THE THERMAL AND MECHANICAL PROPERTIES OF A LOW-DENSITY GLASS-FIBER-REINFORCED ELASTOMERIC ABLATION MATERIAL

by W. T. Engelke, R. W. Robertson, A. L. Bush and C. D. Pears

Prepared under Contract NAS1-11499

SOUTHERN RESEARCH INSTITUTE
BIRMINGHAM, ALABAMA

for

NATIONAL AERONAUTICS AND SPACE ADMINISTRATION

FOREWORD

This report is submitted in accordance with the statement of work of Contract NAS1-11499.

The work was conducted by the Applied Thermal Section of the Mechanical Engineering and Mechanics Division at the Southern Research Institute, Birmingham, Alabama, between March, 1973 and April, 1974. Mr. R. W. Robertson was Project Engineer and Dr. Ronald K. Clark of the Langley Research Center was the technical representative for this contract.

TABLE OF CONTENTS

TABLE OF CONTENTS - CONTINUED

LIST OF ILLUSTRATIONS

LIST OF ILLUSTRATIONS - CONTINUED

LIST OF ILLUSTRATIONS - CONTINUED

LIST OF TABLES

LIST OF TABLES - CONTINUED

LIST OF TABLES - CONTINUED

SUMMARY

An evaluation of the thermal and mechanical properties was performed on a molded low-density elastomeric ablation material designated as Material B. This material contained:

1) Twenty-five parts by weight GE RTV 655 Silicone Resin

2) Fifty parts by weight Union Carbide BJO-0930 phenolic microballons primed with GE SS4155

3) Fifteen parts by weight Emerson Cummings IG101 glass bubbles

4) Ten parts by weight Polymer Corporation Polypenco 66D nylon primed with GE SS4155

5) The above matrix was reinforced with glass fibers 1/4 inch long. The percentage by weight of the glass fibers to the total composite was 15%.

Both the virgin and charred states were examined to provide meaningful inputs to the design of a thermal protection system. This evaluation was a continuation of a previous program where the same properties were determined on another low-density elastomeric composite designated as Material A [1][1].

On the virgin material the thermal conductivity ranged from 0.044 W/m K at 100 K to 0.053 W/m K at 410 K, decreasing to 0.050 W/m K at 520 K. The heat capacity went from 0.55 J/g K at 100 K to 1.75 J/gK at 500 K. The tensile strength at room temperature averaged 41,000 N/m^2 in the "a" direction and 38,000 N/m^2 in the "b" direction. The average compressive strength at room temperature in the "a" direction was 192,000 N/m^2 and in the "b" direction 186,000 N/m^2.

Chars representative of the flight chars formed during ablation were prepared in a laboratory furnace from 600 K to 1700 K and properties of effective thermal conductivity, heat capacity, porosity and permeability were determined on the furnace chars formed at various temperature levels within the range. This provided a "boxing" of the data which will enable the prediction of the transient response of the material during "flight" ablation.

---

[1] Bracketed numbers indicate reference listed at the end of the report.

The properties indicated that in the range of 500 K to 800 K all degradation and volatilization occurs since at 800 K the weight loss was almost maximum and bulk density was minimum. The thermal conductivity at atmospheric pressure increased rapidly from 0.089 W/mK at 800 K to 0.68 W/mK at 1730 K. The heat capacity curve had a relative minimum of 1.6 J/gK at 800 K, increasing to a relative maximum of 2.55 J/gK at 1100 K. Between 1100 K and 1365 K the heat capacity values decreased to 1.95 J/gK and remained constant to 1740 K.

X-ray diffraction analyses were performed on samples from the 1300 K and 1700 K furnace chars and no ordered carbon was detected. Alpha cristobalite was the only identifiable compound.

Comparisons were made between the properties of prior Material A and Material B. Definite trends existed due to the influence of the honeycomb reinforcement in Material A.

THE THERMAL AND MECHANICAL PROPERTIES OF A LOW-DENSITY GLASS-FIBER-REINFORCED ELASTOMERIC ABLATION MATERIAL

INTRODUCTION

Scope

This is the final report to the National Aeronautics and Space Administration, Langley Research Center, for the work performed under Contract NAS1-11499. This program involved the evaluation of thermal and physical properties on a low-density elastomeric ablation material in both the uncharred (virgin) and charred state. It is the second final report under this program. The first final report [1] involved the evaluation of Material A and this report deals with Material B. Material A was a honeycomb reinforced elastomeric composite whereas Material B was an elastomeric composite reinforced with glass fibers.

Background

The material evaluated is being considered as an ablative material to be used in the thermal protection system for the shuttle. Both thermal and mechanical data were measured on both the virgin and charred material to provide meaningful inputs to the design of the thermal protection system. To accomplish this, the evaluation of thermal conductivity, heat capacity, tensile strength and compressive strength for the virgin material was necessary; and for the charred material, thermal conductivity, heat capacity, permeability and porosity were examined.

The properties of the char composite were intended to provide data to predict the transient response of the material during ablation. Therefore, the "boxing" approach developed at Southern Research Institute was used. [2] This method involves predegrading the material at some preselected temperature, preparing specimens and performing property measurements up to the precharring temperature with steady-state devices. The locus of points of property versus precharring temperature represents the transient behavior of the property during the first exposure. The advantages of this method are that it provides a dimensionally stable specimen and allows the use of steady-state measurement techniques. This approach seems to represent the best state-of-the-art technique provided that the structures of the flight and laboratory chars are similar and that additional time-at-temperature during the measurements does not significantly alter the properties.

Program Performed

The evaluation of the virgin material included the thermal conductivity and heat capacity from 150 to 500 K. Tensile and compressive strength and modulus were determined on the virgin material at room temperature. The mechanical properties were determined in the two in-plane directions and the thermal conductivity was determined in the thickness direction.

The first step in evaluating the charred material was the investigation of the methods necessary to prepare chars which would best simulate the chars formed during flight. This investigation was conducted by charring several samples in a furnace under various conditions and comparing the resultant char with two chars supplied by NASA that were formed in the arc-jet torch. The main criteria of the char preparation was to prepare chars suitable for evaluation as well as simulate the char formed during ablation in flights.

The furnace chars were prepared at five temperature levels from 600 K to 1750 K. This temperature range was selected since the arc-jet chars were formed over that range, which is inclusive of the temperatures predicted during flight.

Properties determined on the chars were effective thermal conductivity, heat capacity, permeability and porosity. The effective thermal conductivity was determined in the thickness direction on the various chars up to their formation temperature, enabling a boxing analysis of the data. Values were determined at mean specimen temperatures up to slightly below the char temperature so that the hot face of the specimen did not exceed the temperature at which the char was formed. Data were measured in an environment of nitrogen at 1333 N/m^2, 49,329 N/m^2 and 101,325 N/m^2 (10,370 and 760 torr).

The heat capacity was determined on the various chars up to the formation temperatures. The permeability was determined on the various chars at room temperature, with a few runs being made to 800 K to assess the effect of temperature. The porosity of the chars was determined with bulk and true density measurements at room temperature.

MATERIAL DESCRIPTION AND CUTTING PLANS

Only one material was evaluated under this program and it was designated Material B. It was a molded, low-density, elastomeric material. This material contained:

1) Twenty-five parts by weight GE RTV 655 Silicone Resin

2) Fifty parts by weight Union Carbide BJO-0930 phenolic microballons primed with GE SS4155

3) Fifteen parts by weight Emerson Cummings IG101 glass bubbles

4) Ten parts by weight Polymer Corporation Polypenco 66D nylon primed with GE SS4155

5) The above matrix was reinforced with glass fibers 1/4 inch long. The percentage by weight of the glass fibers to the composite was 5%.

The elastomeric composite of this material (Items 1 through 4) is basically the same as the composite used for Material A with the exception that glass bubbles were used instead of the

silica bubbles. Also, this elastomeric composite was reinforced with glass fibers rather than the honeycomb reinforcement used in Material A.

A total of four panels were received which were 30.5 cm x 30.5 cm square x 4.8 cm thick.

There was no visual basis for assigning in-plane directions to the panels, since there was no preferred direction or orientation of the fibers. Since the mechanical properties were to be determined in both the "a" and "b" directions, the panel used for these evaluations was arbitrarily assigned an "a" and a "b" direction. The "c" direction was in the thickness of the panel. The effective thermal conductivity of the virgin and charred material was determined in the "c" direction, as was the permeability of the charred material.

Cutting plans for the three panels (numbered 1 through 3) used in these evaluations are shown in Figures 1 through 4. These cutting plans show the extraction of specimens for the evaluation of the virgin material and the extraction of blanks employed for charring. The specimens extracted from the char blanks after charring are also indicated in the figures.

A numbering system was devised that designated the type of specimen, specimen number, direction (if applicable), panel number from which it was extracted, material and charring conditions (where applicable).

The numbering system for the virgin specimens was as follows:

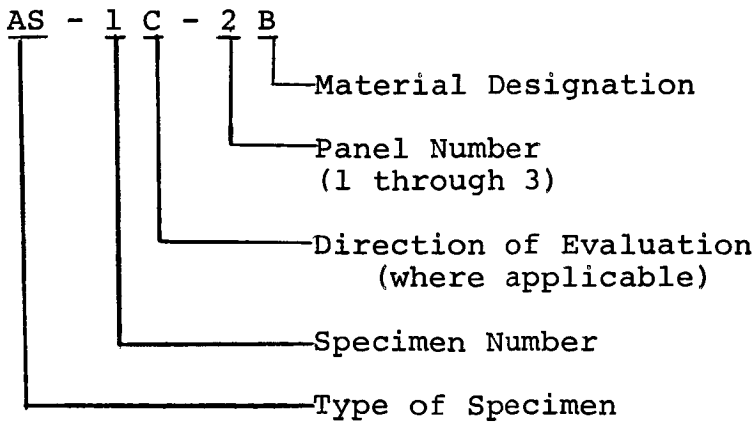

AS - Conductivity Specimen

HC - Heat Capacity Specimen

T - Tensile Specimen

C - Compressive Specimen

The numbering system for the char blanks was as follows:

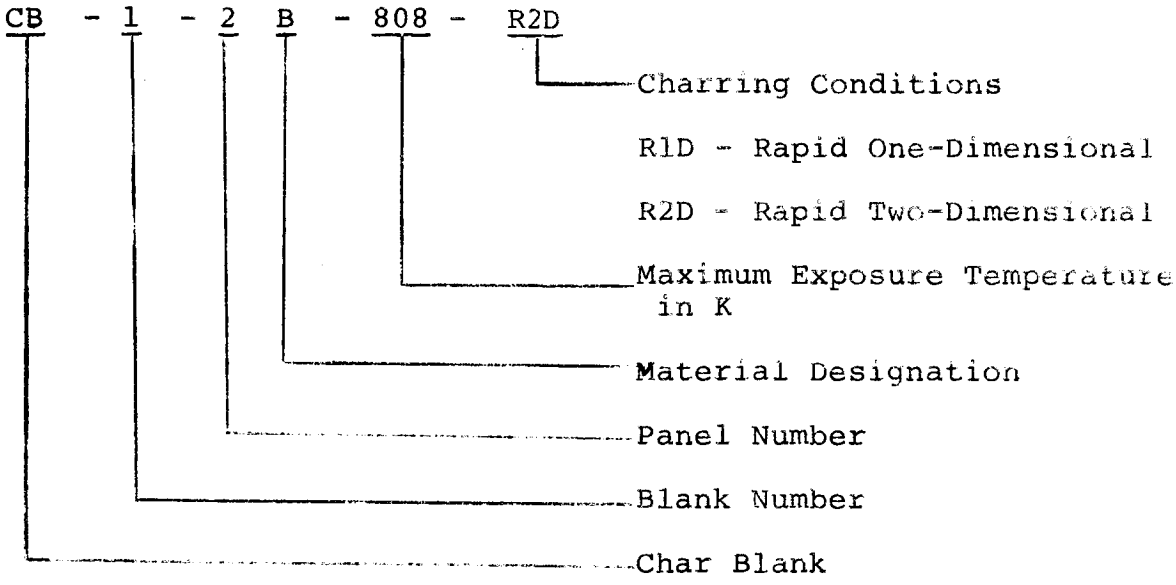

The specimens extracted from the char blanks were designated as follows:

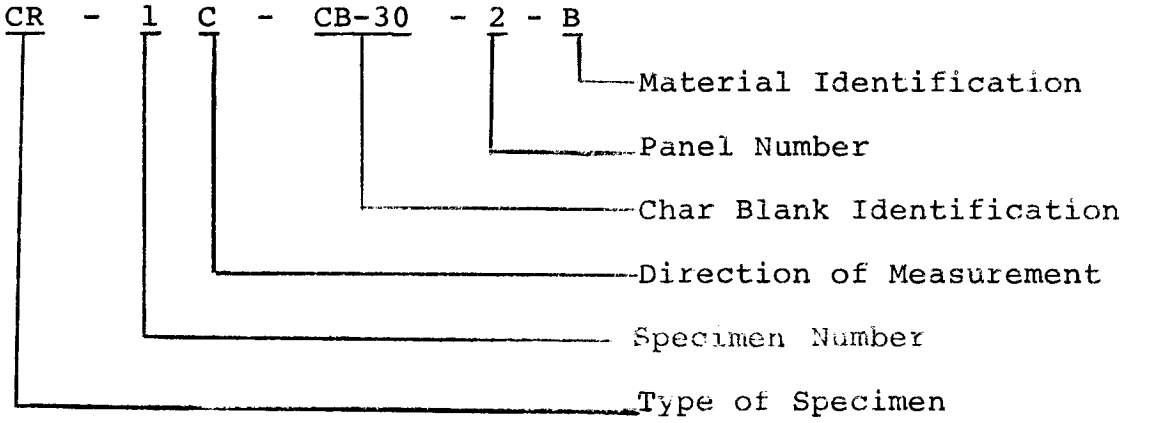

CR - Thermal Conductivity (Comparative Rod)

RI - Thermal Conductivity (Radial Inflow)

HC - Heat Capacity

P - Permeability

BD - Bulk Density

TD - True Density

In addition to the four panels, four blocks were received that had been exposed to the arc-jet. These were necessary to provide a baseline for comparison of the furnace chars prepared at various conditions. The four blocks were about 12.7 cm x 6.3 cm x 3.4 cm thick. Originally, these blocks were 12.7 cm x 12.7 cm that were subjected to the arc-jet and then sectioned in half. Some true density specimens were extracted from one of the blocks. The specimen numbers extracted from the arc-jet were as follows:

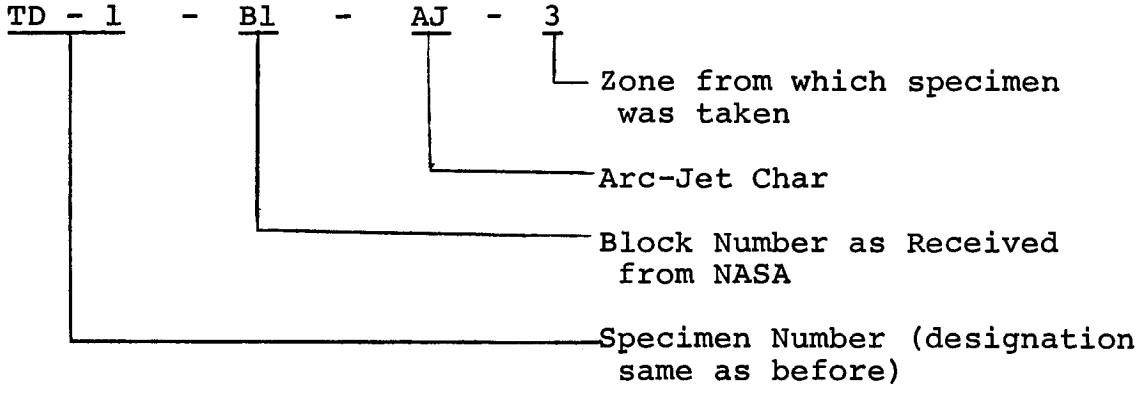

APPARATUSES AND PROCEDURES

Char Preparations

Chars were prepared in a high temperature furnace which employs an electrically heated graphite heater tube. The heater tube is cylindrical in shape. The heater tube temperature is controlled manually with a powerstat which drives a 25 kw transformer.

Chars were prepared by immersion of the char blanks in the furnace after it had been preheated to a selected temperature level. The char blanks which were 3.81 cm wide x 7.62 cm long x 5.08 cm thick were supported in a holder which could be rapidly inserted and extracted from the furnace. A picture of the specimen holder is given in Figure 5. Shown in the figure is the final system decided on after the preliminary char evaluation was completed which will be discussed later. One blank was charred at a time with both faces exposed to the radiant heating from the heater tube of the furnace. The graphite felt insulation around the edges prevented lateral heating. This arrangement provided two-dimensional heating of the blanks which

caused the char formation to progress from both faces to the center.

The maximum temperature was measured for each char prepared. This was done by measuring the face temperature of the char through the sight port in the furnace. Temperatures were measured either with chromel/alumel thermocouples installed at the specimen surface through the sight port or by direct readings with an optical pyrometer. When using the optical pyrometer, appropriate corrections were made for the sight window.

The specimens were cooled rapidly by withdrawing the specimen from the furnace at the end of the heating cycle and immersing it inside a cold cylinder purged with helium. A helium purge was used in the furnace during all of the char work. A helium purge also was inserted at the bottom of the heater tube with the gas traveling from bottom to top to sweep the pyrolysis gases toward the top of the furnace.

The furnace preheat temperatures employed were approximately 600 K, 800 K, 1100 K, 1370 K and 1730 K. The correlation between furnace preheat temperature and cold wall heat flux is given in Table 1. As previously reported [3], the correlation is rather good between the radiant cold wall heat flux and the convective cold wall heat flux in a high enthalpy nitrogen gas stream.

The thermal response of the chars prepared in the laboratory were defined from measurements of temperature at the surface and in-depth. Chromel/alumel thermocouples were installed in the char centrally between the two heated surfaces. In some of the 1100 K, 1300 K and 1700 K furnace chars, a thermocouple was placed about 0.7 cm beneath the surface so the temperature-time history could be obtained for the zone from which the specimen would come. The thermocouple wires were housed in double bore alumina tubing and were inserted in holes drilled parallel to the heated surfaces.

The temperature measurements were used to define the time required for the front face and the in-depth thermocouple to reach equilibrium. This aided in defining the uniformity of the char with regard to temperature exposure. The results of the initial measurements, which established the response, were used throughout the program as being representative for all chars prepared.

Some of the chars prepared at temperature were made into specimens by careful handsanding; however, most of these samples were extremely friable and were impregnated with poly-alphamethylstyrene (Amoco Resin 18-210) prior to the machining operation. Then, the samples were machined to the desired dimensions. The impregnant was removed by baking the machined sample in an inert environment for about 1 hour at 672 K. At this temperature the resin turns to a gas and leaves the specimen with essentially no residue.

It was found that the 800 K specimen for the Guarded Comparative Rod Apparatus could best be obtained by first cutting the specimen shape from the virgin material, then charring the specimen in the furnace which was preheated to 800 K. This minimized handling of the charred material and thus, reduced damage to the specimen. This specimen was designated CR-3C-CB-0-1B. It was designated as coming from char blank 0 since it did not actually come from a char blank.

Thermal Conductivity

Three apparatuses were employed to determine the thermal conductivity of both the virgin and charred material. The ASTM C-177 guarded hot plate was used to 600 K for the virgin and 600 K precharred material. The comparative rod apparatus was used to 1100 K for the chars prepared in the furnace above 800 K. The radial inflow apparatus was used up to 1365 K and 1730 K for the chars prepared at 1365 K and 1730 K, respectively.

Guarded Hot Plate Apparatus - A complete description of the ASTM C-177 guarded hot plate apparatus is included in Appendix A. For these evaluations the smaller apparatus with the 8.25 cm heater plate was employed. Due to the nature of this material, the evaluations required the following exceptions to the described procedures:

1. The specimen discs were split into a central and guard ring to minimize radial heat exchange. Figure 6 is a drawing of the specimen disc employed.

2. Temperatures on both runs were measured internally with thermocouples inserted in 0.1 cm diameter temperature wells (see Figure 7). The internal thermocouple beads were potted in place with an RTV adhesive. The wires were insulated with a double bore alumina tube broken every 0.64 cm along its length to minimize thermal drain from the bead.

3. Temperatures in the guard ring of the specimen were measured and the difference between the guard and the central were maintained within 10 percent of the temperature gradient across the specimen.

Comparative Rod Apparatus - The comparative rod apparatus is described in Appendix B. This apparatus consists basically of two cylindrical reference pieces of known thermal conductivity stacked in series with the cylindrical specimen. A small electrical heater is placed at one end of the rod, to introduce heat through the stack, and a heat sink or a second heater is employed at the opposite end of the stack to maintain the temperature drop through the specimen at the desired level. Radial losses are minimized by means of radial guard heaters surrounding the rod. The annulus between the rod and the guard heaters and surrounding the guard heater is packed with an insulation, usually diatomaceous earth or thermatomic carbon.

This method compares the conductivity of the specimen to that of the references and requires true axial heat flow down the column with a minimum of radial heat exchange.

Modification of this apparatus was necessary for this program since the standard assembly is only accurate for measurements of conductivity above 1.4 W/mK. The reason for this is that analyses [4,5] have shown that heat can shunt the specimen (through the insulation) particularly when the thermal conductivity of the specimen is not an order-of-magnitude or more than that of the insulation and the guard heater is, say, twice the diameter of the specimen or more. Note that the shunting effectively gives a larger specimen area and results in an erroneously low temperature difference in the specimen relative to the reference (assuming that the references have a higher thermal conductivity than the specimen). This yields erroneously high values of thermal conductivity. With certain values for the thermal conductivities of the references, specimen and insulation, guard heater to specimen diameter ratio and guard to specimen temperature profile, these errors can easily reach 100 percent.

Analyses [4, 5, 6] have shown that the heat shunting problem can be overcome if the following conditions are satisfied:

1. The guard profile matches the specimen profile.

2. The ratio of guard diameter to specimen diameter is as near unity as possible.

These concepts were applied to the modified technique used here.

The experimental configuration used for the measurements is shown in Figure 7. The assembly consisted of a central column comprised of 2.54 cm diameter specimen sandwiched between two references of known thermal conductivity. Guard rings made of the same materials as the specimen and references surrounded the central column. The guard rings were constructed to match the specimen and reference lengthwise. The annulus between the central column and guard ring was 0.16 cm wide which gives a ratio guard diameter to specimen diameter of 1.125.

The references used were made from slip cast fused silica, the conductivity of which has been evaluated and well defined from several measurements made in the ASTM guarded hot plate apparatus.

Heaters made of Armco iron were placed on either end of the column to control heat flow and mean temperature. Armco iron was used because its thermal conductivity is about 200 times that of the specimen and; hence, the temperature gradient along a radial line at the top of the build-up was estimated to be no more than one or two degrees. Thus, the guard and central temperatures are matched at the ends. The entire assembly is surrounded by diatomaceous earth insulation contained inside a 10 cm diameter guard heater.

Temperatures are measured at two axial locations in each reference and in the specimen. A beaded chromel/alumel thermocouple was inserted into the drilled holes in a double bore alumina insulator. The insulator was broken about every 0.3 cm to minimize conduction losses. The thermocouples in the specimen were potted in place at the bead with Silastic RTV-731, silicone rubber.

Specimen gage lengths were determined from radiographs or X-rays. The X-rays were examined at 10X magnification to determine the gage distance relative to the overall thickness.

The idea for the assembly shown in Figure 7 was to use identical materials for a guard ring and thus create as closely as possible a matched guard condition to minimize radial heat exchange. Also, a thin specimen, 0.635 cm, is used because this also minimizes radial heat exchange and heat shunting. Further, the annulus is kept small to minimize heat shunting which occurs even with matched guarding.

In practice, perfect matching of the guard and central columns is not achieved. Hence, corrections for radial heat exchange are made to the measured data based on the measured temperature profiles. Further, corrections are made for the heat shunting through the annulus.

Details of the corrections made to the measured data are included in Appendix C. Even though two different corrections are applied to the data, the maximum value for both corrections during this program did not exceed 12 percent. Hence, sizeable uncertainties in the correction procedures do not create large uncertainties to the final data. The combined uncertainty for the several sources of uncertainty present is ±8 percent increasing to ±10 percent above 800 K.

Radial Inflow Apparatus - A complete description of the radial inflow apparatus is included in Appendix D. Due to the structure of this material, cylindrical specimens could not be employed; therefore, the strip assembly was used. A sectional view of this assembly is shown in Figure 8.

The assembly consisted of four specimen strips sandwiched between strips of ATJ graphite which contain wells for temperature measurement. The corners of the build-up were packed with thermatomic carbon to minimize extraneous heat flows. Pyrolytic graphite strips were used on the inside to aid in maintaining the isotherms normal to the directions of heat flow. The assembly was placed concentric about a calorimeter with a 1.27 cm gage section, and the annulus between the calorimeter and the pyrolytic graphite strips was packed with graphite.

Positive interfacial contact between the strips was assured in this assembly by the addition of expansion pistons to the support cylinder. These pistons were designed to counteract differenetial expansions that would cause a separation at the interfaces. For this program the pistons consisted of a stack of two pieces, pyrolytic graphite in "c" direction at 0.254 cm thick, and CS graphite at 0.508 cm thick.

The specimen was built up on the calorimeter tube and guards packed with thermatomic carbon were used above and below the specimen to retard longitudinal heat flow. Graphite felt insulation was used between the specimen and guards. The top guard section contained graphite sight tubes which align with the temperature wells in the specimen and provided access from outside the furnace.

During the run the procedures were similar to those detailed in the appendix.

Thermal conductivity was calculated from the measurements of temperature difference and heat flow. The equation used is:

$$k = \frac{\Delta X}{4A} \frac{Q}{\Delta T} \qquad (1)$$

where

k = thermal conductivity - W/mK

ΔX = thickness of specimen - cm

A = area of gage section of one specimen strip

Q = total measured heat flow - watts

ΔT = temperature difference across specimen strip - K

A correction to the conductivity calculated in Equation 1 is necessary for this assembly. The measured conductivity will be erroneously high due to the heat transferred through the corners packed with thermatomic carbon. The correction required has been determined analytically for the geometry of the assembly by dividing the configuration into several radial segments and assuming the temperature distribution in the thermatomic carbon is the same as in the specimen and surrounding strips. This analysis yields:

$$\frac{k_s}{k_m} = 1 - 0.19 \frac{k_p}{k_m} \qquad (2)$$

where

k_s = true thermal conductivity of the specimen

k_m = measured thermal conductivity of the specimen

k_p = thermal conductivity of the packing in the corners

As observed in Equation 2 the lower the measured conductivity the greater the bias. For these runs the maximum bias was 19 percent.

The uncertainty of the values measured in the radial inflow apparatus can be derived from the summation of the following random uncertainties:

1. Errors associated with the basic equipment that have been set at ±7 percent. This includes the uncertainties involved in temperature measurement, heat flow measurement and other factors as discussed in the appendix.

2. Error in the analytical correction of the measured data. The error involved here is certainly no more than ±50 percent of the correction. With the maximum correction being ±19 percent the maximum error would be ±9 percent.

The combination of the above uncertainties yield a total error for the modified radial inflow system of ±12 percent.

Impregnant Removal from Conductivity Specimens - As part of the procedures for all the conductivity runs where impregnated specimens were employed, the system with specimen was assembled and prior to the measurement of data was baked at above 670 K to remove the impregnant from the specimen.

Heat Capacity

The heat capacity of both the virgin and charred materials were performed in both the adiabatic and ice calorimeter. The adiabatic calorimeter was employed to 800 K and the ice calorimeter from 800 K to 1730 K. Both apparatuses are described fully in Appendices D and E.

A major problem with these materials, particularly that of the chars, is the very low mass times heat capacity product (mCp) due to the low density of the material. With a low mCp, the signal is, of course, very low and the measurement is subject to a lack of precision.

To minimize this problem, the chars were pulverized and packed within an aluminum container for the determinations in the adiabatic calorimeter. The pulverization increased the mCp product sufficiently and the additional mCp of the container remained a very small percentage of total signal; therefore, the correction for the mCp of the container was small. These conditions provided the precision normally obtained with this apparatus.

For the determinations using the ice calorimeter, the low density char was pulverized and packed within our normal graphite container. Unfortunately, the mCp product of the container was a significant percentage (about 50 percent) of the total signal. Since the correction for the container was significant, the heat capacity of the cups employed for the measurements were confirmed with several determinations over the temperature range of interest.

Permeability

All permeability measurements for this program were made with the high temperature permeability apparatus which is described in Appendix F. The low temperature measurements were made in this apparatus because it measures total pressure and is probably better for the high flow rates expected with these chars.

The diameter of all specimens was approximately 2.54 cm, but the thickness varied from 0.630 cm to 1.827 cm. Silicone rubber (Dow Corning RTV-731 Silastic) was used as the sealant for all of the char specimens which were run only at room temperature. The furnace char specimens run at elevated temperatures were sealed in the fixture with Sauereisen 32 cement.

A piece of wire screen was placed on the downstream side of the 1100, 1300 and 1700 K specimens before they were sealed in the fixture. This was done to prevent the specimens' destruction by the differential pressure across it. A calibration curve was obtained for the screen wire giving pressure drop as a function of gas flow rate. This correction was applied to the pressure drop measured across the permeability specimens which were backed with screen wire. The 600 and 800 K specimens were sufficiently strong that this was not necessary. Figure 9 shows a typical specimen assembly. One specimen of the chars formed at 600, 800, 1100, 1300 and 1700 K was run at room temperature using nitrogen and helium as the permeating gases. An additional specimen of the 1100, 1300 and 1700 K chars was run at 800 K using nitrogen and helium as the permeating gases. All specimens which were run at elevated temperatures were run at room temperature before and after the high-temperature measurements. This assisted in ascertaining if any physical change in the specimen occurred during the measurements at elevated temperature. The 600 and 800 K chars were capable of being machined without impregnation. However, because of the

fragile nature of the other chars, the 1100, 1300 and 1700 K specimens were machined by hand. The 600 and 800 K specimens were sealed directly into the specimen holder and allowed to cure. However, a wire screen was placed behind each of the 1100, 1300 and 1700 K specimens before they were sealed in the specimen holder. The specimen assembly was then sealed in the specimen holder and allowed to cure.

Porosity

The porosity of the chars was determined by calculation from measured values of bulk and true density in accordance with the following equation:

$$P = 1 - \frac{\rho_b}{\rho_t} 100 \qquad (3)$$

where

P = total porosity in percent by volume

ρ_b = bulk density

ρ_t = true density

The bulk density was measured by machining a specimen to a definite geometry from which volume and weight were accurately measured.

The true density was determined using a liquid pycnometer in accordance with ASTM 135-66. The sample was pulverized and passed through a 100 mesh screen to assure that all particles were free of voids. The wetting agent used was methanol and a 25 ml pycnometer bulb was used primarily.

On some of the samples, complete wetting was not obtained as evidenced by some (less than 2 percent) particle floatation in the bulb. Apparently, the pulverization and passage through a 100 mesh screen did not remove all of the porosity. The small amount of particle floatation was removed from the bulb and weighed to adjust the results to a corrected value of true density. This correction was less than 5 percent.

Tension

All of the tensile evaluations were made in a Tinius-Olsen Universal Testing Machine at 294 K. Strain gage extensometers were utilized to measure strain over a 5.08 cm gage length. Two specimens were tested in each direction (a and b). Figure 10 shows the tensile specimen configuration. A schematic of the load train is shown in Figure 11. Strain gage extensometers were calibrated over a 0 to 0.305 cm range with 0.020 cm/cm chart calibration, and this calibration was linear within 1.0 percent over the full scale. Load was calibrated to 1 percent accuracy. The specimens had aluminum pads epoxied to each side of each end. These pads provided load transfer to the gage section and support at the pin holes. Chain segments were used in the load train to assure uniaxial alignment.

Compression

All of the compressive evaluations were made in a Tinius-Olsen Universal Testing Machine at 294 K. Strain gage extensometers were used to measure strain over a 5.08 cm gage length. Figure 12 shows the compressive specimen configuration. Two specimens were evaluated in each direction (a and b). The extensometers were calibrated over a 0 to 0.305 cm range with 0.020 cm/cm chart calibration, and this calibration was linear within 1.0 percent over the full scale. Load was calibrated to 1 percent accuracy. The specimens were tested in a special loading fixture to provide uniaxial alignment and avoid specimen buckling. A schematic of the load fixture is shown in Figure 13.

RESULTS OF VIRGIN MATERIAL EVALUATION

Thermal Conductivity

The thermal conductivity from 110 K to 500 K in the "c" or thickness direction of the panel was measured in 1 atmosphere of nitrogen. The data are shown in Figure 14 and Table 2. As seen in the figure, the values increased from 0.045 W/m K at 120 K, reached a maximum value of 0.053 at 425 K. The data for both specimens agreed rather well except for some scatter at 200 K.

The comparative values for Material A [1] were plotted on Figure 14 as a dashed line. From 120 K to 350 K the conductivity values of Material A were about 12 percent higher than those for Material B. The values then diverged so that at 500 K the

conductivity of Material A was 50 percent higher than that of Material B.

There was a significant difference in the character of the two curves. Whereas the conductivity curve for Material A exhibited a marked increase above 297 K, the curve for Material B increased gradually to its peak at 425 K then decreased slightly from 425 K to 500 K. The decreasing character of the conductivity of Material B above 425 K was expected due to the initial degradation of the composite. The honeycomb reinforcement in Material A was an influence since it provided a more continuous shunt of heat flow and would yield the higher values and increasing character of conductivity observed.

Heat Capacity

Enthalpy and heat capacity from 120 K to 490 K were determined. The values of enthalpy and heat capacity are shown in Figure 15 and Table 3.

The heat capacity increased from 0.5 J/g K at 120 K to 1.7 J/g K at 490 K. These values were about 10 percent lower than those measured on Material A.

Attempts to determine the enthalpy at temperatures higher than 500 K resulted in values that were biased high. Observations of the thermal response of the specimen within the furnace indicated that at slightly higher temperatures an exothermic reaction initiates which would obviously alter the measurement of enthalpy.

Tension

The results of the tensile evaluations are shown in Table 4 and the stress-strain curves are included as Figures 16 through 19.

In the "a" direction, ultimate strengths for specimens T-1a-2B and T-2a-2B were 48.27 x 10^3 N/m^2 and 34.48 x 10^3 N/m^2, respectively and elastic modulii were 8825.6 x 10^3 N/m^2 and 7032.9 x 10^3 N/m^2, respectively. In the "b" direction, ultimate strengths for specimens T-1b-2B and T-2b-2B were 42.75 x 10^3 N/m^2 and 32.41 x 10^3 N/m^2, respectively and elastic modulii were 6343.4 x 10^3 N/m^2 and 7032.9 x 10^3 N/m^2, respectively. A typical tensile fracture is shown in Figure 20.

Material B did not exhibit the anisotropic behavior in tension found in Material A. The ultimate strength of Material B was about one-fourth to one-eighth that of Material A while the elastic modulus of Material B was one-half to one-fourth that of Material A. Again the influence of the honeycomb reinforcement of Material A would increase the strength and anisotropy.

Compression

The results of the compressive evaluations are shown in Table 5 and the stress-strain curves are included as Figures 21 through 24.

In the "a" direction, ultimate strengths for specimens C-1a-2B and C-2a-2B were 184.09 x 10^3 N/m^2 and 200.64 x 10^3 N/m^2, respectively and elastic modulii were 9928.8 x 10^3 N/m^2 and 10135.7 x $10^3 N/m^2$, respectively.

In the "b" direction, ultimate strengths for specimens C-1b-2B and C-2b-2B were 208.92 x 10^3 N/m^2 and 162.72 x 10^3 N/m^2, respectively and elastic modulii were 13238.4 x 10^3 N/m^2 and 10963.1 x 10^3 N/m^2, respectively. A typical compressive fracture is shown in Figure 25.

Material B did not exhibit the anisotropic behavior in compression found in Material A. The ultimate strength of Material B was about one-half to one-third that of Material A while the elastic modulus of Material B was one-half to one-fourth that of Material A.

CHAR PREPARATION IN THE LABORATORY FURNACE

Criteria

To conduct a meaningful evaluation of the thermal properties of a char formed during re-entry, one must be able to prepare suitable specimens from the char. Obviously, these specimens must be stable, compatible with the environment and other conditions of the test and be representative of the char formed during flight. In addition, to characterize a char formed at specific temperatures, the char specimen must be prepared under isothermal conditions.

Of course, the best simulation of a flight char is one that is made under a high enthalpy arc-jet stream; however, the chars prepared in an arc-jet are normally not practical for use as a specimen. This is due to a large temperature gradient that exists during char formation. Therefore, the chars were prepared in a furnace under this program, and the conditions of charring were selected to provide the best representation of the flight char.

To best meet the criteria of char preparation, an initial evaluation of optimum procedures was conducted, the first step of which was a study of the arc-jet chars prepared by NASA. It was assumed that they represented flight chars.

Arc-Jet Char Description

Two samples of char formed in the arc-jet were received for our inspection and formed a baseline for comparison of the furnace chars at various conditions.

The arc-jet specimens for Material B were prepared in the same manner as those for Material A. The arc-jet specimens were prepared by mounting the block on a wedge and the hot gases impinged the surface at an angle under a constant heating rate cycle of 20 minutes. The cold wall heat flux was monitored from the leading edge to the back edge. At the midpoint, the cold wall heat flux density was 18.2×10^4 W/m^2 (16 Btu/ft^2 sec). The variation in heat flux density was linear and it ranged from 30.1×10^4 W/m^2 (26.5 Btu/ft^2 sec) at the leading edge to 7.26×10^4 W/m^2 (6.4 Btu/ft^2 sec) at the trailing edge. Assuming only radiation heat loss from the sample and an emittance of 0.6 (probably low), the maximum equilibrium temperature of the crust on the arc-jet was calculated to be 1728 K or 2650°F. Therefore, the maximum charring temperature used in this program was about 1730 K.

A photograph of Arc-Jet-B-1 as received from NASA is shown in Figure 26. Arc-Jet-B-2 is shown in Figure 27. A visual inspection of Arc-Jet-B-2 and a discussion with the technical monitor of NASA resulted in the conclusion that this sample had been subjected to excessive oxidation and was unsuitable as a standard of comparison. The crust of Arc-Jet-B-2 was cracked and completely separated from the remainder of the sample. The outer surface of the crust had a dark yellow-green coloring.

Arc-Jet-B-1 had a crust with a light-burgundy coloration on its outer surface. There were areas where the firm crust had been eroded away possibly by oxidation and/or the action of the arc-jet. The fibers on the surface were glazed and appeared darker than the surrounding material. Immediately beneath the crust was a grey powdery area in which the fibers were quite fragile. Beneath this was a darker area which was hard and brittle and tended to granulate when scraped with a sharp blade. The coloration of this zone was unique in that the upper portion of the zone was dark brownish while the lower portion was dark grey. The fibers in this zone were almost indiscernible. The next zone was black and somewhat powdery with dark, brittle fibers. The next zone was dark grey and very powdery with light-colored, pliable fibers. The bottom zone was spongy and somewhat darker than the virgin material.

There were no pronounced cracks in Arc-Jet-B-1. There were several small random cracks within 1/2 inch of the heated surface, but there were no cracks on the surface itself. Since this material was not reinforced with a honeycomb, this macroscopic structure of the char was quite different than that of Material A. As related in NASA CR 132281 [1], Material A had several major separations and gaps due to the shrinkage of the elastomeric composite from the honeycomb wall. Therefore, the char (furnace or arc-jet) of Material B, was more homogenious than that of Material A since it consisted of a more even distribution of porosity and cracks.

Suitable Monitors

To properly conduct the initial evaluation of optimum char preparation in the furnace, suitable monitors and inspection procedures were necessary. The evaluation and selection of the best inspection procedures were thoroughly reviewed under CR 132281 [1] concerning the evaluation of Material A. Due to the similarities of these two materials, the optimum inspection techniques developed for Material A were used here.

The best inspection procedure appeared to be the examination of the chars' gross physical structure. Consideration was given to parameters such as density, color, texture and appearance of the fibers. The manner in which the chars reacted to scraping with a sharp blade or crushing were also considered.

The use of the 10X to 20X stereo microscope assisted in the visual inspection. The specimens were viewed in a natural state without preparation such as polishing and impregnation. This permitted observation and comparison of the structure, color of the beads and fibers in the various chars.

As was the case for Material A, the temperatures of char formation for Material B were too low to permit any use of the monitors which quantitized degree of graphitization or ordering of the crystallites. These were very effective monitors under a previous program performed under Contract NAS1-10517 [3]. Some X-ray diffraction tests were run and no ordered carbon was detected. The results of the X-ray diffraction measurements presented later did indicate the presence of alpha cristobalite which was obviously from the glass present in the virgin material. The technique used in preparing the X-ray diffraction samples was not controlled, therefore the results of these analyses could not be compared precisely. However, these results were used to make general comparisons.

Preliminary Char Preparation and Selection of Charring Conditions

Two methods were attempted to provide representative chars prepared in the furnace. These methods are referred to as:

1) Rapid one-dimensional (R1D)

2) Rapid two-dimensional (R2D)

The term rapid refers to the chars formed by a rapid heating rate which was obtained by immersion into a furnace preheated to the desired temperature. Typical temperature versus time curves for the surface and internally at depths of 1.27 and 2.54 cm (on the 5.08 cm thick char blanks) from the heated surface are included in Figure 28.

One-dimensional and two-dimensional indicated the application of heat to the specimen. The one-dimensional chars were prepared by allowing exposure of only one surface to the radiant heat from the heater tube. This was done by using the assembly discussed under "Apparatuses and Procedures" section but two specimens were installed back-to-back with a piece of graphite felt inserted between them. This provided an insulated back face boundary condition and allowed one-dimensional heating to occur.

The two-dimensional heating allowed radiant heating to both surfaces of a specimen as discussed under the "Apparatuses and Procedures" section.

Table 6 summarizes all the char blanks prepared during the preliminary investigation. The table includes various measurements made to characterize and compare the blanks made. Some of the same measurements were made on the arc-jet specimens for a basis of comparison.

The rapid one-dimensional chars warped severely, rendering them unsuitable for specimen preparation. This method was, therefore, not pursued and the rapid two-dimensional charring was studied in more detail and finally selected. Preparation of samples under 2.54 cm produced chars unsuitable for evaluation; however, thicker samples formed sufficiently thick charred areas near the surfaces. These charred areas proved to be representative of the flight chars. The sample thickness of 5 cm was used. The visual appearance of these two-dimensional chars was quite similar to the arc-jet char except for the crust (1700 K char). The 1700 K furnace char was a dark grey color whereas the arc-jet char was light grey, possibly resulting from oxidation.

The effect of residence time (time-at-temperature) was examined with three char blanks (CB-35-1B, CB-34-1B and CB-20-1B), all of which were 1700 K chars. Char blank CB-34-1B was held at temperature for one second, CB-35-1B was held for 25 seconds and CB-20-1B for 18-1/2 minutes. Visual inspection and X-ray diffraction showed chars CB-34-1B and CB-35-1B to be the same and they compared favorably with the arc-jet chars. However, X-ray diffraction revealed that very little alpha cristobalite remained in char CB-20-1B and visual inspection revealed that the interior was grey intermingled with white areas which was unlike that of the arc-jet char. A hard crust about 10 mils thick had formed on the surface, but thoughout the rest of the char, the material was soft and spongy.

The above study led to the selection of the rapid two-dimensional (R2D) heating to process the charred specimens.

All the chars prepared for evaluation under this program were done under the (R2D) conditions with the exception of the 600 K thermal conductivity char. Here the 8.26 cm diameter guarded hot plate was employed for the conductivity measurement and two discs shown in Figure 6 were employed. To accommodate this configuration, a chamber was constructed which enclosed the

specimens and the chamber was purged with helium and installed within a laboratory oven. The heating cycle consisted of heating the material to 590 K in 90 minutes, holding it at constant temperature for 30 minutes and allowing it to cool within the oven after power shut down.

The R2D chars were prepared, as discussed previously in the Apparatuses and Procedures section, by immersing a 3.81 x 7.62 x 5.08 cm thick char blank, insulated around the edges, within the preheated furnace and holding it for about 30 seconds after thermal equilibrium was established. The 1300 K and 1700 K chars were impregnated with Amoco resin 18-210; however, it was possible to make specimens from the other chars without impregnation. Specimens were taken from each half of the char, as close to the heated surface as possible, since the central region was of poor structure and not representative of the arc-jet char. Since these chars were two inches thick, it was rather easy to avoid this central area. Therefore, as far as the specimen was concerned, the formation of char during preparation progressed from one surface to the other rather than a progression from both surfaces into the center.

Typical temperature versus time plots for the furnace chars employed for evaluation are shown in Figure 28.

Table 7 is a summary of all the char blanks prepared and the specimens extracted from them. Included in the table are various physical measurements made prior to and after the cycle.

DATA AND RESULTS

Thermal Conductivity

Thermal conductivity curves are included in Figures 32 through 36. The curves for Material A are also included in these figures. Tables 8 through 14 include the thermal conductivity data.

The thermal conductivity of each char was determined at mean temperatures up to just below the charring value since the hot face temperature of the specimen was not allowed to exceed the prechar temperature. To determine the thermal conductivity at the charring temperature, the curve was extrapolated a small amount. The thermal conductivity values of the virgin material and all of the chars were plotted versus charring temperature in Figure 37.

Since there were no major separations or cracks in this material to provide gross anomalies in the structure, such as there were for Material A, the value measured was an effective conductivity of the composite and needed no adjustments to account for major anomalies.

For some of the evaluations, the data scatter was high since this material was not conducive to conducting precise thermal conductivity evaluations. Intimate interfacial contact necessary for precise measurement was not possible due to the porous nature of the material as well as the glass fibers that protruded from the surfaces. Due to the flexibility of the glass fibers, machining the surfaces did not cut the fibers flush with the surface; therefore, leaving the surface with a brush like texture primarily for the 600 K and 800 K chars.

Another problem involved a deterioration of the surfaces on a 1300 K char specimen during the run in the comparative rod apparatus. This was noticed during the disassembly of the comparative rod apparatus after the run. Even though the run was performed in an inert atmosphere obtained within two vacuum cycles and back-filling with nitrogen, the combination of silica and carbon can (as we have observed previously) oxidize the carbon. This apparently occured in varying degrees for the 1300 and 1700 K char specimens.

Since a residence time of about 20 minutes seemed to affect the structure of the 1700 K chars, (as discussed before) X-ray diffraction analysis was performed on several thermal conductivity specimens in an attempt to see if the material was altered during the run. One guarded comparative rod specimen and one radial inflow specimen of the 1300 K and 1700 K chars were examined after being run and compared with char blanks which had been prepared under the same conditions as those from which the specimens were removed. A comparison of the alpha cristobalite content gave no indication of a change in the 1300 K specimen due to the additional exposure to temperature during the run. However, there was an indication of a possible decrease in alpha cristobalite content of the 1700 K guarded comparative rod specimen and a definite decrease in alpha cristobalite content in the 1700 K radial inflow specimen.

Thus, the results of the post mortem examination of the 1700 K radial inflow specimen indicates that some material in the 1700 K char was not "frozen" upon initial exposure to temperature. Subsequent exposure to temperatures up to the charring temperature caused some alteration in the 1700 K char.

With the above problems inherent with this material, it must be emphasized that the thermal conductivity data are approximate and will only serve to provide trends and general characterization of the material's conductivity during degradation.

Referring to Figure 37, the boxed values of thermal conductivity were fairly consistent with those measured on the virgin material. The curve increased gradually from 0.045 W/m K at 100 K to 0.093 W/m K at 810 K. Between 810 K and 1365 K the slope of the curve increased and was extrapolated between 1365 K and 1730 K resulting in a value of 0.680 W/m K at 1730 K. The curve for the data measured at 49,329 N/m^2 (370 torr) had a similar character, being about 5 percent below the atmospheric curve. The data taken at 1333 N/m^2 (10 torr) fell between 21 percent and 44 percent below the atmospheric curve.

Visual comparison of the arc-jet and furnace chars and post mortem X-ray diffraction analyses suggested that we were unable to model the arc-jet crust exactly. Therefore, the thermal conductivity curves in Figure 37 were extrapolated from 1370 K to 1730 K as was done for Material A. It was believed that this gave a more realistic value of the thermal conductivity of the crust.

In comparison with Material A, the values for Material B were generally lower. This would be expected since Material A contained the honeycomb reinforcement which did provide a more continuous path for heat flow.

Porosity

The porosity of the charred material was calculated from the bulk and true densities. Some true density measurements were also made on the arc-jet char.

Figure 38 and Table 16 report the bulk densities measured versus char formation temperature. The values decreased from 0.255 gm/cm^3 at 300 K (virgin material) to a minimum of 0.18 gm/cm^3 at 810 K. Between 810 K and 1370 K the bulk density increased to 0.222 gm/cm^3 but decreased slightly to 0.202 gm/cm^3 at 1740 K.

The minimum bulk density occurring at 810 K is attributed to the material's high initial weight loss (outgassing of volatiles) and low shrinkage. The effect of char temperature on char blank shrinkage is evident in Figure 30.

The true density is shown in Figure 39 and Table 17. There was general agreement between the true density of the arc-jet and furnace chars except at 810 K where the value for the arc-jet was 23 percent higher.

The porosity is shown in Figure 40 and Table 18. The values increased from 83 percent at 600 K to 87 percent at 810 K and remained fairly constant (2 percent variation) above that temperature. This value was as expected and was slightly below that of Material A which contained more major cracks and separations.

Heat Capacity

The enthalpy and heat capacity data are shown in Figures 41 through 44 and Tables 19 through 25. The heat capacity curves for Material A are plotted as a dashed line on these figures. As was found with the previously tested Material A, the enthalpy did decrease in magnitude with increasing temperature of char formation.

A boxing analysis was performed to predict the heat capacity of Material B during degradation. The results of this analysis is shown in Figure 45 along with the curve for Material A. Below 500 K the values shown are those measured on the virgin material. Above 500 K initial degradation occurs and when the charring temperature reaches 810 K a weight loss of about 37 percent occurs indicating the complete loss of all volatiles in the virgin material. There is a slight decrease in heat capacity during initial degradation up to 810 K. From 810 K to 1100 K, the heat capacity increases to its maximum value of 2.55 J/gK. The percentage weight loss reaches its maximum of 42 percent at 1100 K. Since the weight loss between 810 K and 1100 K is only about five percent, the increase in heat capacity represents normal behavior for a stable material. Between 1100 K and 1370 K there was only a slight decrease in weight loss but the heat capacity decreased indicating a variation in material composition. Between 1370 K and 1739 K the heat capacity remains almost constant, indicating stabilization of the material.

The heat capacity curve for Material A exhibits the same general character as that for Material B up to 830 K, with the two curves varying no more than 15%.

Permeability

The permeability was determined on all the furnace chars prepared at the five charring temperatures. The values were measured at room temperature on all the chars while measurements at elevated temperatures were made on the 800 K, 1100 K, 1300 K and 1700 K furnace chars. The intent of the permeability measurements was to predict the pressure gradient through the thickness of the flight char as it was formed.

The permeability coefficients were derived from the Cornell and Katz plots shown in Figures 46 through 50. The calculations required for the Cornell and Katz plot are shown in Tables 26 through 30.

The data for the two 600 K permeability specimens showed good agreement, but the room temperature data for the two specimens from the 800 K, 1100 K, 1300 K and 1700 K chars did not agree. There did not appear to be a correlation between this variation and the densities of the duplicate specimens.

The trend of the Cornell and Katz plots for the 800 K, 1100 K, 1300 K and 1700 K specimens at the various run temperatures was unexpected. The viscous flow coefficient, α, decreased from the room temperature run to the 811 K run on the 800 K, 1100 K and 1300 K specimen as expected. However, for the 1700 K specimen the viscous flow coefficient was higher for the 811 K run than for the room temperature run. The value of α for the room temperature return on the 800 K specimen was higher than that for the 811 K run but lower than the original room temperature run. For the 1100 K and 1300 K chars, α was higher on room temperature return than on the initial room temperature run. The room temperature return run for the 1700 K char was inconclusive since the helium and nitrogen data did not agree. The data points were plotted in Figure 50 but no curve was drawn.

The values of β, the inertial coefficient were also unusual. In several instances the value of β was zero (see Table 31), indicating purely viscous flow.

It appeared that the reason for the inconsistency of the permeability data on the furnace chars of Material B was the fragile nature of the chars. The pressure gradient across the specimen, the temperature to which the specimen was exposed and the flow of gas through the specimen could have combined to produce unpredictable changes in the flow of the permeating gas, especially

since there was no reinforcement within the material itself. That Material A had a reinforcing honeycomb was probably the main reason for its more consistent permeability coefficients. The major portion of the flow in Material A was in the cracks between the honeycomb and filler material. Material B had no one such obvious path of low resistance to the flow of the permeating gas.

The room temperature Cornell and Katz plot for Material A is shown on each of Figures 47 through 50. The plot for the 600 K char of Material A is not shown since it would be off scale. The plots for the 800, 1100 and 1300 K chars show that Material A was more permeable than Material B. This was probably due to the cracks between the filler and reinforcement of Material A. The plot for the 1700 K char shows that Material A was less permeable than Material B. This was possibly due to the thickness of the specimen as well as the variability in the crust formed on the two materials.

Conclusions

This study has characterized Material B in both the virgin and charred states. The data have revealed the typical progression of various thermal and physical properties that will occur during the process of ablation upon re-entry.

The degradation of the virgin material seems to initiate at about 500 K as was observed with the apparent exothermic reaction that occurred above 500 K with the heat capacity specimens and the decrease in thermal conductivity at 500 K. A summary of the properties measured on Material B by the boxing technique is given in Figure 51.

The weight loss history and bulk density profile indicate that all degradation and volatilization occurs between 500 K and 800 K. The maximum weight loss and the greatest decrease in bulk density occur between 600 K and 800 K.

Between 800 K and 1100 K carbonization of the material is indicated by a significant increase in thermal conductivity and true density. Heat capacity also increases appreciably in this temperature range. Between 1100 K and 1740 K the thermal conductivity continues to increase, although above 1365 K the increase is not as rapid. Above 1100 K the true density values are fairly constant and the heat capacity values decrease to a constant value

between 1100 K and 1365 K. Although carbonization is apparent, X-ray diffraction analyses showed that the charring temperatures used in this program did not produce any ordered carbon.

The permeability values, although not precise, should serve as an order-of-magnitude estimate of the values for the degrading system.

The variation in behavior and properties between Material A and B are mainly due to the influence that the honeycomb reinforcement has on the elastomeric composite. The thermal conductivities are higher in Material A, virgin and char, due to the continuous conduction path provided by the honeycomb wall. The heat capacities were similar with Material A being slightly higher in the virgin state. The strengths were higher for the virgin Material A again due to the continuous reinforcement provided by the honeycomb structure.

The structures of the two materials in the charred states were physically different due to the influence of the honeycomb reinforcement. The rigid honeycomb and shrinking elastomeric composite in Material A allowed gross separations and cracks to develop, which obviously increased the permeability porosity and effective thermal conductivity (radiant shine through) over that of the more homogeneous structure of Material B. A crust formed on both materials but the crust on Material A seemed firmer and was well supported by the honeycomb structure. The mechanical integrity of the charred Material A seemed better due to the firmer crust and honeycomb confinement.

ACKNOWLEDGMENTS

The mechanical property evaluations under this program were conducted by Austin Bush, Associate Engineer in the Applied Mechanics Section. Andre P. Wooten, Technical Specialist in the Applied Thermal Section was responsible for much of the specimen coordination and experimental work. Coordination of the program and the remaining evaluations was performed by Ronald Robertson, Associate Engineer in the Applied Thermal Section.

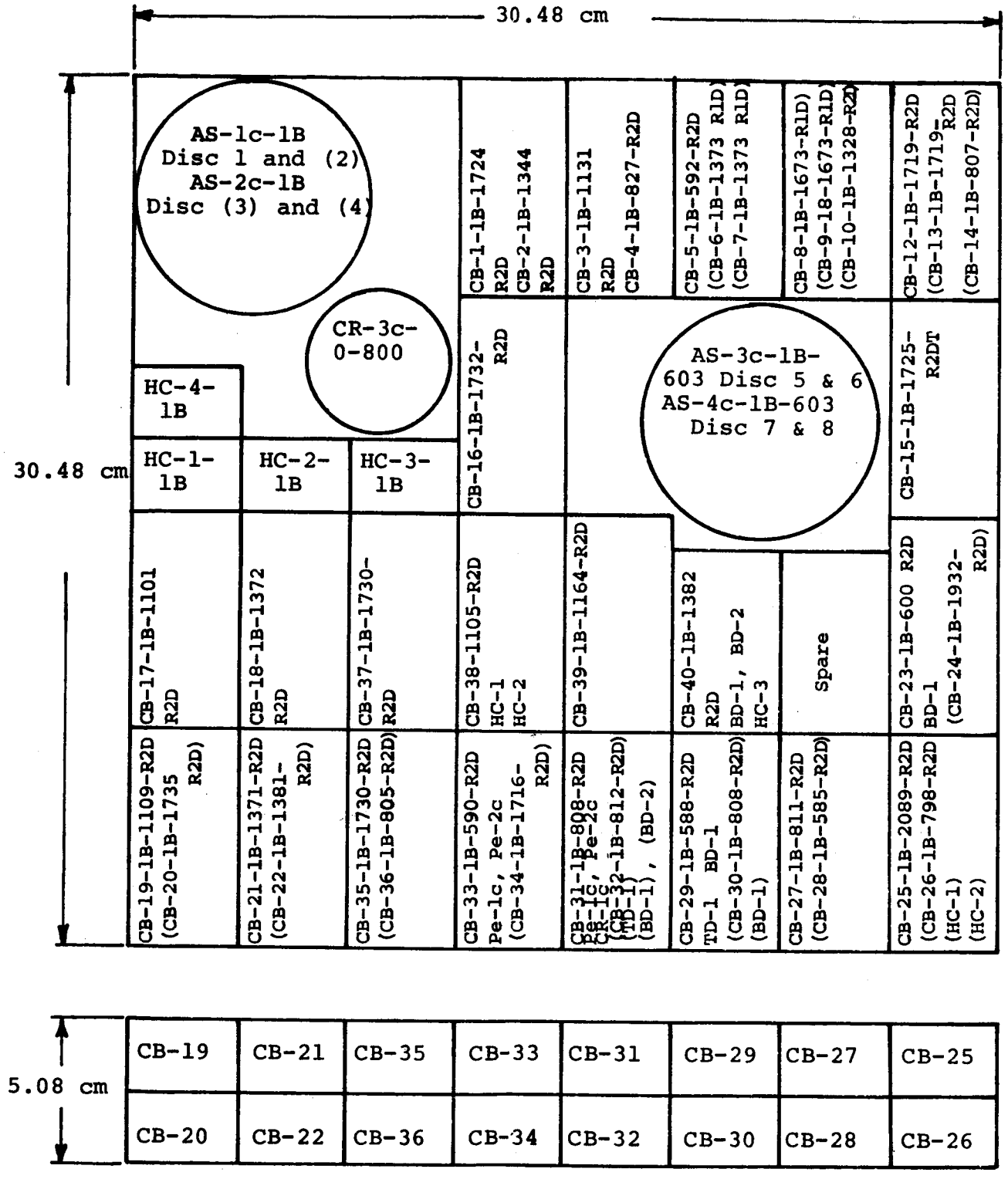

Note: Numbers in () are specimens removed from lower half of panel thickness.

Figure 1. Cutting Plan for Panel 1 of Material B

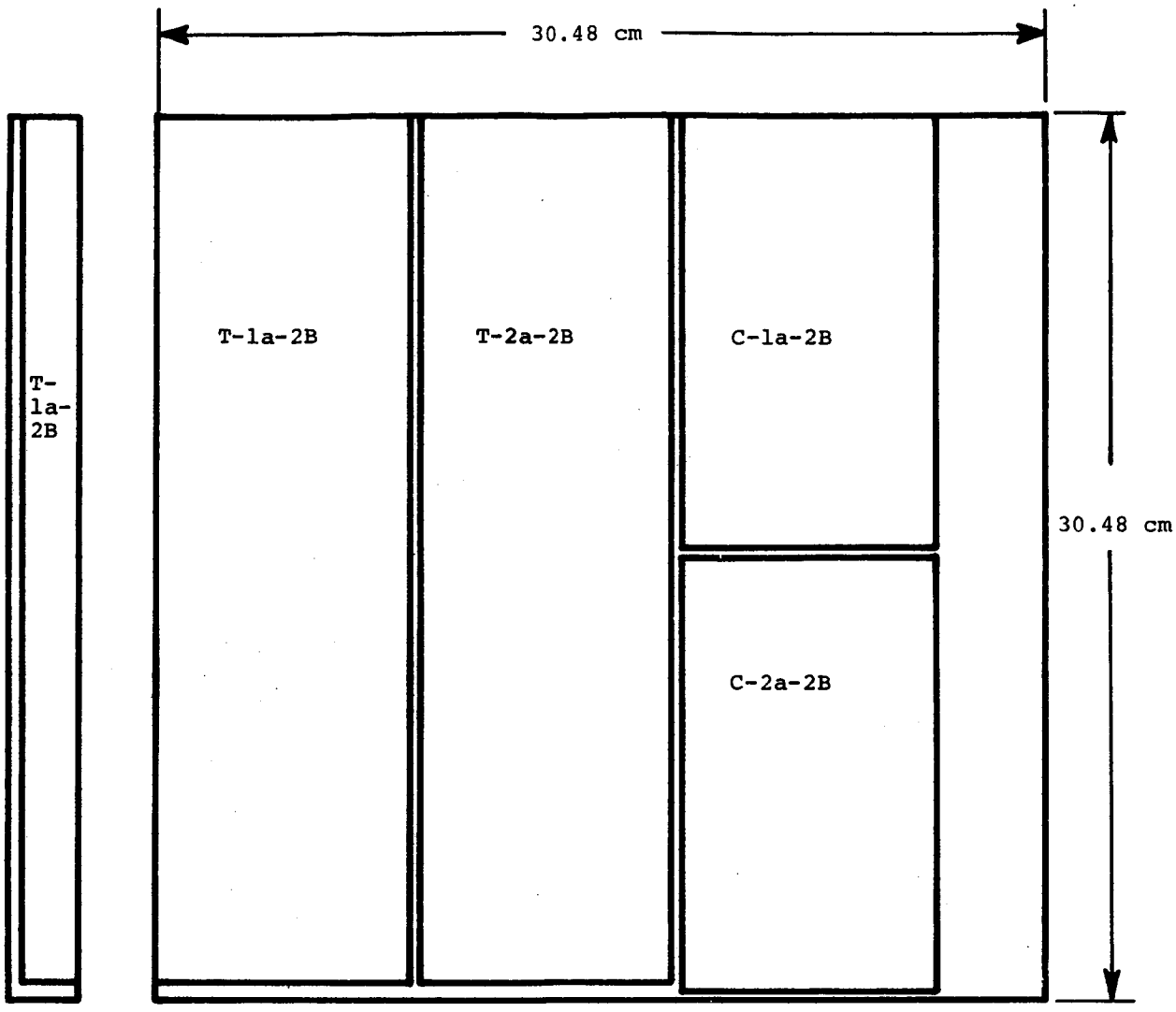

Figure 2. Cutting Plan for Top Half of Panel No. 2 of Material B

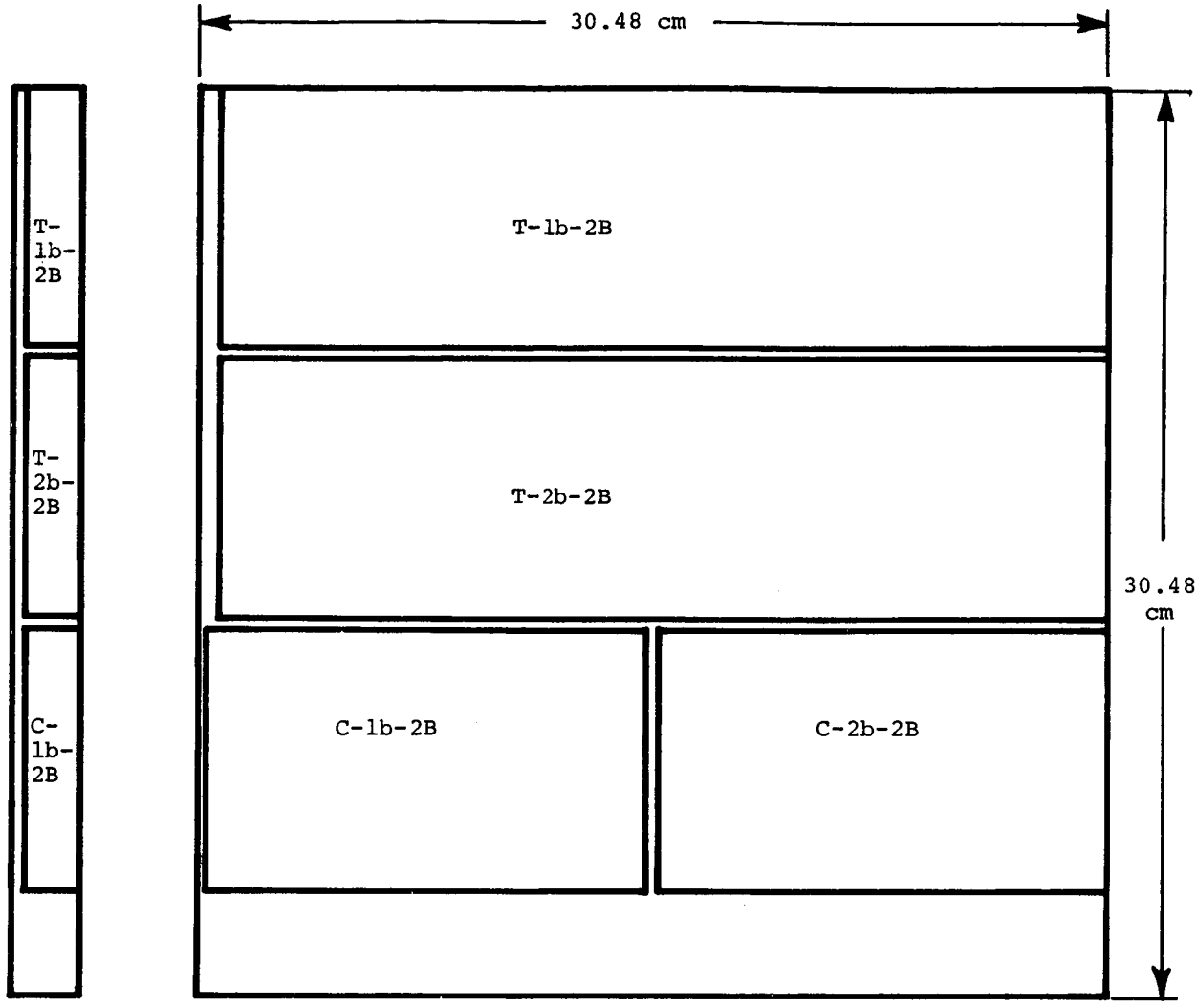

Figure 3. Cutting Plan for Bottom Half of Panel No. 2 of Material B

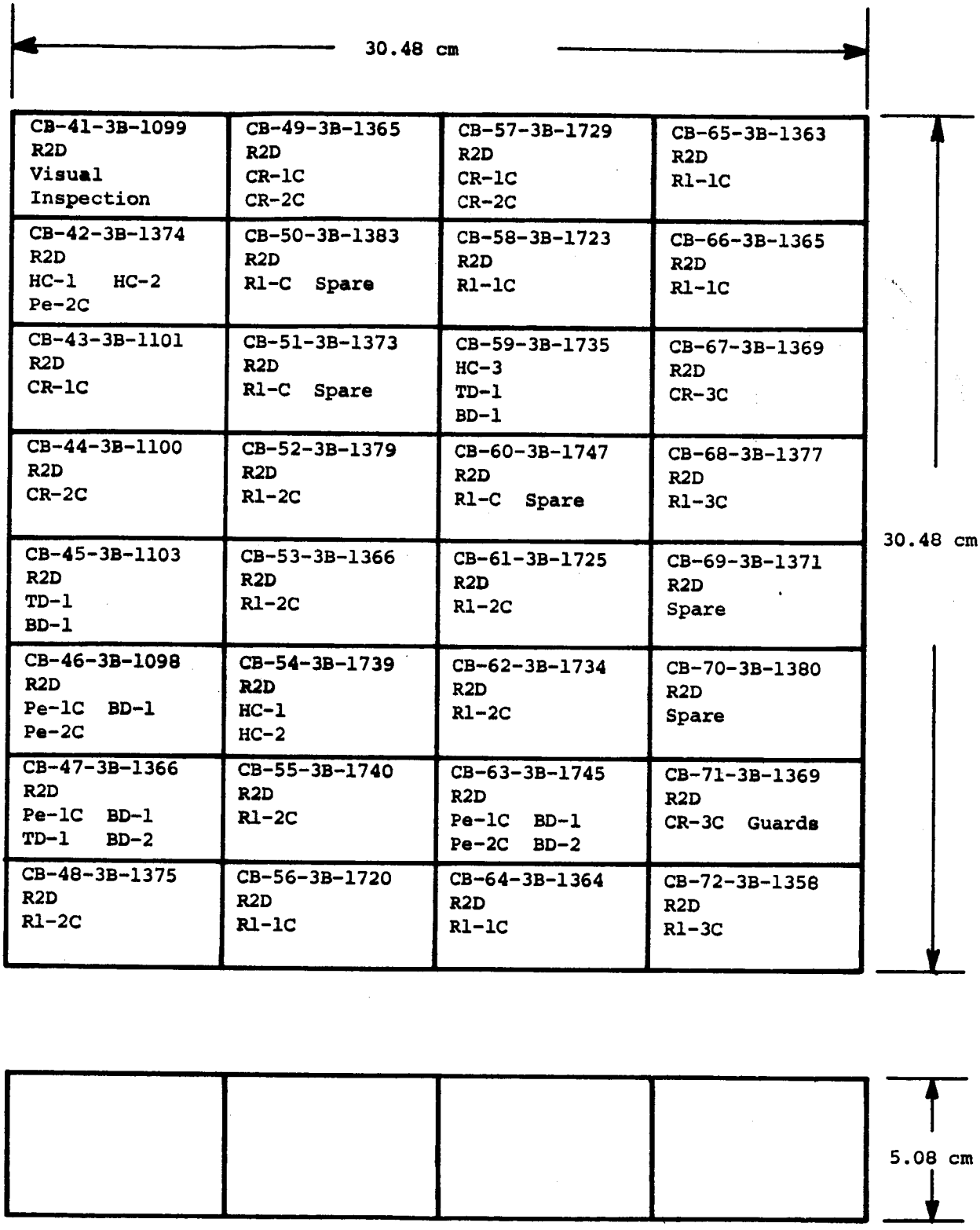

Figure 4. Cutting Plan for Panel 3 of Material B

Notes:

1. One specimen 3.81 cm wide x 7.62 cm long x 5.08 cm
2. Specimen is inserted in heater tube with 7.5 cm diameter
3. Temperature measured through sight port in furnace by sighting at center of specimen

Figure 5. Photograph of Specimen Holder for Preparing Char Samples Shown With Virgin Specimen Installed

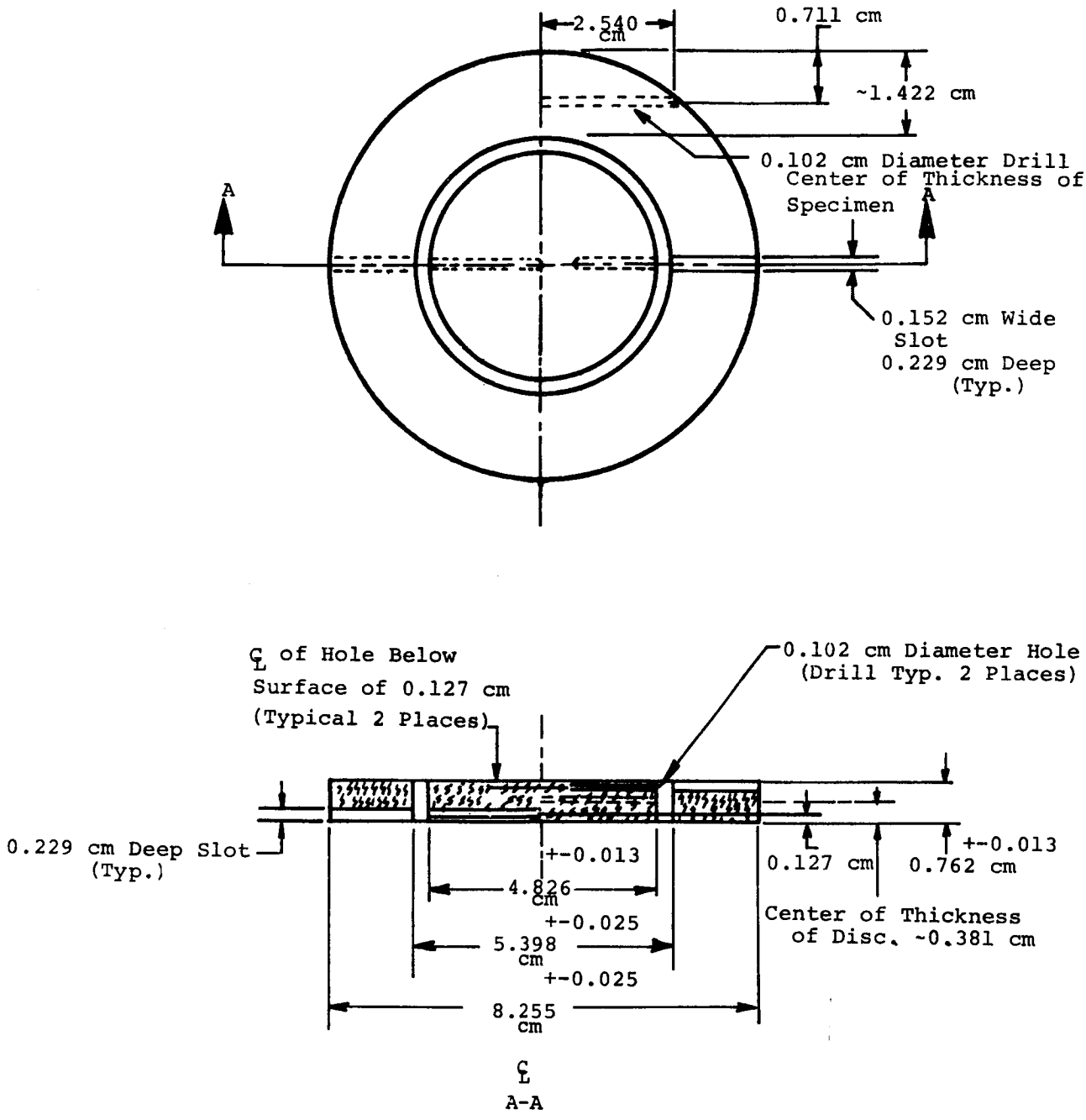

Figure 6. Thermal Conductivity Specimen for Guarded Hot Plate Apparatus

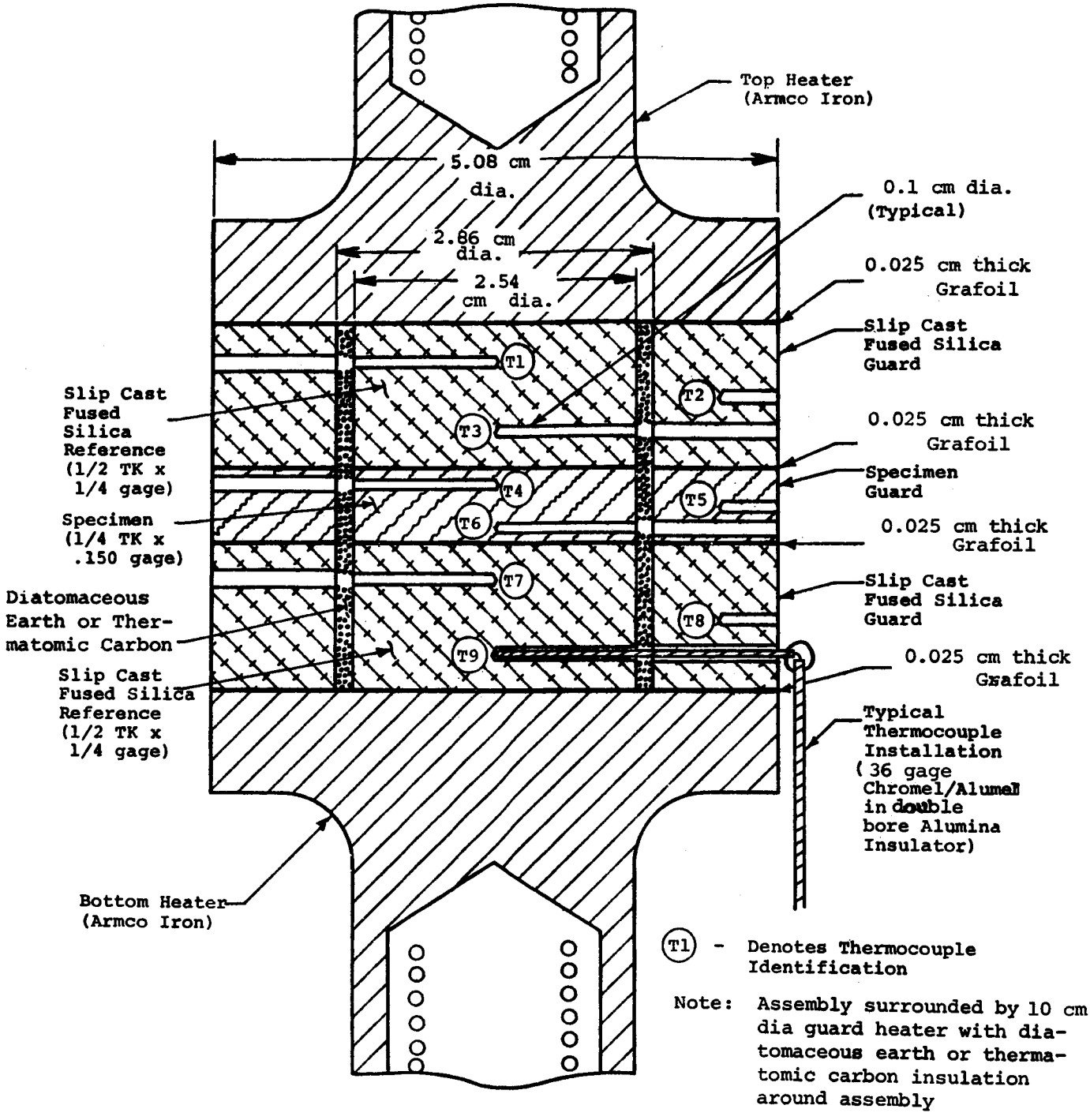

Figure 7. Assembly of Guarded Comparative Rod Apparatus

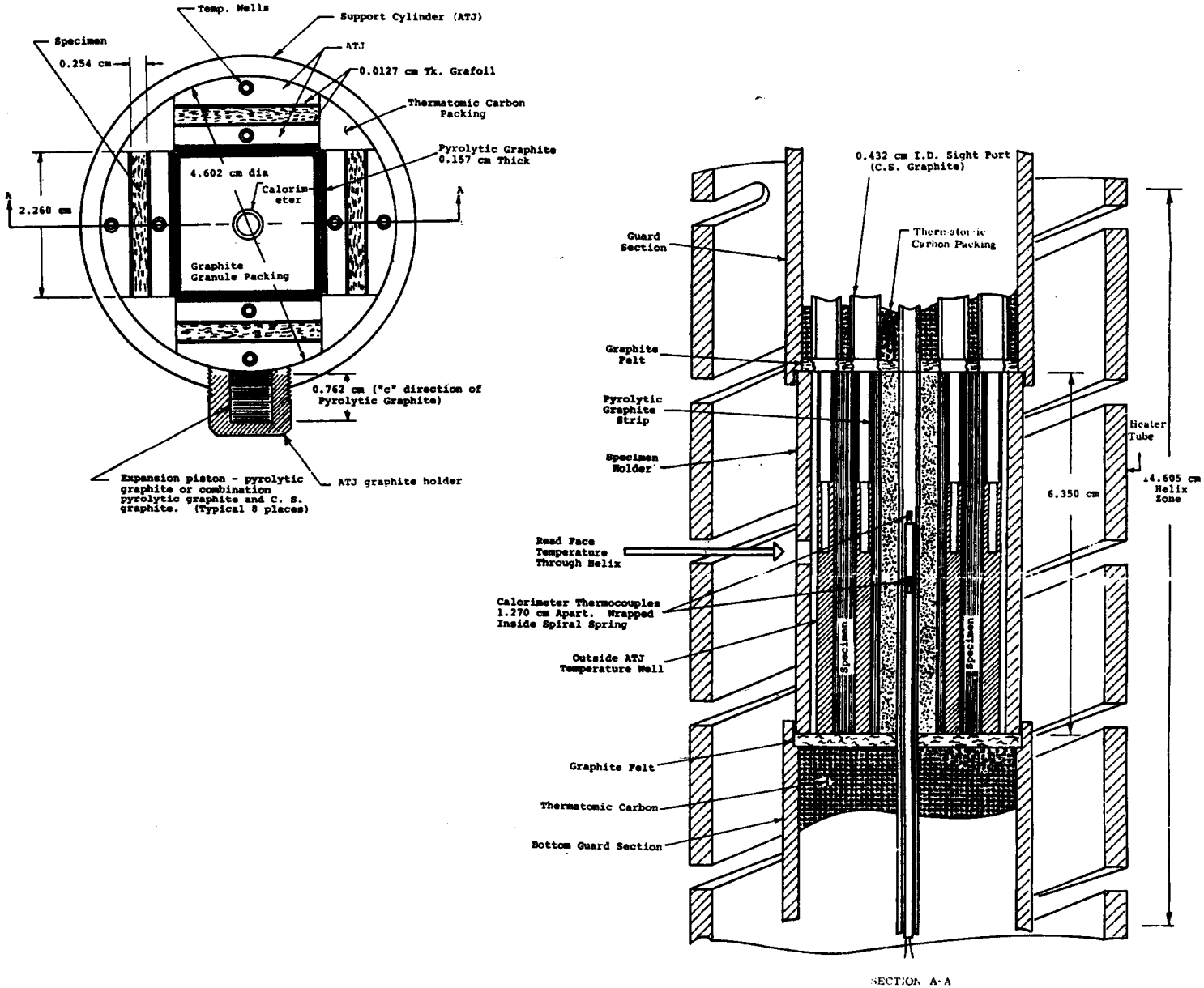

Figure 8. Schematic of Strip Specimen Configuration for Thermal Conductivity Measurements in Radial Inflow Apparatus

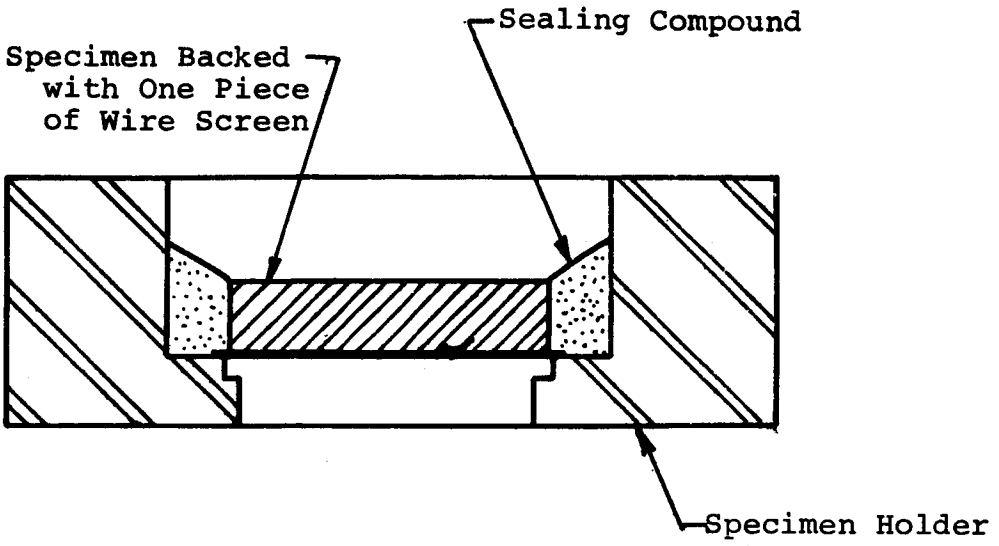

Figure 9. Typical Permeability Specimen Build-Up

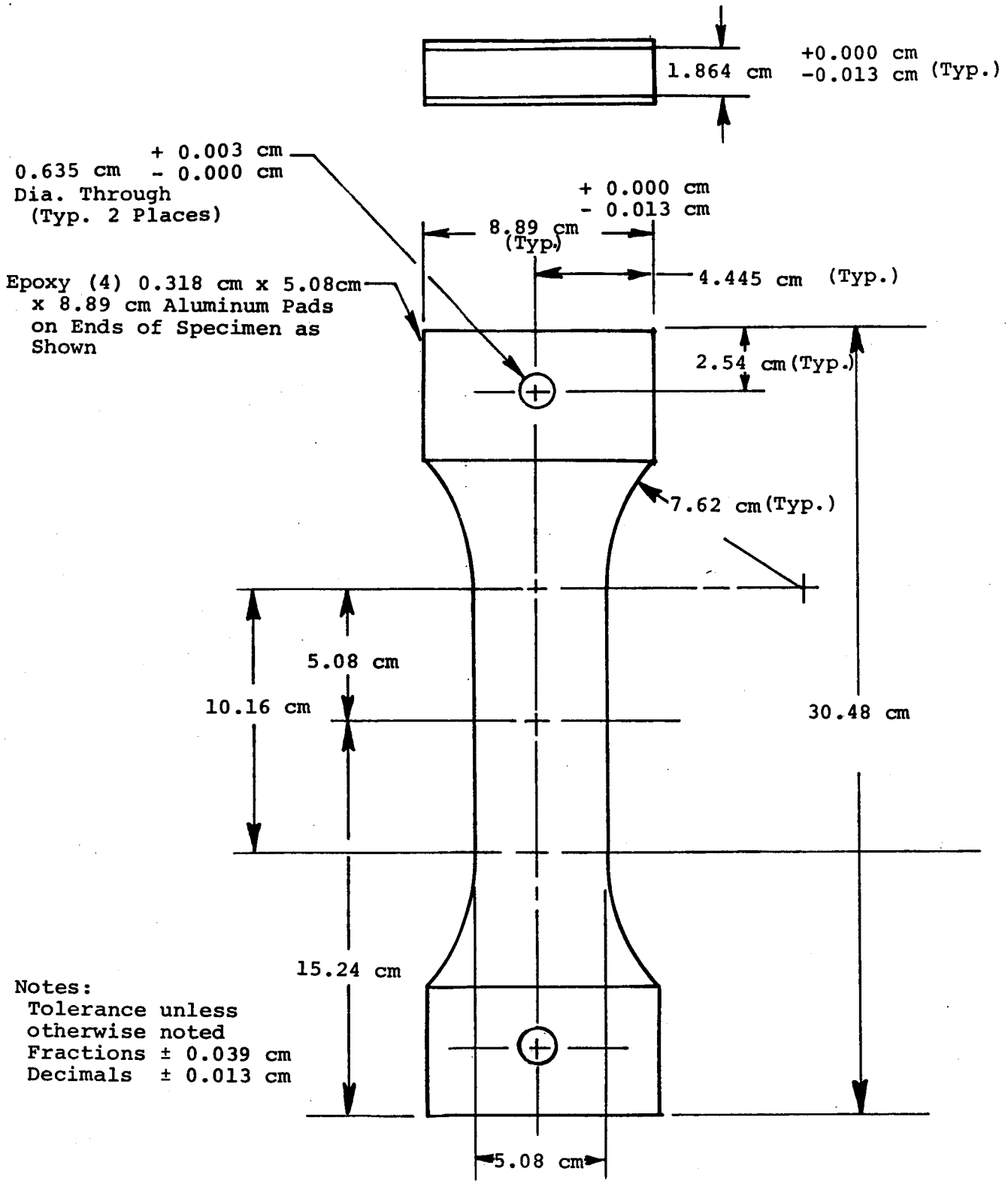

Figure 10. Tensile Specimen Configuration

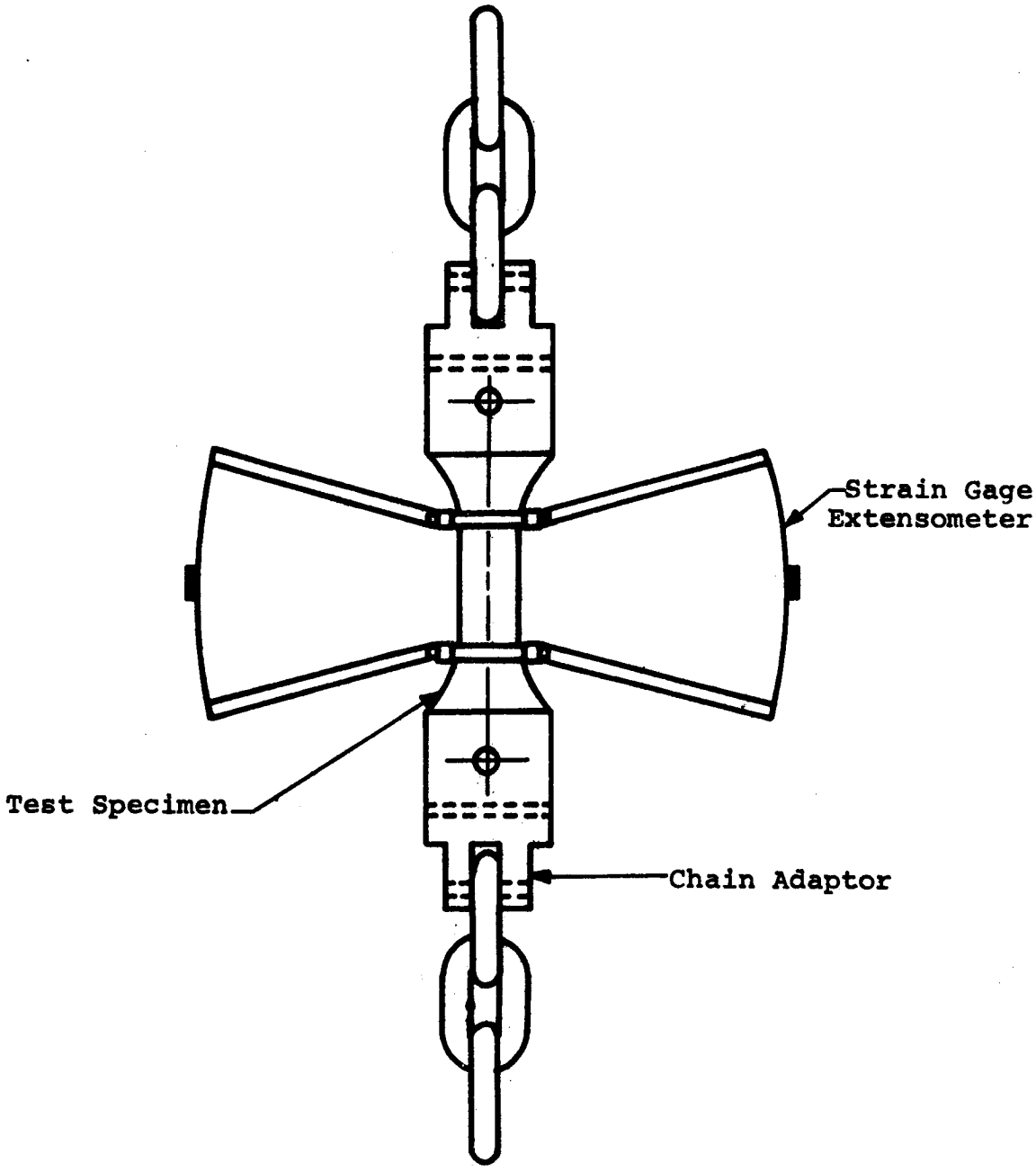

Figure 11. Schematic of Tensile Load Train Assembly.

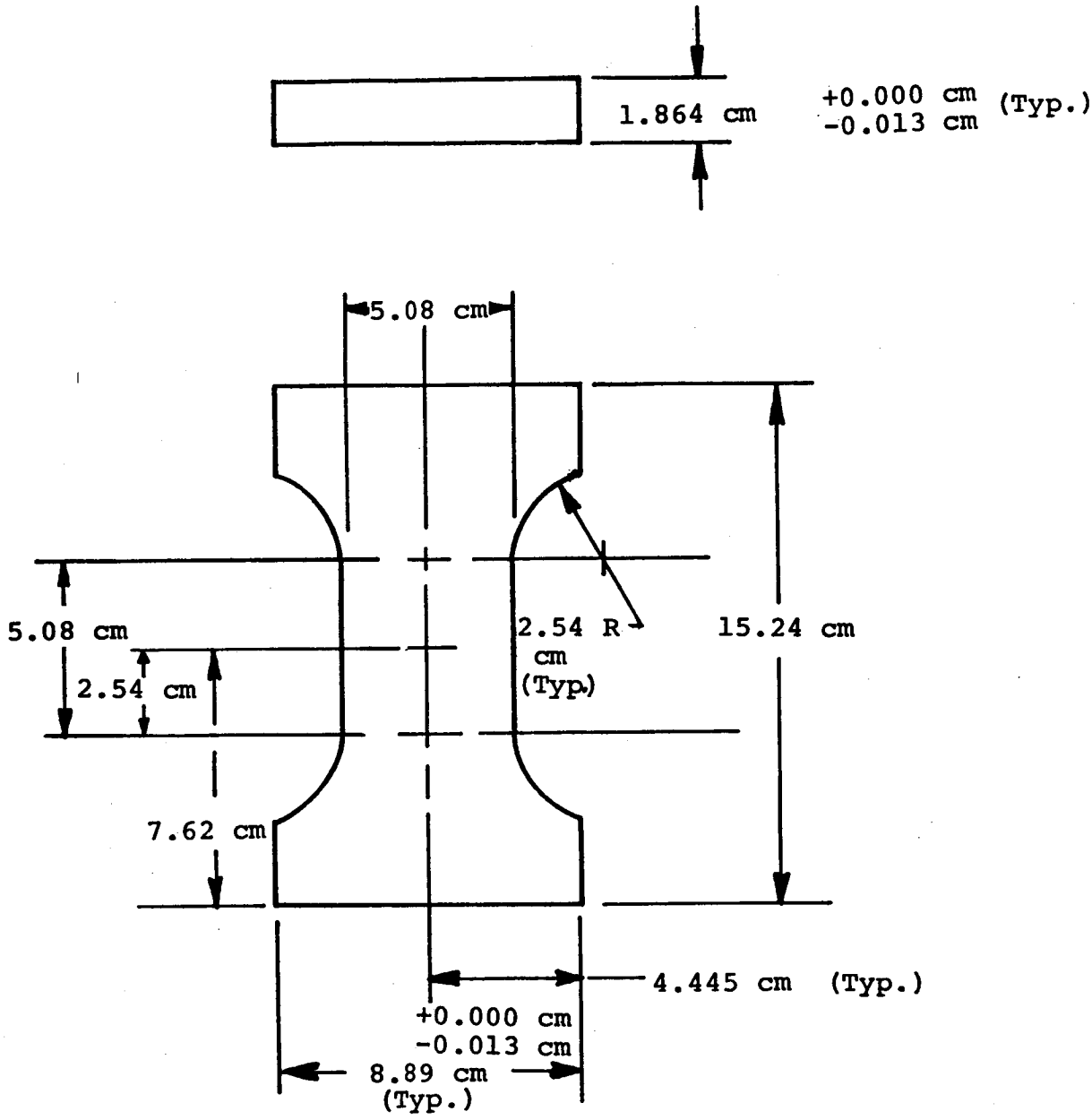

Notes:

1. Tolerances Unless Otherwise Noted
   Fractions ± 0.016 cm
   Decimals ± 0.013 cm

Figure 12. Compressive Specimen Configuration

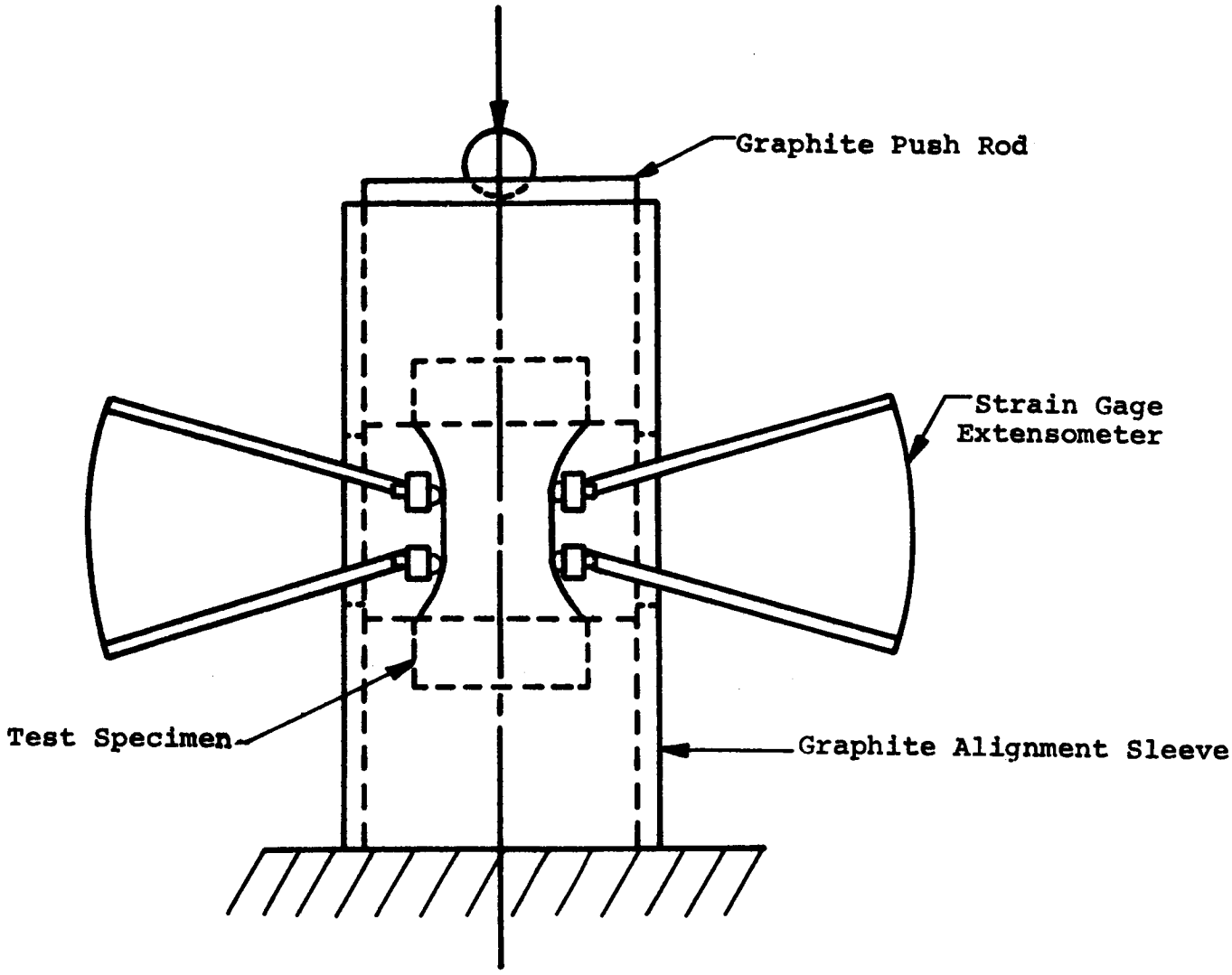

Figure 13. Schematic of Compressive Load Train Assembly

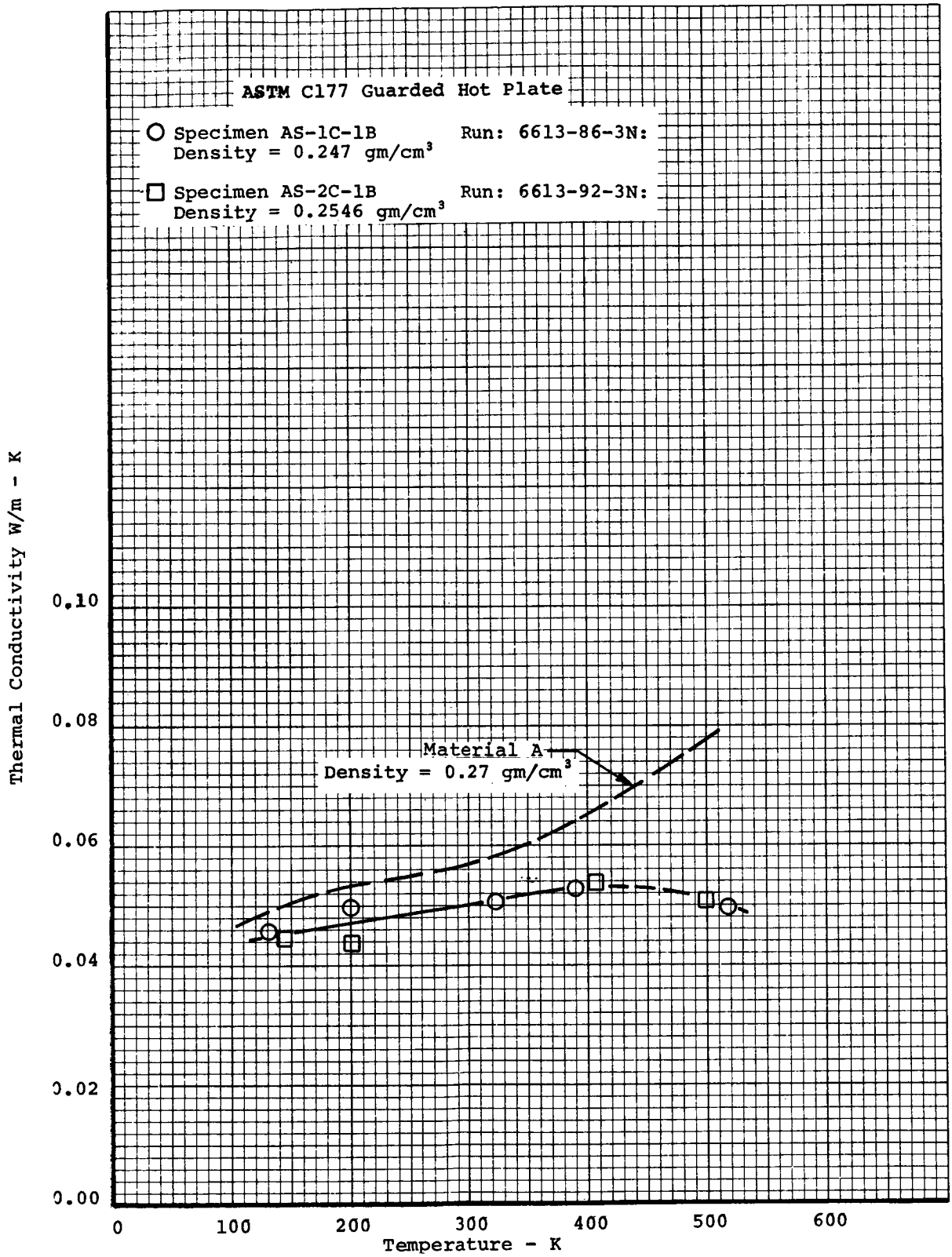

Figure 14. Thermal Conductivity of a Low-Density Elastomeric Ablation Material (Material B) in 1 Atmosphere of Dry Nitrogen.

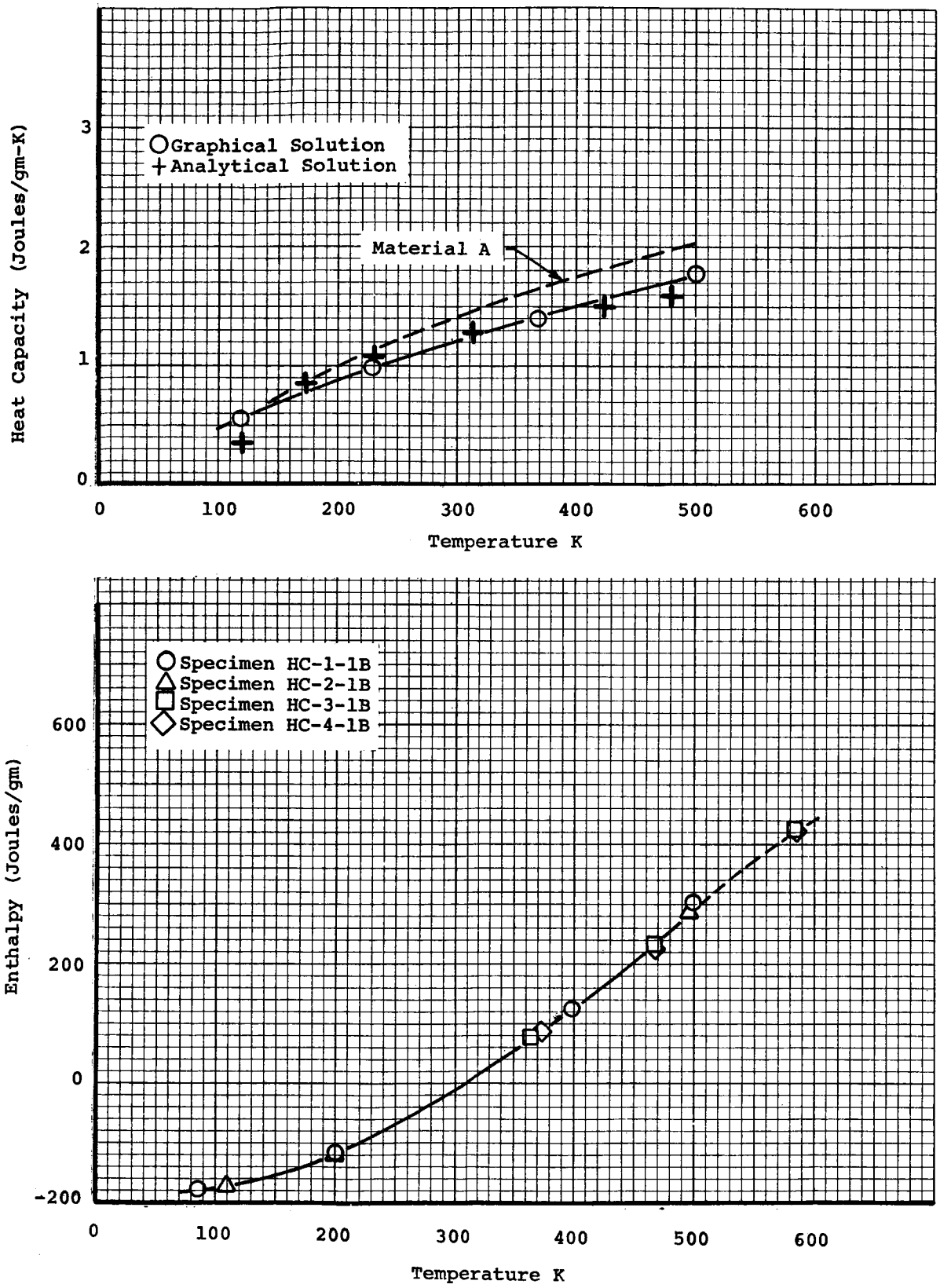

Figure 15. Enthalpy and Heat Capacity of a Low-Density Elastomeric Material (Material B)

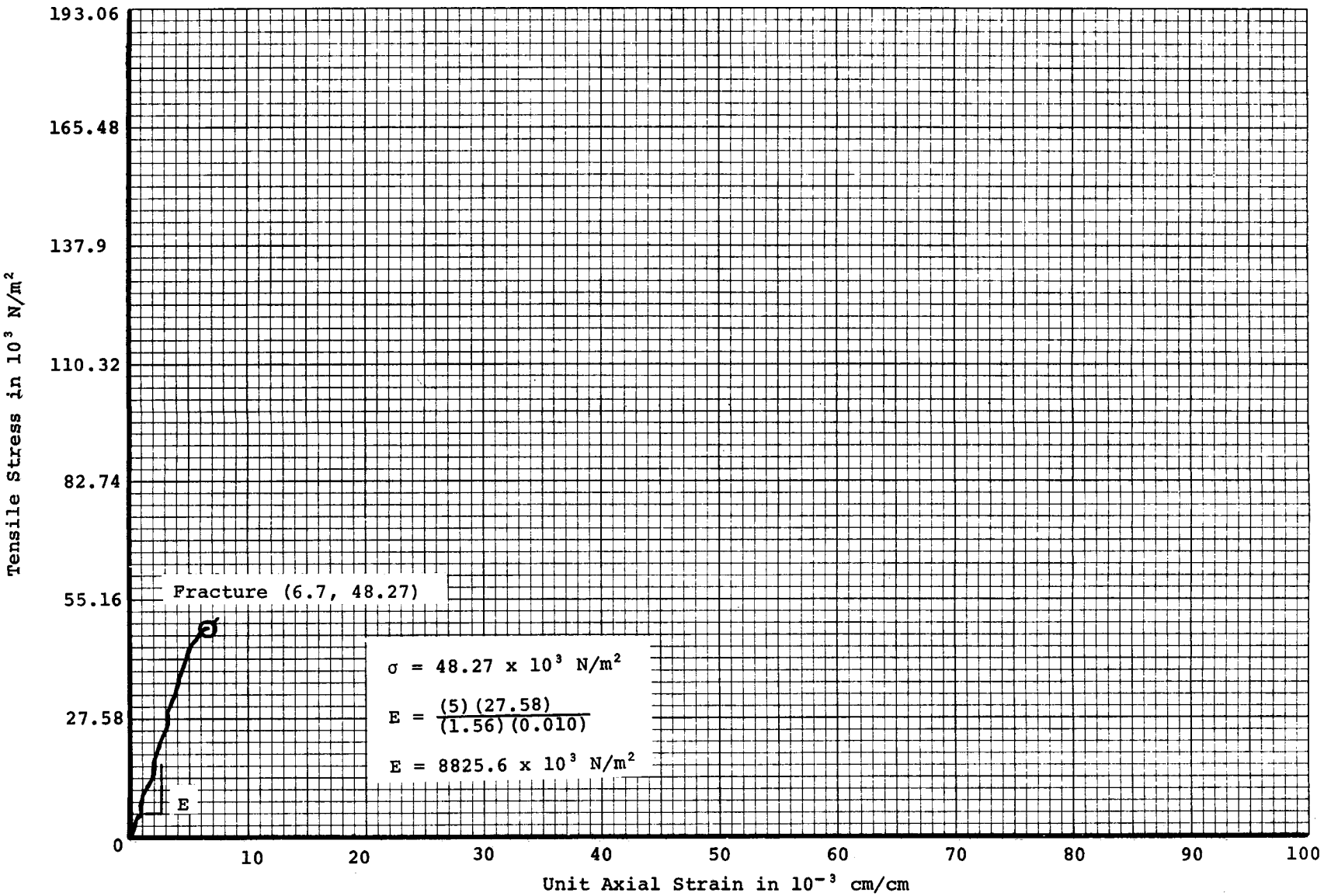

Figure 16. Tensile Stress versus Axial Strain for Specimen T-1a-2B

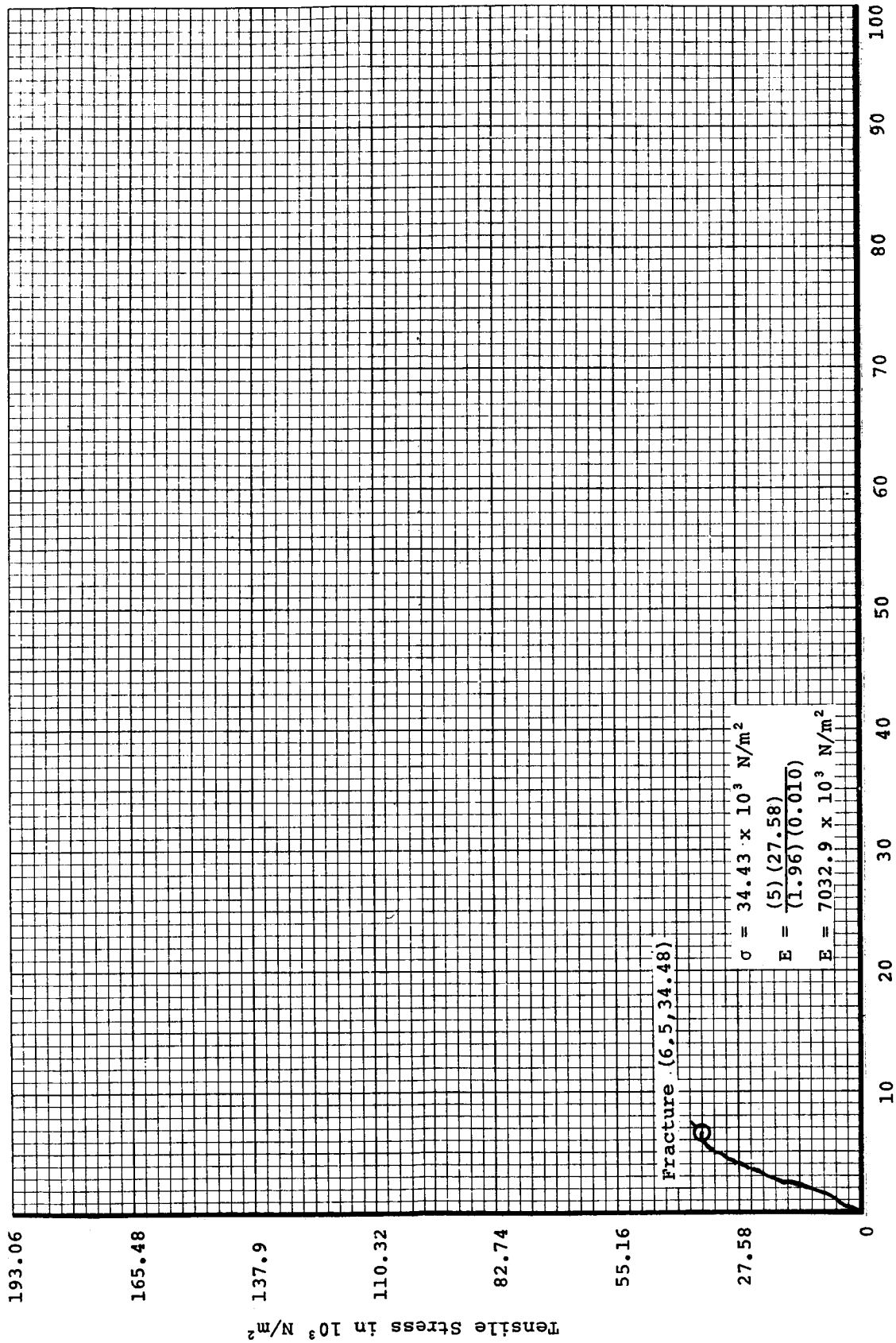

Figure 17. Tensile Stress versus Axial Strain for Specimen T-2a-2B

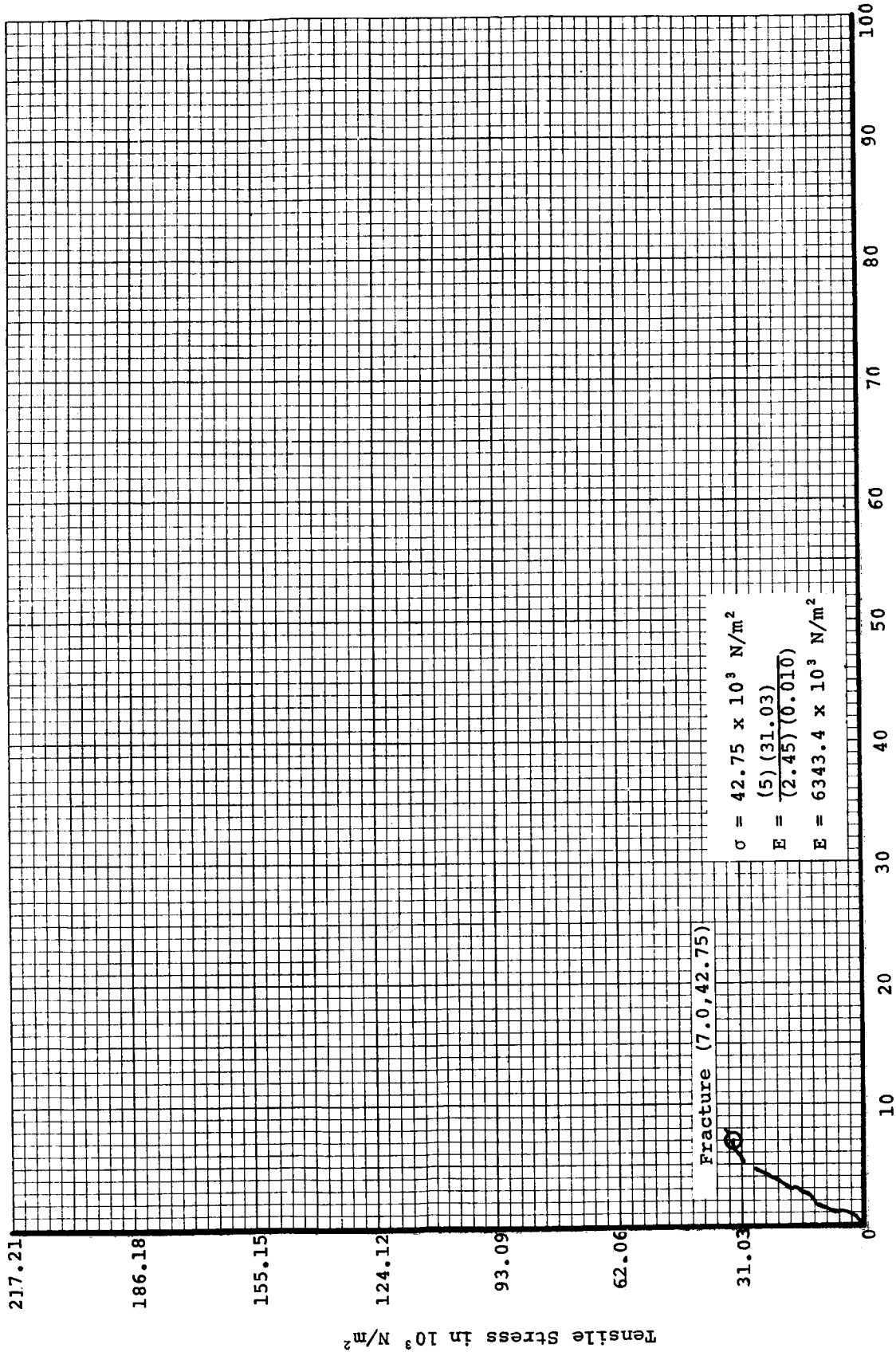

Figure 18. Tensile Stress versus Axial Strain for Specimen T-1b-2B

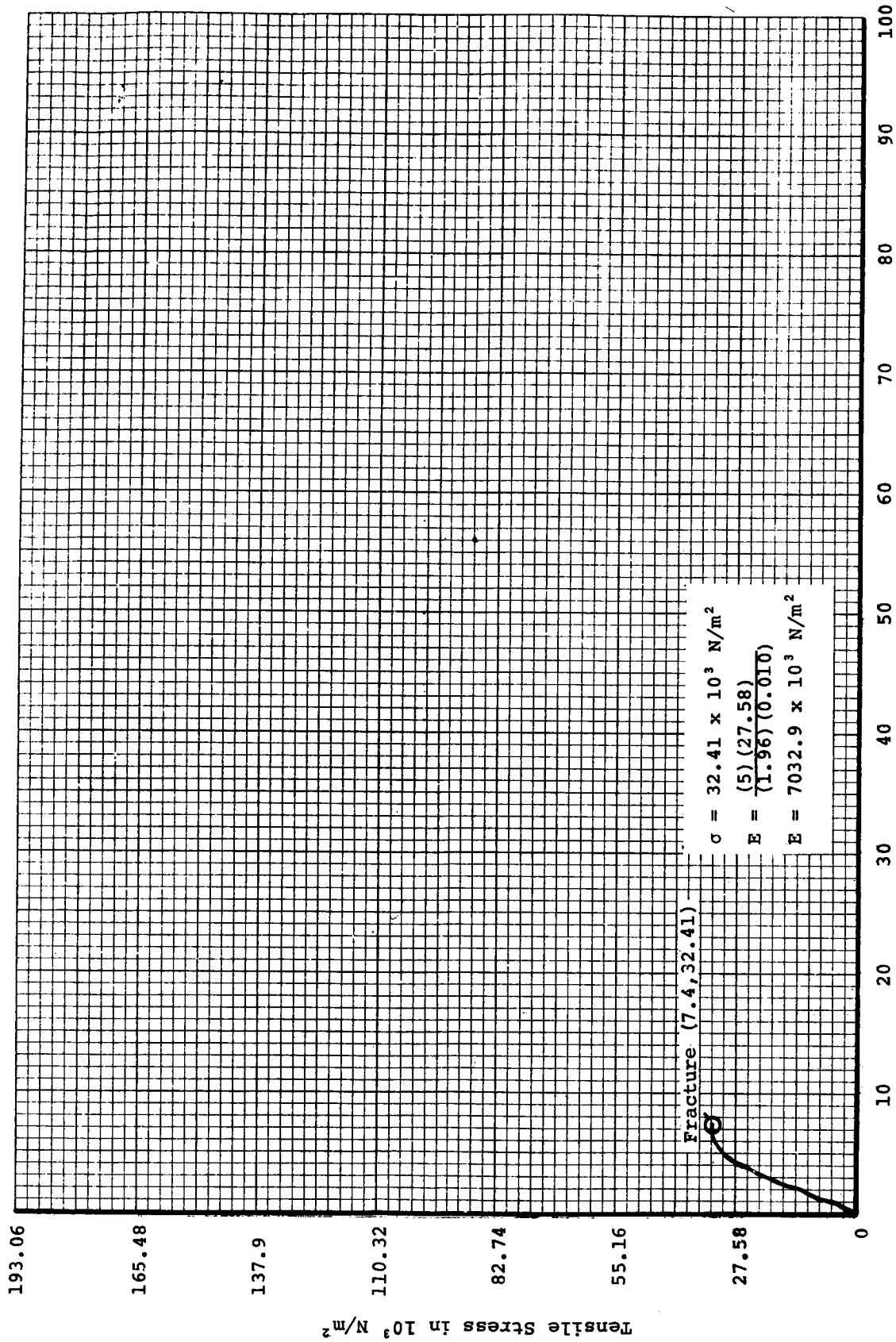

Figure 19. Tensile Stress versus Axial Strain for Specimen T-2b-2B

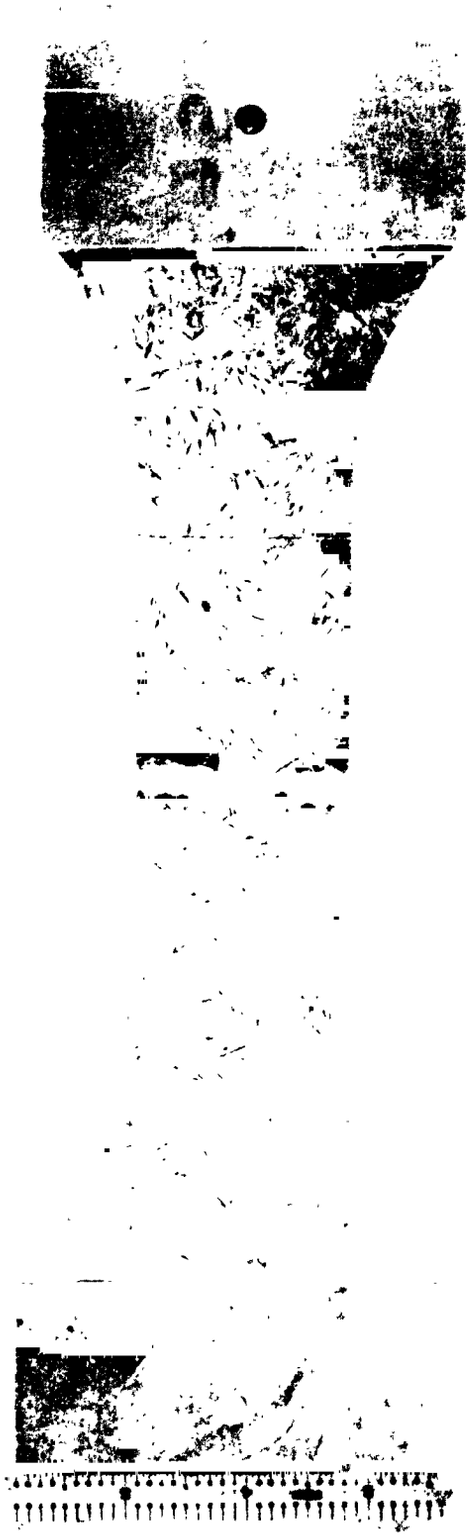

Figure 20. Typical Fracture for Tensile Specimen

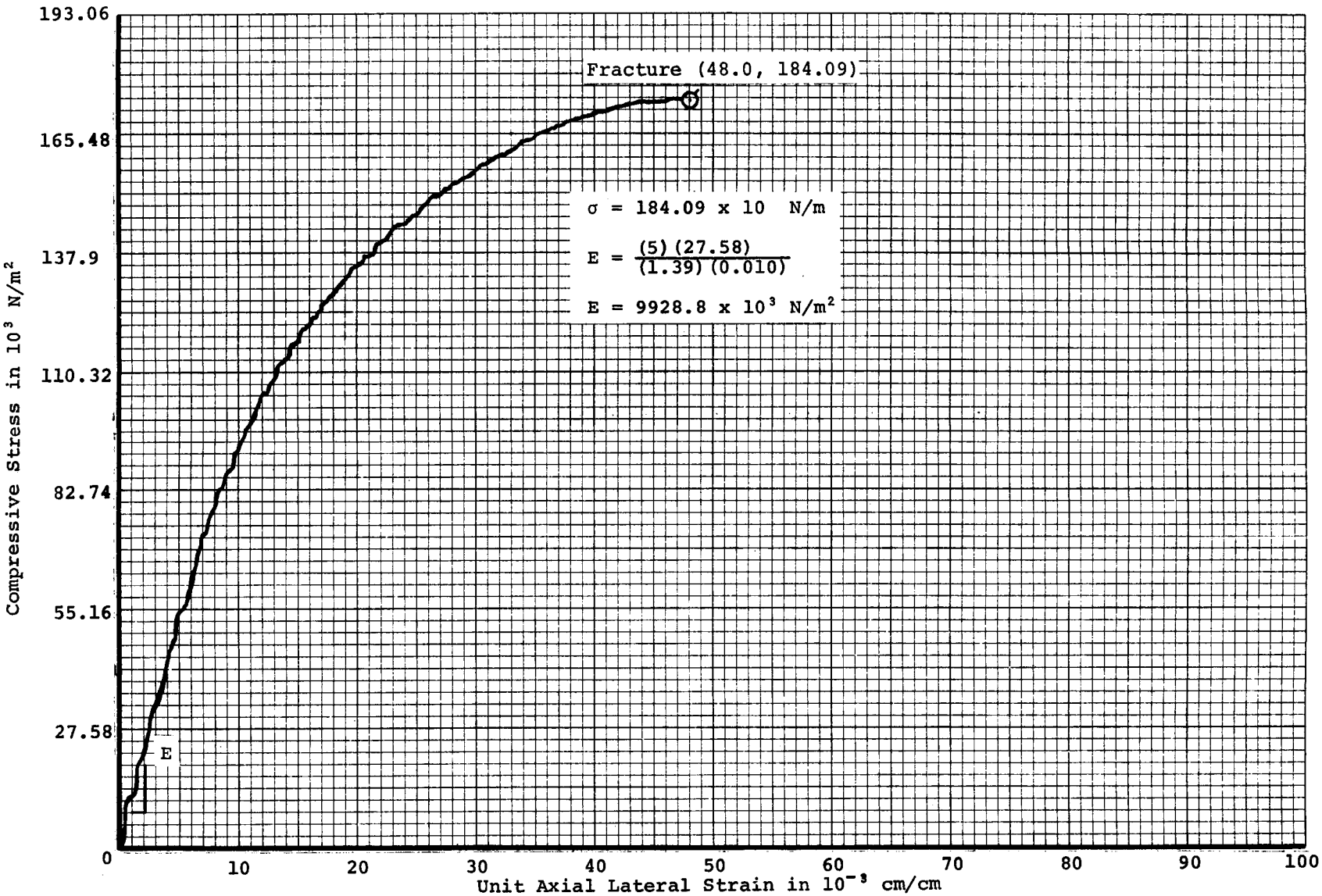

Figure 21. Compressive Stress versus Axial Strain for Specimen C-1a-2B

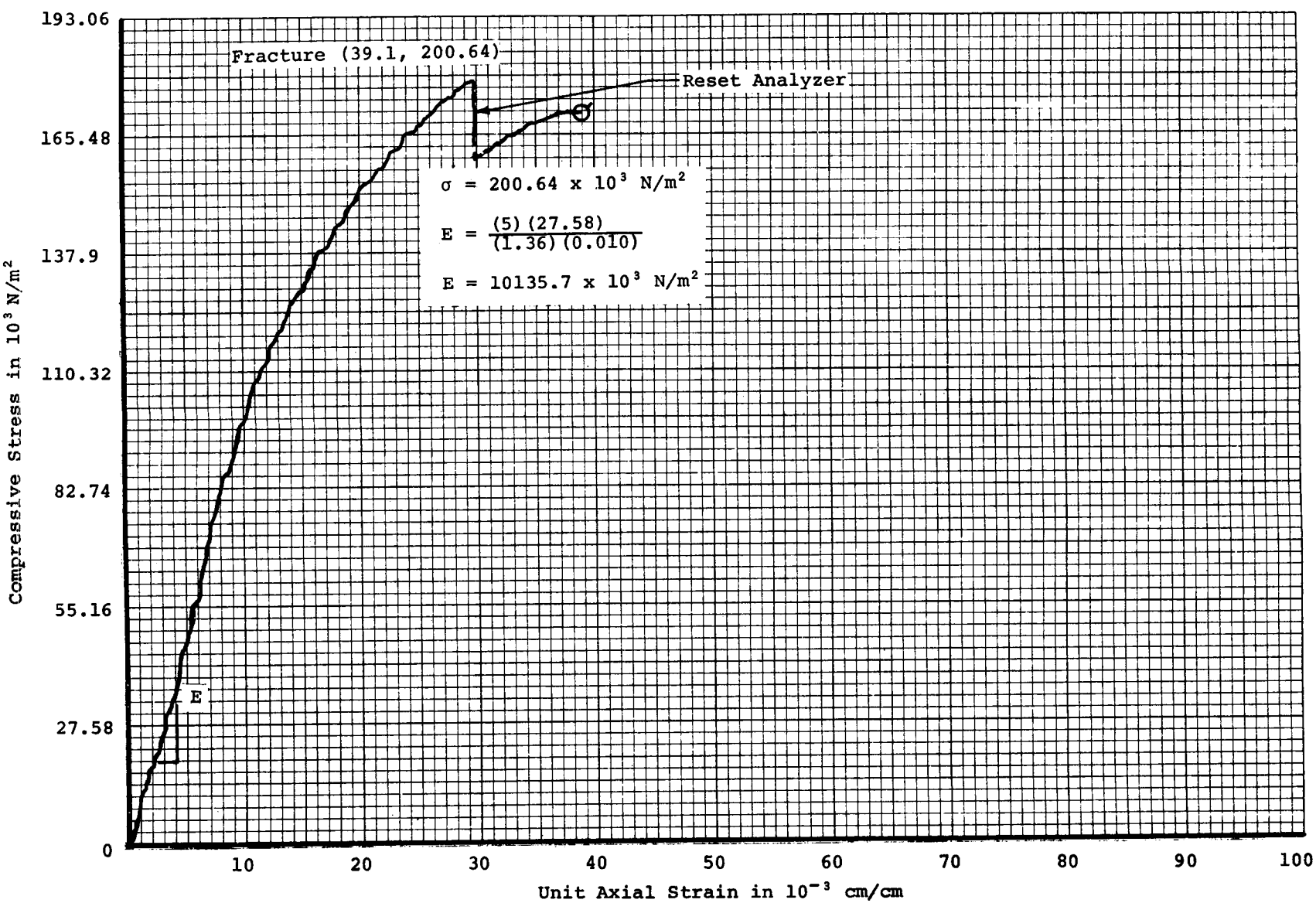

Figure 22. Compressive Stress versus Axial Strain for Specimen C-2a-2B

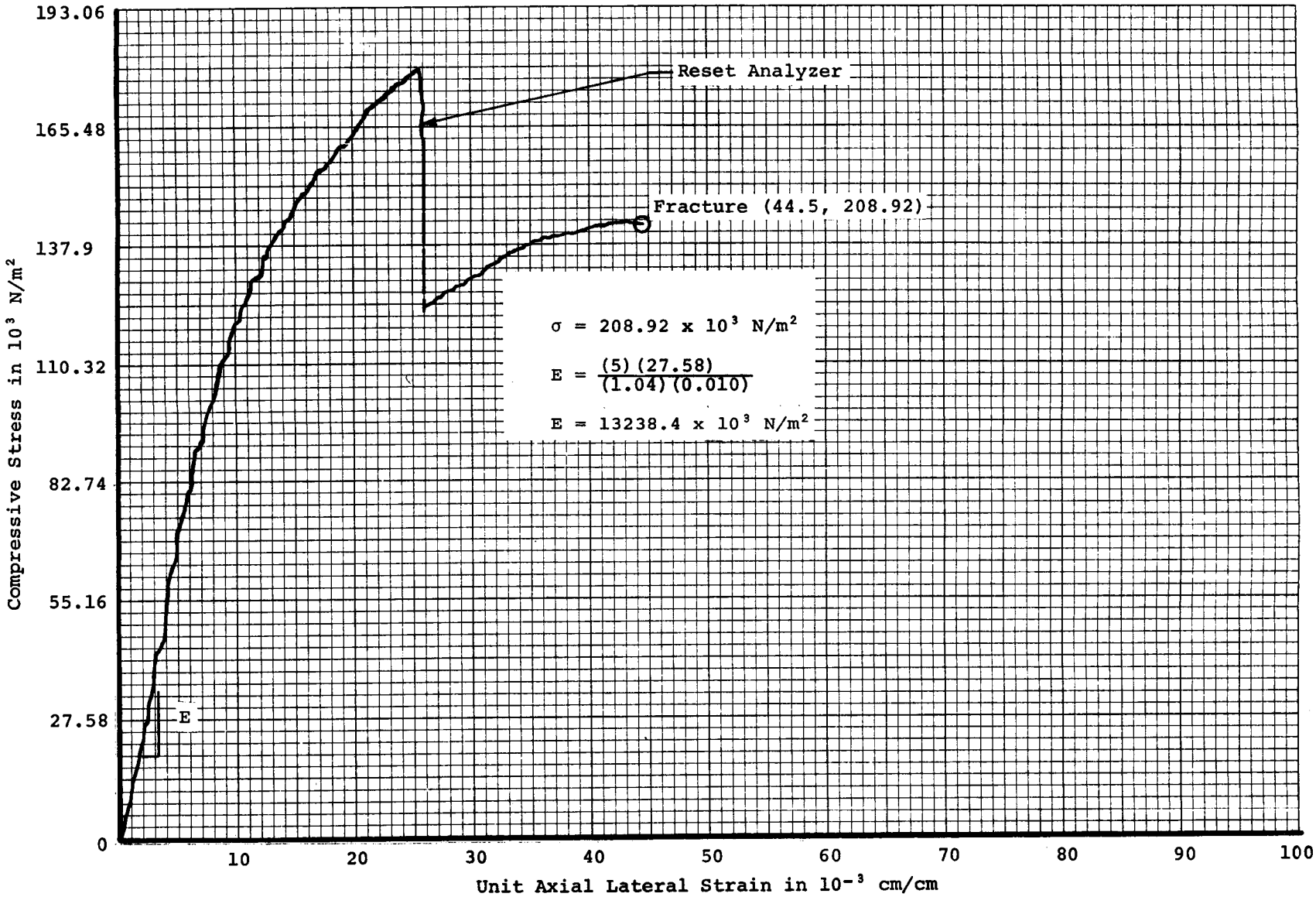

Figure 23. Compressive Stress versus Axial Strain for Specimen C-1b-2B

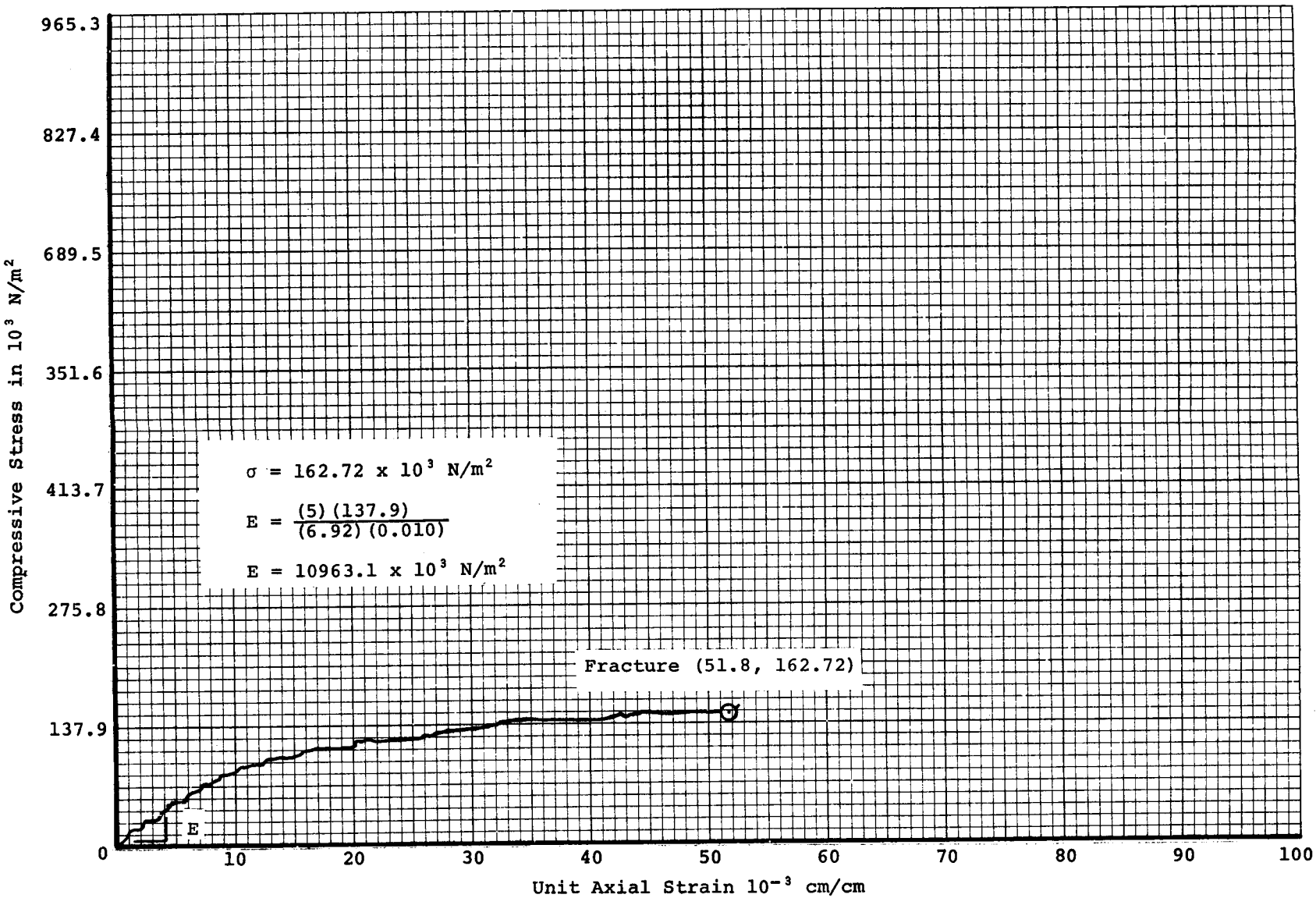

Figure 24. Compressive Stress versus Axial Strain for Specimen C-2b-2B

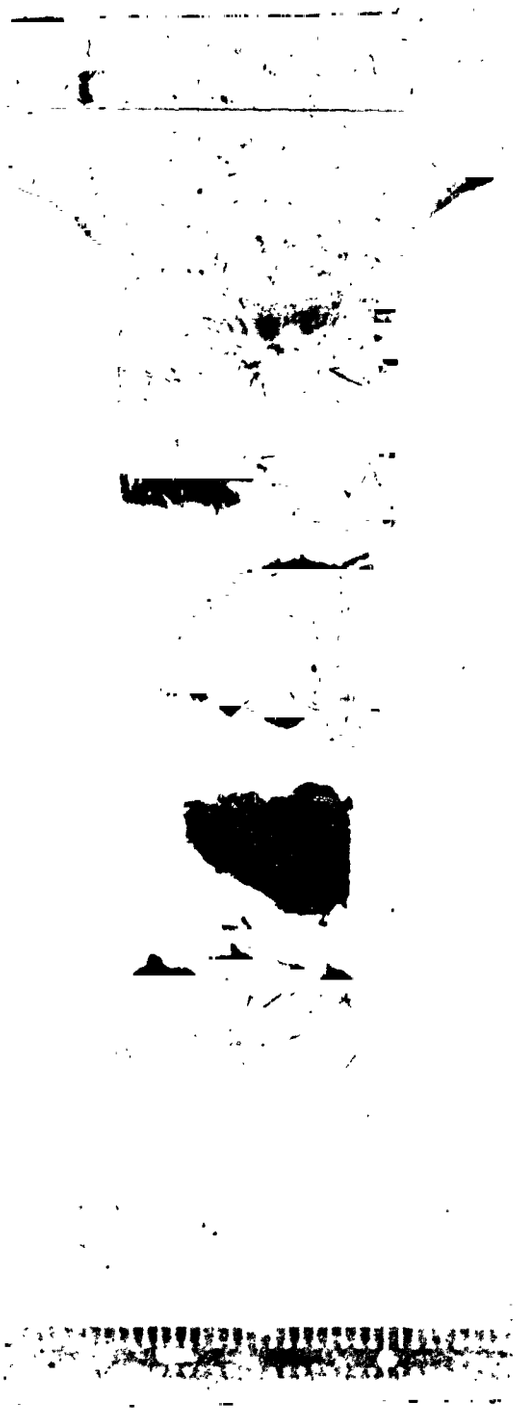

Figure 25. Typical Fracture for Compressive Specimen

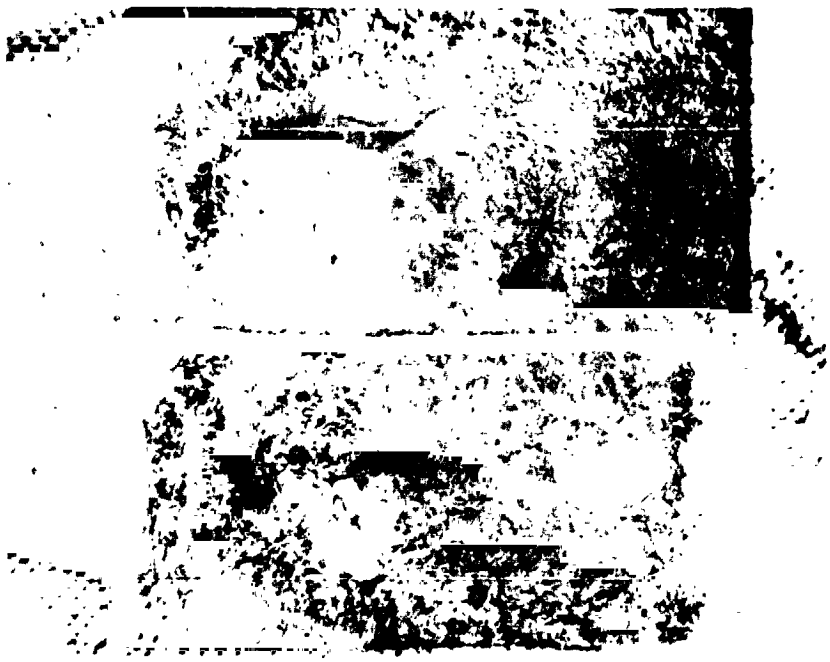

Sectioned
by NASA

Top View

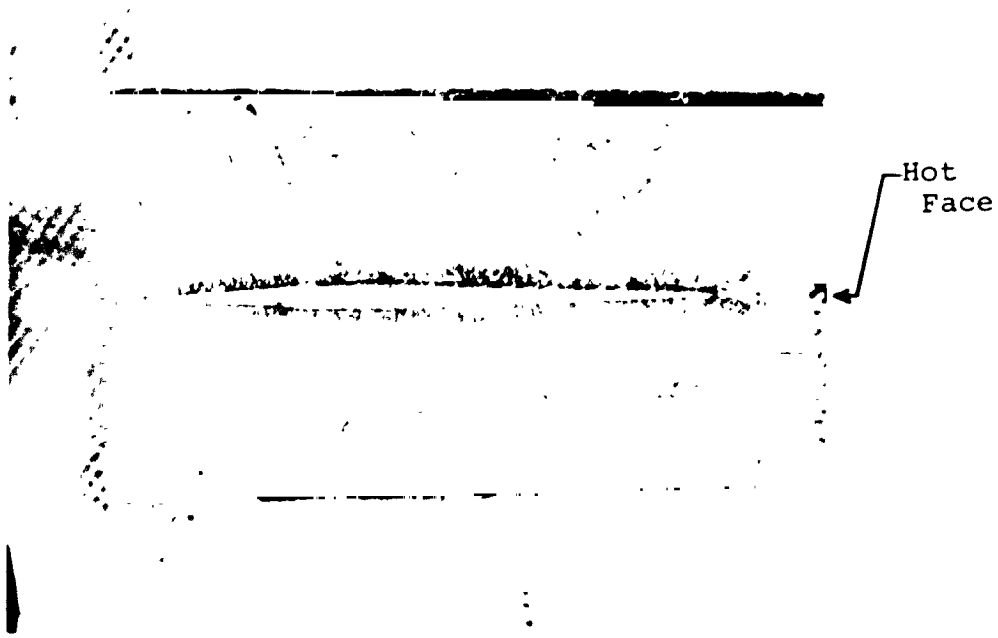

Side View

Figure 26. Photograph of Arc-Jet Char of Material B Prepared by NASA (Specimen 1)

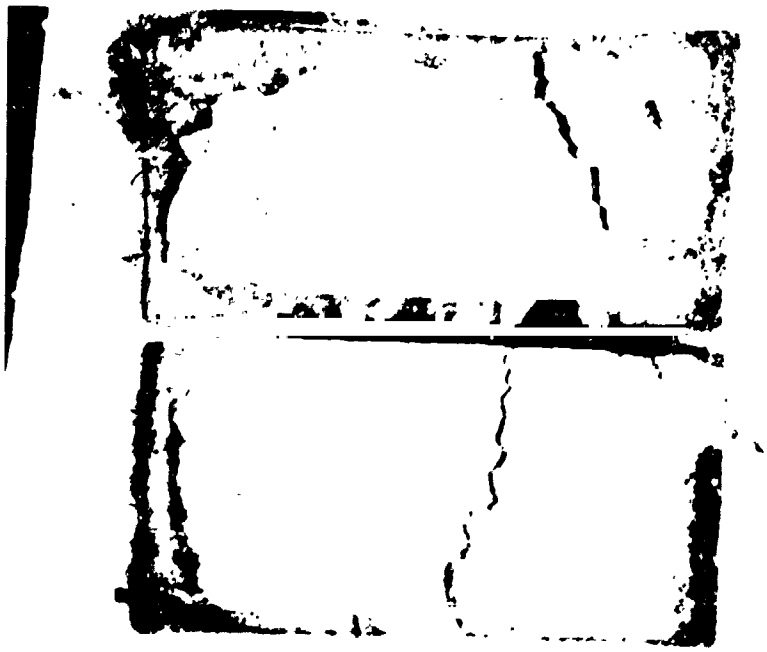

Sectioned by NASA

Top View

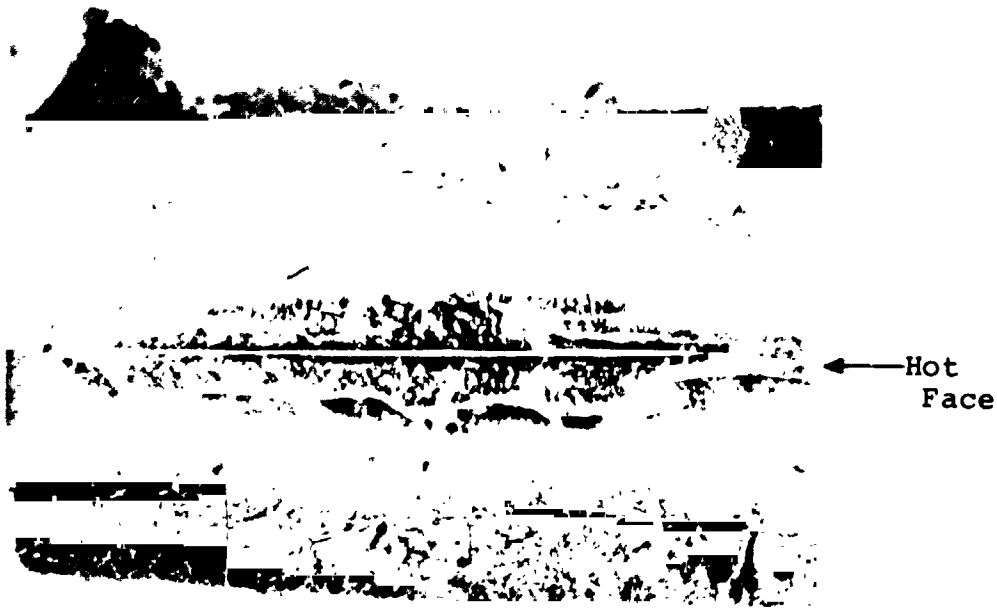

Side View

Figure 27. Photograph of Arc-Jet Char of Material B Prepared by NASA (Specimen 2)

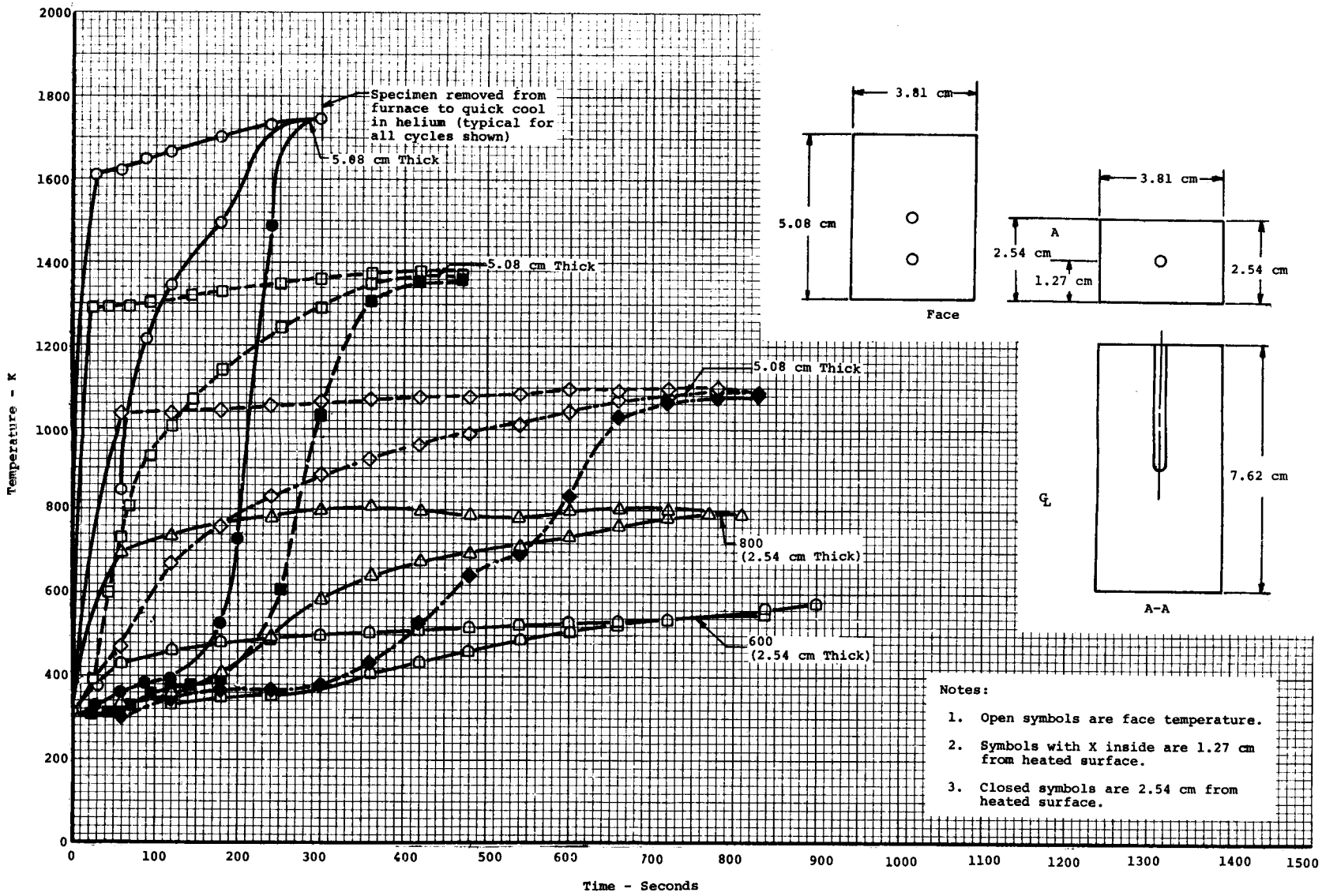

Figure 28. Typical Temperature versus Time Curves for Furnace Char Prepared by Rapid 2D Heating

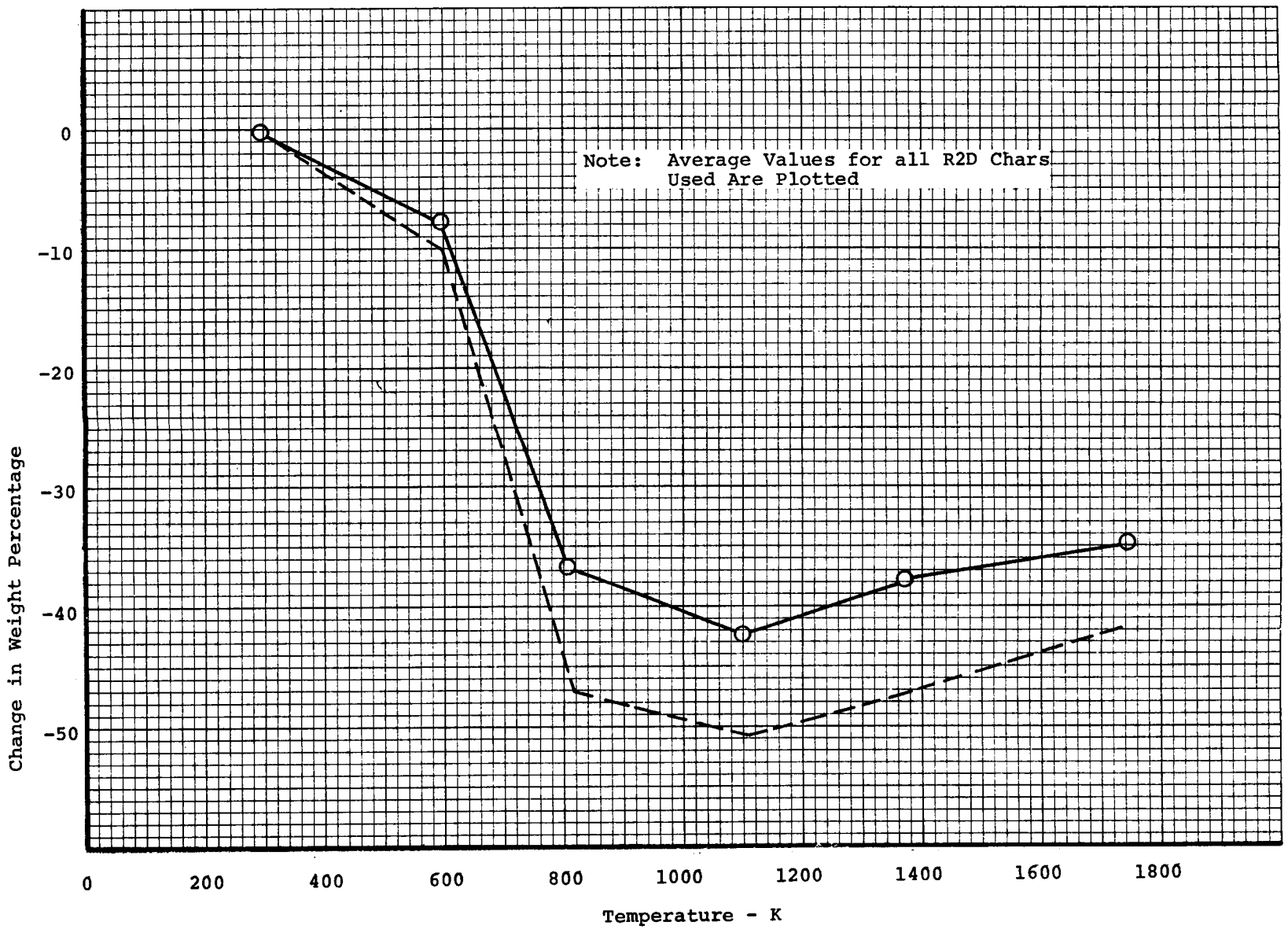

Figure 29. Effect of Char Temperature on Percentage Weight Loss for R2D Furnace Chars Prepared from Material B

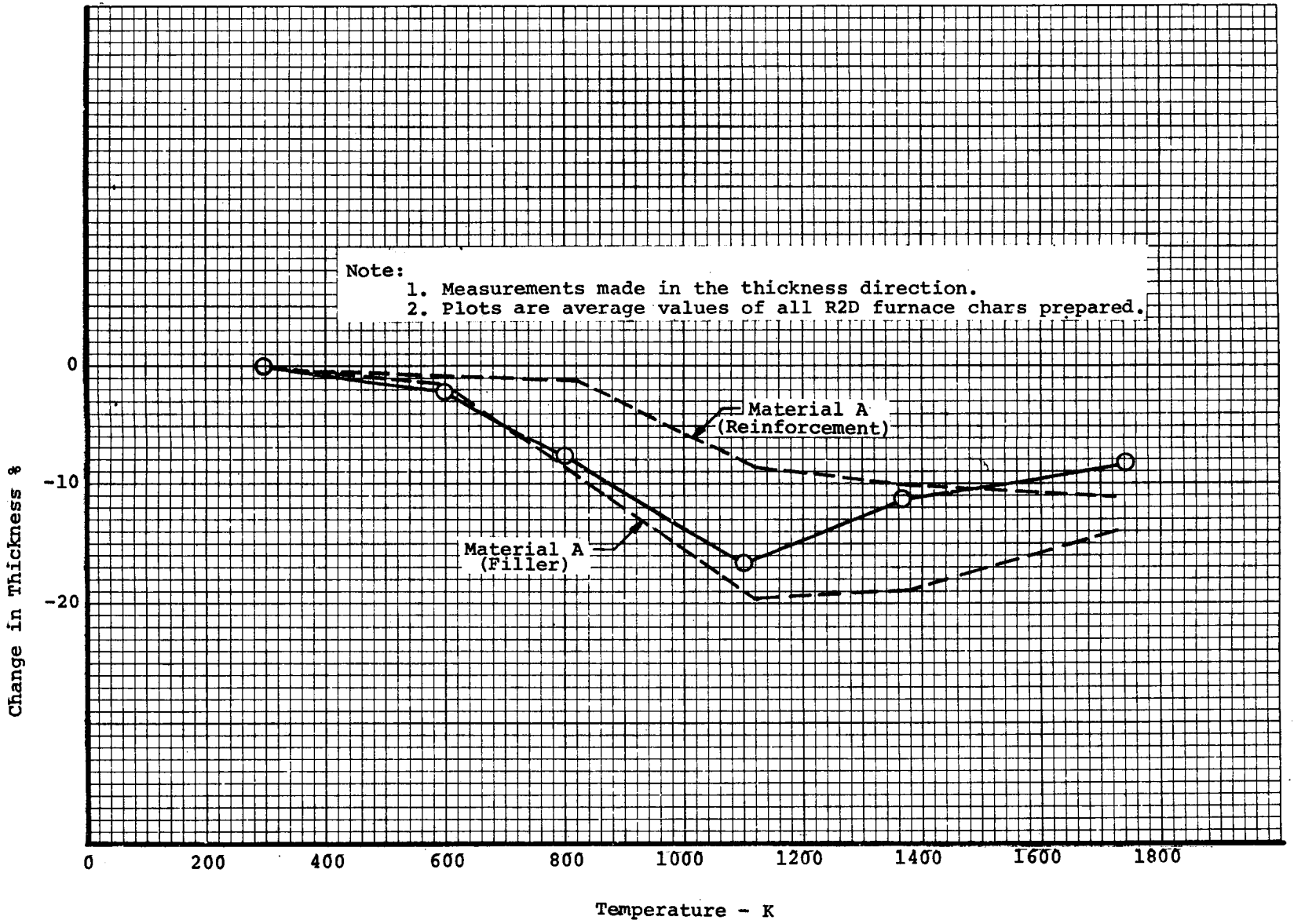

Figure 30. Effect of Char Temperature on Shrinkage for R2D Furnace Chars Prepared from Material B

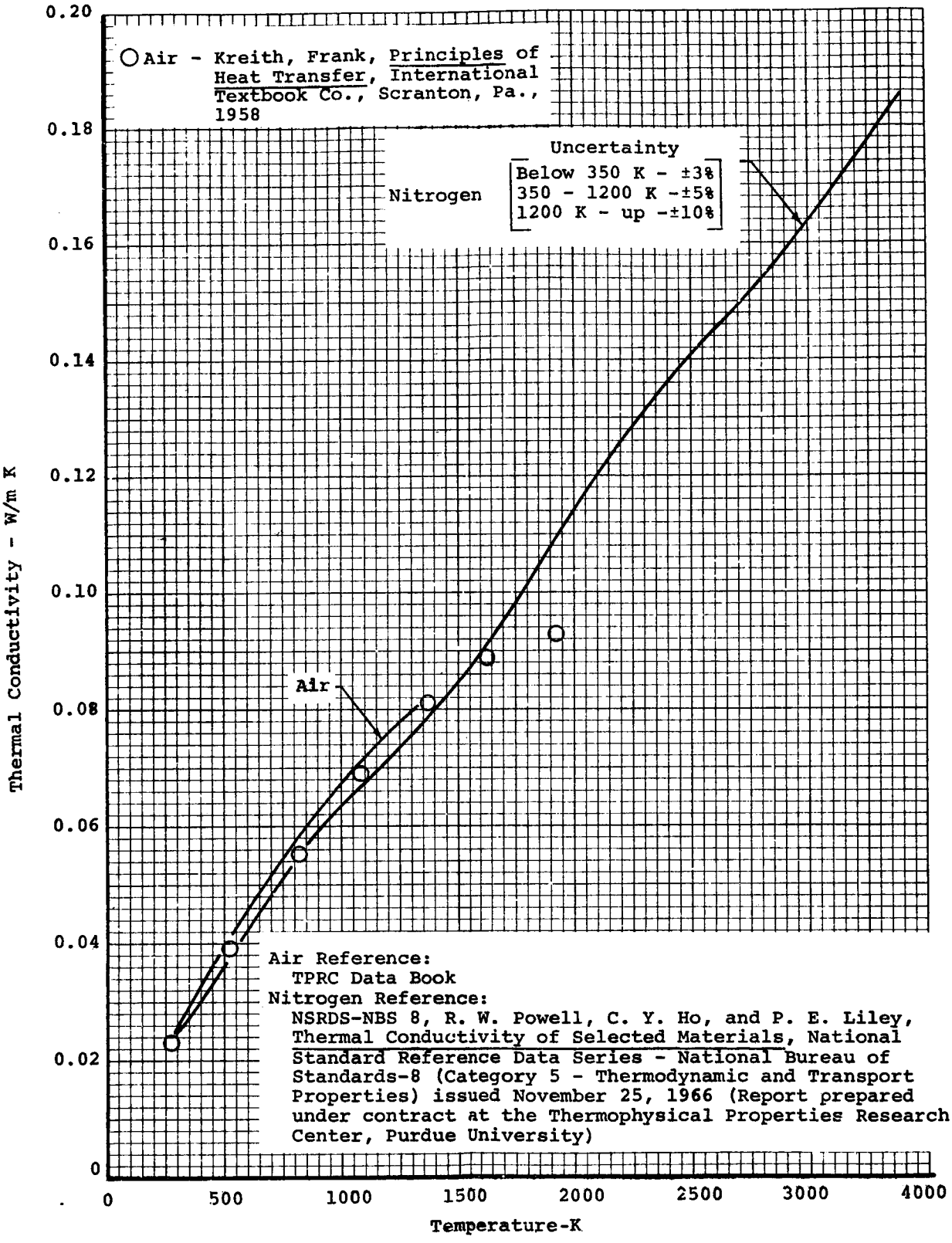

Figure 31. The thermal conductivities of gaseous nitrogen at pressure of 1 atmosphere

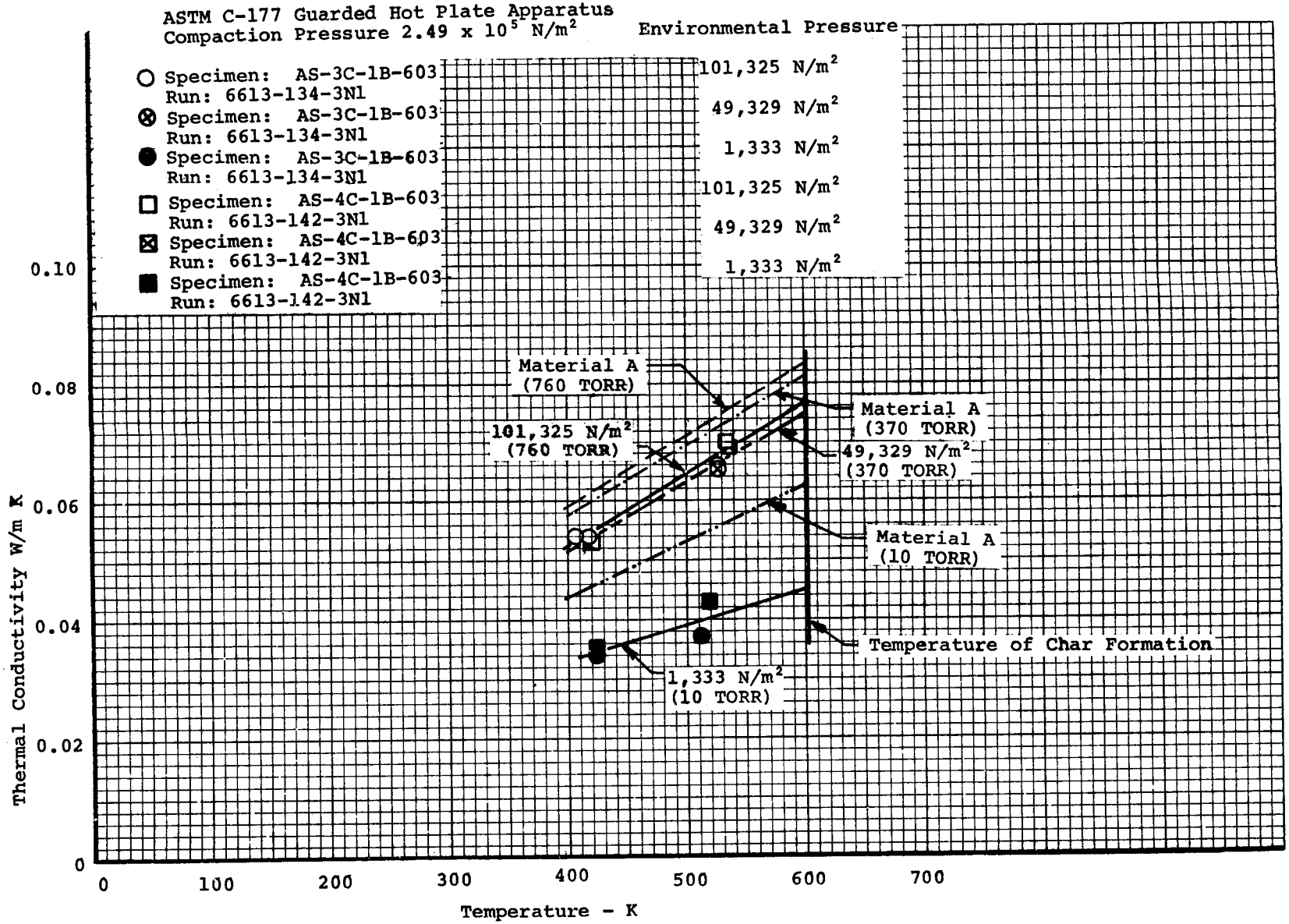

Figure 32. Thermal Conductivity of the Furnace Char of Material B Formed at 603 K

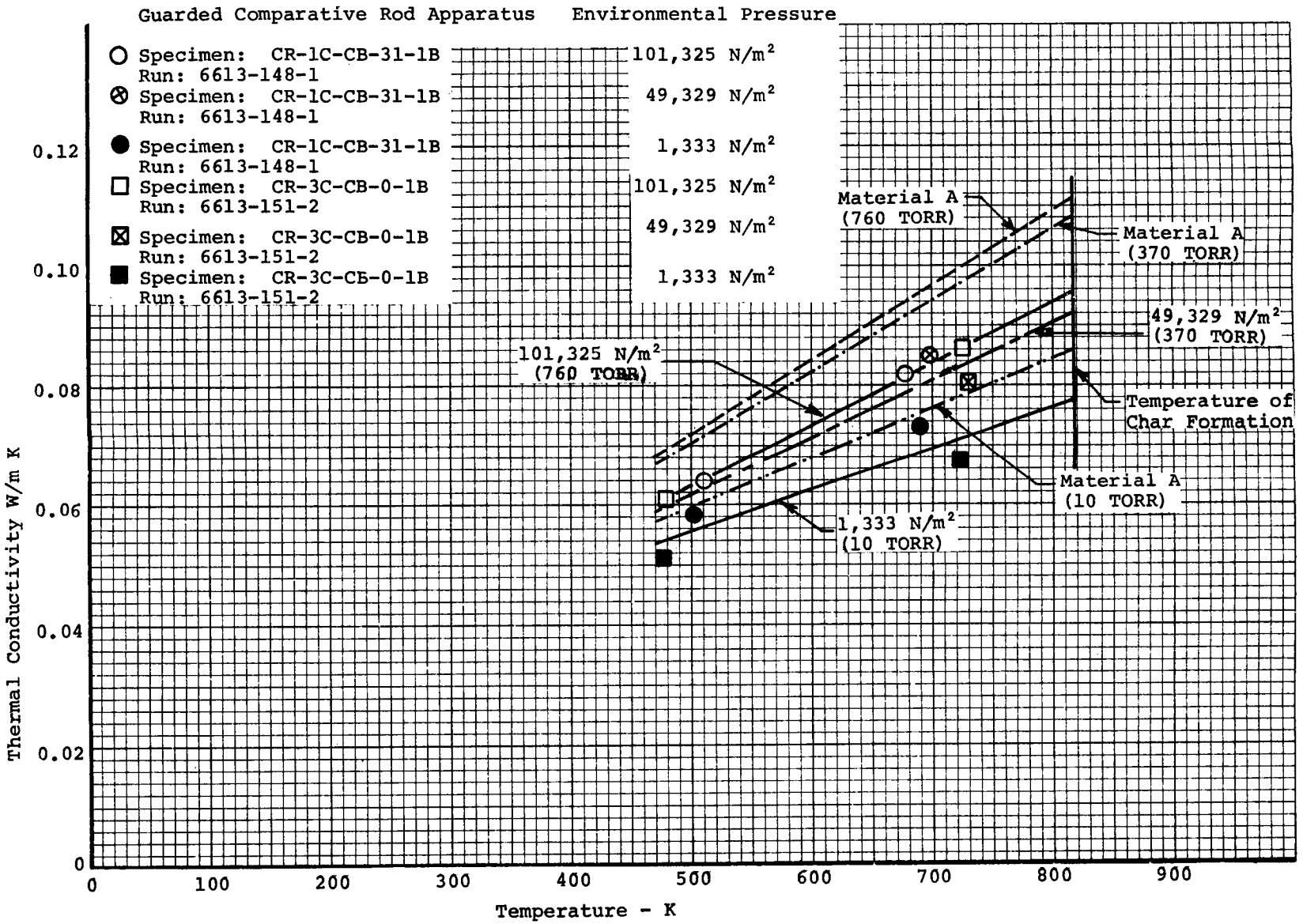

Figure 33. Thermal Conductivity of the Furnace Char of Material B Formed at 800 K

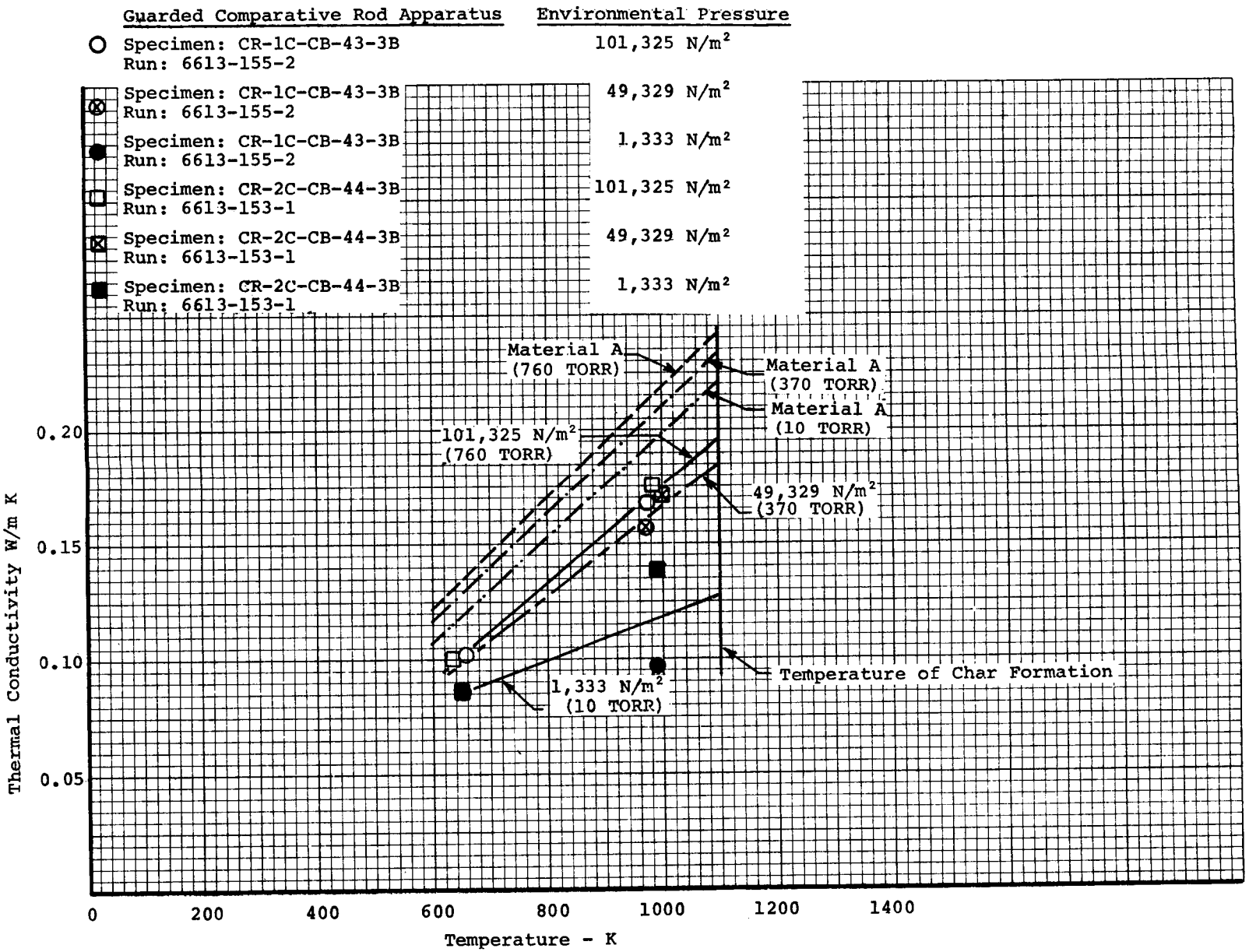

Figure 34. Thermal Conductivity of the Furnace Char of Material B Formed at 1100 K.

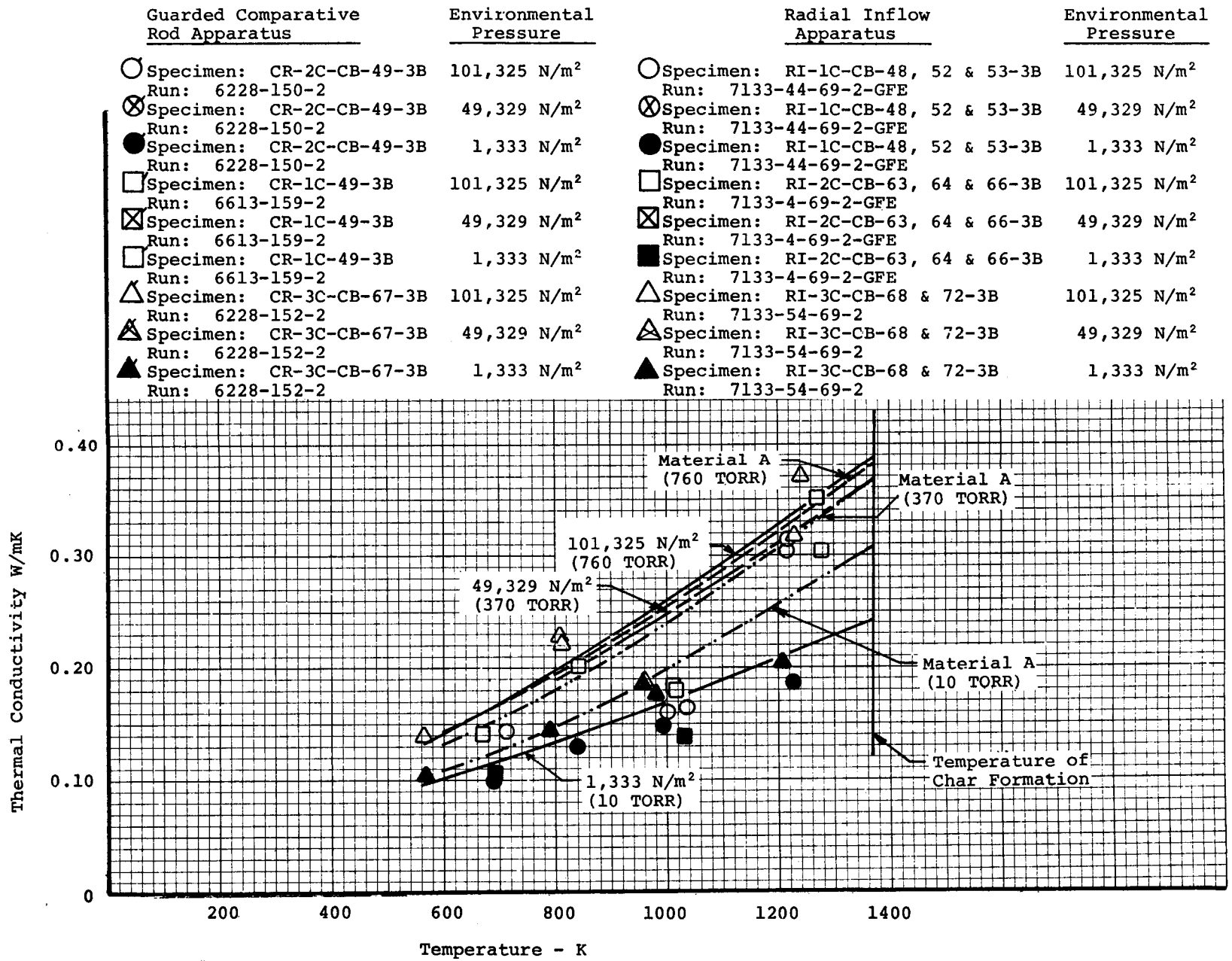

Figure 35. Thermal Conductivity of the Furnace Char of Material B Formed at 1365 K

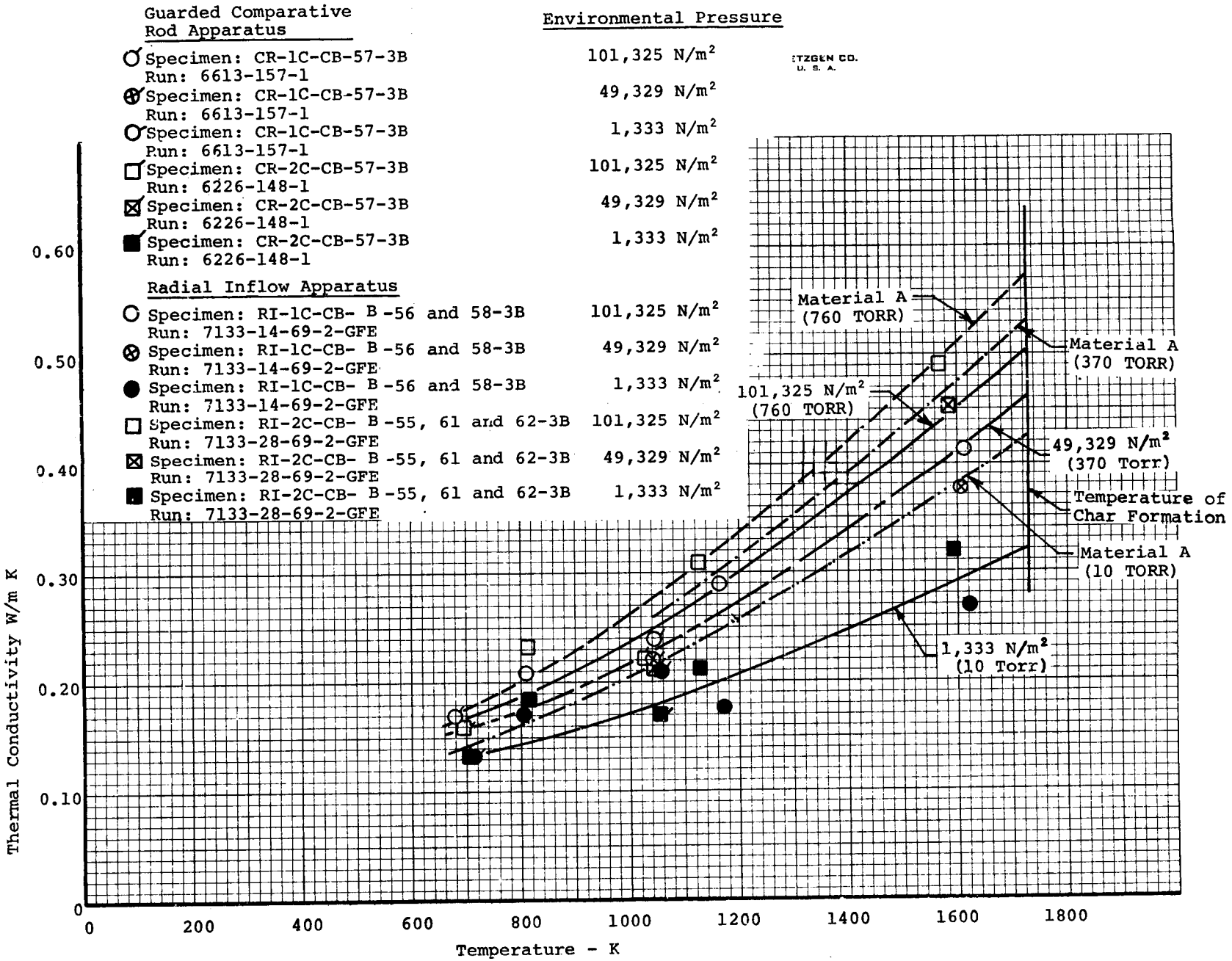

Figure 36. Thermal Conductivity of the Furnace Char of Material B Formed at 1729 K

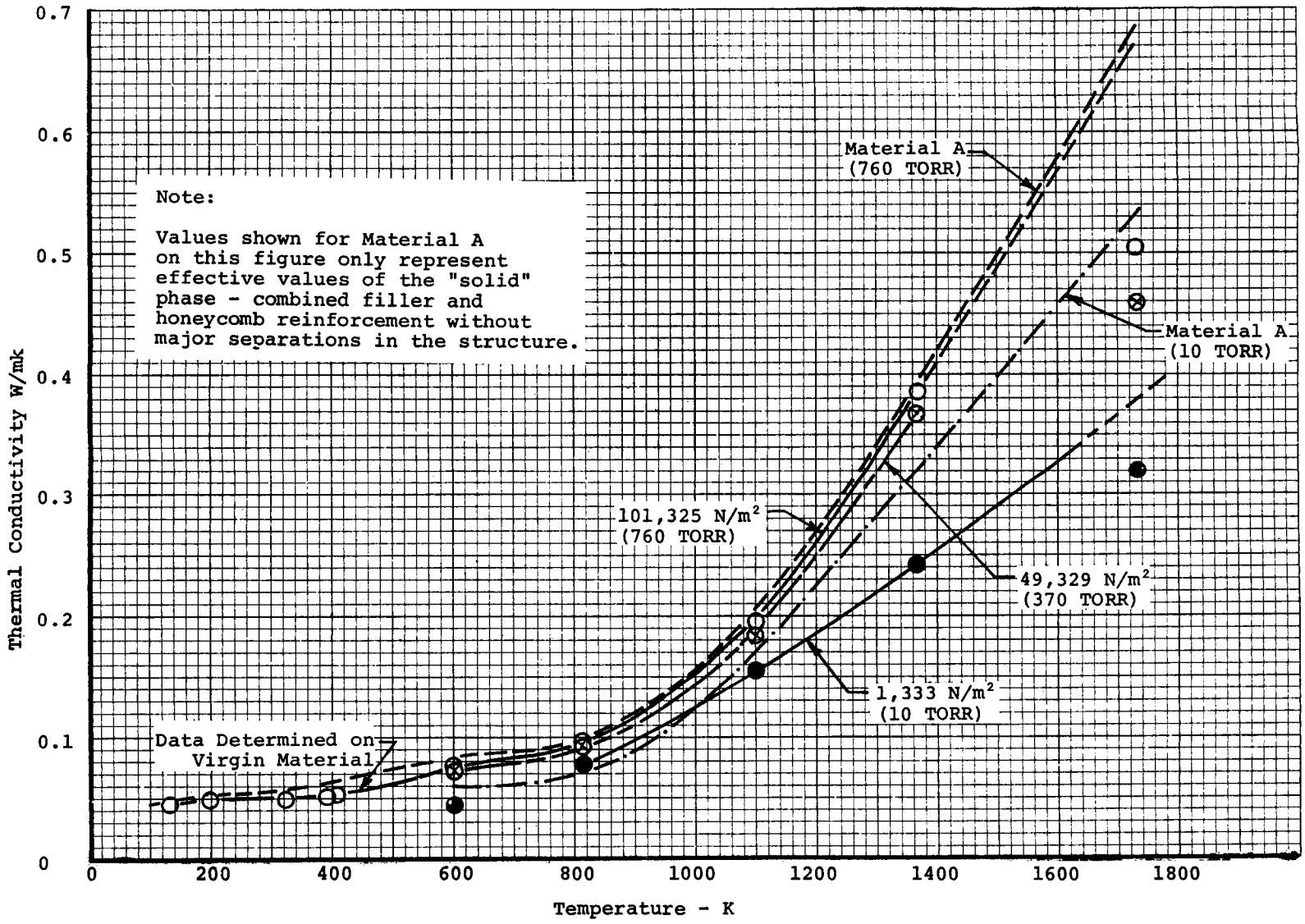

Figure 37. Thermal Conductivity of Material B During Ablative Charring Using the Boxing Analysis

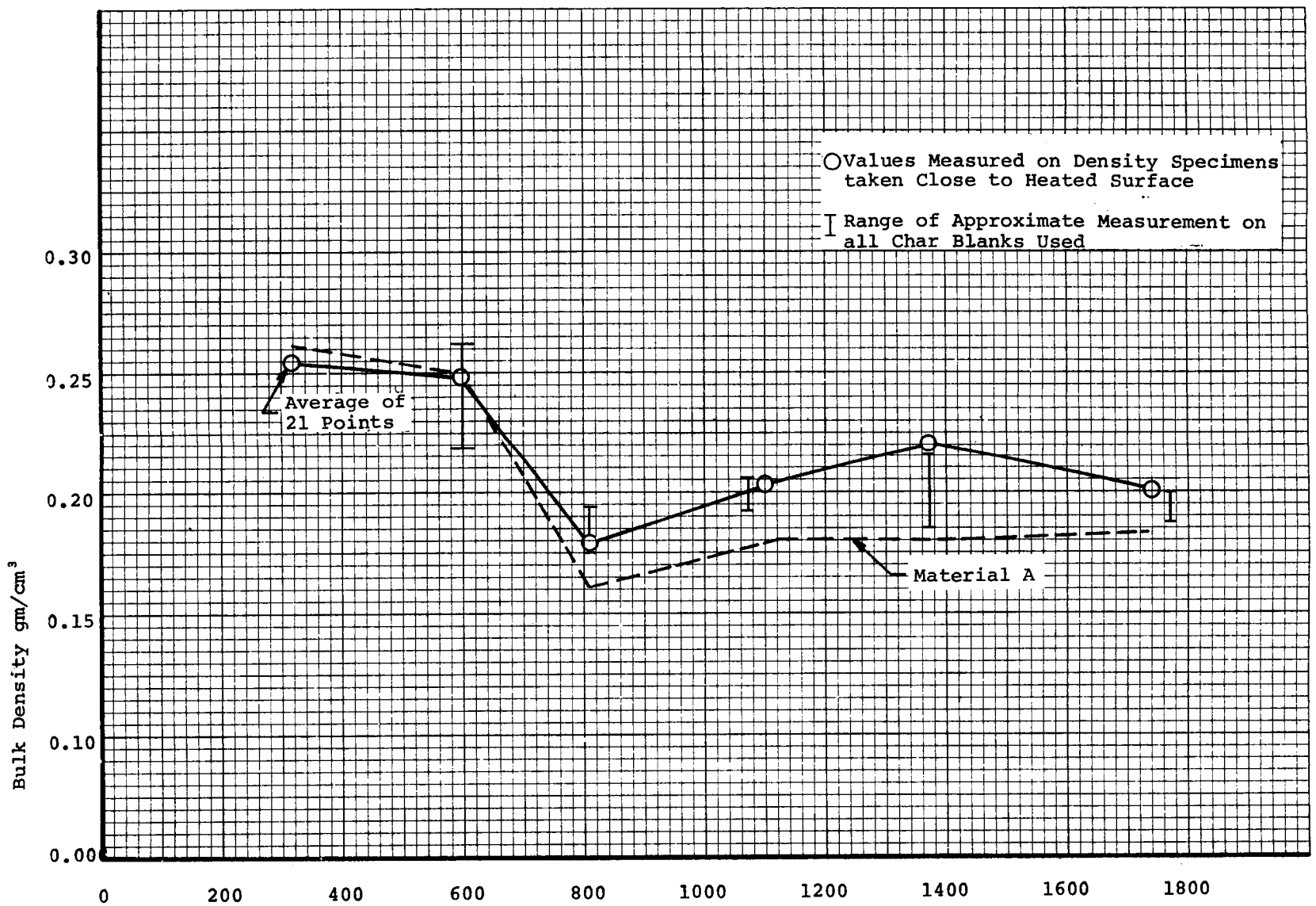

Figure 38. Bulk Density of Furnace Chars of Material B

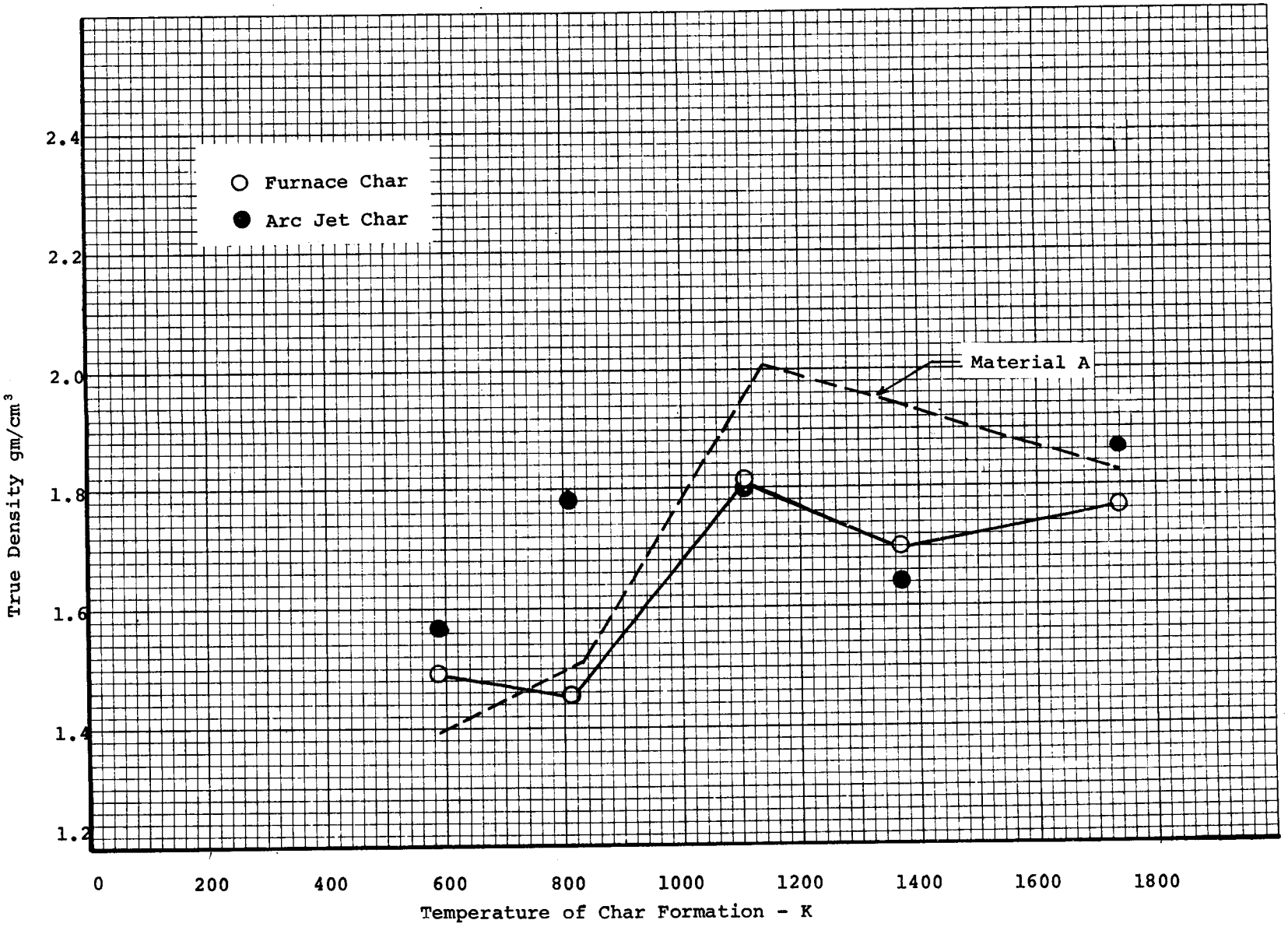

Figure 39. True Density of Furnace and Arc-Jet Chars of Material B

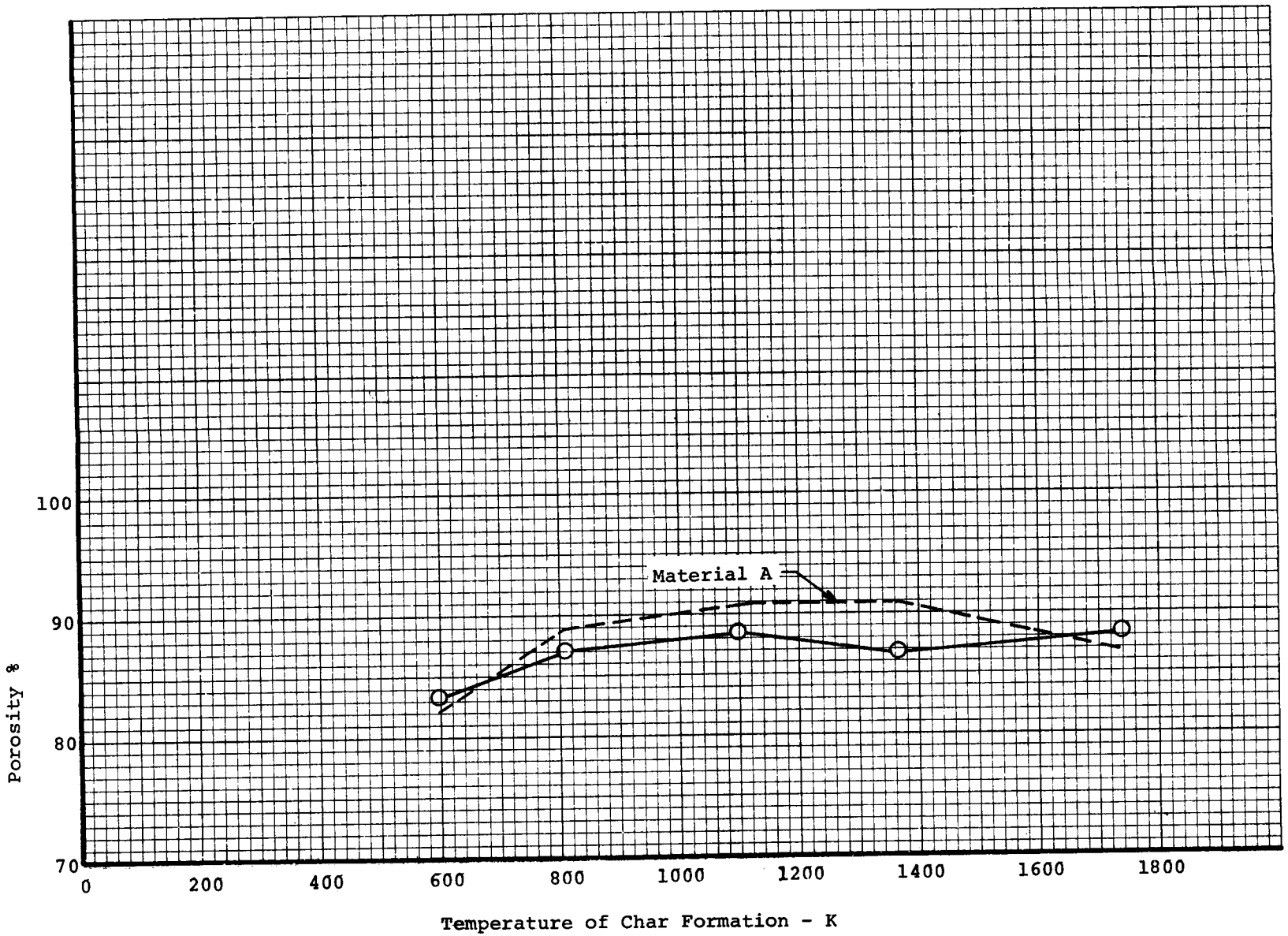

Figure 40. Total Porosity of Furnace Char of Material B

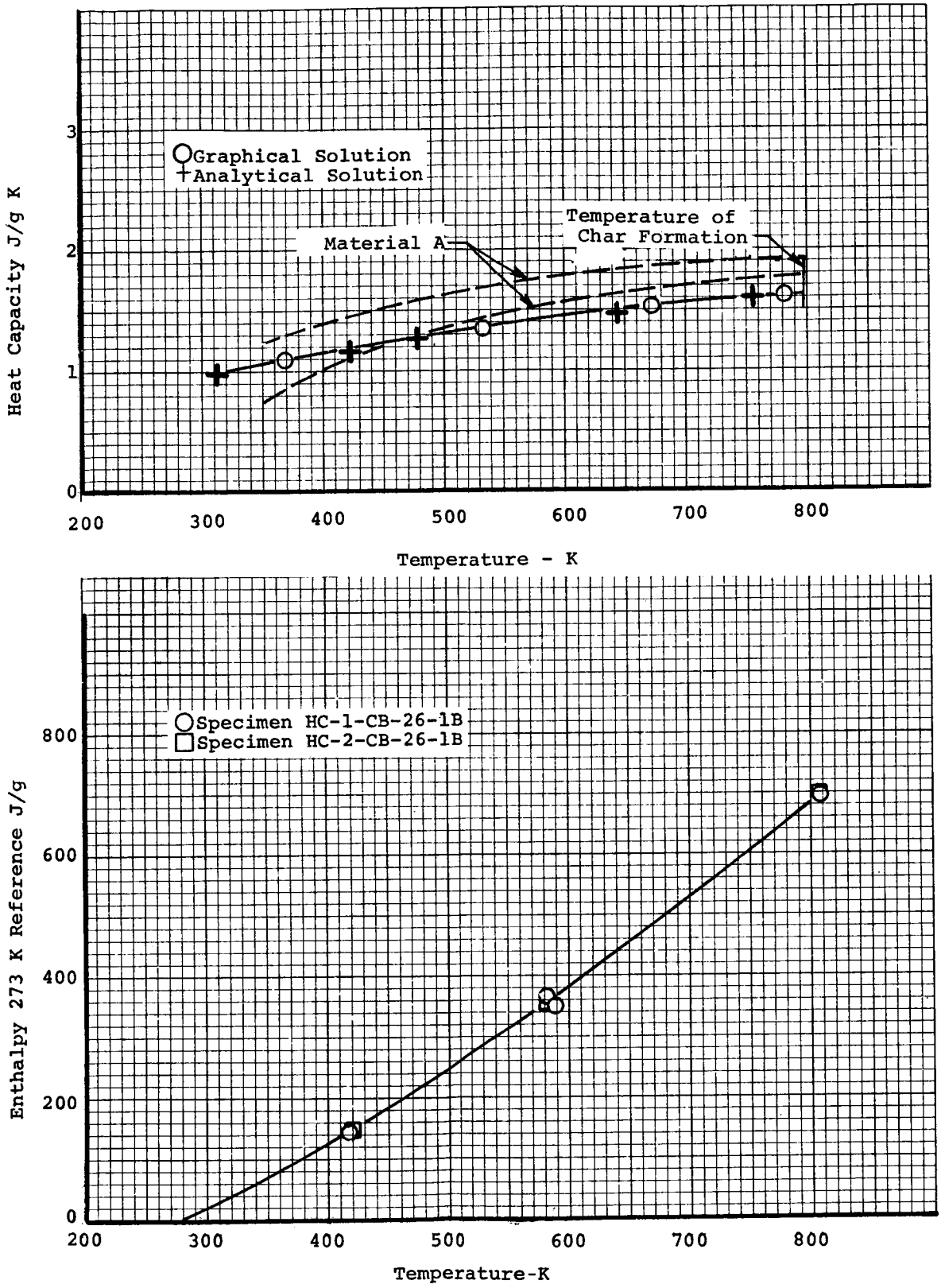

Figure 41. Enthalpy and Heat Capacity of the Furnace Char of Material B Formed at 798 K

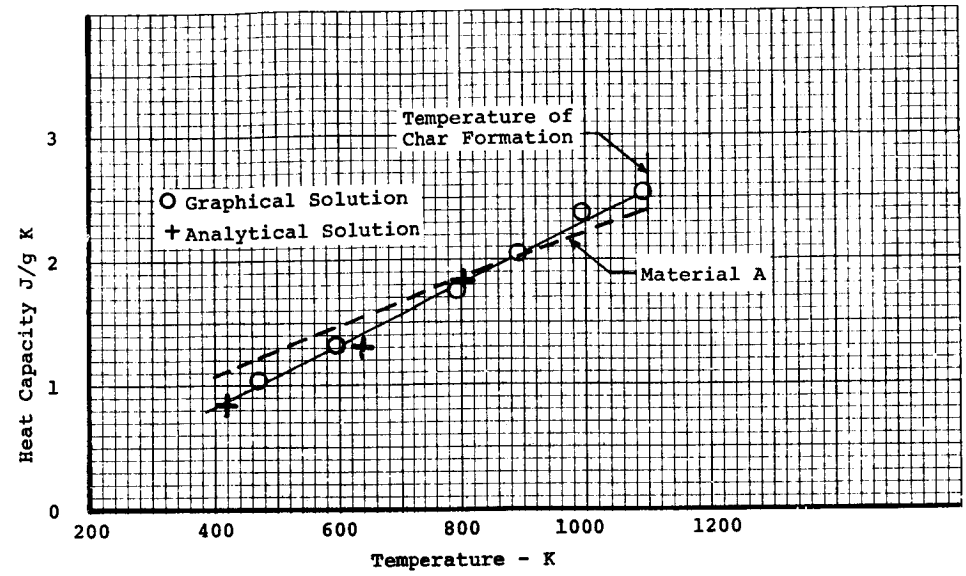

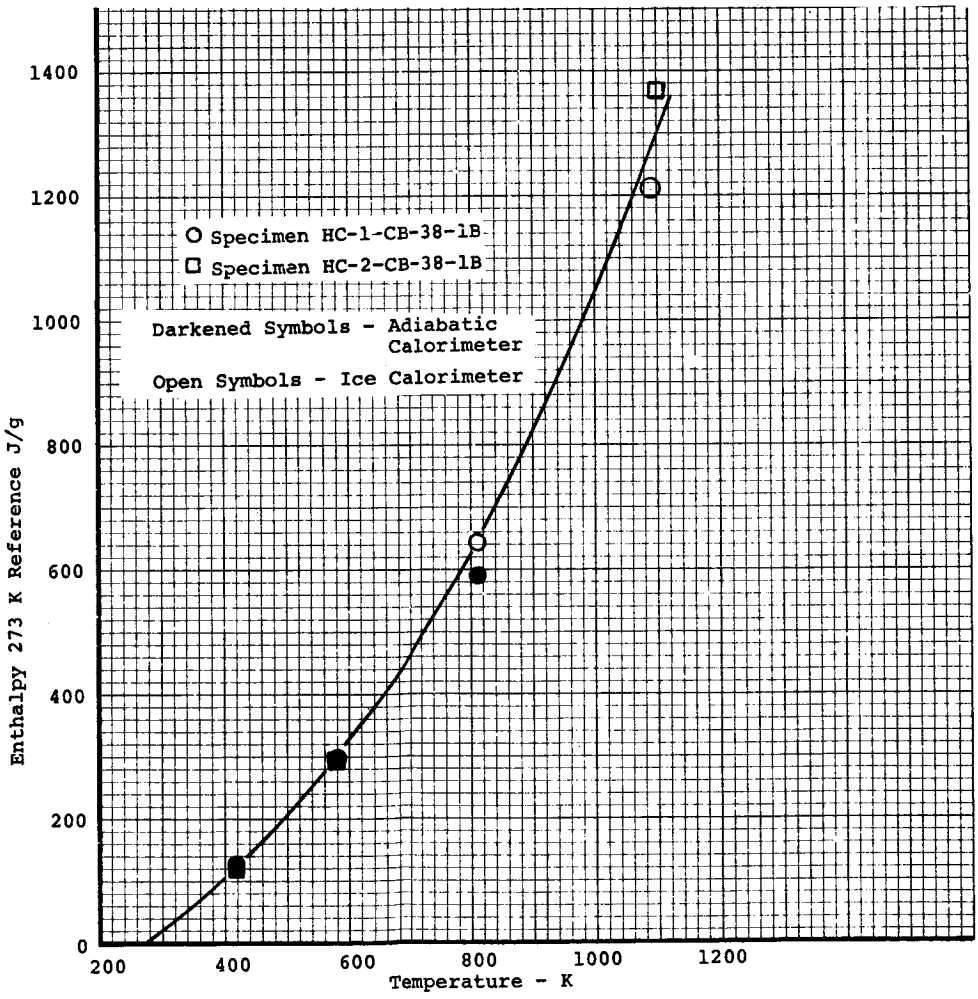

Figure 42. Enthalpy and Heat Capacity of the Furnace Char of Material B Formed at 1105 K

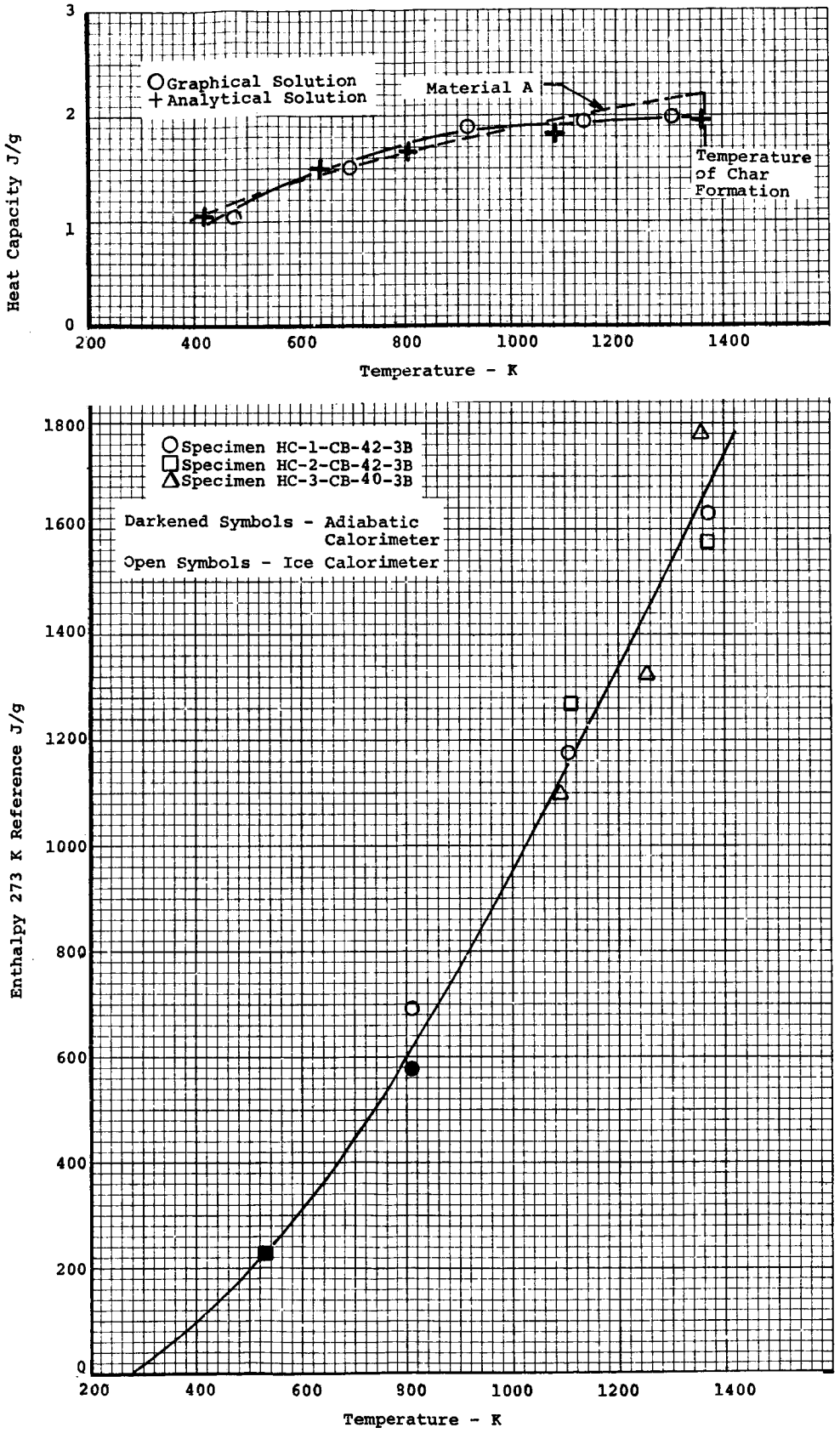

Figure 43. Enthalpy and Heat Capacity of the Furnace Char of Material B Formed at 1374 K

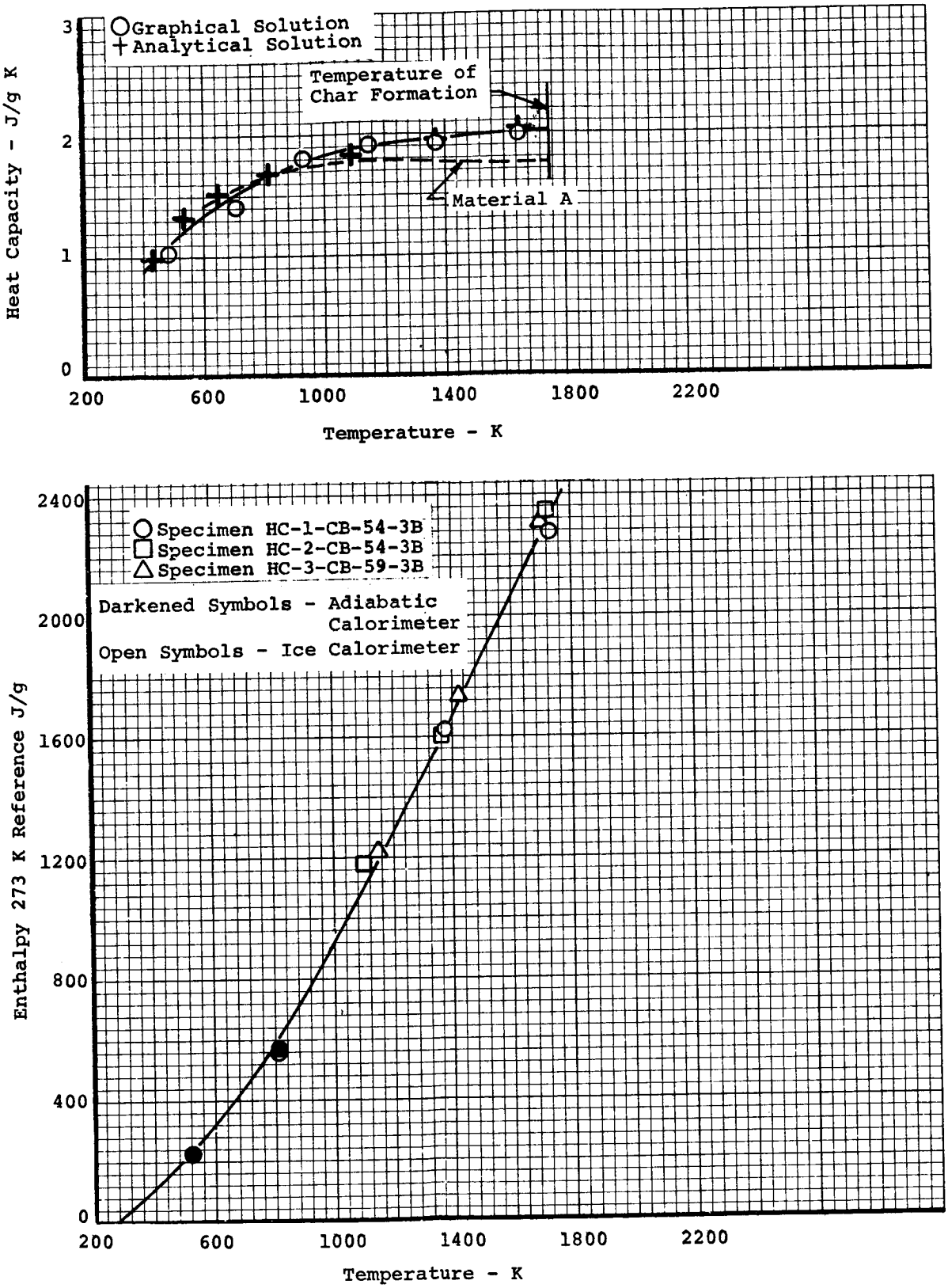

Figure 44. Enthalpy and Heat Capacity of the Furnace Char of Material B Formed at 1739 K

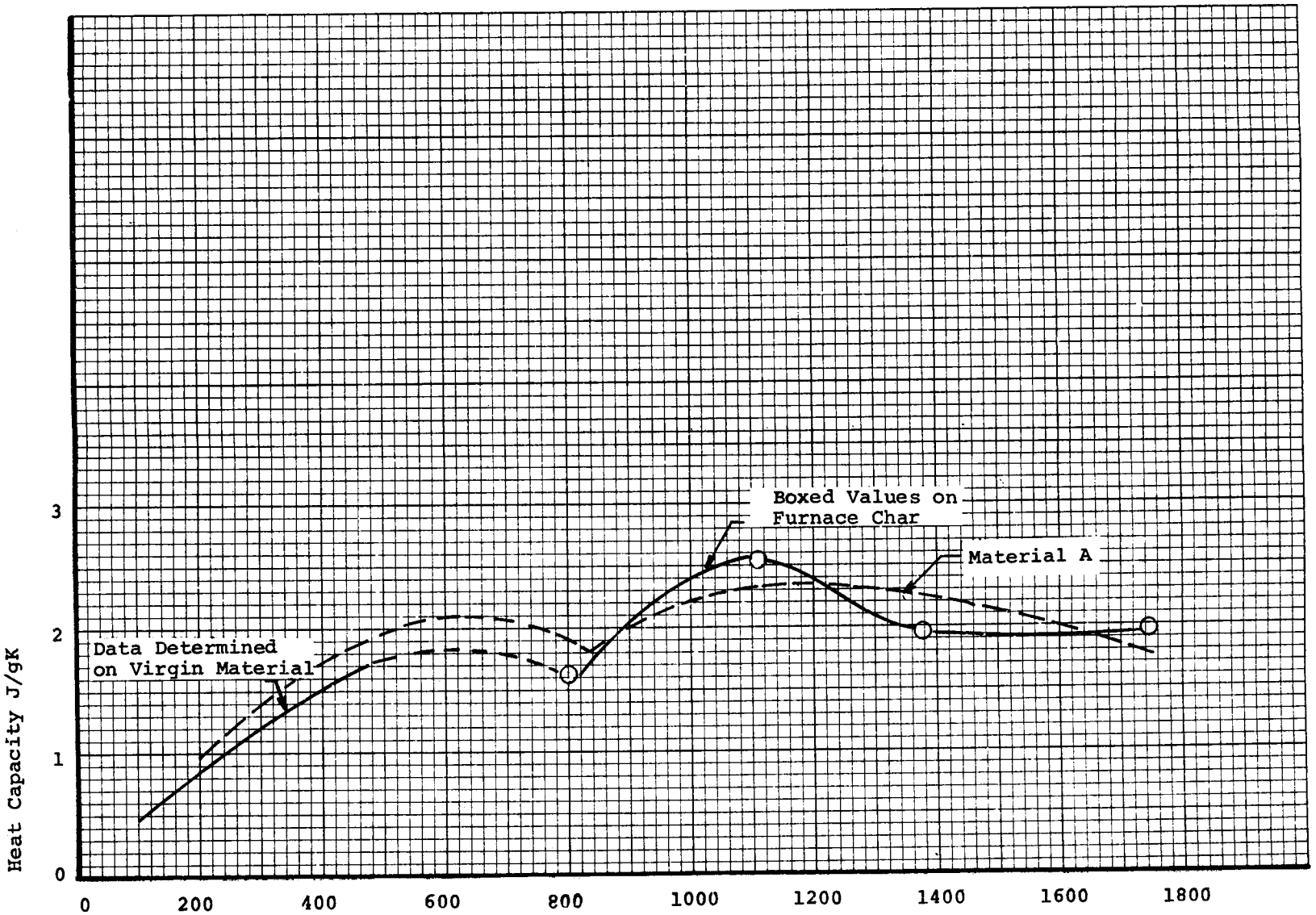

Figure 45. Heat Capacity of Material B During Ablative Charring Using the Boxing Analysis

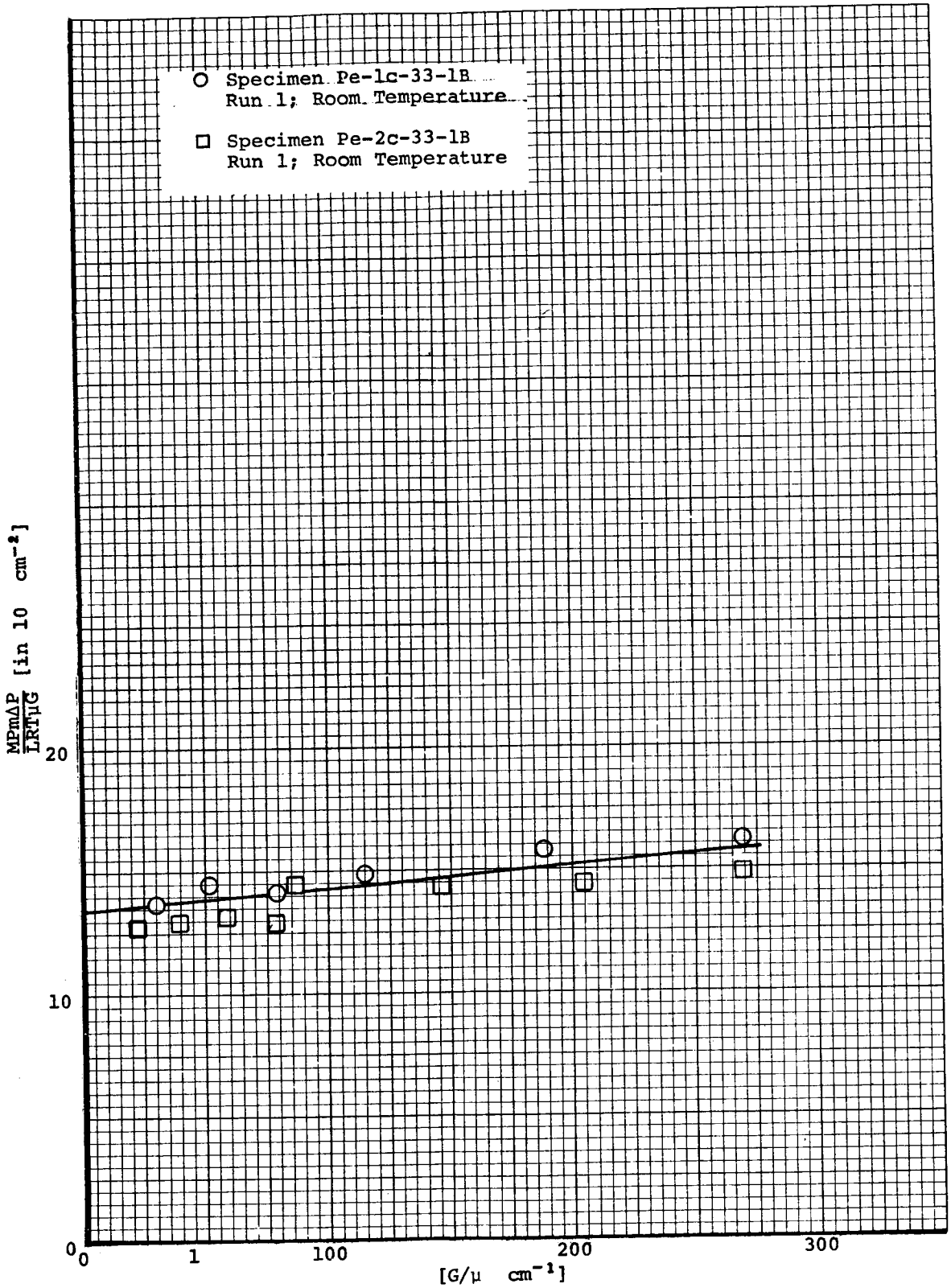

Figure 46. The Permeability of the Furnace Char of Material B Formed at 600 K

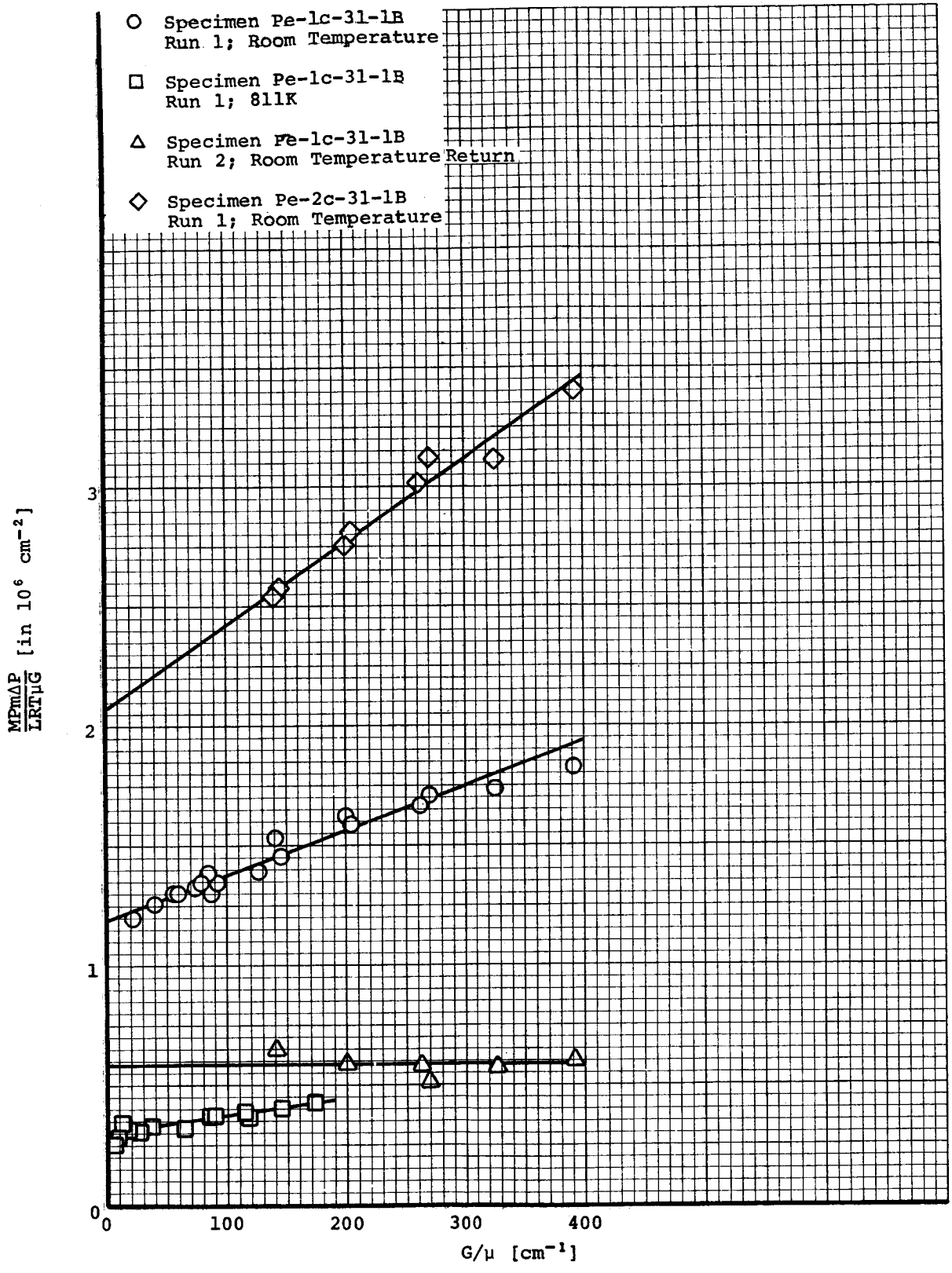

Figure 47. The Permeability of the Furnace Char of Material B Formed at 800 K

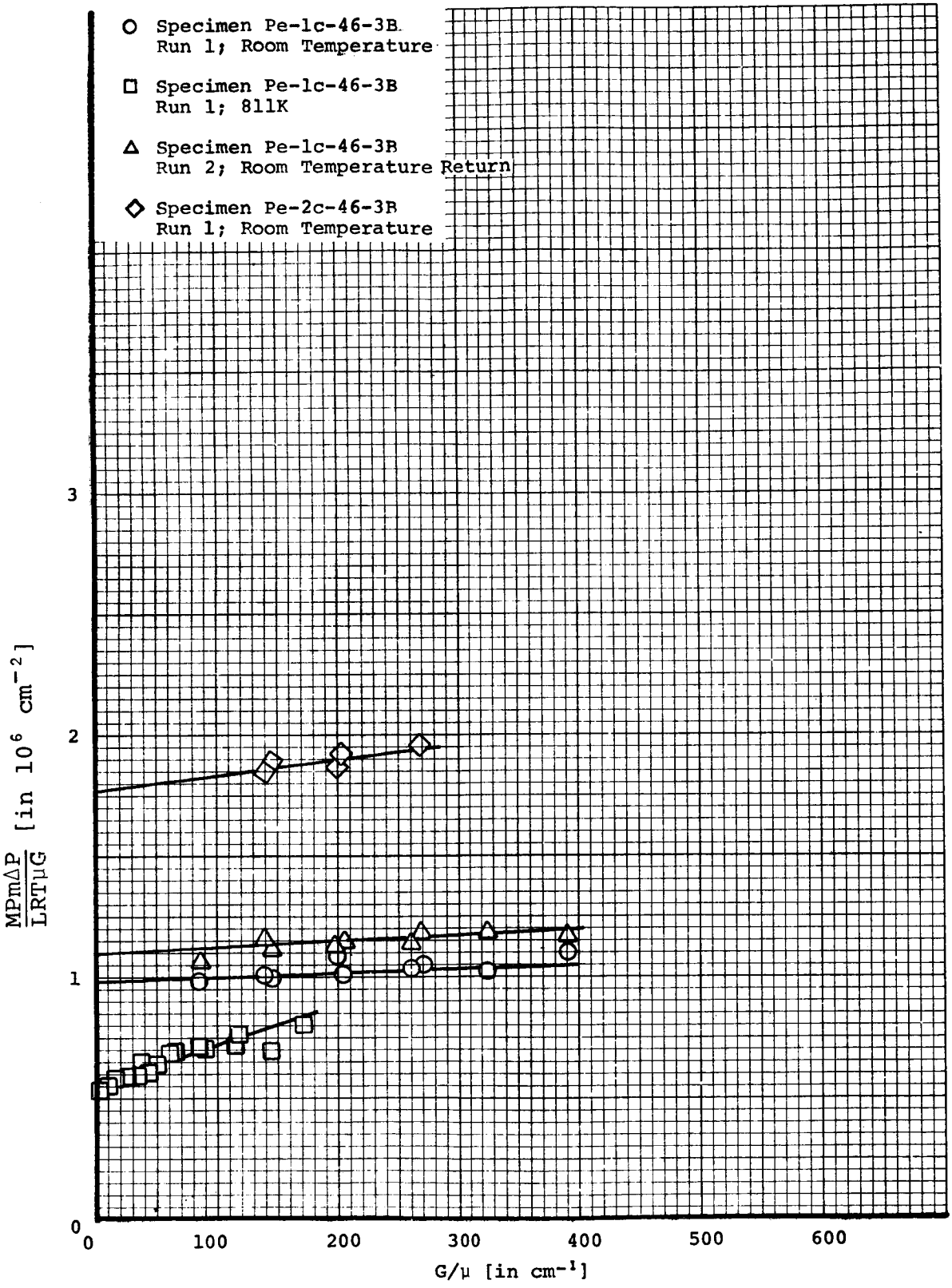

Figure 48. The Permeability of the Furnace Char of Material B Formed at 1098 K

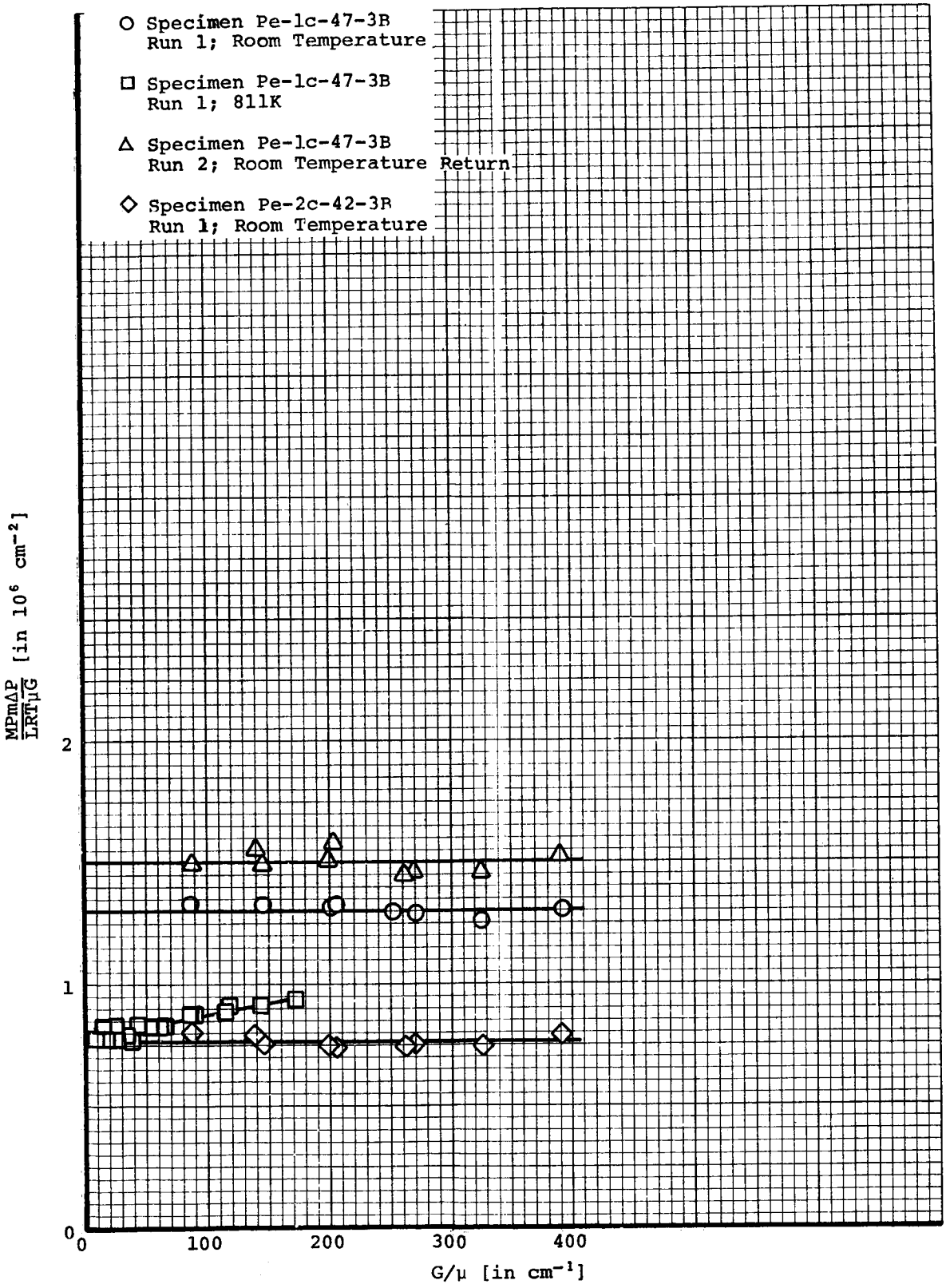

Figure 49. The Permeability of the Furnace Char of Material B Formed at 1366 K

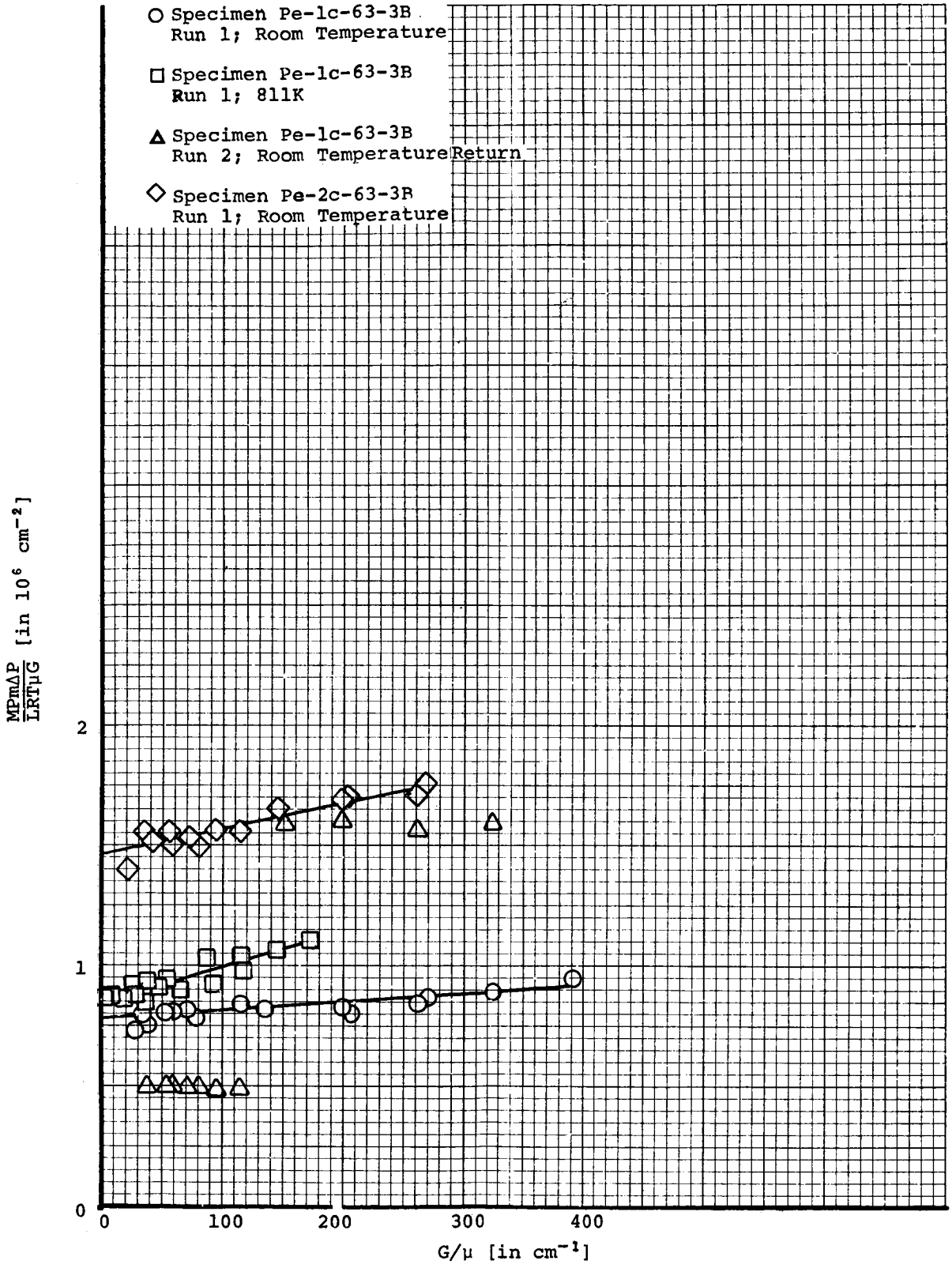

Figure 50. The Permeability of the Furnace Char of Material B Formed at 1745 K

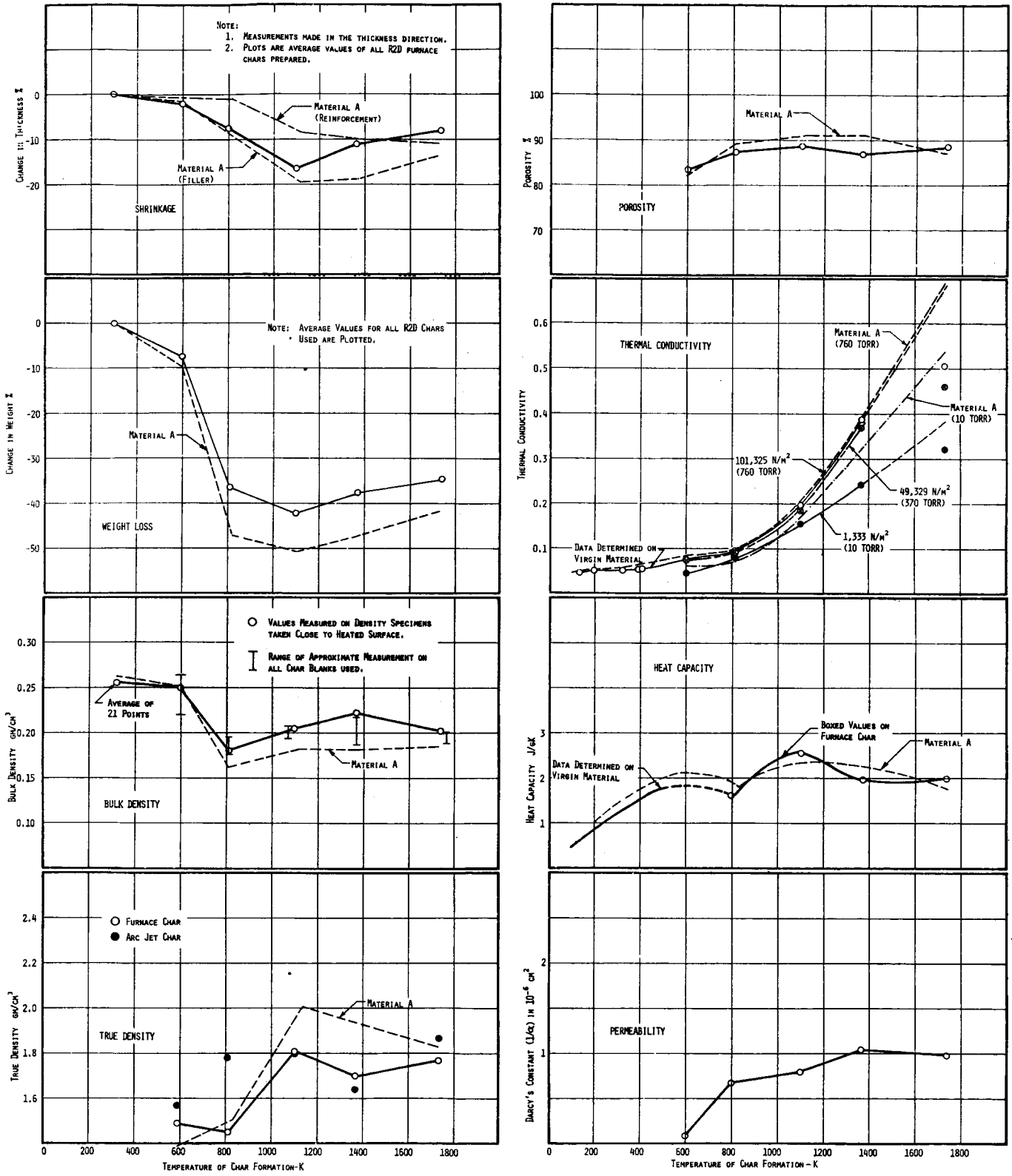

Figure 51. Composite of Properties Determined on Material B During Degradation and Char Formation

TABLE 1

COLD WALL HEAT FLUX
OF FURNACE CHARS

Furnace Preheat Temperature K	Approximate Cold Wall Heat Flux W/m-K
600	0.6×10^2
800	17.0×10^3
1100	65.0×10^3
1370	160.0×10^3
1730	400.0×10^3

Note: Cold wall heat fluxes are for immersion of specimen within preheated furnace. Emittance of surface assumed at 0.8.

TABLE 2

THERMAL CONDUCTIVITY OF A LOW-DENSITY ELASTOMERIC ABLATION MATERIAL (MATERIAL B) IN 1 ATMOSPHERE NITROGEN MEASURED IN ASTM C177 GUARDED HOT PLATE APPARATUS

Avg. Specimen Mean Temp. K	Total Heat Input Watts	Average Specimen ΔT K	Specimen Gage[2] cm	Specimen Thermal Conductivity W/m - K	Time to Temperature[3] hr
Specimen AS-1C-1B Run: 6613-86-3 Ni					
132.4	1.583	49.4	0.527	0.046	2.5
132.3	1.583	49.4	0.527	0.046	3.0
202.8	4.051	116.9	0.527	0.050	2.0
199.6	4.051	116.7	0.527	0.050	2.7
323.9	1.019	25.7	0.467	0.051	16.0
323.9	1.019	25.7	0.467	0.051	16.5
393.2	1.719	37.1	0.419	0.053	3.0
393.4	1.419	37.1	0.419	0.053	3.5
520.1	2.808	52.4	0.338	0.050	2.5
521.3	2.808	52.4	0.338	0.050	3.0
Specimen AS-2C-1B Run: 6613-92-3 Ni					
145.9	1.862	59.7	0.525	0.045	1.8
146.0	1.862	59.7	0.525	0.045	2.3
202.5	3.325	108.8	0.525	0.044	4.0
202.7	3.325	108.8	0.525	0.044	4.5
409.7	1.827	37.7	0.409	0.054	16.0
409.6	1.827	37.7	0.409	0.054	16.5
501.7	2.812	52.2	0.348	0.051	3.0
501.7	2.812	52.1	0.348	0.051	3.5

Notes:

1. Diameter of central heater = 4.826 cm.
2. Thermal conductivity values based on measured gage at each temperature level.
3. Time to temperature implies the time elapsed between adjustment of power and obtaining data.

Bulk Density and Specimen Weights

AS-1C-1B Bottom Disc 0.2498 gm/cm^3; Initial Weight, 3.5534 gm
Final Weight, 3.2652

Top Disc 0.2433 gm/cm^3; Initial Weight, 3.4826 gm
Final Weight, 3.2045 gm

AS-2C-1B Bottom Disc 0.2486 gm/cm^3; Initial Weight, 3.5112 gm
Final Weight, 3.2913 gm

Top Disc 0.2607 gm/cm^3; Initial Weight, 3.6975 gm
Final Weight, 3.4332 gm

TABLE 3

ENTHALPY OF A LOW-DENSITY ELASTOMERIC ABLATION MATERIAL (MATERIAL B)
MEASURED IN THE ADIABATIC CALORIMETER

Specimen	Run	Initial Cup Temp. °K	Final Cup Temp. °K	Change in Cup Temp. °K	Initial Sample Temp. °K	Initial Wt. of Sample gm	Final Wt. of Sample gm	Enthalpy Joules/gm Above 303°K
HC-1-1B	1	298.07	295.93	-2.14	86.11	6.3000	6.2912	-177.0
HC-1-1B	2	298.48	297.15	-1.33	201.11	6.2912	6.2968	-113.3
HC-1-1B	3	297.02	298.62	+1.60	400.00	6.2968	6.0890	126.8
HC-1-1B	4	297.76	301.38	3.62	501.11	6.0890	5.9157	306.3
HC-2-1B	1	298.52	296.33	-2.19	110.00	6.6363	6.6326	-172.0
HC-2-1B	2	298.58	297.15	-1.43	201.11	6.6326	6.6100	-115.4
HC-2-1B	3	297.47	299.08	1.61	399.44	6.6100	6.3974	122.1
HC-2-1B	4	297.95	301.52	3.57	498.89	6.3974	6.2225	287.5
HC-3-1B	1	296.90	298.03	1.12	365.56	6.7733	6.6766	78.9
HC-3-1B	2	299.02	302.08	3.06	468.89	6.6766	6.5087	235.8
HC-3-1B	3	299.48	304.44	4.96	586.39	6.5087	5.9095	425.2
HC-4-1B	1	298.03	299.11	1.09	374.72	6.0615	5.8549	89.0
HC-4-1B	2	296.51	299.16	2.66	469.72	5.8549	5.8172	225.1
HC-4-1B	3	299.44	303.87	4.43	586.39	5.8172	5.3050	421.9

TABLE 4

TENSILE STRENGTH PROPERTIES OF A LOW-DENSITY ELASTOMERIC ABLATION MATERIAL (MATERIAL B)

Load Direction	Temp °F	Rate	Specimen Number	Bulk Density gm/cm^3	Ultimate Strength N/m^2	Initial Elastic Modulus N/m^2	Total Unit Axial Strain cm/cm
a	70	-	T-1A-B	0.2440	48.27	8825.6	0.0067
		-	T-2A-B	0.2462	34.48	7032.9	0.0065
b	70	-	T-1B-B	0.2531	42.75	6343.4	0.0070
		-	T-2B-B	0.2483	32.41	7032.9	0.0074

TABLE 5

COMPRESSIVE STRENGTH PROPERTIES OF A LOW-DENSITY ELASTOMERIC ABLATION MATERIAL (MATERIAL B)

Load Direction	Temp °F	Rate	Specimen Number	Bulk Density gm/cm^3	Ultimate Strength $10^3 N/m^2$	Initial Elastic Modulus $10^3 N/m^2$	Total Unit Axial Strain cm/cm
a	70	-	C-1A-B	0.2476	194.09	9928.8	0.0480
		-	C-2A-B	0.2532	200.64	10135.7	0.0391
b	70	-	C-1B-B	0.2625	208.92	13238.4	0.0445
		-	C-2B-B	0.2499	162.72	10963.1	0.0518

TABLE 6

SUMMARY OF CHAR BLANKS PREPARED DURING THE PRELIMINARY INVESTIGATIONS

Temperature Category	Total Time in Furnace Seconds	Maxium Temperature K	Specimen Blank Number[1]	Thickness cm	Virgin Bulk Density gm/cm³	Weight Loss %	Shrinkage in Thickness %	Char[2] Bulk Density gm/cm³	Change in Bulk Density %	X-ray Diffraction Intensities at d=4.05	X-ray Diffraction Intensities at d=2.485
800K	780	827	CB- 4-1B- 827 (R2D)	2.54	0.2588	40.23	10.30	0.1785	31.02		
	1200	807	CB-14-1B- 807 (R2D)	2.54	0.2602	43.93	12.42	0.1742	33.95		
1100K	375	1131	CB- 3-1B-1131 (R2D)	2.54	0.2600	42.34	21.92	0.2215	14.80		
	420	1101	CB-17-1B-1101 (R2D)	5.08	0.2549	41.86	11.47	0.1750	31.34		
	1200	1109	CB-19-1B-1109 (R2D)	2.54	0.2755	45.01	21.86	0.2217	20.39		
	600	1164	CB-39-1B-1164 (R2D)	5.08	0.2446	42.67	15.08	0.2011	17.78		
1370K	260	1344	CB- 2-1B-1344 (R2D)	2.54	0.2586	37.33	13.91	0.2047	20.84		
	270	1373	CB- 6-1B-1373 (R1D)	1.27	0.2562	41.48	22.00	0.2213	13.62		
	270	1373	CB- 7-1B-1373 (R1D)	0.64	0.2534	43.62	25.37	0.2285	9.82		
	270	1328	CB-10-1B-1328 (R2D)	1.27	0.2576	43.87	14.78	0.1898	26.31		
	270	1326	CB-11-1B-1366 (R2D)	0.64	0.2529	46.03	20.54	0.2355	11.62		
	420	1372	CB-18-1B-1372 (R2D)	5.08	0.2475	40.31	14.91	0.1980	20.00		
	1200	1371	CB-21-1B-1371 (R2D)	2.54	0.2551	39.79	14.03	0.1975	22.57		
	1200	1381	CB-22-1B-1381 (R2D)	2.54	0.2619	42.75	12.65	0.1860	28.98		
1730K	180	1724	CB- 1-1B-1724 (R2D)	2.54	0.2608	34.08	11.57	0.2054	21.24	6100	900
	150	1673	CB- 8-1B-1673 (R1D)	1.27	0.2514	38.60	15.67	0.1993	20.72		
	210	1673	CB- 9-1B-1673 (R1D)	0.64	0.2485	41.48	21.57	0.1976	20.48		
	150	1719	CB-12-1B-1719 (R2D)	1.27	0.2485	37.78	17.81	0.2043	17.78		
	150	1719	CB-13-1B-1719 (R2D)	0.64	0.2475	44.93	18.18	0.1812	26.78		
	Transient	1725	CB-15-1B-1725 (R2D)	5.08	0.2530	26.94	5.00	0.2013	20.43		
	420	1732	CB-16-1B-1732 (R2D)	5.08	0.2652	37.54	5.47	0.1856	30.01	4000	550
	1200	1735	CB-20-1B-1735 (R2D)	2.54	0.2485	53.89	12.79	0.1429	42.49	500	900
	90	1716	CB-34-1B-1716 (R2D)	2.54	0.2628	33.14	14.72	0.2196	16.43	4300	500
	120	1730	CB-35-1B-1730 (R2D)	2.54	0.2676	34.58	10.92	0.2105	21.33	4500	700
	120	1730	CB-37-1B-1730 (R2D)	5.08	0.2655	34.20	9.20	0.2034	23.42	4800	700
1900K	180	1932	CB-24-1B-1932 (R2D)	2.54	0.2591	43.40	11.14	0.1742	32.76	Slight	800
2100K	240	2089	CB-25-1B-2089 (R2D)	2.54	0.2567	59.30	7.78	0.1167	54.53	Slight	2200
Arc Jet Char			Zone 1[3] AJ-B-1					0.219		9100	1300
			Zone 1[3] AJ-B-2							11200	1400
			Zone 2[3] AJ-B-2							7300	1000
			Zone 2[3] AJ-B-1					0.256			

[1]Specimen number contains designation R1D, R2D which infer the following:

R1D - Rapid heating rate, immersed in preheated furnace at desired temperature. One dimensional heating
R2D - Same as R1D except two-dimensional heating

[2]Bulk density of char measured approximately on entire block after extraction from the furnace

[3]Diagram of Arc Jet Char with Zones 1 through 5 indicated

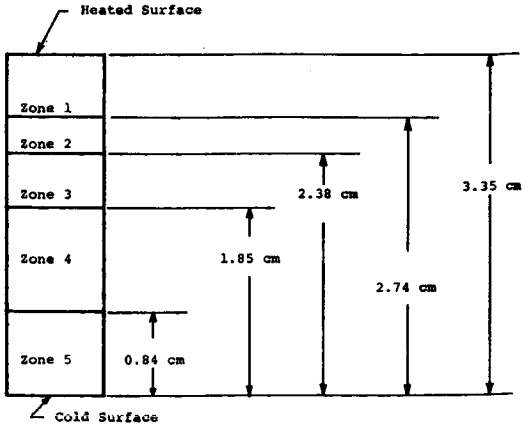

TABLE 7

SUMMARY OF CHAR BLANKS PREPARED (RAPID TWO-DIMENSIONAL) FOR EVALUATION

Temperature Category	Specimen Blank Number	Virgin Bulk Density gm/cm³	Maximum Temperature K	Total Time in Furnace sec	Weight Loss %	Shrinkage %	Char Bulk Density gm/cm³	Change in Bulk Density %	Specimen Prepared					
									Cp	Permeability	Density	CRA	RIA	Visual Inspection or Specimen Guards
600K	CB-23-1B-600(R2D)	0.2576	600	1200	13.33	3.51	0.2200	14.59			1			
	CB-28-1B-585(R2D)	0.2622	585	1080	5.44	1.48	0.2520	3.89	2					
	CB-29-1B-588(R2D)	0.2640	588	1080	5.42	2.48	0.2640	3.01			1			
	CB-33-1B-590(R2D)	0.2675	590	1080	6.07	0.61	0.2541	5.00		2				
	Average	0.2628			7.56	2.02	0.2475	6.62						
800K	CB-26-1B-798(R2D)	0.2523	798	810	37.84	8.63	0.1763	30.12	2					
	CB-27-1B-811(R2D)	0.2677	811	810	40.13	11.64	0.1835	31.45						2
	CB-30-1B-808(R2D)	0.2596	808	810	35.67	7.67	0.1853	28.62			1			
	CB-31-1B-808(R2D)	0.2673	808	810	33.68	7.56	0.1951	27.01		2		2		
	CB-32-1B-812(R2D)	0.2778	812	810	37.94	7.08	0.1913	31.13			2			
	CB-36-1B-805(R2D)	0.2588	805	810	34.30	9.75	0.1934	25.27						2
	Average	0.2639			36.59	8.72	0.1874	28.93						
1100K	CB-38-1B-1105(R2D)	0.2652	1105	770	40.40	14.80	0.2039	23.10	2					
	CB-41-3B-1099(R2D)	0.2634	1099	830	42.10	16.90	0.2036	22.70						2
	CB-43-3B-1101(R2D)	0.2566	1101	830	42.50	17.40	0.2003	21.90				1		
	CB-44-3B-1100(R2D)	0.2552	1100	830	42.60	16.60	0.2007	21.40				1		
	CB-45-3B-1103(R2D)	0.2580	1103	830	42.40	17.90	0.2075	19.60			3			
	CB-46-3B-1098(R2D)	0.2488	1098	830	42.90	16.30	0.1942	21.90		2	1			
	Average	0.2578			42.15	16.65	0.2017	21.77						
1370K	CB-40-1B-1382(R2D)	0.2600	1382	466	39.43	11.72	0.2071	20.34	1		2			
	CB-42-3B-1374(R2D)	0.2571	1374	456	36.50	10.60	0.1983	22.90	2	1				
	CB-47-3B-1366(R2D)	0.2508	1366	470	37.00	12.20	0.1964	21.70		1	4			
	CB-48-3B-1375(R2D)	0.2460	1375	470	36.70	10.90	0.1882	23.50					2	
	CB-49-3B-1365(R2D)	0.2644	1365	470	36.30	11.30	0.2021	23.60				2		1
	CB-50-3B-1383(R2D)	0.2598	1383	470	36.80	10.90	0.2017	22.40					1	
	CB-51-3B-1373(R2D)	0.2570	1373	470	36.10	11.30	0.2176	15.30					1	
	CB-52-3B-1379(R2D)	0.2565	1379	470	37.10	11.10	0.1977	22.90					1	
	CB-53-3B-1366(R2D)	0.2636	1366	470	37.60	11.60	0.2040	22.60					2	
	CB-64-3B-1364(R2D)	0.2697	1364	470	38.37	11.15	0.2064	23.47					1	
	CB-65-3B-1363(R2D)	0.2548	1363	470	38.36	10.42	0.1900	25.43					1	
	CB-66-3B-1365(R2D)	0.2544	1365	470	41.15	10.83	0.1872	25.41					2	
	CB-67-3B-1369(R2D)											1		
	CB-68-3B-1377(R2D)												2	
	CB-69-3B-1371(R2D)													1
	CB-70-3B-1380(R2D)													1
	CB-71-3B-1369(R2D)													1
	CB-72-3B-1358(R2D)												2	
	Average	0.2578			37.62	11.17	0.1997	22.46						
1730K	CB-54-3B-1739(R2D)	0.2583	1739	300	35.80	8.00	0.1926	25.40	2					
	CB-55-3B-1740(R2D)	0.2553	1740	300	34.60	8.10	0.1892	25.90					2	
	CB-56-3B-1720(R2D)	0.2514	1720	300	34.80	7.90	0.1945	22.60					2	
	CB-57-3B-1729(R2D)	0.2507	1729	300	34.10	7.60	0.1970	21.40				2		1
	CB-58-3B-1723(R2D)	0.2551	1723	300	34.60	8.50	0.2003	21.50					1	
	CB-59-3B-1735(R2D)	0.2526	1735	300	34.90	7.70	0.1891	25.10	1		3			
	CB-60-3B-1747(R2D)	0.2530	1747	300	34.60	8.20	0.1972	22.10		1			1	
	CB-61-3B-1725(R2D)	0.2573	1725	300	34.60	8.10	0.2016	21.60						1
	CB-62-3B-1734(R2D)	0.2505	1734	300	33.90	8.90	0.1992	20.50					2	
	CB-63-3B-1745(R2D)	0.2622	1745	300	34.60	7.90	0.1977	24.59		2	2			
	Average	0.2546			34.65	8.09	0.1958	23.07						

TABLE 8

THERMAL CONDUCTIVITY OF THE FURNACE CHAR OF MATERIAL B FORMED AT 600K
MEASURED IN ASTM C177 GUARDED HOT PLATE APPARATUS

Average Specimen Mean Temperature K	Total Heat Input Watts	Average Specimen ΔT K	Specimen Gage[2] cm	Specimen Thermal Conductivity W/m-K	Time to Temperature[3] hr	Environmental Conditions Press Nitrogen N/m^2
Specimen: AS-3C-1B-603 Run: 6613-134-3N1						
424	1.377	52	0.477	0.034	6.8	1,333
425	1.380	52	0.477	0.034	7.4	1,333
419	1.995	48	0.477	0.054	14.5	101,325
420	1.995	48	0.477	0.054	15.1	101,325
513	2.295	82	0.477	0.037	1.0	1,333
513	2.295	82	0.477	0.037	1.6	1,333
529	3.611	73	0.477	0.065	4.3	49,329
529	3.611	73	0.477	0.065	4.8	49,329
529	3.850	76	0.477	0.066	1.0	101,325
529	3.850	76	0.477	0.066	1.4	101,325
407	1.722	41	0.477	0.054	17.7	101,325
407	1.722	41	0.477	0.054	18.2	101,325
Specimen: AS-4C-1B-603 Run: 6613-142-3N1						
422	1.816	46	0.480	0.053	17.4	101,325
422	1.816	46	0.480	0.053	18.0	101,325
425	1.318	50	0.480	0.035	5.2	1,333
425	1.318	50	0.480	0.035	5.8	1,333
534	3.947	74	0.480	0.070	2.0	101,325
534	3.947	74	0.480	0.070	2.5	101,325
536	3.810	72	0.480	0.070	4.3	49,329
536	3.810	72	0.480	0.069	4.8	49,329
520	2.558	77	0.480	0.043	2.4	1,333
521	2.558	77	0.480	0.043	3.0	1,333

Notes:

1. Diameter of central heater = 4.826 cm.
2. Thermal Conductivity values based on measured thickness at each temperature level.
3. Time to temperature implies the elasped between adjustment of power and obtaining data.

TABLE 9

THERMAL CONDUCTIVITY OF THE FURNACE CHAR OF MATERIAL B FORMED AT 808 K
MEASURED IN THE GUARDED COMPARATIVE ROD APPARATUS

Specimen	Measured Temperature K: Top Reference And Guard T1 K	T2 K	T3 K	Specimen And Guard T4 K	T5 K	T6 K	Bottom Reference And Guard T7 K	T8 K	T9 K	ΔT_1 Top Reference K	K_1 Top Reference W/mK	ΔT_2 Bottom Reference K	K_2 Bottom Reference W/mK	ΔT_s Specimen K	Environmental Pressure N/m^2	Mean Temperature Specimen K	Measured Thermal Conductivity W/m K	True Thermal Conductivity Corrected For Radial Heat Exchange and Axial Heat Shunting W/m K
CR-1C-CB-31-1B	642.5	630.4	627.9	596.3	463.1	408.6	372.6	367.6	357.6	14.6	1.11	15.0	0.98	187.7	1333	502	0.061	0.058
Run: 6613-148-1	642.5	630.4	628.0	596.4	463.1	408.7	372.7	367.6	357.6	14.5	1.11	15.1	0.98	187.7	1333	503	0.061	0.058
	631.7	619.8	617.5	590.5	473.7	428.6	397.1	392.6	382.0	14.2	1.11	15.1	1.00	161.9	101325	510	0.071	0.064
Initial Thickness:	631.6	619.3	617.4	590.4	473.7	428.5	397.0	392.6	381.9	14.2	1.11	15.2	1.00	161.9	101325	509	0.071	0.064
0.635 cm	832.9	816.8	811.3	778.8	637.7	578.1	535.8	528.4	513.2	21.6	1.16	22.6	1.08	200.7	101325	678	0.091	0.082
Final Thickness:	832.9	816.9	811.3	778.8	637.7	578.0	535.7	528.4	513.1	21.6	1.16	22.6	1.08	200.8	101325	678	0.091	0.082
0.559 cm	862.6	844.9	839.4	804.1	654.1	591.3	546.5	537.2	521.9	23.2	1.17	24.6	1.08	212.8	49329	698	0.093	0.085
	862.6	845.2	839.5	804.2	654.2	591.4	546.6	537.4	522.0	23.2	1.17	24.6	1.08	212.8	49329	698	0.093	0.085
	850.1	836.2	830.6	795.5	652.3	585.0	541.1	534.4	521.1	19.5	1.16	19.9	1.08	210.4	1333	690	0.078	0.073
	849.9	836.1	830.5	795.3	652.1	584.8	540.9	534.2	521.0	19.4	1.16	19.9	1.08	210.5	1333	690	0.078	0.073
CR-3C-CB-0-1B	586.5	575.0	574.1	532.0	504.4	429.2	370.2	365.3	357.3	12.4	1.10	12.9	0.98	102.8	101325	481	0.068	0.061
Run: 6613-151-2	586.5	575.0	574.1	532.1	504.4	429.2	370.2	365.3	357.3	12.3	1.10	12.9	0.98	102.9	101325	481	0.068	0.061
	585.5	576.5	575.6	530.6	503.9	425.9	368.8	365.5	358.3	10.0	1.10	10.5	0.98	104.6	1333	478	0.054	0.051
Initial Thickness:	585.7	576.6	575.6	530.7	503.9	426.1	368.9	365.6	358.4	10.1	1.10	10.5	0.98	104.6	1333	478	0.054	0.052
0.691 cm	885.9	868.5	867.0	803.4	762.3	644.8	535.9	532.5	515.4	18.9	1.17	20.6	1.08	158.6	1333	724	0.075	0.067
Final Thickness:	886.1	868.3	867.3	803.6	762.5	645.1	536.2	528.3	515.7	18.8	1.17	20.6	1.08	158.5	1333	724	0.074	0.068
0.640 cm	886.8	876.4	866.1	806.0	768.9	655.0	545.8	537.3	522.7	20.7	1.17	23.1	1.08	151.0	49329	731	0.087	0.080
	887.0	876.6	866.1	806.1	769.0	655.1	545.9	537.3	522.8	20.8	1.17	23.1	1.08	151.0	49329	731	0.087	0.081
	878.0	858.4	855.6	799.9	763.7	651.9	544.8	535.3	519.1	22.4	1.17	25.7	1.08	148.1	101325	726	0.097	0.086
	878.2	858.7	855.7	800.1	763.9	652.0	545.0	535.5	519.3	22.5	1.17	25.7	1.08	148.1	101325	726	0.097	0.086

TABLE 10

THERMAL CONDUCTIVITY OF THE FURNACE CHAR OF MATERIAL B FORMED AT 1101 K
MEASURED IN THE GUARDED COMPARATIVE ROD APPARATUS

Specimen	Measured Temperature K: Top Reference And Guard T1 K	T2 K	T3 K	Specimen And Guard T4 K	T5 K	T6 K	Bottom Reference And Guard T7 K	T8 K	T9 K	ΔT_1 Top Reference K	K_1 Top Reference W/m K	ΔT_2 Bottom Reference K	K_2 Bottom Reference W/m K	ΔT_s Specimen K	Environmental Pressure N/m^2	Mean Temperature Specimen K	Measured Thermal Conductivity W/m K	True Thermal Conductivity Corrected For Radial Heat Exchange and Axial Heat Shunting W/m K
CR-1C-CB-43-3B	780.3	764.8	761.3	717.3	641.6	600.1	547.2	543.0	527.3	19.1	1.14	19.9	1.09	117.2	101325	659	0.114	0.102
Run: 6613-155-2	780.6	765.0	761.5	717.5	641.9	600.4	547.4	543.3	527.4	19.0	1.14	19.9	1.09	117.1	101325	659	0.114	0.102
	756.6	747.4	744.0	699.7	655.5	602.9	556.0	551.4	543.0	12.5	1.14	13.0	1.09	96.8	1333	651	0.090	0.085
Initial Thickness:	756.8	747.6	744.3	700.0	655.8	603.1	556.2	551.5	543.1	12.5	1.14	13.1	1.09	96.8	1333	652	0.090	0.085
0.635 cm	1125.0	1110.0	1103.5	1064.9	989.9	914.9	858.7	855.4	835.9	21.5	1.25	22.8	1.17	150.0	1333	990	0.110	0.097
Final Thickness:	1125.0	1110.3	1103.5	1064.9	989.9	914.9	858.6	855.3	835.9	21.5	1.25	22.7	1.17	150.0	1333	990	0.109	0.097
0.483 cm	1107.0	1091.9	1076.6	1039.8	973.2	906.6	861.9	854.6	830.6	30.4	1.24	31.3	1.17	133.2	49329	973	0.171	0.157
	1107.1	1092.0	1076.8	1040.0	973.3	906.8	862.1	854.8	830.8	30.4	1.25	31.3	1.17	133.2	49329	973	0.171	0.157
	1114.3	1097.4	1080.4	1042.4	973.8	905.2	859.3	851.0	825.6	33.8	1.25	33.6	1.16	137.2	101325	974	0.182	0.167
	1114.3	1097.4	1080.4	1042.5	973.9	905.3	859.3	851.1	825.7	33.8	1.25	33.6	1.16	137.2	101325	974	0.182	0.167
CR-2C-CB-44-3B	721.7	712.0	709.9	680.1	638.7	592.4	560.6	555.5	548.4	11.8	1.13	12.1	1.09	87.7	101325	636	0.108	0.100
Run: 6613-153-1	721.8	712.3	710.1	680.3	638.9	592.6	560.7	555.6	548.6	11.7	1.13	12.0	1.09	87.7	101325	636	0.107	0.099
	755.9	746.5	743.1	706.2	654.9	595.1	555.2	550.6	542.3	12.8	1.14	12.9	1.09	111.1	1333	651	0.092	0.087
Initial Thickness:	756.2	746.6	743.9	706.3	655.0	595.3	555.3	550.8	542.5	12.3	1.14	12.8	1.09	111.1	1333	651	0.090	0.085
0.635 cm	1133.7	1115.4	1109.4	1065.8	1007.8	923.2	854.9	853.1	828.9	24.3	1.26	26.1	1.16	142.6	1333	994	0.153	0.138
Final Thickness:	1133.4	1115.3	1109.1	1065.5	1007.5	923.0	854.7	853.4	828.9	24.3	1.26	25.8	1.16	142.5	1333	994	0.152	0.137
0.483 cm	1134.1	1114.1	1107.0	1066.0	1013.8	938.9	873.8	864.9	845.6	27.1	1.26	28.2	1.17	127.1	49329	1002	0.189	0.171
	1134.3	1114.3	1107.2	1066.1	1014.0	939.1	874.0	865.0	845.7	27.1	1.26	28.3	1.17	127.1	49329	1003	0.189	0.171
	1113.1	1092.4	1086.5	1046.5	994.9	924.1	860.4	850.1	832.0	26.6	1.25	28.3	1.17	122.4	101325	985	0.193	0.175
	1113.1	1092.3	1086.5	1046.5	995.0	924.1	860.4	850.2	832.1	26.6	1.25	28.3	1.17	122.4	101325	985	0.193	0.175

TABLE 11

THERMAL CONDUCTIVITY OF THE FURNACE CHAR OF MATERIAL B FORMED AT 1365 K
MEASURED IN THE GUARDED COMPARATIVE ROD APPARATUS

Specimen	Measured Temperature K									ΔT_1 Top Reference K	K_1 Top Reference W/m K	ΔT_2 Bottom Reference K	K_2 Bottom Reference W/m K	ΔT_s Specimen K	Environmental Pressure N/m^2	Mean Temperature Specimen K	Measured Thermal Conductivity W/m K	True Thermal Conductivity Corrected For Radial Heat Exchange and Axial Heat Shunting W/m K
	Top Reference And Guard			Specimen And Guard			Bottom Reference And Guard											
	T-1 K	T-2 K	T-3 K	T-4 K	T-5 K	T-6 K	T-7 K	T-8 K	T-9 K									
CR-2C-CB-49-3B	771.5	762.2	760.9	740.1	715.8	682.9	669.0	662.3	657.9	10.6	1.14	11.1	1.12	57.2	101325	711	0.153	0.143
Run: 6228-150-2	771.6	762.3	761.0	740.1	715.8	683.0	669.1	662.4	658.0	10.6	1.14	11.1	1.12	57.1	101325	712	0.153	0.144
Initial Thickness:	779.8	770.1	768.1	735.6	700.0	644.7	620.1	614.0	607.7	11.7	1.14	12.4	1.11	90.8	1333	690	0.107	0.101
0.637 cm	779.9	770.1	768.2	735.6	700.0	644.7	619.8	614.1	607.8	11.7	1.14	12.0	1.11	90.9	1333	690	0.105	0.100
Final Thickness:	1134.8	1114.6	1111.3	1059.7	1008.5	930.1	892.0	879.8	867.8	23.6	1.26	24.3	1.18	129.6	1333	995	0.161	0.148
0.569 cm	1134.9	1114.8	1111.3	1059.8	1008.5	930.1	892.0	879.8	867.8	23.6	1.26	24.2	1.18	129.7	1333	995	0.160	0.148
	1160.5	1139.1	1137.0	1092.6	1042.6	976.4	946.2	932.4	921.4	23.5	1.27	24.8	1.19	116.2	49329	1034	0.183	0.165
	1160.5	1138.0	1137.0	1092.6	1040.9	976.3	946.4	932.4	921.3	23.6	1.27	25.2	1.19	116.3	49329	1034	0.185	0.166
	1134.8	1112.3	1110.4	1063.8	1009.1	941.3	910.1	894.5	884.6	24.4	1.26	25.5	1.18	122.4	101325	1003	0.178	0.161
CR-1C-CB-49-3B	733.6	727.1	723.4	700.5	664.4	645.2	619.0	615.6	608.4	10.3	1.13	10.6	1.11	55.3	101325	673	0.151	0.142
Run: 6613-159-2	733.7	727.2	723.4	700.6	664.4	645.2	619.0	615.6	608.4	10.3	1.13	10.6	1.11	55.4	101325	673	0.151	0.142
Initial Thickness:	769.6	759.8	759.5	730.0	686.8	657.9	624.2	623.1	613.4	10.0	1.14	10.7	1.11	72.1	1333	694	0.116	0.107
0.638 cm	769.6	759.9	759.6	730.0	686.9	658.0	624.3	623.3	613.5	10.0	1.14	10.7	1.11	72.1	1333	694	0.116	0.107
Final Thickness:	1196.8	1174.3	1172.4	1105.4	1032.3	959.1	877.1	867.4	850.4	24.4	1.29	26.8	1.17	145.2	1333	1032	0.154	0.139
0.566 cm	1196.9	1174.4	1172.4	1105.4	1032.3	959.2	877.2	866.9	850.4	24.4	1.29	26.8	1.17	146.2	1333	1032	0.154	0.139
	1175.9	1162.0	1148.1	1082.9	1017.0	951.2	875.6	864.0	845.6	27.8	1.28	30.0	1.17	131.7	49329	1017	0.192	0.180
	1175.9	1162.0	1148.1	1082.8	1016.9	951.1	875.5	863.9	845.5	27.8	1.28	30.0	1.17	131.7	49329	1017	0.192	0.180
	1168.5	1154.8	1140.9	1075.9	1009.5	946.0	871.5	860.3	840.9	27.6	1.27	30.6	1.17	129.9	101325	1011	0.195	0.183
	1168.6	1154.8	1141.0	1076.0	1011.0	946.0	871.5	860.3	841.0	27.6	1.27	30.4	1.17	129.9	101325	1011	0.195	0.182
CR-3C-CB-67-3B	653.4	641.4	637.6	605.4	557.3	521.6	484.2	478.3	467.5	15.8	1.11	16.7	1.06	83.8	101325	563	0.149	0.140
Run: 6228-152-2	653.5	641.4	637.6	605.4	557.3	521.5	484.1	478.3	467.5	15.8	1.11	16.6	1.06	83.8	101325	563	0.149	0.140
Initial Thickness:	656.3	646.6	644.3	612.0	559.6	525.1	485.2	481.5	472.5	12.1	1.11	12.6	1.06	86.9	1333	569	0.109	0.104
0.634 cm	656.3	646.5	644.3	612.0	559.6	525.1	485.2	481.6	472.6	12.0	1.11	12.6	1.06	86.9	1333	569	0.109	0.104
Final Thickness:	1144.5	1113.7	1108.7	1035.6	951.7	875.0	797.5	783.7	756.8	35.8	1.26	40.7	1.14	160.6	1333	955	0.202	0.186
0.635 cm	1144.6	1113.7	1108.7	1035.6	951.7	875.1	797.5	783.8	756.8	35.9	1.26	40.7	1.14	160.5	1333	955	0.203	0.186
	1150.3	1123.6	1113.3	1043.3	959.7	875.7	804.4	787.5	761.2	37.0	1.26	43.3	1.15	167.6	49329	960	0.203	0.187
	1143.5	1115.9	1106.4	1036.5	952.8	870.1	799.1	781.9	755.8	37.1	1.26	43.3	1.14	166.4	101325	953	0.205	0.187
	1171.5	1141.9	1136.7	1063.4	977.9	897.3	816.2	802.6	776.2	34.8	1.27	40.0	1.15	166.1	1333	980	0.193	0.177

TABLE 12

THERMAL CONDUCTIVITY OF THE FURNACE CHAR OF MATERIAL B FORMED AT 1365K
MEASURED IN THE RADIAL INFLOW APPARATUS

	Time	Outer Face Temperature K	Average ΔT of Each Strip K	Heat Flow to Calorimeter Watts	Average Mean Temperature of Specimen K	Average Thermal Conductivity $\frac{W}{mK}$	Environmental Pressure $\frac{N}{m^2}$
Specimen No. RI-1C-CB-48,52 & 53-3B	On 7:30		204 213 -				
	Read 9:00		212 —				
Run: 7133-44-69-2-GFE	Avg		210	13	841	0.130	1333
Initial Thickness 0.254 cm	Read 10:20		—				
	Avg	1334	266	40	1212	0.306	101325
			248 263 -				
	Read 10:50		262 —				
	Avg	1311	258	40	1217	0.314	49329
			249 257 -				
	Read 11:25		251 —				
	Avg	1338	252	24	1224	0.187	1333
Specimen No. RI-2C-CB-53,64 & 66-3B	On 10:45		144 135 134				
	Read 12:15		137 —				
Run: 7133-4-69-2-GFE	Avg		137	13	843	0.202	101325
Initial Thickness 0.254 cm			165 149 157				
Final Thickness 0.246 cm	Read 2:30		159 —				
	Avg	1356	157	24	1276	0.306	101325
			154 139 147				
	Read 3:00		149 —				
	Avg	1343	147	26	1269	0.353	49329
			124 112 120				
	Read 3:25		126 —				
	Avg	1354	121	14	1286	0.241	1333
Specimen No. RI-3c-CB-68 & 72-3B			204 216 206				
	On 2:15		203 —				
Run: 7133-54-69-2	Avg		207	15	789	0.146	1333
Initial Thickness 0.254 cm			188 203 196 192				
	3:30		—				
	Avg		194	21	811	0.221	49329
			195 204 197 192				
	4:45		—				
	Avg		197	22	809	0.229	101325
			261 268 262 264				
	6:45		—				
	Avg		264	27	1203	0.206	1333
			259 268 257 257				
	8:05		—				
	Avg		261	41	1225	0.320	49329
			259 271 258 257				
	9:15		—				
	Avg		261	48	1239	0.372	101325

Note: Calculation of Thermal Conductivity

$$K = \frac{Q\Delta X}{A\Delta T}$$

where

- K = thermal conductivity
- ΔX = specimen thickness
- Q = heat flow to 1.27 cm calorimeter gage section
- A = gage area of specimen (total for 4 strips) = 11.5 cm^2
- ΔT = temperature drop across specimen

TABLE 13

THERMAL CONDUCTIVITY OF THE FURNACE CHAR OF MATERIAL B FORMED AT 1729 K
MEASURED IN THE GUARDED COMPARATIVE ROD APPARATUS

Specimen	Measured Temperature K									ΔT_1 Top Reference K	K_1 Top Reference W/m K	ΔT_2 Bottom Reference K	K_2 Bottom Reference W/m K	ΔT_s Specimen K	Environmental Pressure N/m^2	Mean Temperature Specimen K	Measured Thermal Conductivity W/m K	True Thermal Conductivity Corrected For Radial Heat Exchange and Axial Heat Shunting W/m K
	Top Reference And Guard			Specimen And Guard			Bottom Reference And Guard											
	T1 K	T2 K	T3 K	T4 K	T5 K	T6 K	T7 K	T8 K	T9 K									
CR-1C-CB-57-3B	768.8	756.5	748.8	720.1	679.2	641.1	601.0	595.4	579.3	20.1	1.14	21.8	1.10	78.9	101325	681	0.182	0.171
Run: 6613-157-1	768.9	756.5	748.7	720.0	679.2	641.1	601.0	595.4	579.3	20.2	1.14	21.8	1.10	78.9	101325	681	0.183	0.171
	828.1	811.3	806.0	767.8	626.3	656.8	598.9	593.3	575.9	22.1	1.16	23.0	1.10	111.0	1333	712	0.141	0.133
Initial Thickness:	828.2	811.4	806.1	767.9	726.4	656.9	599.0	593.4	575.9	22.1	1.16	23.0	1.10	111.0	1333	712	0.141	0.133
0.635 cm	1197.9	1176.8	1165.4	1115.1	1055.2	1001.3	935.7	929.3	899.6	32.5	1.29	35.4	1.19	113.8	1333	1058	0.226	0.208
Final Thickness:	1198.0	1176.9	1165.5	1112.5	1055.3	1000.9	935.1	929.9	899.9	32.6	1.29	35.3	1.19	111.6	1333	1057	0.231	0.212
0.533 cm	1166.4	1144.3	1137.1	1090.7	1040.8	995.9	943.4	932.9	911.0	29.3	1.27	32.4	1.19	94.8	49329	1043	0.246	0.222
	1166.5	1144.3	1137.1	1090.8	1040.9	996.0	943.4	932.9	911.0	29.3	1.27	32.4	1.19	94.8	49329	1043	0.246	0.222
	1177.0	1160.8	1144.5	1095.1	1042.2	995.1	940.1	927.5	905.1	32.5	1.28	35.0	1.19	100.1	101325	1045	0.255	0.240
CR-2C-CB-57-3B	779.8	768.1	762.1	734.1	697.9	661.8	636.3	628.8	617.4	17.7	1.14	17.9	1.11	72.3	101325	698	0.170	0.160
Run: 6226-148-1	779.9	768.2	762.1	734.1	698.0	661.8	636.4	628.9	618.5	17.7	1.14	17.9	1.11	72.3	101325	698	0.170	0.160
	783.2	773.0	768.5	740.7	703.3	666.3	640.0	635.9	625.6	14.7	1.14	15.3	1.11	74.4	1333	704	0.140	0.133
Initial Thickness:	783.3	773.1	768.6	740.8	703.4	666.4	641.0	636.0	625.6	14.8	1.14	15.4	1.11	74.4	1333	704	0.140	0.133
0.635 cm	1201.5	1180.2	1172.1	1119.3	1057.1	995.0	949.4	937.3	918.1	29.3	1.29	31.2	1.19	124.3	1333	1057	0.186	0.171
Final Thickness:	1201.5	1180.3	1172.2	1119.4	1057.2	995.0	949.5	937.4	918.2	29.3	1.29	31.3	1.19	124.4	1333	1057	0.186	0.171
0.559 cm	1187.9	1165.6	1153.3	1102.6	1043.8	985.0	941.0	926.2	904.5	34.7	1.28	36.5	1.19	117.6	49329	1044	0.229	0.212
	1187.9	1165.6	1153.3	1102.6	1043.8	985.0	941.0	926.1	904.5	34.7	1.28	36.6	1.19	117.6	49329	1044	0.230	0.213
	1168.5	1146.5	1134.3	1084.9	1028.2	971.5	928.6	910.4	891.9	34.3	1.27	36.7	1.19	113.4	101325	1028	0.236	0.221

TABLE 14

THERMAL CONDUCTIVITY OF THE FURNACE CHAR OF MATERIAL B FORMED AT 1729K
MEASURED IN THE RADIAL INFLOW APPARATUS

	Time	Outer Face Temperature K	Average ΔT of Each Strip K	Heat Flow to Calorimeter Watts	Average Mean Temperature of Specimen K	Average Thermal Conductivity $\frac{W}{mK}$	Environmental Pressure $\frac{N}{m^2}$
Specimen No.: RI-1C-CB-55 & 56-3B	On		126				
	7:20		124				
	Read		123				
Run:	8:15		122				
7133-14-69-2-GFE	Avg		124	11	802	0.171	1333
Initial Thickness			141				
			138				
Final Thickness	Read		137				
	8:40		136				
	Avg		138	16	807	0.209	101325
			169				
			166				
	Read		167				
	9:15		163				
	Avg	1239	166	16	1169	0.177	1333
			181				
			178				
	Read		177				
	9:50		174				
	Avg	1239	178	28	1163	0.290	101325
			204				
			202				
	Read		202				
	11:30		198				
	Avg	1722	202	48	1616	0.414	101325
			194				
			200				
	Read		193				
	12:15		-				
	Avg	1711	196	41	1606	0.378	49329
			-				
			181				
	Read		156				
	1:00		-				
	Avg	1722	168	27	1621	0.270	1333
Specimen No.: RI-2C-CB-58,60,62-3B	On		137				
	7:20		-				
	Read		150				
Run:	8:40		144				
7133-28-69-2-GFE	Avg		144	13	819	0.186	1333
Initial Thickness			152				
			-				
Final Thickness	Read		164				
	9:30		153				
	Avg		156	18	815	0.233	101325
			179				
			-				
	Read		194				
	10:30		186				
	Avg	1222	187	20	1130	0.212	1333
			197				
			-				
	Read		209				
	11:00		197				
	Avg		201	32	1127	0.310	101325
			223				
			203				
	Read		226				
	12:10		219				
	Avg	1691	218	56	1568	0.492	101325
			213				
			182				
	Read		203				
	12:45		200				
	Avg	1689	199	47	1586	0.454	49329
			197				
			178				
	Read		184				
	1:25		189				
	Avg	1683	187	32	1596	0.320	1333

Note: Calculation of Thermal Conductivity

$$K = \frac{Q\Delta X}{A\Delta T}$$

where

- K = thermal conductivity
- ΔX = specimen thickness
- Q = heat flow to 1.27 cm calorimeter gage section
- A = gage area of specimen (total for 4 strips) = 11.5 cm^2
- ΔT = temperature drop across specimen

TABLE 15

BOXING ANALYSIS OF THERMAL CONDUCTIVITY

Temperature of Char Formation K	Environmental Pressure N/m^2	Thermal Conductivity W/m K
600	101325 49329 1333	0.076 0.075 0.045
808	101325 49329 1333	0.096 0.092 0.078
1100	101325 49329 1333	0.197 0.185 0.127
1365	101325 49329 1333	0.343 0.323 0.201
1729	101325 49329 1333	0.507 (0.68)[1] 0.461 (0.54) 0.322 (0.38)

[1]Values in parentheses extrapolated from trend of data at lower temperatures since furnace char at 1700; did not appear to represent flight char crust.

Table 16

Bulk Density of Furnace Chars of Material B
Formed at Temperatures from 600K to 1700K

Specimen No.	Maximum Temperature K	Length cm	Width cm	Thickness cm	Weight gm	Bulk Density gm/cm^3	Average Bulk Density gm/cm^3
BD-1-CB-29-1B	588	3.81	3.642	1.687	6.1335	0.2620	
BD-1-CB-23-1B	600	3.746	3.449	2.299	7.0438	0.2371	0.2495
BD-1-CB-32-1B	812	3.510	0.218	0.914	1.2218	0.1742	
BD-2-CB-32-1B	812	3.696	3.668	0.945	2.3795	0.1857	0.1800
BD-1-CB-30-1B	808	4.013	3.797	0.686	1.8820	0.1800	
BD-1-CB-45-3B	1103	7.290	3.467	0.883	4.4015	0.1958	
BD-1-CB-46-3B	1098	7.280	3.378	0.698	3.6625	0.2132	0.2045
BD-1-CB-47-3B1	1366	1.674	1.283	0.307	0.1450	0.2197	
BD-2-CB-47-3B2	1366	1.524	1.415	0.521	0.2228	0.1983	
BD-1-CB-40-1B1	1382	3.383	2.172	0.538	0.9255	0.2339	0.2223
BD-2-CB-40-1B2	1382	3.536	2.939	0.470	1.1600	0.2376	
BD-1-CB-59-3B	1735	7.640	3.548	0.495	2.7028	0.2012	
BD-1-CB-63-3B1	1745	3.632	3.581	0.594	1.6322	0.2110	0.2025
BD-2-CB-63-3B2	1745	3.038	1.918	0.310	0.3528	0.1954	

Note: Specimens prepared from near heated surface; core or center of char blanks were not used.

TABLE 17

TRUE DENSITY OF THE FURNACE
AND ARC-JET CHARS OF MATERIAL B

Specimen No.	Maxium Temperature of Formation K	True Density at 299K gm/cm^3
TD-CB-29-1B	588	1.49
TD-CB-32-1B	812	1.43
TD-CB-45-3B	1103	1.81
TD-CB-47-3B	1366	1.70
TD-CB-59-3B	1735	1.77
TD-1-B1-AJ-5*	-	1.57
TD-1-B1-AJ-4	-	1.78
TD-1-B1-AJ-3	-	1.80
TD-1-B1-AJ-2	-	1.64
TD-1-B1-AJ-1	-	2.40

* Diagram of Arc Jet Char with Zones 1 through 5 indicated.

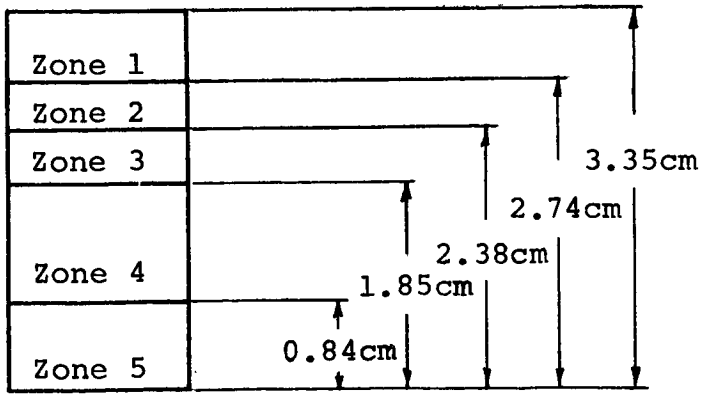

TABLE 18

TOTAL POROSITY OF THE FURNACE CHARS
OF MATERIAL B

Temperature of Char Formation K	True Density gm/cm^3	Bulk Density gm/cm^3	Total Porosity %
600	1.49	0.2495	83
812	1.43	0.1800	87
1103	1.81	0.2045	89
1366	1.70	0.2223	87
1735	1.77	0.2025	89

TABLE 19

ENTHALPY OF THE FURNACE CHAR OF MATERIAL B FORMED AT 800K
MEASURED IN THE ADIABATIC CALORIMETER

Specimen and Run Number	Initial Cup Temp. K	Final Cup Temp. K	Change in Cup Temp. K	Initial Sample Temp. K	Time at Temp. Min	Initial Wt. of Sample gm	Final Wt. of Sample gm	Enthalpy 303K Reference J/g	Enthalpy 273K Reference J/g
CB-26-1B-798 (R2D) - 1									
Run No. 1	296.18	297.24	1.06	417.22	20	3.9263	3.8229	120.8	146.4
Run No. 2	298.08	300.91	2.83	583.33	20	3.8229	3.7804	343.7	369.3
Run No. 3	301.28	303.96	2.68	590.39	20	3.7804	3.7785	327.9	353.5
Run No. 4	297.21	302.47	5.27	810.00	20	3.7785	3.6340	670.0	695.6
CB-26-1B-798 (R2D) - 2									
Run No. 1	297.28	298.06	0.78	420.28	20	2.7869	2.7357	123.8	149.3
Run No. 2	300.84	302.82	1.98	583.61	20	2.7357	2.7107	332.2	357.7
Run No. 3	300.14	303.93	3.79	809.83	20	2.7107	2.5715	672.4	697.9

TABLE 20

ENTHALPY OF THE FURNACE CHAR OF MATERIAL B FORMED AT 1100K
MEASURED IN THE ADIABATIC CALORIMETER

Specimen and Run Number	Initial Cup Temp. K	Final Cup Temp. K	Change in Cup Temp. K	Initial Sample Temp. K	Time at Temp. Min	Initial Wt. of Sample gm	Final Wt. of Sample gm	Enthalpy 303K Reference J/g	Enthalpy 273K Reference J/g
CB-38-1B-1105 (R2D) - 1									
Run No. 1	295.38	296.51	1.126	420.56	20	4.6421	4.5100	109.8	128.4
Run No. 2	297.78	300.52	2.74	585.00	20	4.5100	4.4143	286.1	304.7
Run No. 3	295.62	301.06	5.44	811.94	20	4.4143	4.3906	573.9	592.5
CB-38-1B-1105 (R2D) - 2									
Run No. 1	296.56	297.75	1.18	420.94	20	5.3185	5.0847	104.1	122.7
Run No. 2	300.48	303.47	2.99	583.89	20	5.0847	5.0582	277.2	295.8

TABLE 21

ENTHALPY OF THE FURNACE CHAR OF MATERIAL B FORMED AT 1100K
MEASURED IN THE ICE CALORIMETER

Specimen Number	SRI Run Number	Drop Temperature K	Initial Weight Grams	Final Weight Grams	Enthalpy 273K Reference J/g
CB-38-1B-1105 (R2D) -1	7155-21				
	Run No. 1	815.56	2.1442	2.0426	647.6
	Run No. 2	1095.56	2.0426	2.0080	1207.7
CB-38-1B-1105 (R2D) -2					
	Run No. 1	1103.33	2.1925	2.0606	1373.1

TABLE 22

ENTHALPY OF THE FURNACE CHAR OF MATERIAL B FORMED AT 1370K
MEASURED IN THE ADIABATIC CALORIMETER

Specimen and Run Number	Initial Cup Temp. K	Final Cup Temp. K	Change in Cup Temp. K	Initial Sample Temp. K	Time at Temp. Min	Initial Wt. of Sample gm	Final Wt. of Sample gm	Enthalpy 303K Reference J/g	Enthalpy 273K Reference J/g
CB-42-3B-1374 (R2D) - 1									
Run No. 1	297.16	298.59	1.43	528.06	20	3.2306	3.0625	210.7	229.3
Run No. 2	298.62	302.29	3.67	812.39	20	3.0625	3.0505	559.2	577.8
CB-42-3B-1374 (R2D) - 2	298.52	299.91	1.39	528.33	20	3.1730	3.0134	209.5	228.1

TABLE 23

ENTHALPY OF THE FURNACE CHAR OF MATERIAL B FORMED AT 1370K
MEASURED IN THE ICE CALORIMETER

Specimen Number	SRI Run Number	Drop Temperature K	Initial Weight Grams	Final Weight Grams	Enthalpy 273K Reference J/g
CB-42-3B-1374 (R2D) -1	7155-22				
	Run No. 1	813.33	2.3615	2.2805	692.8
	Run No. 2	1108.89	2.2736	2.2506	1175.5
	Run No. 3	1371.67	2.2506	2.1925	1625.7
CB-42-3B-1374 (R2D) -2	7155-23				
	Run No. 1	1113.89	2.5041	2.3807	1265.5
	Run No. 2	1371.67	2.3807	2.3142	1571.9
CB-40-1B-1382 (R2D) -1	7155-29				
	Run No. 1	1095	2.1570	2.0465	1095.2
	Run No. 2	1259.44	2.0465	2.0305	1321.1
	Run No. 3	1360.56	2.0305	1.9872	1775.2

TABLE 24

ENTHALPY OF THE FURNACE CHAR OF MATERIAL B FORMED AT 1740K
MEASURED IN THE ADIABATIC CALORIMETER

Specimen and Run Number	Initial Cup Temp. K	Final Cup Temp. K	Change in Cup Temp. K	Initial Sample Temp. K	Time at Temp. Min	Initial Wt. of Sample gm	Final Wt. of Sample gm	Enthalpy 303K Reference J/g	Enthalpy 273K Reference J/g
CB-54-3B-1739 (R2D) - 1									
Run No. 1	299.45	301.39	1.94	530.56	20	4.4052	4.2616	207.4	223.7
Run No. 2	300.26	305.35	5.09	812.22	20	4.2616	4.2363	561.2	577.4
CB-54-3B-1739 (R2D) - 2									
Run No. 1	301.10	302.75	1.65	530.56	20	3.7790	3.6559	207.4	223.7

TABLE 25

ENTHALPY OF THE FURNACE CHAR OF MATERIAL B FORMED AT 1740K
MEASURED IN THE ICE CALORIMETER

Specimen Number	SRI Run Number	Drop Temperature K	Initial Weight Grams	Final Weight Grams	Enthalpy 273K Reference J/g
CB-54-3B-1739 (R2D) -1	7155-25				
	Run No. 1	810.56	2.4754	2.3807	555.6
	Run No. 2	1377.22	2.3710	2.3525	1624.4
	Run No. 3	1730.00	2.3525	2.0709	2271.3
CB-54-3B-1739 (R2D) -2					
	Run No. 1	1101.11	2.4376	2.3322	1181.7
	Run No. 2	1363.33	2.3322	2.3117	1605.4
	Run No. 3	1721.67	2.3117	1.5205	2344.1
CB-59-3B-1735 (R2D) -3					
	Run No. 1	1150.56	2.2434	2.1608	1224.4
	Run No. 2	1427.78	2.1608	2.1467	1728.9
	Run No. 3	1702.22	1.9033	1.7394	2302.7

TABLE 26

THE PERMEABILITY OF THE FURNACE CHAR OF MATERIAL B FORMED AT 590 K

Permeating Gas	Gage Pressure at Flowmeter (N/m^2)	Pressure Drop through Specimen (P_2-P_1) ΔP (N/m^2)	Downstream Gage Pressure P_1 (N/m^2)	Absolute Mean Specimen Pressure P_m (N/m^2)	Downstream Gas Temperature K	Volumetric Flow Rate Corrected to Standard Conditions Qstp (cm^3/sec)	$\frac{MPm\Delta P}{LTR\mu G}$ (cm^{-2})	$\frac{G}{\mu}$ (cm^{-1})
Specimen: Pe-1c-33-1B; A = 5.108 cm^2; T = 0.631 cm; Density = 0.2540 gm/cm^3								
Helium	68950	6094.44	0.00	104404	294	187	13.7 $x10^6$	30
	68950	10834.56	0.00	106774	294	323	14.4	52
Helium	68950	15574.68	0.00	109144	294	483	14.2	79
Nitrogen	68950	2844.72	2.49	102781	294	89	14.9	115
	68950	4897.31	4.98	103810	294	146	15.8	188
Nitrogen	68950	7084.40	7.47	104906	294	208	16.2	269
Specimen: Pe-2c-33-1B; A = 5.087 cm^2; T = 0.634 cm; Density = 0.2560 gm/cm^3								
Helium	68950	3995.24	0.00	103354	294	130	12.7	21
	68950	7381.04	2.49	105050	294	240	12.9	39
	68950	10902.28	4.98	106813	294	353	13.1	58
Helium	68950	14558.94	7.47	108643	294	483	13.1	79
Nitrogen	68950	2099.20	0.00	102406	294	67	14.4	86
	68950	3453.52	2.49	103086	294	112	14.3	145
	68950	4875.55	2.49	103797	294	158	14.4	205
Nitrogen	68950	6568.45	2.49	104643	294	208	14.8	270

TABLE 27

THE PERMEABILITY OF THE FURNACE CHAR OF MATERIAL B FORMED AT 800 K

Permeating Gas	Gage Pressure at Flowmeter (N/m^2)	Pressure Drop through Specimen (P_2-P_1) ΔP (N/m^2)	Downstream Gage Pressure P_1 (N/m^2)	Absolute Mean Specimen Pressure P_m (N/m^2)	Downstream Gas Temperature K	Volumetric Flow Rate Corrected to Standard Conditions Qstp (cm^3/sec)	$\frac{MPm\Delta P}{LTR\mu G}$ (cm^{-2})	$\frac{G}{\mu}$ (cm^{-1})
Specimen: Pe-1c-31-1B; A = 5.077 cm^2; T = 1.827 cm; Density = 0.2300 gm/cm^3								
Helium	68950	1101.02	2.49	101901	294	130	1.1 x10^6	21
	68950	2127.31	4.98	102425	294	240	1.2	39
	68950	3238.30	7.47	102983	294	353	1.3	58
	68950	4513.69	9.96	103623	294	483	1.3	79
	103425	3019.09	12.45	102879	294	330	1.3	54
	103425	4135.06	17.44	103441	294	447	1.3	73
	103425	5330.74	22.42	104044	294	570	1.3	93
Helium	103425	7333.50	34.87	105058	294	765	1.3	126
Nitrogen	68950	553.00	0.00	101633	294	67	1.3	87
	68950	1031.27	0.00	101872	294	112	1.4	145
	68950	1574.31	2.49	102146	294	158	1.5	205
	68950	2231.94	2.49	102475	294	208	1.7	270
	103425	577.91	0.00	101645	294	66	1.3	85
	103425	1041.24	2.49	101880	294	108	1.5	140
	103425	1574.31	4.98	102149	294	154	1.6	200
	103425	2107.39	7.47	102418	294	202	1.6	262
	103425	2730.14	9.96	102732	294	252	1.7	327
Nitrogen	103425	3427.62	12.45	103083	294	302	1.8	392
Helium	68950	388.60	0.00	101551	795	36	0.2	2
	68950	1619.15	2.49	102169	794	130	0.3	10
	68950	3093.82	4.98	102908	789	240	0.3	18
Helium	68950	4438.96	9.96	103586	787	353	0.3	27
Nitrogen	68950	318.85	0.00	101516	792	23	0.3	13
	68950	856.90	2.49	101787	794	67	0.3	38
	68950	1404.92	186.83	102246	793	112	0.3	64
	68950	2281.76	149.46	102647	795	158	0.3	90
	68950	2949.34	548.02	103379	797	208	0.3	119
	103425	2202.04	24.91	102482	799	154	0.3	88
	103425	3029.06	49.82	102921	797	202	0.3	115
	103425	3935.78	69.75	103394	796	252	0.4	144
	103425	4972.04	74.73	103917	794	302	0.4	173
	103425	443.40	12.45	101591	294	108	0.6	140
	103425	572.93	49.82	101693	294	154	0.5	200
	103425	747.30	97.15	101827	294	202	0.5	262
	103425	911.71	146.97	101959	294	252	0.5	327
	103425	1140.88	201.77	102129	294	302	0.6	392
Nitrogen	68950	687.52	169.39	101870	294	208	0.5	270
Specimen: Pe-2C-31-1B; A = 5.077 cm^2; T = 0.640 cm; Density = 0.1812 gm/cm^3								
Nitrogen	68950	637.70	0.00	101675	294	112	2.5	145
	68950	976.47	0.00	101845	294	158	2.8	205
	68950	1424.85	0.00	102069	294	208	3.1	270
	103425	602.82	0.00	101658	294	108	2.5	140
	103425	936.62	7.47	101832	294	154	2.7	200
	103425	1335.18	7.47	102032	294	202	3.0	262
	103425	1718.79	9.96	102226	294	252	3.1	327
Nitrogen	103425	2236.92	12.45	102487	294	302	3.3	392

TABLE 28

THE PERMEABILITY OF THE FURNACE CHAR OF MATERIAL B FORMED AT 1098 K

Permeating Gas	Gage Pressure at Flowmeter (N/m^2)	Pressure Drop through Specimen (P_2-P_1) ΔP (N/m^2)	Downstream Gage Pressure P_1 (N/m^2)	Absolute Mean Specimen Pressure P_m (N/m^2)	Downstream Gas Temperature K	Volumetric Flow Rate Corrected to Standard Conditions Qstp (cm^3/sec)	$\frac{MPm\Delta P}{LRT\mu G}$ (cm^{-2})	$\frac{G}{\mu}$ (cm^{-1})
Specimen: Pe-1c-46-3B; A = 5.067 cm^2; T = 0.699 cm; Density = 0.1618 gm/cm^3								
Nitrogen	68950	159.42	2.49	101439	294	67	0.9 x10^6	87
	68950	274.01	2.49	101496	294	112	1.0	146
	68950	388.60	2.49	101553	294	158	1.0	205
	68950	533.07	4.98	101628	294	208	1.0	271
	103425	264.05	2.49	101491	294	108	1.0	140
	103425	408.52	2.49	101563	294	154	1.0	200
	103425	508.16	2.49	101613	294	202	1.0	263
	103425	632.71	7.47	101680	294	252	1.0	328
Nitrogen	103425	812.07	7.47	101770	294	302	1.1	393
Helium	68950	308.88	4.98	101516	809	36	0.5	2
	68950	1150.84	14.95	101947	810	130	0.5	10
	68950	2202.04	24.91	102482	809	240	0.5	18
	68950	3327.98	29.89	103050	809	353	0.5	27
	68950	4458.89	39.86	103626	808	483	0.5	37
	103425	2057.57	19.93	102405	812	218	0.5	16
	103425	3093.82	27.40	102931	811	330	0.5	25
	103425	4329.36	44.84	103566	813	447	0.6	34
	103425	5495.15	52.31	104156	813	570	0.6	44
Helium	103425	6984.76	77.22	104926	813	690	0.6	53
Nitrogen	68950	672.57	7.47	101700	814	67	0.6	38
	68950	1165.79	14.95	101954	813	112	0.6	64
	68950	1688.90	19.93	102221	812	158	0.7	90
	68950	2401.32	24.91	102582	811	208	0.7	119
	103425	1125.93	9.96	101929	813	108	0.6	61
	103425	1649.04	14.95	102196	812	154	0.7	88
	103425	2202.04	22.42	102480	810	202	0.7	115
	103425	2635.48	32.38	102707	809	252	0.6	144
Nitrogen	103425	3646.82	39.86	103220	810	302	0.8	173
	68950	174.37	0.00	101444	294	67	1.0	87
	68950	303.90	2.49	101511	294	112	1.1	146
	68950	438.42	4.98	101581	294	158	1.1	205
	68950	602.82	7.47	101665	294	208	1.1	271
	103425	303.90	2.49	101511	294	108	1.1	140
	103425	423.47	4.98	101573	294	154	1.1	200
	103425	557.98	7.47	101643	294	202	1.1	263
	103425	727.37	12.45	101733	294	252	1.1	328
Nitrogen	103425	861.89	17.44	101805	294	302	1.1	393
Specimen: Pe-2c-46-3B; A = 5.067 cm^2; T = 0.765 cm; Density = 0.1861 gm/cm^3								
Nitrogen	68950	557.98	4.98	101640	294	112	1.8	146
	68950	802.10	7.47	101765	294	158	1.9	205
	68950	1076.11	12.45	101907	294	208	1.9	271
	103425	528.09	4.98	101626	294	108	1.8	140
	103425	757.26	12.45	101748	294	154	1.8	200

TABLE 29

THE PERMEABILITY OF THE FURNACE CHAR OF MATERIAL B FORMED AT 1366 K

Permeating Gas	Gage Pressure at Flowmeter (N/m^2)	Pressure Drop through Specimen (P_2-P_1) ΔP (N/m^2)	Downstream Gage Pressure P_1 (N/m^2)	Absolute Mean Specimen Pressure P_m (N/m^2)	Downstream Gas Temperature K	Volumetric Flow Rate Corrected to Standard Conditions Qstp (cm^3/sec)	$\frac{MP_m\Delta P}{LRT\mu G}$ (cm^{-2})	$\frac{G}{\mu}$ (cm^{-1})
Specimen: Pe-1c-47-3B; A = 5.067 cm^2; T = 0.630 cm; Density = 0.2108 gm/cm^3								
Nitrogen	68950	194.30	0.00	101454	294	67	1.3 x10^6	87
	68950	323.83	0.00	101518	294	112	1.3	146
	68950	458.34	0.00	101586	294	158	1.3	205
	68950	592.86	4.98	101658	294	208	1.2	271
	103425	443.40	0.00	101578	294	154	1.3	200
	103425	577.91	7.47	101653	294	202	1.3	263
	103425	692.50	9.96	101713	294	252	1.2	328
Nitrogen	103425	861.89	9.96	101797	294	302	1.3	393
Helium	68950	1454.74	14.95	102099	809	130	0.7	10
	68950	2665.37	19.93	102709	808	240	0.7	18
	68950	3925.82	29.89	103349	809	354	0.7	27
	68950	5236.08	39.86	104014	808	483	0.7	37
	103425	2640.92	19.93	102697	814	218	0.8	16
	103425	3927.53	27.40	103348	813	330	0.8	25
	103425	5010.98	32.38	103894	812	447	0.7	34
	103425	6703.88	47.33	104756	811	570	0.8	44
Helium	103425	8058.20	64.77	105450	812	693	0.8	53
Nitrogen	68950	737.34	0.00	101725	811	67	0.8	38
	68950	1275.39	2.49	101997	811	112	0.8	64
	68950	1868.25	7.47	102298	810	158	0.8	90
	68950	2570.71	14.95	102657	811	208	0.9	119
	103425	1220.59	4.98	101972	813	108	0.8	61
	103425	1848.32	9.96	102291	812	154	0.8	88
	103425	2421.25	14.95	102582	812	202	0.8	115
	103425	3093.82	19.93	102923	811	252	0.9	144
	103425	3846.10	32.38	103312	811	302	0.9	173
	68950	219.21	0.00	101466	294	67	1.4	87
	68950	363.69	2.49	101541	294	112	1.4	146
	68950	513.15	2.49	101616	294	158	1.4	205
	68950	667.59	4.98	101695	294	208	1.4	271
	103425	368.67	0.00	101541	294	108	1.5	140
	103425	508.16	0.00	101611	294	154	1.5	200
	103425	642.68	2.49	101680	294	202	1.4	263
	103425	807.08	4.98	101765	294	252	1.4	328
Nitrogen	103425	1011.35	4.98	101867	294	302	1.5	393
Specimen: Pe-2c-42-3B; A = 5.067 cm^2; T = 0.635 cm; Density = 0.1894 gm/cm^3								
Nitrogen	68950	69.75	0.00	101391	294	23	1.3	29
	68950	119.57	0.00	101416	294	67	0.8	87
	68950	189.32	0.00	101451	294	112	0.7	146
	68950	259.06	0.00	101486	294	158	0.7	205
	68950	353.72	0.00	101533	294	208	0.7	271
	103425	189.32	0.00	101451	294	108	0.7	140
	103425	254.08	0.00	101484	294	154	0.7	200
	103425	338.78	0.00	101526	294	202	0.7	263
	103425	418.49	9.96	101576	294	252	0.7	328
	103425	533.07	17.44	101640	294	302	0.7	393

TABLE 30

THE PERMEABILITY OF THE FURNACE CHAR OF MATERIAL B FORMED AT 1745 K

Permeating Gas	Gage Pressure at Flowmeter (N/m^2)	Pressure Drop through Specimen (P_2-P_1) ΔP (N/m^2)	Downstream Gage Pressure P_1 (N/m^2)	Absolute Mean Specimen Pressure P_m (N/m^2)	Downstream Gas Temperature K	Volumetric Flow Rate Corrected to Standard Conditions Qstp (cm^3/sec)	$\frac{MPm\Delta P}{LRT\mu G}$ (cm^{-2})	$\frac{G}{\mu}$ (cm^{-1})
Specimen: Pe-1c-63-3B; A = 5.067 cm^2; T = 0.762 cm; Density = 0.2204 gm/cm^3								
Helium	68950	553.00	196.79	101830	294	240	0.7 x10^6	39
	68950	856.90	276.50	102061	294	354	0.8	58
	68950	1155.82	368.67	102303	294	485	0.7	80
	103425	518.13	204.26	101820	294	218	0.7	35
	103425	807.08	286.46	102047	294	330	0.8	54
	103425	1101.02	368.67	102276	294	447	0.8	73
	103425	1743.70	553.00	102781	294	693	0.8	114
Helium	103425	2027.67	640.19	103011	294	820	0.8	135
Nitrogen	103425	338.78	171.88	101698	294	154	0.8	200
	103425	458.34	206.75	101792	294	202	0.8	263
	103425	597.84	249.10	101905	294	252	0.8	328
	103425	762.25	296.43	102034	294	302	0.9	393
	68950	44.84	94.66	101474	294	23	0.7	29
	68950	338.78	179.35	101705	294	158	0.8	205
Nitrogen	68950	478.27	219.21	101815	294	208	0.8	271
Helium	68950	541.73	24.91	101652	816	36	0.8	2
	68950	1963.76	32.38	102371	814	130	0.8	10
	68950	3588.95	32.38	103183	812	241	0.8	18
	68950	5281.85	82.20	104080	811	354	0.8	27
	68950	6974.75	87.18	104931	810	484	0.8	37
	103425	5146.42	57.29	103987	802	330	0.9	25
	103425	6703.88	64.77	104773	800	447	0.8	34
	103425	8667.65	72.24	105763	801	570	0.9	44
Helium	103425	10766.84	82.20	106822	802	694	0.9	53
Nitrogen	68950	1041.24	24.91	101902	814	67	0.9	38
	68950	1654.02	24.91	102208	811	112	0.9	64
	68950	2406.31	37.36	102597	810	158	0.9	90
	68950	3327.98	37.36	103058	811	208	0.9	119
	103425	2600.60	79.71	102737	808	154	1.0	88
	103425	3442.56	82.20	103160	811	202	1.0	115
	103425	4369.21	94.66	103636	809	252	1.0	144
Nitrogen	103425	5405.47	99.64	104159	808	302	1.1	173
Helium	68950	1101.02	57.29	33014	294	240	0.4	39
	68950	1589.26	57.29	33258	294	354	0.4	58
	68950	2157.21	57.29	33542	294	485	0.4	80
	103425	1504.56	39.86	33199	294	330	0.4	54
	103425	2007.75	39.86	33450	294	447	0.4	73
	103425	2530.86	49.82	33722	294	570	0.4	94
Helium	103425	3093.82	52.31	34066	294	693	0.4	114
Nitrogen	103425	493.22	24.91	101628	294	118	1.5	153
	103425	652.64	24.91	101708	294	154	1.6	200
	103425	836.98	24.91	101800	294	202	1.5	263
Nitrogen	103425	1061.17	24.91	101912	294	252	1.5	328
Specimen: Pe-2c-63-3B; A = 5.067 cm^2; T = 0.711 cm; Density = 0.2178 gm/cm^3								
Helium	68950	503.18	19.93	101628	294	130	1.3	21
	68950	1011.35	19.93	101882	294	240	1.5	39
	68950	1469.69	19.93	102111	294	354	1.4	58
	68950	2012.73	22.42	102385	294	485	1.4	80
	103425	941.60	9.96	101837	294	218	1.5	35
	103425	1424.85	12.45	102081	294	330	1.5	54
	103425	1903.12	14.95	102323	294	447	1.5	73
	103425	2471.07	19.93	102612	294	570	1.5	94
Helium	103425	2979.24	24.91	102871	294	693	1.5	114
Nitrogen	68950	458.34	49.82	101635	294	112	1.6	146
	68950	667.59	12.45	101703	294	158	1.7	205
	68950	906.72	17.44	101827	294	208	1.7	271
	103425	642.68	7.47	101685	294	154	1.	200
Nitrogen	103425	851.92	9.96	101792	294	202	1.	263

TABLE 31

SUMMARY OF PERMEABILITY COEFFICIENTS

Specimen	Temperature of Char Formation	Temperature K	α [cm^{-2}]	$k = \alpha$ [cm^{-2}]	β [cm^{-1}]	ρ [gm/cm^3]
Pe-1c-33-1B	600	294	13.5×10^{6}	0.074×10^{-6}	8.25×10^{3}	0.2540
Pe-2c-33-1B	600	294	13.5	0.074	8.25	0.2560
Pe-1c-31-1B	800	294	1.19×10^{6}	0.84×10^{-6}	1.85×10^{3}	0.2300
Pe-1c-31-1B	800	811	0.31	3.22	0.70	0.2300
Pe-1c-31-1B	800	294	0.58	1.72	-0-	0.2300
Pe-2c-31-1B	800	294	2.07	0.48	3.42	0.1812
Pe-1c-46-3B	1098	294	0.98×10^{6}	1.02×10^{-6}	0.17×10^{3}	0.1618
Pe-1c-46-3B	1098	811	0.55	1.82	1.68	0.1618
Pe-1c-46-3B	1098	294	1.10	0.91	0.24	0.1618
Pe-2c-46-3B	1098	294	1.77	0.56	0.60	0.1861
Pe-1c-47-3B	1366	294	1.30×10^{6}	0.77×10^{-6}	-0-	0.2108
Pe-1c-47-3B	1366	811	0.78	1.28	0.60×10^{3}	0.2108
Pe-1c-47-3B	1366	294	1.50	0.67	-0-	0.2108
Pe-2c-42-3B	1374	294	0.77	1.30	-0-	0.1894
Pe-1c-63-3B	1745	294	0.78×10^{6}	1.28×10^{-6}	0.33×10^{3}	0.2204
Pe-1c-63-3B	1745	811	0.85	1.18	1.50	0.2204
Pe-1c-63-3B	1745	294	-	-	-	0.2204
Pe-2c-63-3B	1745	294	1.47	0.68	1.05	0.2178

REFERENCES

1. Engelke, W. T., et al: "Thermal and Mechanical Properties of an Elastomeric Filled Honeycomb Designated Material A", NASA Contractor Report, NASA CR-132281, September, 1973.

2. Pears, C. D., and Schoffner, J. E.: "The Thermal Response of Ablative Materials". Presented at VIII National Symposium of SAMPLE, San Francisco, California, May 25-28, 1965.

3. Smyly, E. D., and Pears, C. D.: The Effects of the Conditions of Char Formation on the Physical Properties of a Charred Phenolic-Nylon, NASA Contractor Report, NASA CR-112136, July, 1972.

4. Flynn, D. R., "Thermal Guarding of Cut-Bar Apparatus", Conference on Thermal Conductivity Methods, Batelle Memorial Institute, 1961.

5. Robinson, H. E., "Thermal Conductivity Reference Standards", Proceedings of the Second Conference on Thermal Conductivity, 1962.

6. Flynn, D. R., "Thermal Conductivity of Ceramics", Mechanical and Thermal Properties of Ceramics, edited by J. B. Wachtman, Jr., NBS Special Publication 303, Washington, D. C., May, 1969, pp. 63-123.

APPENDICES

APPENDIX A

THERMAL CONDUCTIVITY TO 1000°F

THERMAL CONDUCTIVITY TO 1000°F

Apparatus and Procedure

Thermal conductivity runs can be made with any of the three guarded hot plate apparatuses which are slightly modified from the standard ASTM C177-45 design. All three are identical in operating procedure and design except in size and are classified as either the 14", 7", or 3" apparatus depending on the diameter of the specimen used. Actually the diameters for the 7" and 3" apparatuses are 7-3/8" and 3-1/4", respectively. Specimen thicknesses are from 1/8" to 3" and duplicate specimens are required per run. Figure 1 is a schematic of a typical assembly used for all three apparatuses.

The apparatus consists of a central heater plate surrounded by a guard heater, each separately controlled. The guard ring is maintained at the same temperature as the central heater so that all of the heat flow is normal to the specimen surfaces. The temperature differences between the guard and central sections are measured by means of differential-thermocouple junctions connected in series. The 14" and 7" apparatuses contain eight differential junctions, whereas the 3" apparatus contains four. The heater plate is sandwiched between layers of filler material, the hot-face thermocouples, the specimen, cold-face thermocouples, filler material, a copper plate, and finally a cold source to dissipate the heat. The cold source consists of a copper coil enclosed in an aluminum box on the 14" apparatus, a copper coil soldered to a copper plate on the 7" apparatus, and a spiral baffled copper container on the 3" apparatus. In addition to the thermocouples in contact with the specimen, thermocouples are located in the central heater and the outer copper cold plates.

To provide intimate contact at all interfaces, the entire sandwich assembly is pressed firmly together by spring loading with the total load application desired, which is usually 600 pounds.

Normally for the determinations between -50°F to 150°F, a filler material of gum rubber is used. From 150°F to 1000°F Fiberfrax paper is used as a filler. The overlapping data at 150°F provides a check on any possible uncertainty due to poor intimate contact resulting from either specimen or filler surface irregularities. If the data agree within approximately 5%, the run is continued; however, if the agreement is not within 5%, the thermocouples are replaced, the specimen is removed, surfaces are resanded, and the run is repeated.

The thermocouples used on the hot and cold side of the specimen are made from 0.005" diameter chromel-alumel wire electrically insulated with 0.003" teflon tape. The junction is made by soldering the wires to a small square of 0.002" thick brass shim stock called a "getter". The teflon insulated leads are sandwiched between the specimen and filler material to assure isothermal conditions along the length of the wire. This arrangement insures that there is no air film between the specimen and the thermocouples, and that good, intimate contact exists at all interfaces.

Single thermocouples in the center of the heater plate and cold plate monitor the temperatures of the heater and cold plates in order to obtain the over-all temperature drop through the assembly.

The assembly is arranged to operate with the specimen placed in the apparatus horizontally, as shown in Figure 1. The specimen required are flat panels sized to fit the apparatus. The assembly is insulated around the edges by either Fiberfrax or glass wool batt.

A constant voltage transformer is used in conjunction with variable voltage transformers to assure a constant power supply at each setting. The central heater and guard heater are controlled individually by the variable voltage transformers. The voltage and current to the central heater are monitored by means of a voltmeter and an ammeter which are switched out of the circuit except when actually being read. The voltage to the guard heater is monitored constantly by a voltmeter.

All of the thermocouple readings are taken on a Leeds and Northrup K-3 potentiometer in conjunction with a galvanometer of 0.43 microvolts per mm deflection sensitivity.

To obtain mean sample temperatures above room temperature, water is circulated through the cooling section. For mean sample temperatures below room temperature, cold trichloroethylene is pumped through the cooling section. This coolant is chilled by circulating it through copper coils in a trichloroethylene dry-ice bath. Equilibrium conditions are certified before readings are taken.

Coefficients of thermal conductivity are calculated from the expression:

$$k_s = \frac{Ql_s}{A\Delta t}$$

Q = total heat flow - Btu/hr

l_S = average thickness of specimens - inches

A = area of central heater section - square feet

Δt = sum of temperature drop across each sample - °F

Theoretically, Q, the heat input, should split, with exactly half of the input flowing through each sample. The temperature drops indicate that this condition rarely exists. Instead, there is a slight unbalance in the heat flow. The above formula then permits a calculation of the arithmetic average for the two panels. In this calculation the temperatures are measured directly at the faces of the specimen by the "getters", resulting in a "direct" method.

As a check, the thermal conductivity is calculated for the specimen with a "series-resistance" or "composite" expression. This method utilizes the same run data, except that the temperature difference between the heater plate and the cold plate is utilized and, since the resistance of the filler is measured separately in the same apparatus, the following series-resistance equation can be used to determine the thermal conductivity of the specimen:

$$k_S = \frac{l_S}{(l_T/k_T) - (l_F/k_F)} \qquad (2)$$

l_S = thickness of the specimen - inches

k_S = thermal conductivity of the specimen - Btu in./hr ft^2°F

(l_T/k_T) = thermal resistance of the total composite of filler and specimen, calculated from the temperature difference between the hot and cold plate

(l_F/k_F) = thermal resistance of the filler alone, determined under the same conditions that exist for (l_T/k_T)

The (l_F/k_F) term for the gum rubber filler is determined both with and without copper plates inserted between the rubber pads to simulate interface resistance that is present during the evaluation of the specimen.

Improvement and Calibrations on the ASTM C177-5 Technique

The ASTM C177-45 guarded hot plate apparatus is only recommended for determining values below 5 Btu in./hr $ft^2°F$. Due to the higher conductivities of many of the new reinforced plastics such as the phenolic graphites and carbons, considerable work was necessary before the above procedures were incorporated, which provides accurate data between 5 and 10 Btu in./hr $ft^2°F$. The following is a resume of the work and analysis performed which extended the range to 10 Btu in./hr $ft^2°F$.

It was decided at the beginning of the investigation that data from -50°F to 150°F would be determined using a filler of gum rubber and determining the conductivity of the specimen by both "direct" measurement of the temperature drop across the specimen and a "series-resistance" or "composite" method, as explained. From 150°F to the maximum temperature, the data would be obtained by using an asbestos filler and determining the conductivity by a "direct" calculation from the measured face temperatures of the specimen. Both methods were used at the 150°F to determine if any uncertainty existed due to poor intimate contact resulting from either specimen or filler surface irregularities.

Considerable deviation of approximately 20 percent to 30 percent occurred between the values obtained for the "composite" method and the "direct" method for the higher conductivity materials. The evaluations with plexiglas and pyrex at that time indicated the following (see Table 1):

1. The "composite" method, when calibrated with pyrex and plexiglas, exhibited somewhat high values of 8 Btu in./hr $ft^2°F$ at 150°F and +1.23 Btu in./hr $ft^2°F$ at 150°F, respectively. The major difficulty was the great scatter between different data.

2. The "direct" method, when calibrated with pyrex, was in error by exhibiting values averaging about 20 percent low. However, the plexiglas calibration indicated excellent agreement.

The above results indicated that the conductivity data for values above 5 Btu in./hr $ft^2°F$ should be determined using the composite method, with the direct method employed for the lower values. However, the composite method is much too critical under certain conditions, and data scatter was as high as 30 percent. By considering equation 2 in close detail, it was found that normal experimental error in determining (l_F/k_F) can result in a magnified error of k_s if (l_F/k_F) is critically close to (l_T/k_T). With certain conditions,

an error of 3 percent in (l_F/k_F) can result in a 10 percent to 50 percent error in k_s. Therefore, it was mandatory that the direct method be improved for use over the entire range of values, and that the composite be used only as a check.

It was determined that a majority of the error obtained with the direct method was due to the lack of intimate contact at the interfaces of the specimens when the load and fillers were improperly selected. This error was magnified (even percentagewise) when the conductivities were about 5 Btu in./hr $ft^2°F$. In order to obtain intimate contact at the interfaces, proper selection of compaction load and filler material for each test material is required. An extensive evaluation was performed on the effect of measured conductivity of increased compaction loading using either no filler material or fillers of gum rubber, Fiberfrax, or asbestos. The specimens used in this evaluation were plexiglas, pyrex, and other plastic materials, which represented a range of conditions including different surface finish, flatness, flexibility, and conductivity. Table 1 presents the calibration data obtained for pyrex and plexiglas in the 3" and 7" diameter and 14" square ASTM C177-45 guarded hot plate apparatuses.

Under the normal compaction load of approximately 600 pounds, the 3" diameter apparatus provided reliable data for plexiglas using either filler or no filler, and for pyrex using the filler only. Under the normal load the 14" apparatus provided accurate data for plexiglas; however, the values were occasionally low on the pyrex using the direct method of calculation. The 7" diameter apparatus provided data about 8 percent low for pyrex under normal load with a gum rubber filler. For plexiglas, the 7" diameter apparatus provided accurate data under normal compaction loads with no filler and gum rubber of Fiberfrax filler; however, the data were 7 percent low using an asbestos filler. Subsequent work indicated that the 7" apparatus was somewhat erratic, so the heater was rebuilt and the agreement with standards improved even more to within about 5 percent, although the trend remained similar. Such extensive data were not reobtained.

Under varying load, the 7" diameter apparatus with gum rubber filler provided values for pyrex that increased 7.5 percent as the load was increased from 100 pounds to 600 pounds and only increased 3 percent more from 600 pounds to 4000 pounds. The excessively high compaction pressures provided values on plexiglas with a gum rubber filler that were not orderly and were noticeably higher than reported in the literature for this material, regardless of the technique.

The data obtained with increasing load on the other plastic materials (not standards) demonstrated in most cases that an increase in compaction load from the normal 600 pounds did not increase the values insignificantly but did introduce unorderly changes. It was apparent, therefore, that excessively high loadings were neither required nor desirable. As a matter of fact, the bonds between the resin and reinforcement on some materials could be influenced, thermally, by such high pressures. Further, stress fields are created and data obtained here have indicated an influence of stress on the conductivity of the structures involved for a material such as plexiglas. The mechanism is probably one of the induced alignment of the chains.

The major requirements was to provide intimate thermal contact on all faces, which could be done by the proper selection of compaction load and filler, depending on the properties of the particular specimen. The actual load on the sandwich was more important than the pressure since it is the load and not the pressure that best correlates with flattening a curved plate or specimen. For example, it requires more load to flatten a 7" plate than it does a 14" plate. So, if the same pressure were maintained on the two apparatuses, the lower compaction force on the smaller one would not flatten the bow. The pressure would be important in providing deformations, locally, of the filler and/or specimen where a low or high spot may exist; however, the data on plexiglas and pyrex with rubber and Fiberfrax, particularly, clearly demonstrated that small compaction loads were sufficient to provide enough pressure to deform the filler into local areas. The compaction load needed was not as excessive as had been suggested in some literature in which the pressure was considered of major importance. An indication of the importance of the load-filler combination rather than pressure was apparent from the data, which provided higher conductivities on the 7" rig with the rubber filler and 600 pound load than on the same rig with no filler at 3000 pound load. Higher conductivities were obtained with the lower pressure by substituting the proper combination of load-filler.

From the above, it has been decided that the higher thermal conductivity materials can be evaluated accurately by the direct measurement method using a filler if the flat surfaces are held flat, and the compaction loads are held at a nominal level sufficient to provide intimate contact at the interfaces. The amount of loading depends on the flatness, the flexibility of the specimen, and the type of filler used. For very rigid materials like pyrex, it is doubtful if enough pressure could be applied when run without filler without breaking the specimen. No one technique is adequate for the determination of the conductivity of all specimens over the full temperature range. Careful judgement is required by the investigator in each case to select the compaction load, the filler (or no filler), the heat flow level, and to evaluate the condition of the apparatus.

The above analysis led to the modifications and improvements which have been made on the ASTM apparatuses beyond those normally employed to assure better accuracy of the data. The screw loading device on the 14" apparatus has been modified to incorporate spring loading at the center and edge clamps to insure more uniform loading, and thus provide flatter surfaces and more intimate contact. The edges are monitored with 1 mil pull-out tabs to insure that no gaps existed in the plates. The thermocouple wires are more carefully placed along the isothermal surface of the specimen. The Fiberfrax paper has been adopted as a high temperature filler, since it conformed to any irregularities on the surface exceptionally well allowing the placement of the small thermocouple wires, electrically insulated with 0,003" teflon tape, without disrupting the intimate contact required. It has also been noted that increasing the heat level, and thus the temperature difference, across the specimen provides less deviation at the 150°F overlap temperature. The minimum heat flow level depends on the conductivity of the material and cannot be defined at a given temperature drop. The random deviation between values on the same specimen as evaluated with rubber filler from -50°F to 150°F, and with Fiberfrax filler from 150°F to 1000°F, has been reduced to a maximum of about 5 percent. Past experience has shown that the Fiberfrax filler provides slightly higher data on 30 percent of the runs and slightly lower data on the remaining runs at the change-over temperature (from one filler to the other) at about 150°F.

Table 1 presents the many calibrations performed on the apparatuses for both before and after the above improvements were incorporated.

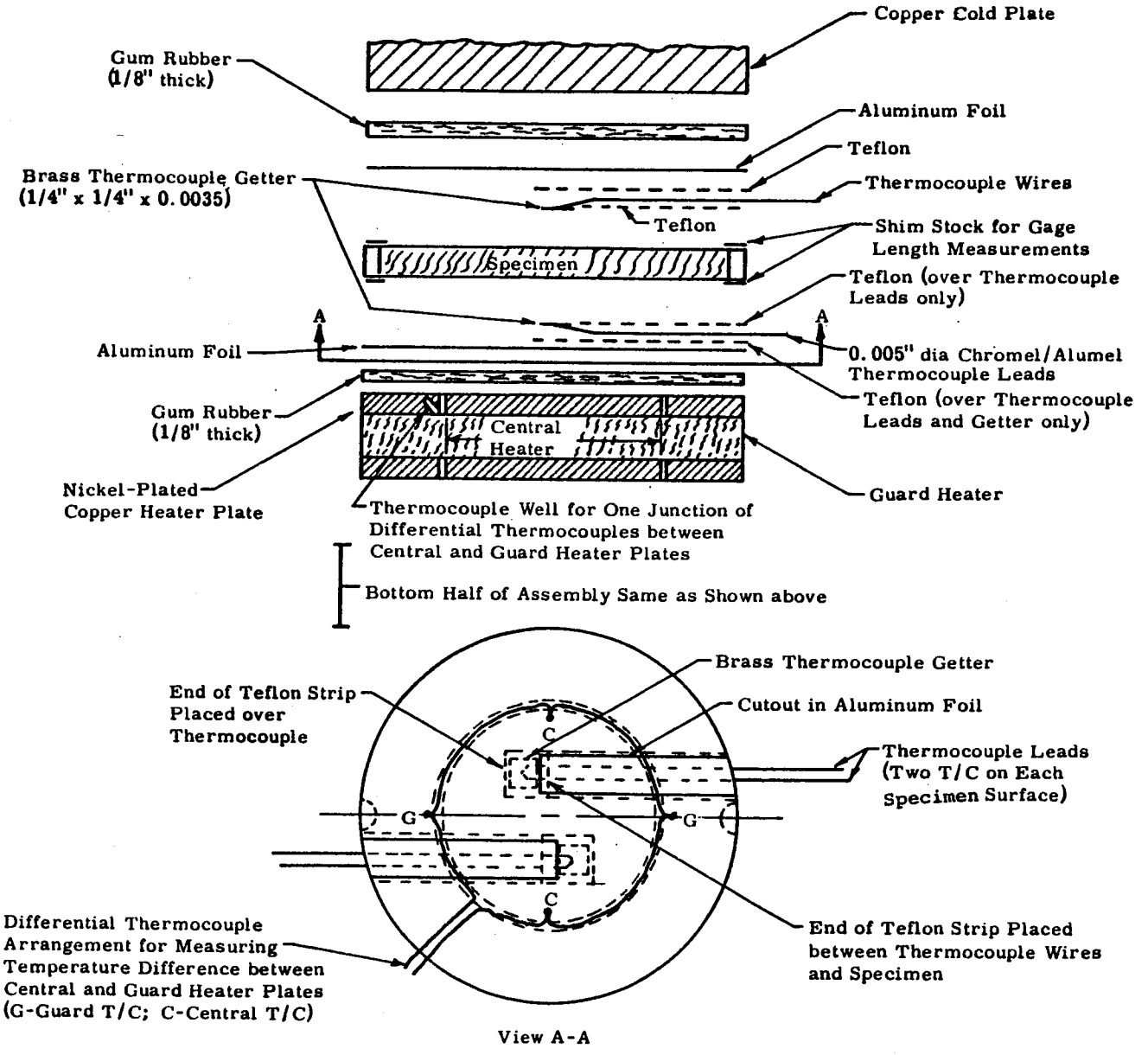

Notes:

1. Buildup shown is used up to 150°F.
2. Above 150°F, gum rubber on hot surface of specimen is replaced by two Fiberfrax discs each 1/8 inch thick and a Fiberfrax disc of the same thickness is placed between the gum rubber and the specimen on the cold surface.
3. At elevated temperatures, an asbestos disc can be placed between the gum rubber and Fiberfrax at the cold surfaces to control temperature drop across the specimen.

Figure 1. Schematic of buildup used for ASTM C177 guarded hot plate thermal conductivity apparatus

Table 1

CALIBRATIONS OF ASTM C 177 APPARATUSES AND PROCEDURES WITH PLEXIGLAS AND PYREX 7740 STANDARDS AT ABOUT 150°F to 200°F (DIRECT METHOD UNLESS OTHERWISE NOTED)

Apparatus	Plexiglas Thermal Conductivity Btu/hr/ft²/°F/in.	Pyrex Thermal Conductivity Btu/hr/ft²/°F/in.
14" rig with asbestos or rubber filler, composite method and 600 pounds	1.33 to 1.39	7.1 to 8.9
14" rig with asbestos filler and 600 pounds	1.17 to 1.20	5.96
14" rig and rubber filler and 600 pounds	1.19 to 1.22 to 1.30	7.35 to 7.39
14" rig with Fiberfrax filler and 600 pounds after improvements made	1.34	7.64 to 7.83
7" diameter rig with rubber filler and compaction of:		
100 pounds	1.25	-7.3%
600 pounds	1.26 to 1.09 with Q	0%, 7.74
1000 pounds	1.25	0%
3000 pounds	-	+2.0%
4000 pounds	1.14 to 1.33 with Q	+2.1%
7" diameter rig with asbestos filler and compaction of:		
100 pounds	-	
600 pounds	1.11 to 1.17	5.0
1000 pounds	1.11	
3000 pounds	-	
4000 pounds	1.16	
7" diameter rig with no filler with compaction loads of:		
100 pounds	1.12	
600 pounds	1.21	4.0
1000 pounds	1.23	
3000 pounds	1.27	
4000 pounds	1.29	
7" diameter rig with Fiberfrax and 600 pounds after improvements made	1.14	7.13 to 8.1
3" diameter rig with rubber filler and 600 pounds	1.17	7.34 to 7.6
3" diameter rig with Fiberfrax filler and 600 pounds	1.15, 1.18, 1.19, 1.41 to 1.19	7.4 to 7.6
3" diameter rig with asbestos filler and 600 pounds	1.16, 1.16, 1.16	7.28
3" diameter rig without filler and 600 pounds	1.18 to 1.19	6.70 to 6.79

1. Literature and previous work reports the thermal conductivity of plexiglas to be 1.19.

2. Literature reports the thermal conductivity of 7740 pyrex to be from 7.1 to 8.1 at about 200°F by Knapp, American Ceramic Society, 1942, and the NBS, respectively. The NBS data are by the series resistance or composite technique. Prior values by the NBS using direct method were about 7.4 to 7.5.

3. Thicknesses of specimens vary with investigator.

APPENDIX B

A COMPARATIVE ROD APPARATUS FOR MEASURING THERMAL CONDUCTIVITY TO 2000°F

A COMPARATIVE ROD APPARATUS FOR MEASURING THERMAL CONDUCTIVITY TO 2000°F

Southern Research Institute's comparative rod apparatus is used to measure thermal conductivities of a wide variety of materials from -300°F to 2000°F. This apparatus, shown schematically in Figure 1, consists basically of two cylindrical reference pieces of known thermal conductivity stacked in series with the cylindrical specimen. Heat is introduced to one end of the rod, composed of the references and specimen, by a small electrical heater. A cold sink or heater is employed at the opposite end of the rod as required to maintain the temperature drop through the specimen at the preferred level. Cylinders of zirconia may be inserted in the rod assembly to assist in controlling the temperature drop. Radial losses are minimized by means of radial guard heaters surrounding the rod and consisting of three separate coils of 16, 18 or 20-gage Kanthal wire wound on a 2 or 4- inch diameter alumina core. The annulus between the rod and the guard heaters is filled with diatomaceous earth, thermatomic carbon, bubbled alumina or zirconia powder. Surrounding the guard is an annulus of diatomaceous earth enclosed in an aluminum or transite shell.

The specimens and references (see Figure 2) are normally 1-inch diameter by 1-inch long. Thermocouples located 3/4 inch apart in radially drilled holes measure the axial temperature gradients. Thermocouples located at matching points in each guard heater are used to monitor guard temperatures, which are adjusted to match those at corresponding locations in the test section.

In operation, the apparatus is turned on and allowed to reach steady state. The guard and rod heaters are adjusted to minimize radial temperature gradients between the rod and guard sections consistent with maintaining equal heat flows in the references. Temperatures are measured on a Leeds and Northrup Type K-3 potentiometer, and the temperature gradients calculated. A typical temperature profile in the test section is shown in Figure 3.

The thermal conductivity of the specimen is calculated from the relation

$$K_s = \frac{K_1 \Delta T + K_2 \Delta T}{2\Delta T_s} \quad \frac{\Delta X_s}{\Delta X_r}$$

where K_1 and K_2 are the thermal conductivities of the upper and lower references; ΔT_1, ΔT_2 and ΔT_s are the temperature differences in the upper and lower references and specimen, respectively; ΔX_s and ΔX_r are the distances between thermocouples in the specimen and references.

Note that for purely axial heat flow, the products $K_1\Delta T_1$ and $K_2\Delta T_2$ should be equal. Due to imperfectly matched guarding and other factors, this condition is seldom attained in practice; therefore, the average of the two values is used in the calculations. Their difference is maintained as small as possible, usually within 5% of the smaller.

For identical specimens, the ratio $\Delta X_s/\Delta X_r$ should be unity but may vary due to the uncertainty in hole locations. To prevent introducing an additional error in calculations, ΔX is determined as follows: the depth of the hole is measured by inserting a snugly fitting drill rod in the hole, measuring the projecting length and subtracting it from the total length of the rod. The slope, or angle the hole makes with the perpendicular to the specimen axis, is determined by making measurements to the face of the hole and the outer end of the drill rod with respect to a datum plane, using a dial gage. From these measurements, the location of the bottom of the hole can be calculated.

Generally, measurements with the comparative rod apparatus are performed in an inert helium environment. The apparatus can also be operated in vacuum and at gas pressures of up to 100 psig. We have had experience operating under all conditions.

The primary reference materials which we use are Code 9606 Pyroceram and Armco iron for measurements on materials with low and high thermal conductivities, respectively. Primary standard reference sets are kept and are used to calibrate other references made from the same materials. The standards of Code 9606 Pyroceram were made from a batch of material which NBS purchased shortly after their measurements on a sample of Code 9606 Pyroceram. The curve which Flynn presented for the thermal conductivity of the Pyroceram is given in Figure 4.[1] Note that the curve is in good agreement

---

[1] Robinson, H.E. and Flynn, D. R., Proceedings of Third Conference on Thermal Conductivity, pages 308-321, 1963 (with author's permission)

with the recommended values from NSRDS-NBS 8[2]. The standards of Armco iron were made from the stock which was used in the round-robin investigations from which Powell[3] developed the most probable values for Armco iron. The curve used for the Armco iron standards is shown in Figure 5. Powell estimated the uncertainty to be within ±2 percent over the temperature range from 0° to 1000°C. Note in Figure 5 that numerous evaluations of Armco iron from other batches of material have agreed within ±3 percent (coefficient of variation about curve) with Powell's original data.

In addition to Code 9606 Pyroceram and Armco iron several other materials have been used as references. These include copper for high conductivity specimens, 316 stainless steel for specimens of intermediate thermal conductivity and Teflon or Pyrex for low conductivity materials.

Copper references have been calibrated against Armco iron and excellent agreement with literature data has been obtained. Thermal conductivity values obtained from calibrations of 316 stainless steel against Pyroceram, Armco iron and a set of 316 stainless steel standards are presented in Figure 6. Note the consistency of the data obtained with the three different sets of references. The coefficient of variation of the data shown in Figure 6, about the curve value, was ±3.3%. These data indicate the internal consistency of the stainless steel and the reference materials. Note that the thermal conductivity values for 316 stainless steel presented in Figure 6 lie between values reported by several steel manufacturers and Lucks and Deem.[4]

The calibrations indicate that for materials with moderate to high thermal conductivities the apparatus operates with a precision of about ±3 percent and a total uncertainty of about ±5 percent at temperatures above 0°F if temperatures between the guard and test section are closely matched. Below 0°F, the precision achieved to date has been about ±7 percent with a total uncertainty of about ±10 percent. We anticipate that the precision and uncertainty at cryogenic temperatures can be improved by additional calibrations.

---

[2] Powell, R. W., C. Y. Ho and P. E. Liley, Thermal Conductivity of Selected Materials, NSRDS-NBS 8, Department of Commerce, November 25, 1966

[3] Powell, R. W., Proceedings of Third Conference on Thermal Conductivity, pages 322-341, 1963

[4] WADC TR58-476, "The Thermophysical Properties of Solid Materials," Armour Research Foundation, November, 1960.

Some additional data obtained on the comparative rod apparatus are shown in Figure 7 and 8. Figure 7 shows thermal conductivity data for ATJ graphite, with grain, using Armco iron as the reference material. These data show excellent agreement with earlier data obtained here and by other sources[5 7]. The maximum scatter of the comparative rod points was about 5 percent.

Figure 8 shows data for thermocouple grade constantan obtained on the comparative rod apparatus using Armco iron references, and on Southern Research Institute's high temperature radial inflow apparatus. Note the excellent agreement. These data also show close agreement with data obtained by Silverman[4] on an alloy of very similar composition.

---

[5] ASD-TDR-62-765, "The Thermal Properties of Twenty-Six Solid Materials to 5000°F or Their Destruction Temperatures," Southern Research Institute, August, 1962

[6] Pears, C. D., Proceedings of Third Conference on Thermal Conductivity, 453-479 (1963)

[7] NSRDS-NBS 16, "Thermal Conductivity of Selected Materials", Part 2, by C. Y. Ho, R. W. Powell and P. E. Liley, National Bureau of Standards, 1968.

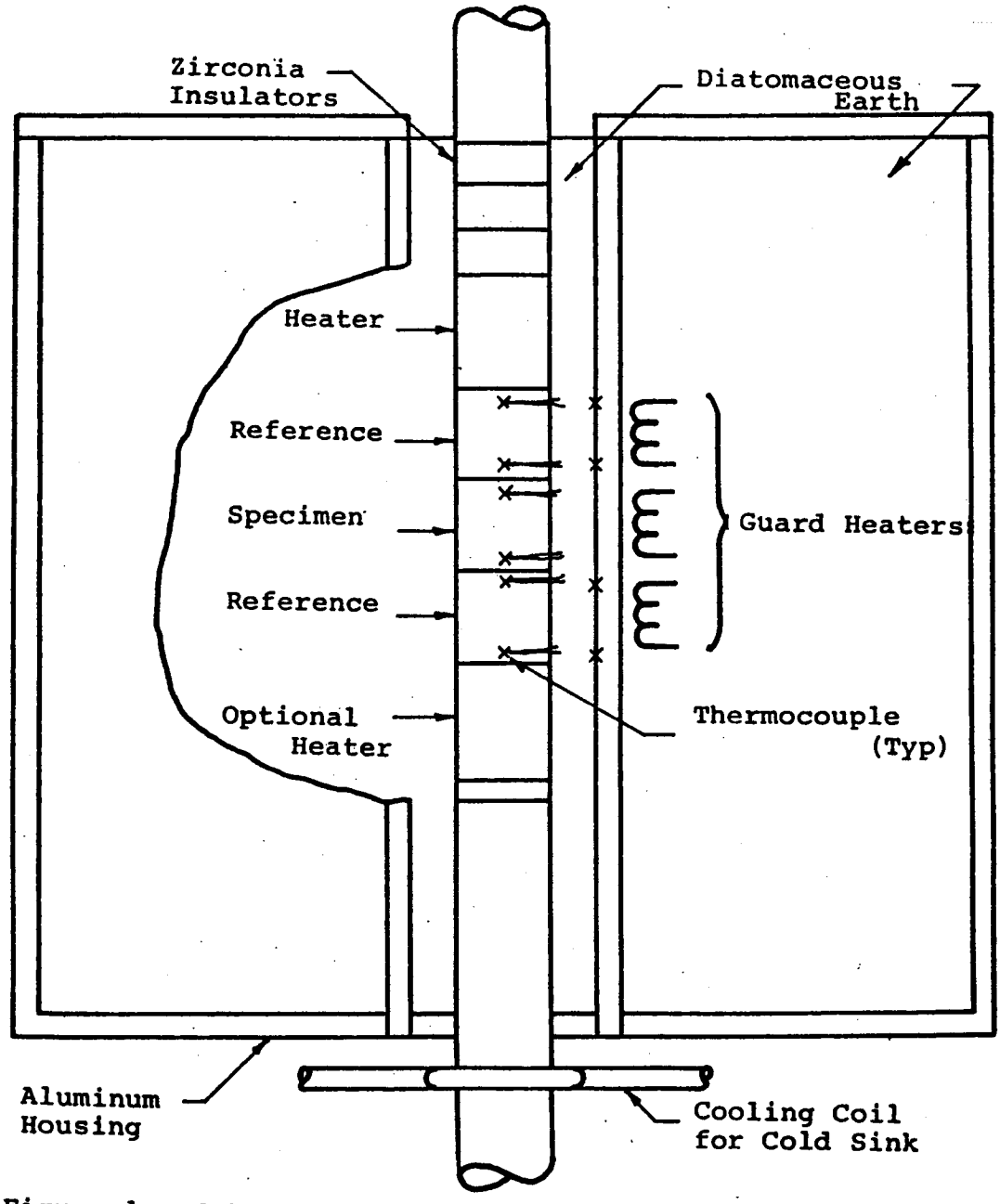

Figure 1. Schematic of Comparative Rod Thermal Conductivity Apparatus

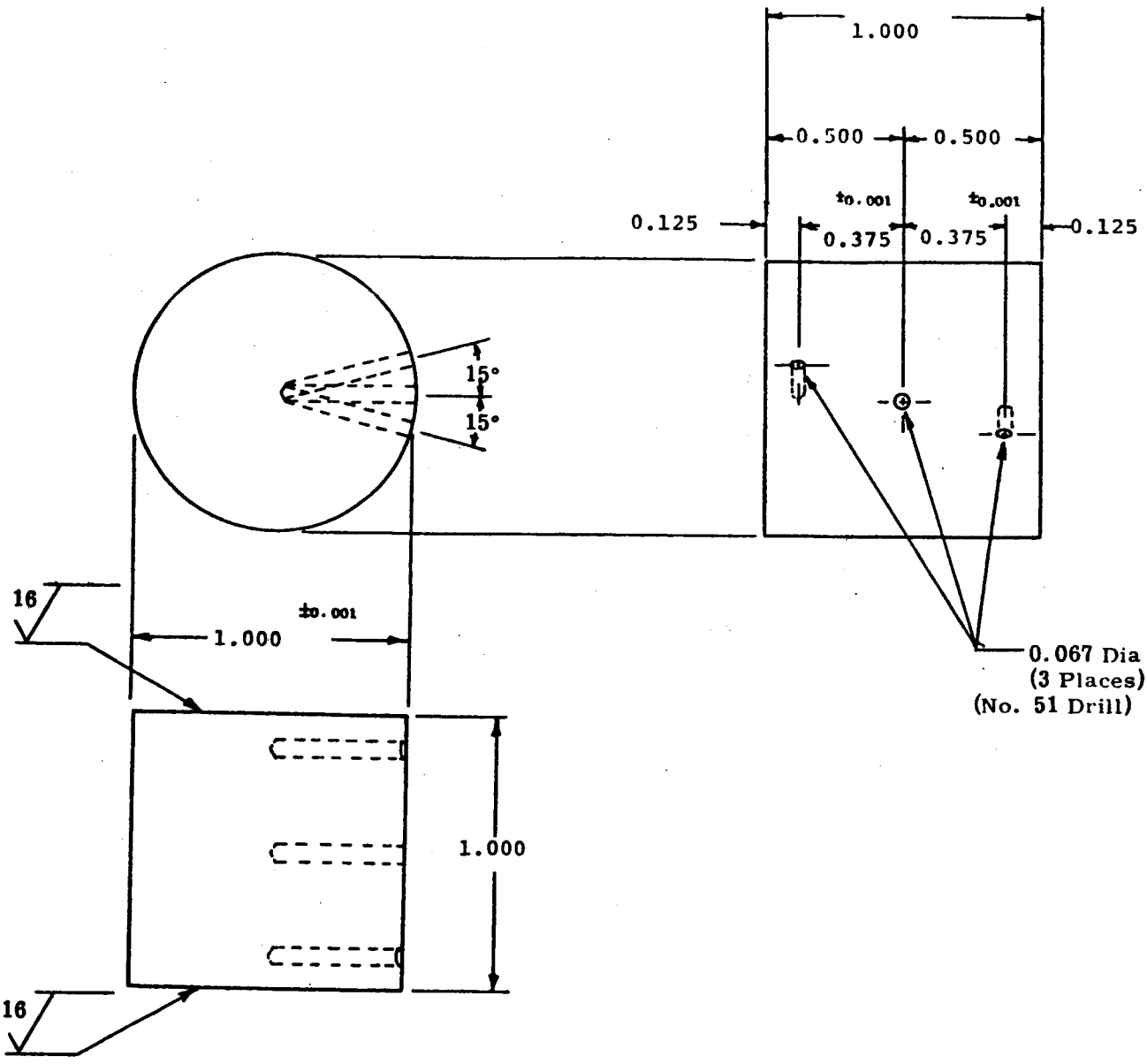

Note: All dimensions ±0.005 except where noted

Figure 2. Drawing of Specimen for Thermal Conductivity Measurements in Comparative Rod Apparatus to 1800°F

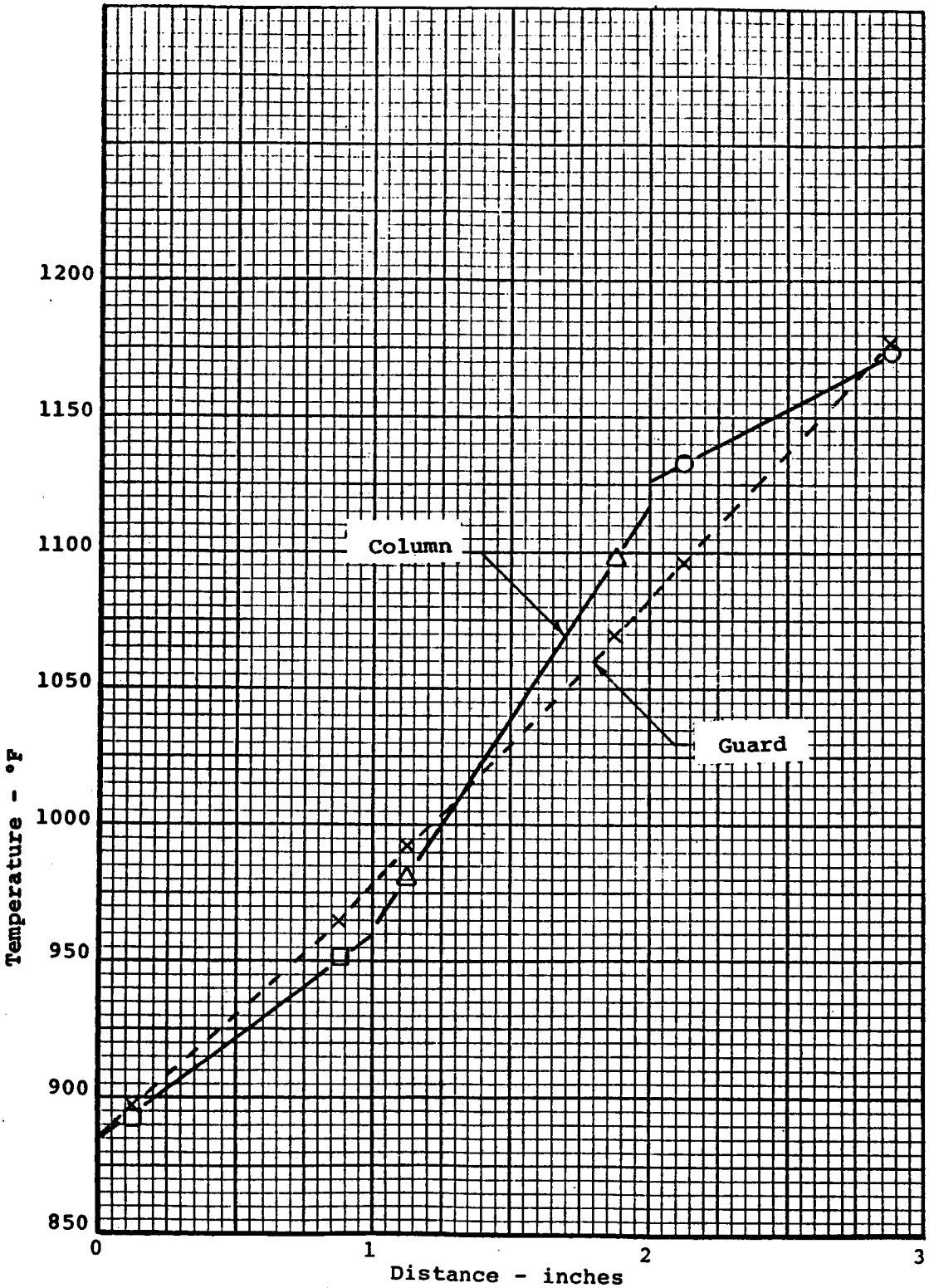

Figure 3. Typical Temperature Profile in Test Section

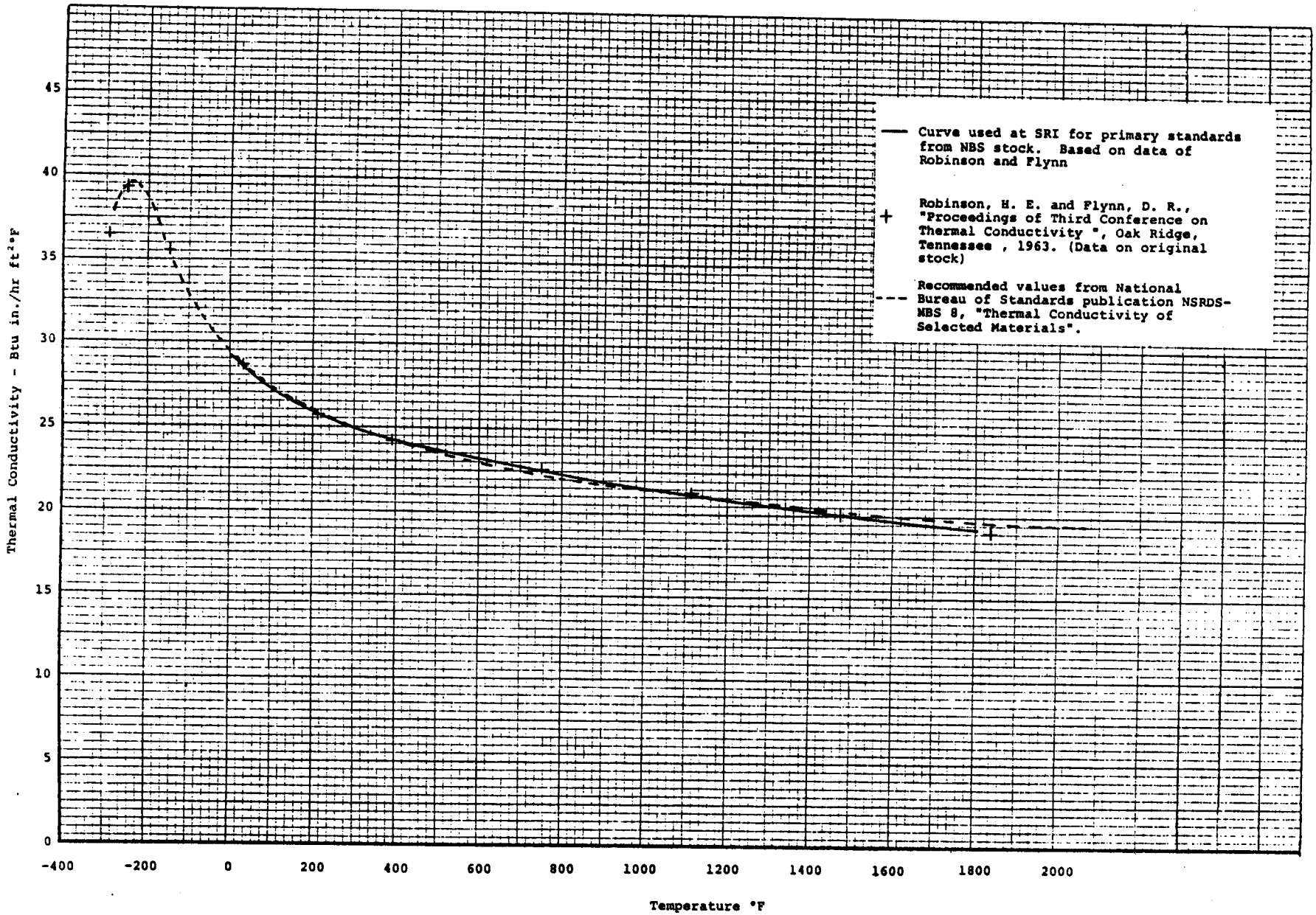

Figure 4. The Thermal Conductivity of Primary SRI Standards from NBS Stock of Code 9606 Pyroceram

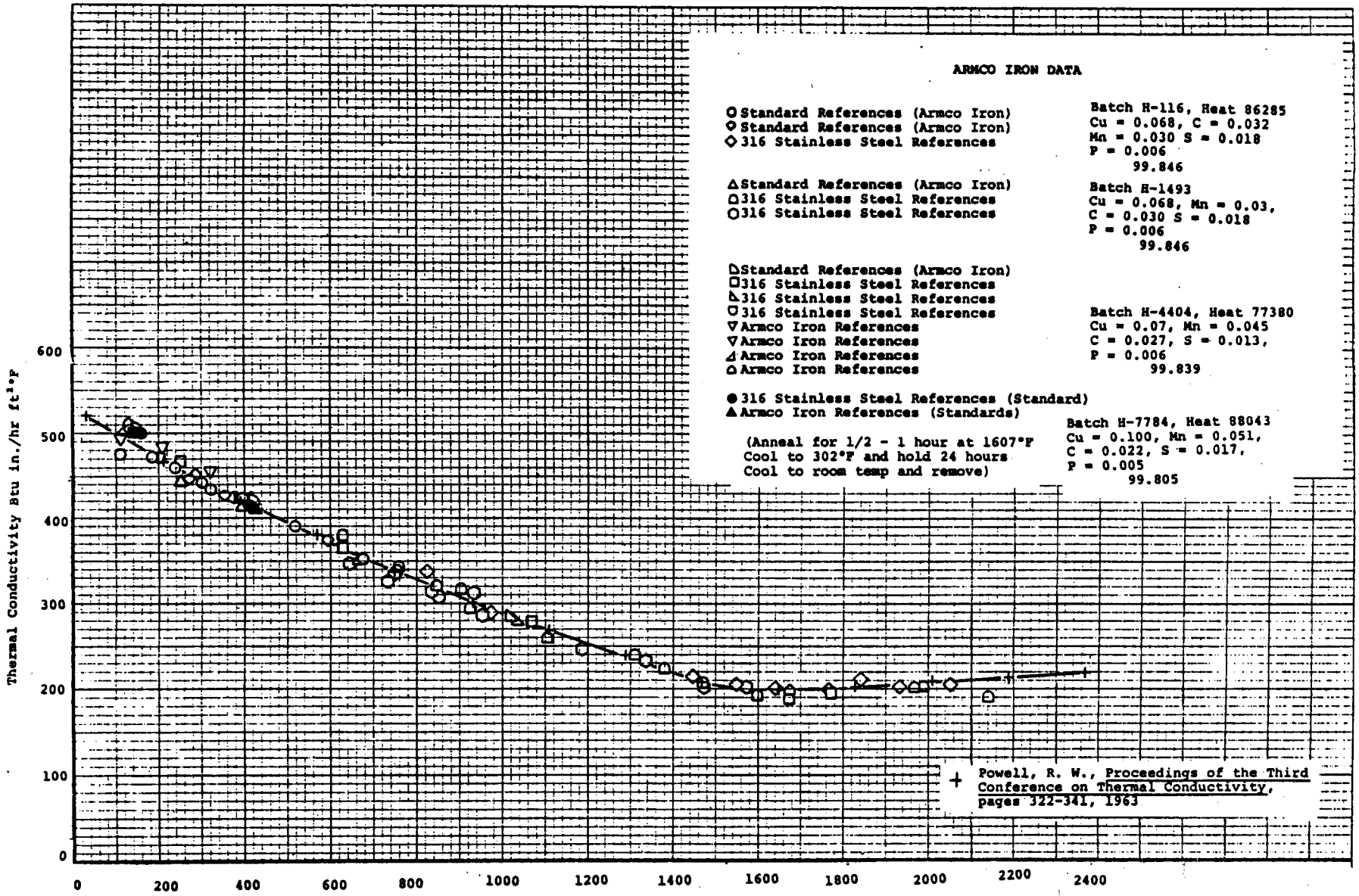

Figure 5. The Thermal Conductivity of Armco Iron

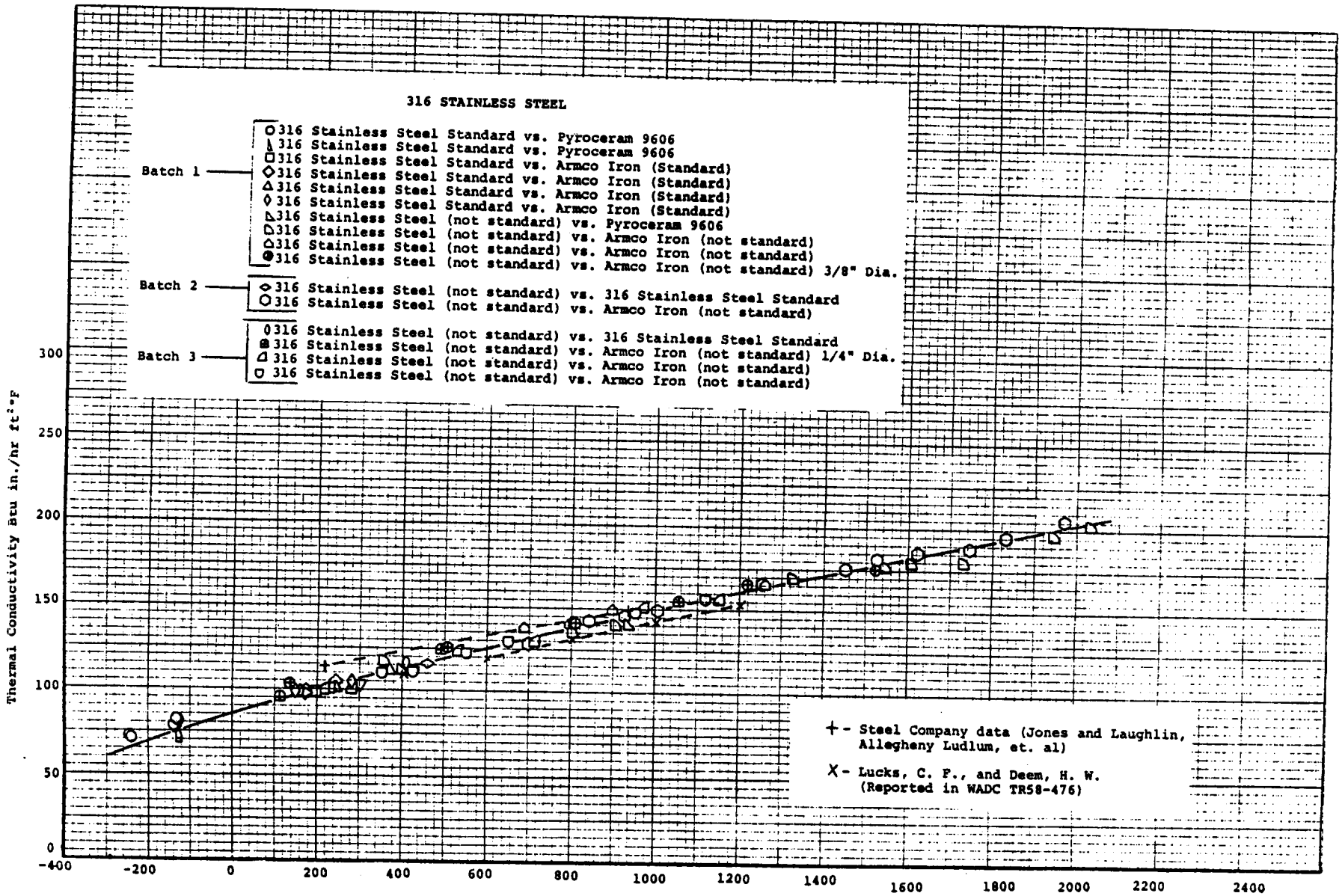

Figure 6. The Thermal Conductivity of 316 Stainless Steel

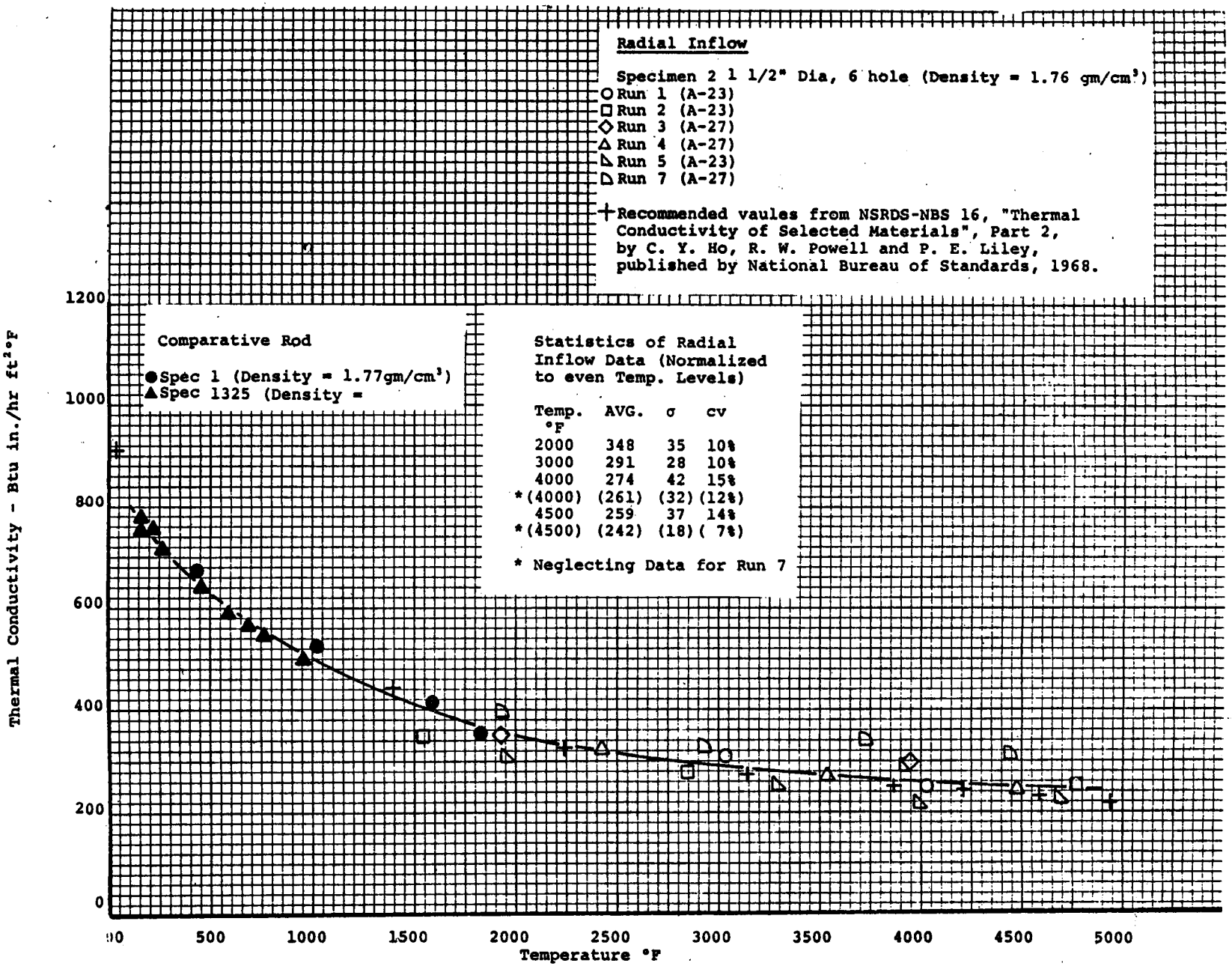

Figure 7. The Thermal Conductivity of ATJ Graphite, With Grain

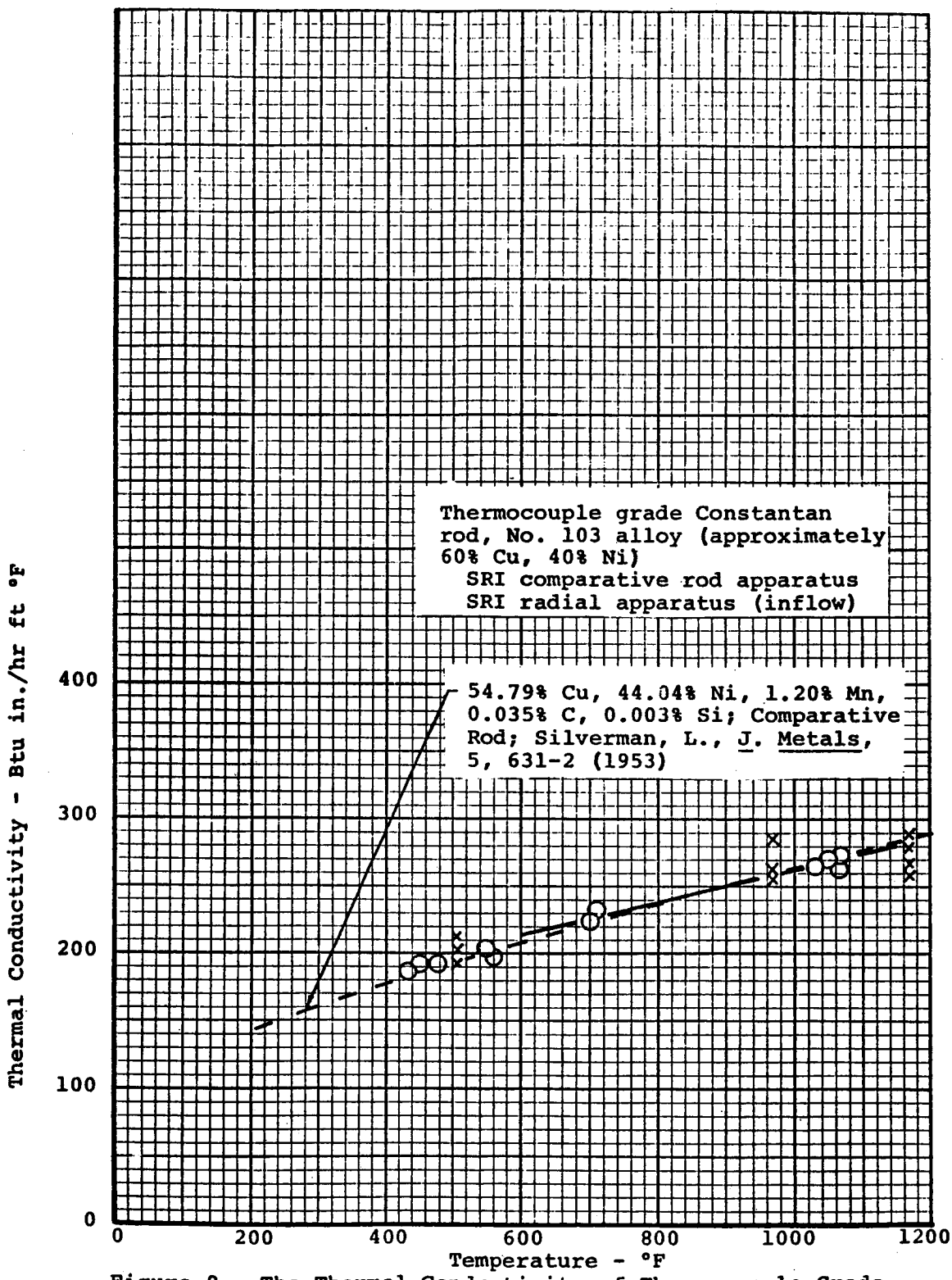

Figure 8. The Thermal Conductivity of Thermocouple Grade Constantan Rod

APPENDIX C

GUARDED COMPARATIVE ROD APPARATUS

GUARDED COMPARATIVE ROD APPARATUS

The guarded comparative rod apparatus is a modified assembly of the basic comparative rod apparatus and is employed for samples with thermal conductivities less than 10 Btu in./hr ft^2 °F.

The reason for this is that analyses [1, 2][1] have shown that heat can shunt the specimen [through the insulation] when the thermal conductivity of the specimen is not an order-of-magnitude or more than that of the insulation and the guard heater is, say, twice the diameter of the specimen or more. Note that the shunting effectively gives a larger specimen area and results in an erroneously low temperature difference in the specimen relative to the reference (assuming that the references have a higher thermal conductivity than the specimen). This yields erroneously high values of thermal conductivity. With certain values for the thermal conductivities of the references, specimen and insulation, guard heater to specimen diameter ratio and guard to specimen temperature profile, these errors can easily reach 100 percent.

Analyses [1, 2[have shown that the heat shunting problem can be overcome if the following conditions are satisfied:

1. The guard profile matches the specimen profile.
2. The ratio of guard diameter to specimen diameter is as near one as possible.

These concepts are applied to the modified technique described here.

The experimental configuration used for the measurements is shown in Figure 1. The assembly consists of a central column comprised of a 1 inch diameter specimen sandwiched between two references of known thermal conductivity. Guard rings made of the same materials as the specimen and references surrounded the central column. The guard rings were constructed to match the specimen and reference lengthwise. The annulus between the central column and guard ring was 1/16 inch wide which gave a guard diameter to specimen diameter of 1.125. A drawing of the specimen and guard ring is given in Figure 2.

---

[1]Bracketed numbers denote references given at end of text.

The references used are slip cast fused silica, the conductivity of which has been defined with the ASTM C 177 guarded hot plate apparatus. The thermal conductivity for the references are shown in Figure 3.

Heaters made of Armco iron are placed on either end of the column to control heat flow and mean temperature. Armco iron is used because its thermal conductivity is about 200 times that of the specimen and; hence, the temperature gradient along a radial line at the top of the build-up was estimated to be no more than one or two degrees. Thus, the guard and central temperatures are matched at the ends. The entire assembly is surrounded by diatomaceous earth or thermatomic carbon insulation depending on the specimen insulation contained inside a 4 inch diameter guard heater.

Temperatures are measured at two axial locations in each reference and in the specimen. A beaded chromel/alumel thermocouple is inserted into the drilled holes in a 1/32 inch double bore alumina insulator. The insulator is broken about every 1/8 inch to minimize conduction losses. The thermocouples in the specimen are potted in place at the bead with Silastic RTV-731, silicone rubber.

Specimen gage lengths are determined from post-run radiographs or X-rays. The X-rays are examined at 10 x magnification to determine the gage distance relative to the overall thickness. Then the relative distances were converted to true distances from the actual thickness of the specimens.

The idea for the assembly shown in Figure 1 is to use identical materials for a guard ring and thus create as closely as possible a matched guard condition to minimize radial heat exchange and heat shunting. Further, the annulus is kept small to minimize heat shunting which occurs even with matched guarding.

In practice, perfect matching of the guard and central columns is not achieved. Hence, corrections for radial heat exchange are made to the measured data based on the measured temperature profiles. Further, corrections are made for the heat shunting through the annulus. The following paragraphs discuss these corrections.

Note in Figure 1 that guard temperatures are measured at the center of each of the three guard sections. These temperatures are used in the analysis of radial heat exchange. For the analysis a one-dimensional fin-type heat transfer analysis is used. The analysis is applied to determine the actual heat flux density into and out of the specimen based on the measured temperatures in the references and under the assumption of a linear temperature profile

in the guard. Consider the following sketch for the top reference and guard (see Figure 1 for identification of thermocouples):

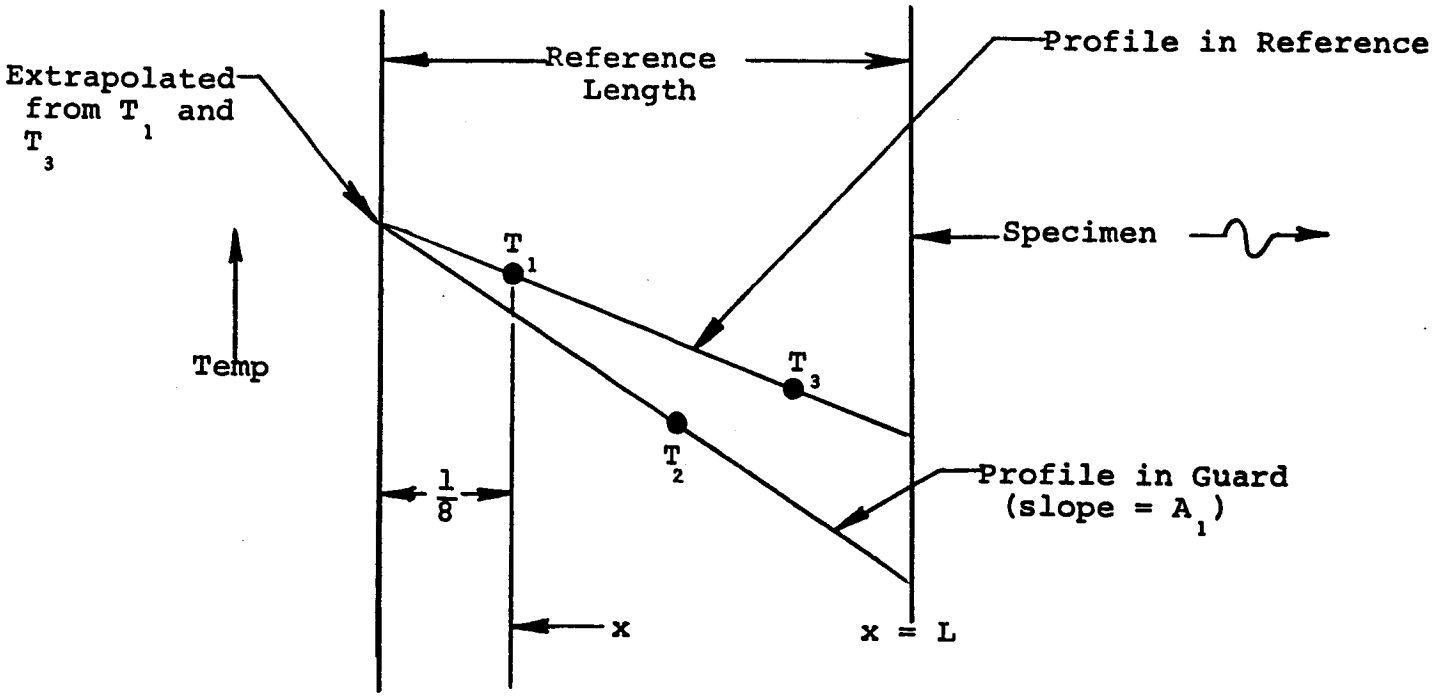

The temperature profile in the reference is given by

$$t = C_1 e^{Nx} + C_2 e^{-Nx} + T_2 + A_1 \left(\frac{1}{8} - x\right) \qquad (1)$$

where

t = temperature

C_1, C_2 = constants of integration

$$N = \sqrt{\frac{hp}{k}}$$

h = effective heat transfer coefficient between two points of radial temperature measurement

p = perimeter of reference

k = thermal conductivity of reference

To solve for Q_S, the heat flux density into the specimen at X = L, equation (1) is subjected to the following boundary conditions:

$$t = T_1 \quad @ \; x = o \tag{2}$$

$$k = \frac{dt}{dx} = -Q_S \quad @ \; X = L \tag{3}$$

A solution is obtained from equation (1) and boundary conditions (2) and (3). There are two unknowns in the resulting equation; namely, Q_S and t. Q_S is determined from the known temperature, T_3, at x = 0.25 inch. Note that the interface temperature at the heater is determined from a linear extrapolation of the reference temperatures. The interface temperature at the heater is assumed to be the same for the central and guard columns and is used along with T_2, the guard temperature, to calculate the temperature gradient in the guard, A_1.

The same type of analysis is used to calculate the actual heat flux into the surface of the bottom reference.

The radial heat loss along the specimen is calculated by assuming a linear temperature profile through the specimen and through the guard. The actual heat flux into the top of the specimen is used and heat fluxes are calculated at each thermocouple location, at the midpoint of the specimen and at the bottom of the specimen. If the heat flux calculated at the bottom of the specimen differed from that calculated from the measurements at the bottom reference, the difference is halved and the heat flux at the top of the specimen is adjusted by that amount. The calculations for the heat flux profile through the specimen are then repeated with the adjusted value. Then, the average heat flux between the points of temperature measurement in the specimen is calculated from

$$Q_{sp} = \frac{Q_{s_1} + 2\,Q_{s_2} + Q_{s_3}}{4} \tag{4}$$

where

Q_{sp} = average heat flux through specimen

Q_{s_1} = heat flux at thermocouple No. 4

Q_{s_2} = heat flux at midpoint of specimen

Q_{s_3} = heat flux at thermocouple No. 6

Now, the measured thermal conductivity is based on the average heat fluxes through the top and bottom references as calculated under the assumption of a linear temperature gradient and no heat losses. The measured thermal conductivity is converted to the corrected value by the equation

$$k_{cr} = \frac{Q_{sp}\ k_m}{Q_m} \tag{5}$$

where

k_{cr} = effective thermal conductivity of specimen corrected for radial heat exchange

Q_{sp} = average heat flow through specimen calculated from analysis

Q_m = average heat flow in references under assumption of no heat loss

k_m = measured thermal conductivity of sample

Next, the method of obtaining the heat transfer coefficients for use in the analysis of radial heat exchange will be considered. Note in Figure 1 that the space between points of radial temperature measurements is filled with either the fused silica or the specimen and the insulation in the annulus between the central column and guard. The thermal conductivities of these elements and the radial thicknesses are used to compute an effective heat transfer coefficient for the analysis. For example, the heat transfer coefficient across the 1/16 inch gap between the central column and guard column is calculated from the equation

$$h = \frac{k}{R_s \ln (R_2/R_1)} \tag{6}$$

where

k = thermal conductivity of material between R_1 and R_2

R_s = radius of central column

R_2 = outer radius

R_1 = inner radius

The thermal resistances of the slip cast fused silica and the specimen between the points of radial temperature measurement are also included in the effective heat transfer coefficients. For the central column the effective heat transfer coefficient is calculated assuming radii (for Equation 6) of 0.25 and 0.5 inch.

For the guard ring, the radii used in Equation 6 are 0.562 and 0.781 inch. Of course, for this analysis the thermal conductivity used in Equation 6 is that of the slip cast fused silica or the specimen.

The overall heat transfer coefficient used in the analysis of radial heat exchange is calculated from the equation

$$h = \frac{h_s\, h_a\, h_g}{h_s\, h_g + h_a\, h_s + h_a\, h_g} \qquad (7)$$

where

h = overall heat transfer coefficient used in Equation 1 $\left[N = \sqrt{\frac{hp}{k}}\right]$

h_s = effective heat transfer coefficient due to radial thermal resistance of central column

h_a = effective heat transfer coefficient of annulus between central and guard sections

h_g = effective heat transfer coefficient of guard ring from inner radius to thermocouple location

The heat transfer coefficients are calculated as a function of temperature. In the analysis of radial heat losses, different values of the heat transfer coefficient are used for the top reference, specimen and bottom reference based on the mean temperatures at those locations.

The thermal conductivity values for the slip cast fused silica which are used to calculate the heat transfer coefficients are presented in Figure 3. The thermal conductivity values which are used for the calculation of the effective heat transfer coefficient of the insulations of diatomaceous earth or thermatomic carbon in nitrogen at 760mm and vacuum are presented in Figure 4, 5 and 6. Also shown in Figure 4 are thermal conductivity values for nitrogen. Literature values for the thermal conductivity of the diatomaceous earth in air (nitrogen) were found to a temperature of 800°F and were extrapolated to 2000°F. Values for the thermatomic carbon were obtained from previous measurements made in our radial inflow apparatus.

With the above information and the measured thermal conductivity of the specimen, the heat transfer coefficients in Equation 7 are calculated.

In addition to the errors associated with radial heat exchange, there are errors due to the shunting heat flow around the specimen through the insulation. This error occurs even with perfect temperature matching of the central and guard columns. This error has been defined analytically by Flynn [3] as

$$\alpha = k_i \left[\frac{1}{k_r} - \frac{1}{k_{cr}}\right] F_g \tag{8}$$

$$k_c = \frac{k_{cr}}{1-\alpha} \tag{9}$$

where

k_c = final corrected thermal conductivity

k_{cr} = measured thermal conductivity corrected for radial heat exchange

k_i = thermal conductivity of insulation

k_r = thermal conductivity of references

F_g = a geometrical factor

Flynn [3] gives the following equation for the maximum value of F_g

$$F_g \leq \left[\frac{(b^2/a^2) - 1}{2 \ln (b/a)}\right] - 1 \tag{10}$$

where

a = radius of specimen
b = inner radius of guard cylinder

Equations 8, 9 and 10 are used to correct for the shunting heat flow. The value used for F_g is 0.116 which is calculated from Equation (10) for the geometry of our system.

Note that two different corrections are applied to the experimental data. However, lest one should become overly concerned with this it should be considered that the maximum value for both corrections is about 10 percent. Hence, sizeable uncertainties in the correction procedures do not lend large

uncertainties to the final data. The several sources of uncertainty and the estimated values are summarized below:

1. Uncertainty in final data due to uncertainty in correction analysis, property data used in analysis and radial temperature differences = 5 percent (maximum).

2. Uncertainty in thermal conductivity of fused silica references = 5 percent to 500°F, 7 percent to 1800°F

3. Uncertainty in gage length = 2 percent.

4. Uncertainty in temperature difference measurements = 2 percent.

The combined uncertainty for the several sources of uncertainty listed above is ±8 percent to 500°F and ±10 percent to 1800°F.

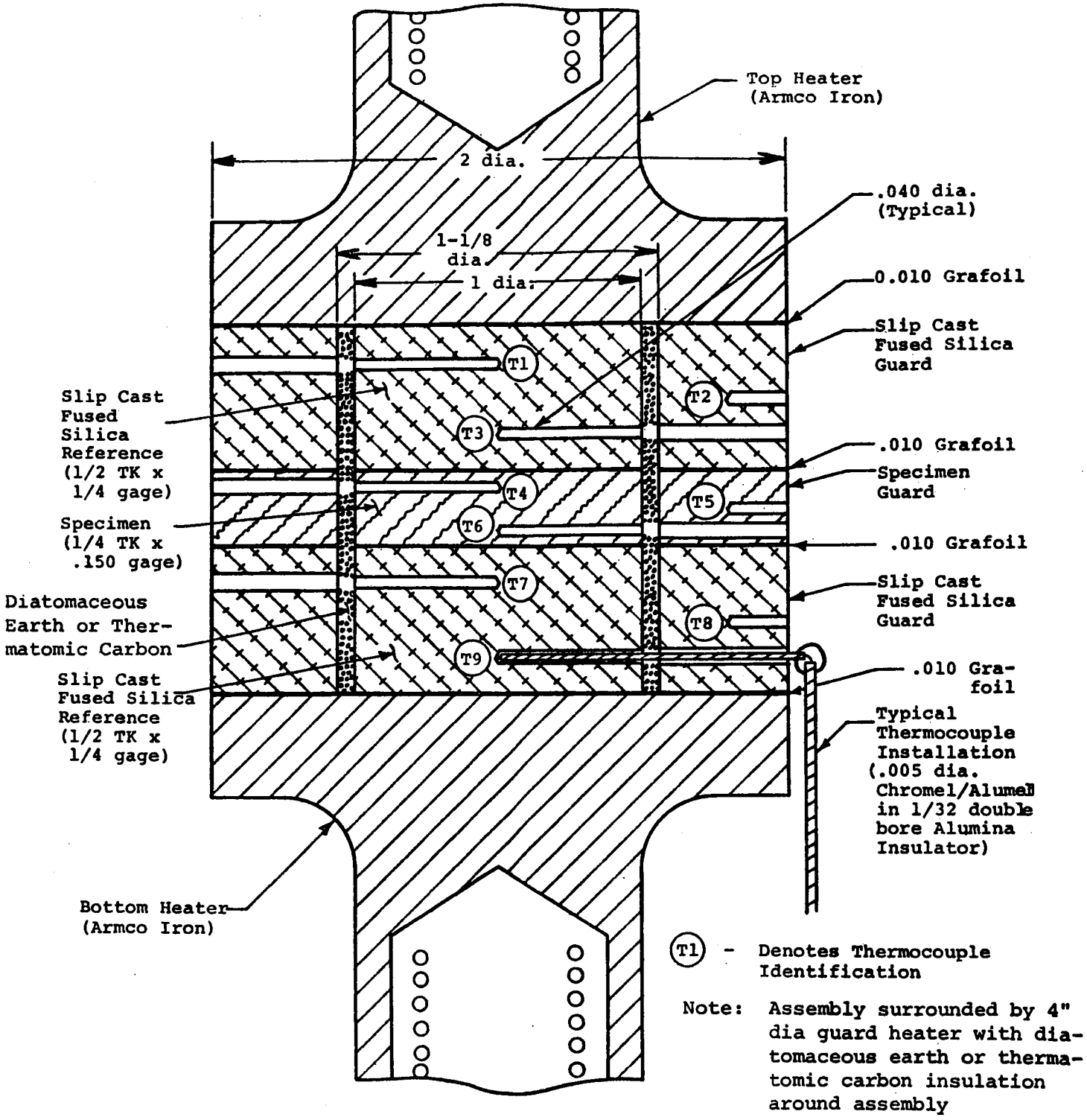

Figure 1. Assembly of Guarded Comparative Rod Apparatus

Note: Size thickness of specimen and guard ring at same time for thickness match.

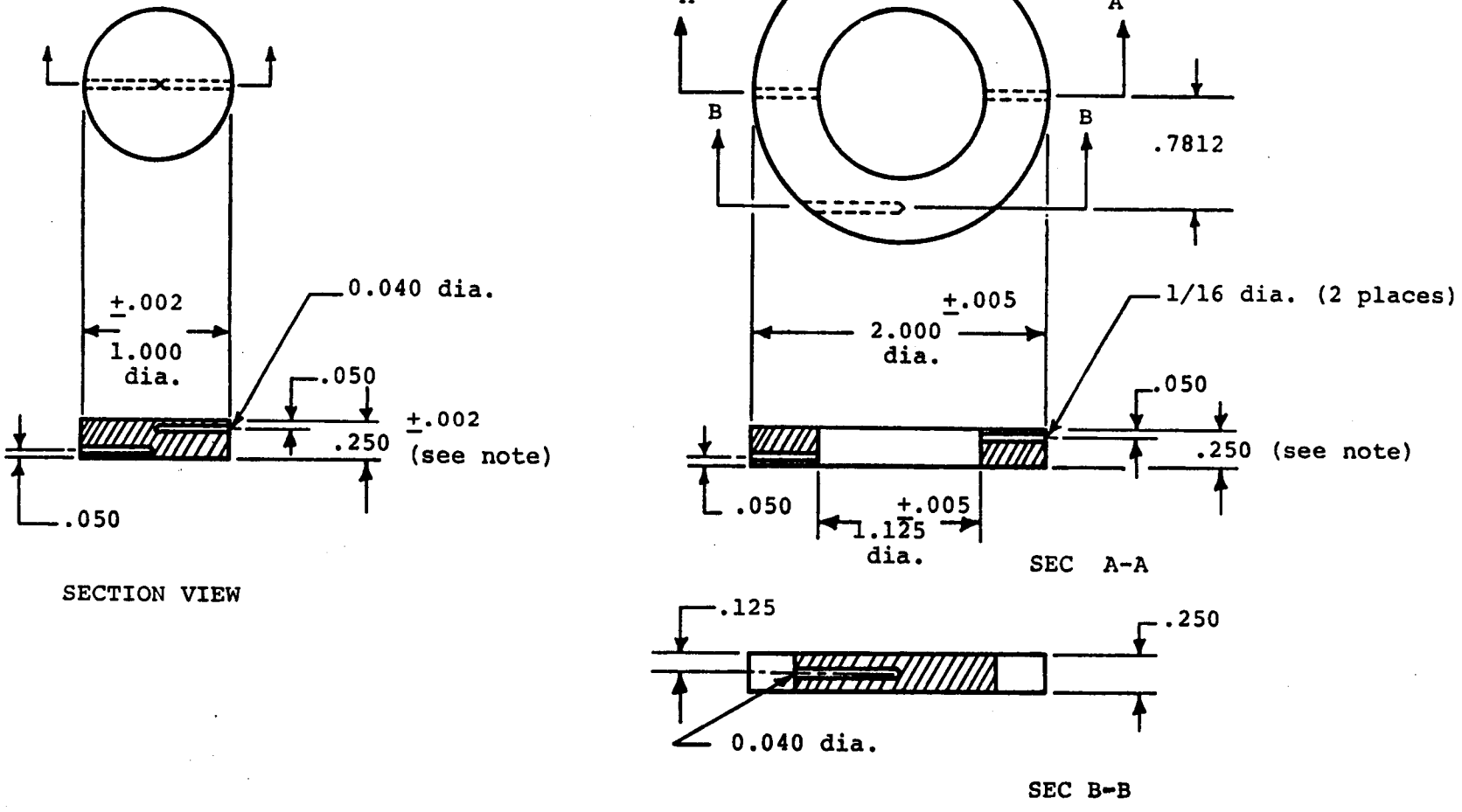

Figure 2. Specimen and Guard Ring for Measurements in Guarded CRA.

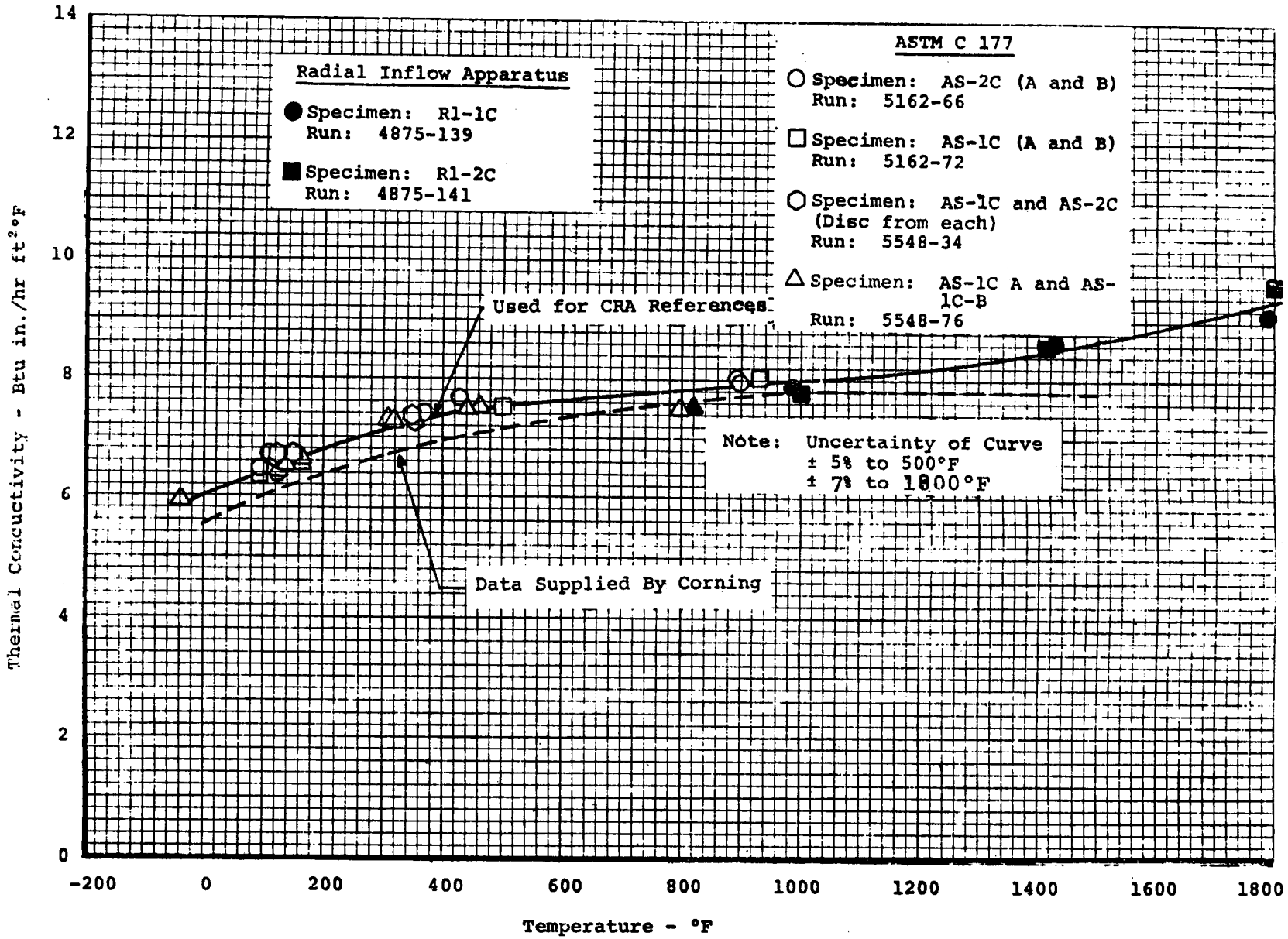

Figure 3. Thermal Conductivity of the Slip Cast Fused Silica References Used in the Comparative Rod Apparatus

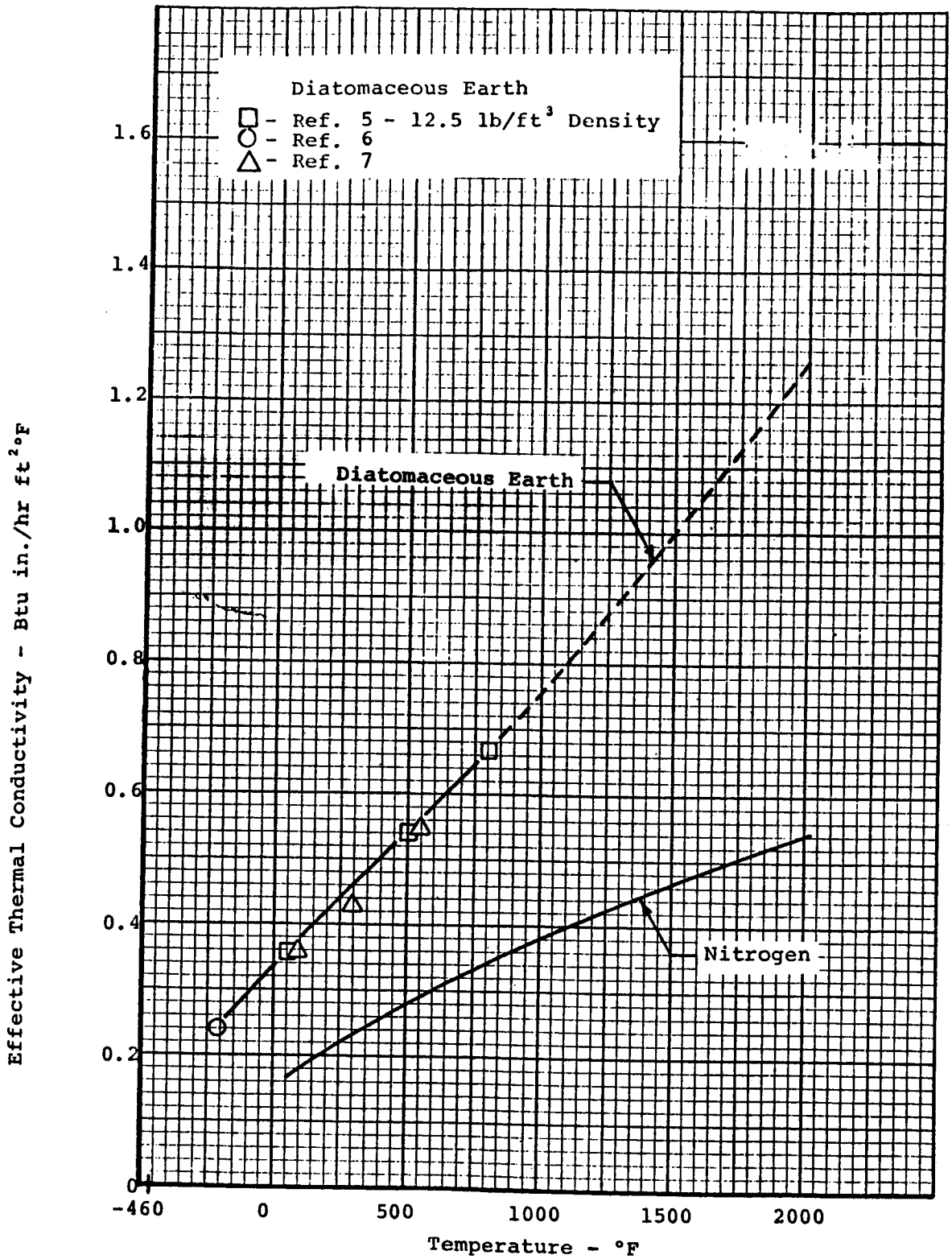

Figure 4. Thermal Conductivity of Diatomaceous Earth in Air (Nitrogen).

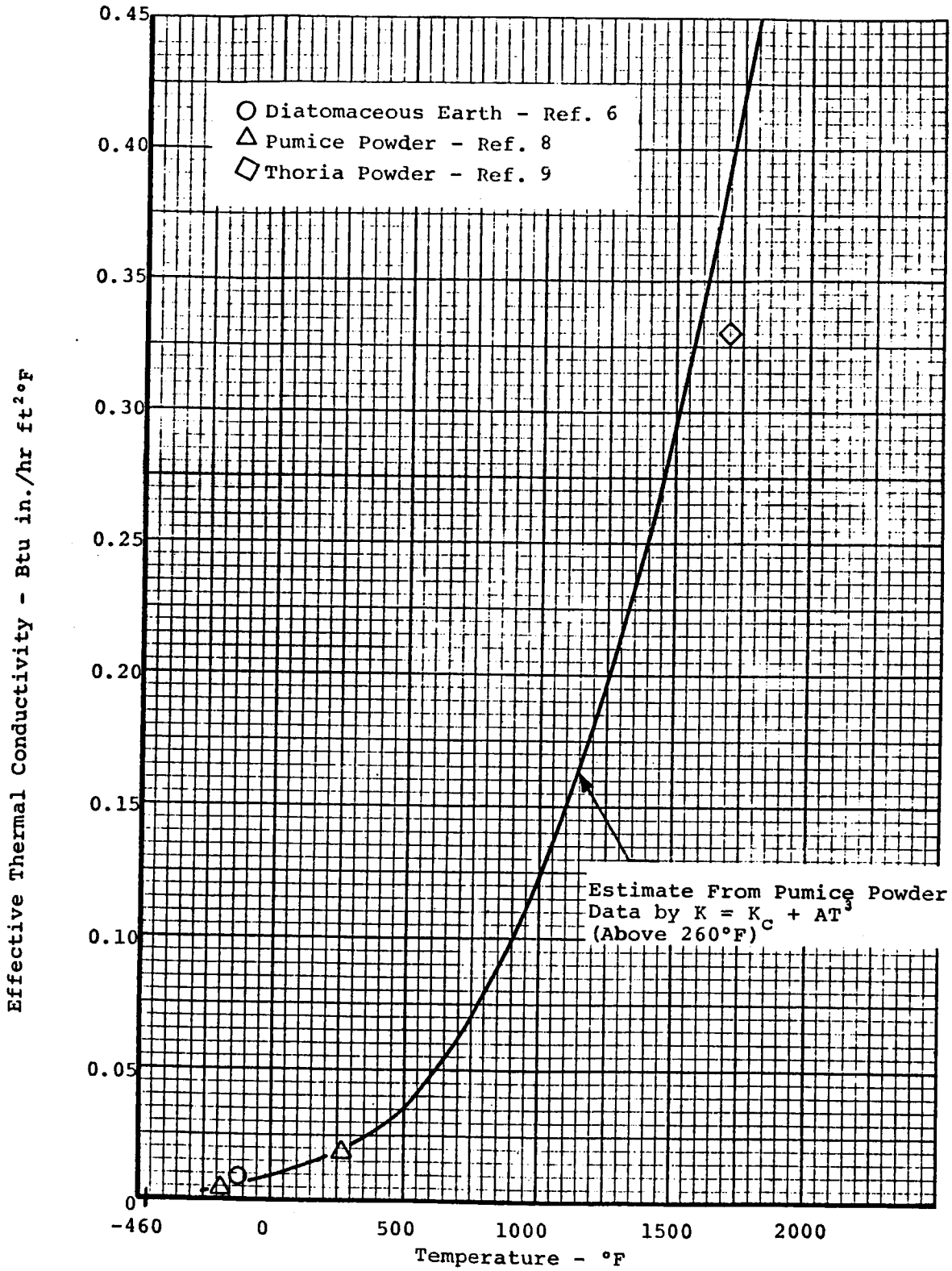

Figure 5. Estimated Thermal Conductivity of Diatomaceous Earth in Vacuum.

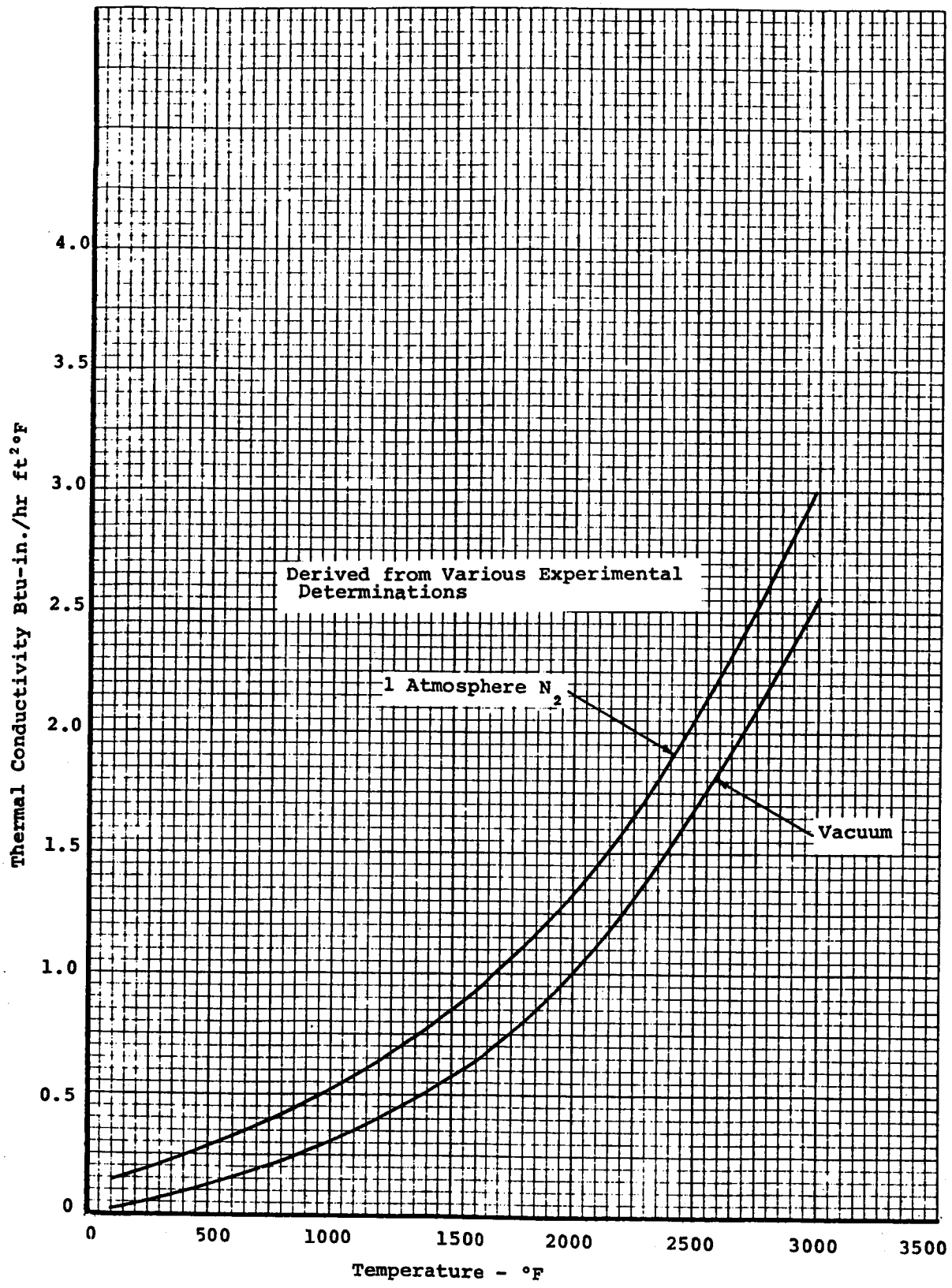

Figure 6. Thermal conductivity of thermatomic carbon in nitrogen and vacuum

specimen. The outer ends of the specimen guards are insulated with graphite tubes filled with thermatomic carbon. These tubes also hold the specimen in alignment. The combined effect of specimen guards and thermatomic carbon insulation permits a minimum axial temperature gradient within the specimen. This gradient is not detectable by optical pyrometer readings. Visual inspection of the specimens after runs have verified that no large axial temperature gradient exists in the specimen. The guards, made of specimen material, display axial distortion of the isothermal lines for approximately 1/4" from the outer ends before reaching an apparent constant axial temperature.

When sufficient material is available the alternate specimen configuration shown in Figure 5 is employed. This specimen, being 1.5" in diameter, provides a larger gage length (0.357") between temperature wells and allows the installation of three holes on each radius without excessively distorting the radial temperature profiles. Thus this specimen configuration permits a more precise measurement of the average temperature at each radial location. As with the smaller specimen, the location of the temperature wells must be altered for transversely anisotropic specimens.

The annulus between the specimen inside diameter and the 7/32" outside diameter of the calorimeter tube is packed with either copper granules, graphite or zirconia powder. This packing provides a positive method for centering the calorimeter within the specimen and promotes good heat transfer between specimen and calorimeter.

Temperatures up to 2000°F are measured with Chromel/Alumel thermocouples inserted into the specimen through the sight tubes. At high temperatures, the temperatures are measured through the certical sight tubes using a right-angle mirror device and optical pyrometer.

In Figures 1 and 3 showing a typical conductivity calorimeter apparatus ready for insertion into a furnace for a run, a water-cooled copper section can be seen at the top of the unit. This section provides permanent sight tubes to within about 2-1/2" of the guard specimen, in addition to a permanent mount for the right-angle mirror device used with the optical pyrometer. Within the short zone between the water-cooled section and the top guard, thin-walled graphite sight tubes are fitted. The remainder of the annulus is filled with thermatomic carbon insulation.

During thermal conductivity runs, the following data are recorded: (1) power input, (2) specimen face temperature, (3) specimen temperatures in the gage section at the two radii, (4) temperature of the calorimeter water at two points 1/2" apart axially within the specimen center and (5) water flow rate through the calorimeter. At least 5 readings are made at each general temperature range to determine the normal data scatter and to minimize the error that might be encountered in a single reading.

All thermocouple readings are measured on a Leeds and Northrup K-3 null balance potentiometer used in conjunction with a galvanometer of 0.43 microvolts per mm deflection sensitivity. All optically measured temperatures are read with a Leeds and Northrup Type 8622 optical pyrometer. The flow rate of the calorimeter water is measured with a Fischer and Porter Stabl-Vis Flowrater.

The thermal conductivity values are computed from the relation

$$K = \frac{Q \ln \frac{r_2}{r_1}}{2\pi L \, (T_{r_2} - T_{r_1})}$$

where

Q = the heat flow to and measured by the calorimeter
r_2 = the radius to the outer temperature well
r_1 = the radius to the inner temperature well
T_{r_2} = temperature at r_2
T_{r_1} = temperature at r_1
L = the gage length over which the calorimeter ΔT is measured, for our present calorimeter is 1/2 inch

Based on an extensive error analysis and calibrations on homogeneous isotropic materials of known thermal conductivities, such as Armco iron and tungsten, the precision (coefficient of variation) in the measurements has been established at ±7 percent over the temperature range. For multiple runs on samples having similar properties, the uncertainty in a smooth curve through the data can be established to within ±7 percent. A detailed error analysis has been presented in a paper by Mann and Pears.[1]

Data obtained here on several high temperature materials are presented in Figures 6, 7 & 8. Figure 6 is a plot of data obtained here on tungsten. The specimen for these determinations were fabricated from stacks of 0.060 inch washers cut from hot rolled sheet stock. Also plotted are values reported by other investigators including "recommended values" given by Powell, Ho and Liley[2] based on a compilation of 103 sets of data. Agree-

---

[1]Mann, W. H. Jr., and C. D. Pears, "A Radial Heat Flow Method for the Measurement of Thermal Conductivity to 5200°F", presented at the Conference on Thermal Conductivity Methods, Battelle Memorial Institute, October 26-28, 1961.

[2]Powell, R. W., C. Y. Ho and P. E. Liley, "Thermal Conductivity of Selected Materials", NSRDS-NBS 8, National Standard Reference Data Series - National Bureau of Standards - 8, 1966, pp. 11, 54-59.

ment of the recommended values is excellent throughout the temperature range.

Figure 7 shows data obtained here on ATJ graphite, with grain. This material is premium grade, medium grain graphite having a density range of 1.73 to 1.78 gm/cm^3. The crosses (+) shown in the figure are "recommended values" given by Ho, Powell and Liley.[3] Again agreement is excellent.

Figure 8 shows data obtained on AXM-5Q1. These data were obtained under a program sponsored by the Air Force Materials Laboratory to develop high temperature thermal conductivity standards. Measurements were made on this material by four laboratories in addition to Southern Research Institute. The bands shown in Figure 8 represent the range of data reported by the other participating organizations. A complete presentation and discussion of the data are given in AFML-TR-69-2.[4]

---

[3]Ho, C. Y., R. W. Powell and P. E. Liley, "Thermal Conductivity of Selected Materials, Part 2, "NSRDS-NBS 16 National Standard Reference Data Series - National Bureau of Standards-16, pp. 89-128.

[4]AFML-TR-69-2, "Development of High Temperature Thermal Conductivity Standards" submitted by Arthur D. Little, Inc., under Contract AF33 (615)-2874, 1969, pp. 115-127.

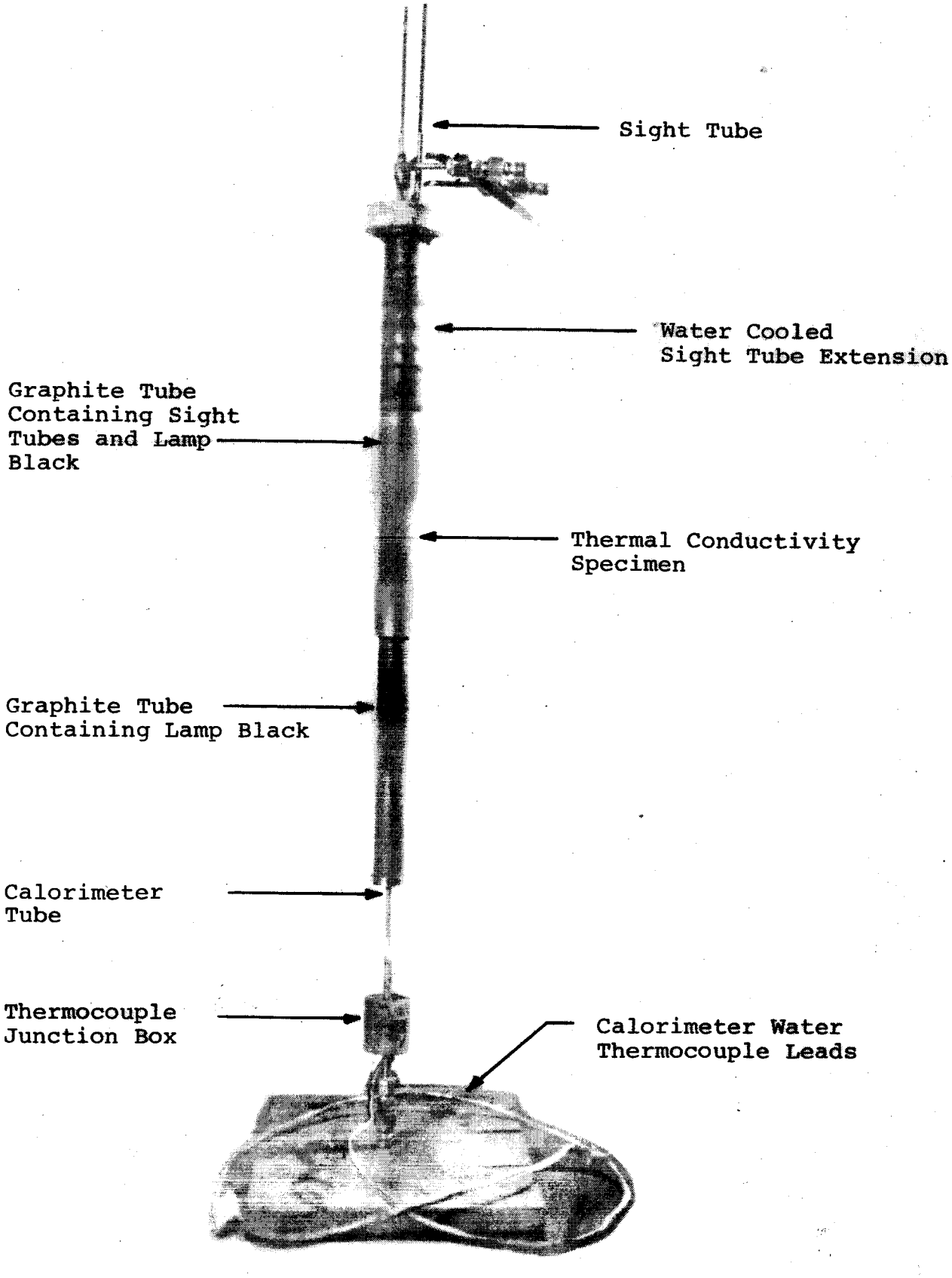

Figure 1. Photograph of the Radial Thermal Conductivity Apparatus

Figure 2. Furnace with Thermal Conductivity Apparatus Installed

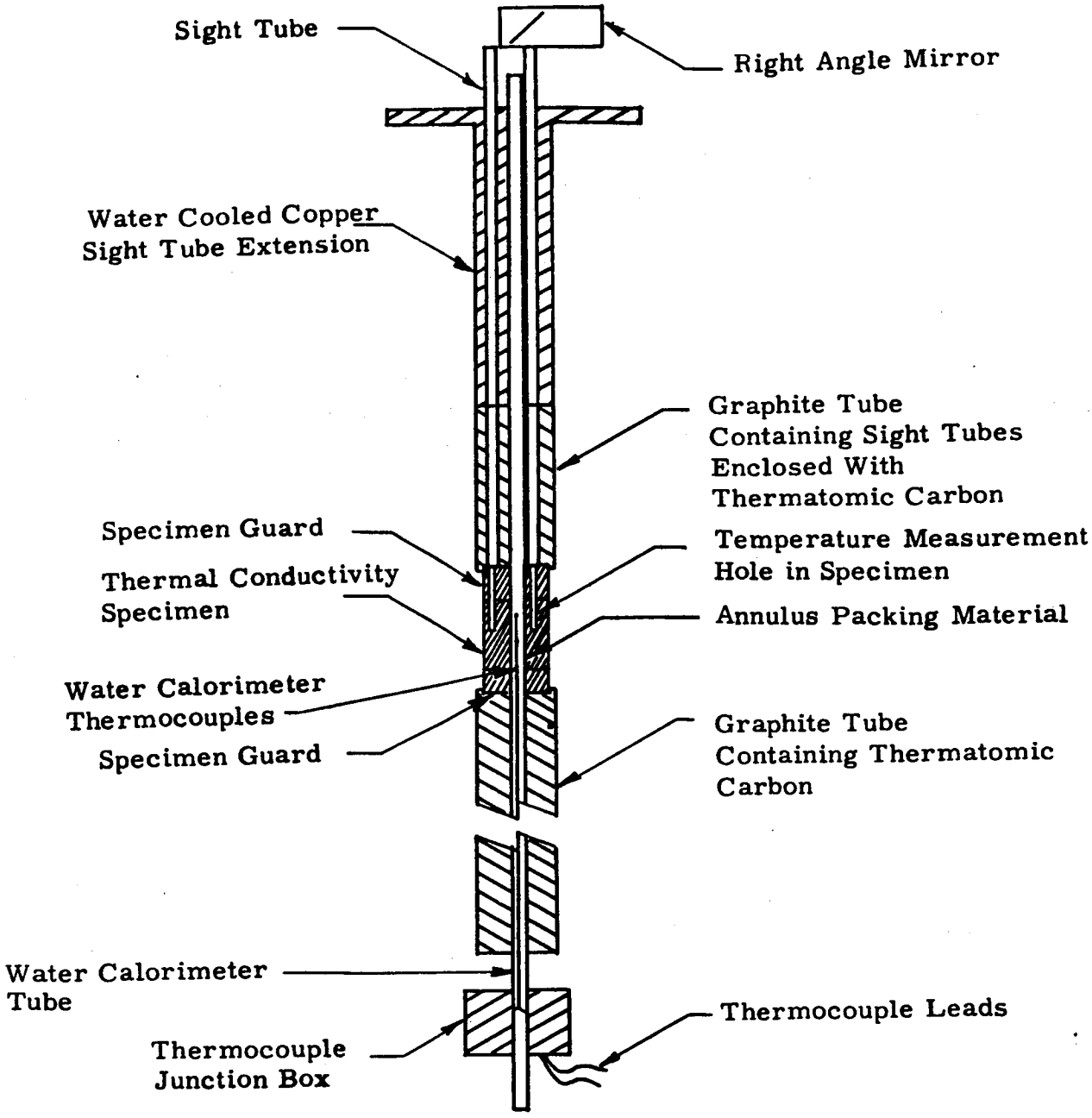

Figure 3. Cross-section Schematic of the Thermal Conductivity Apparatus

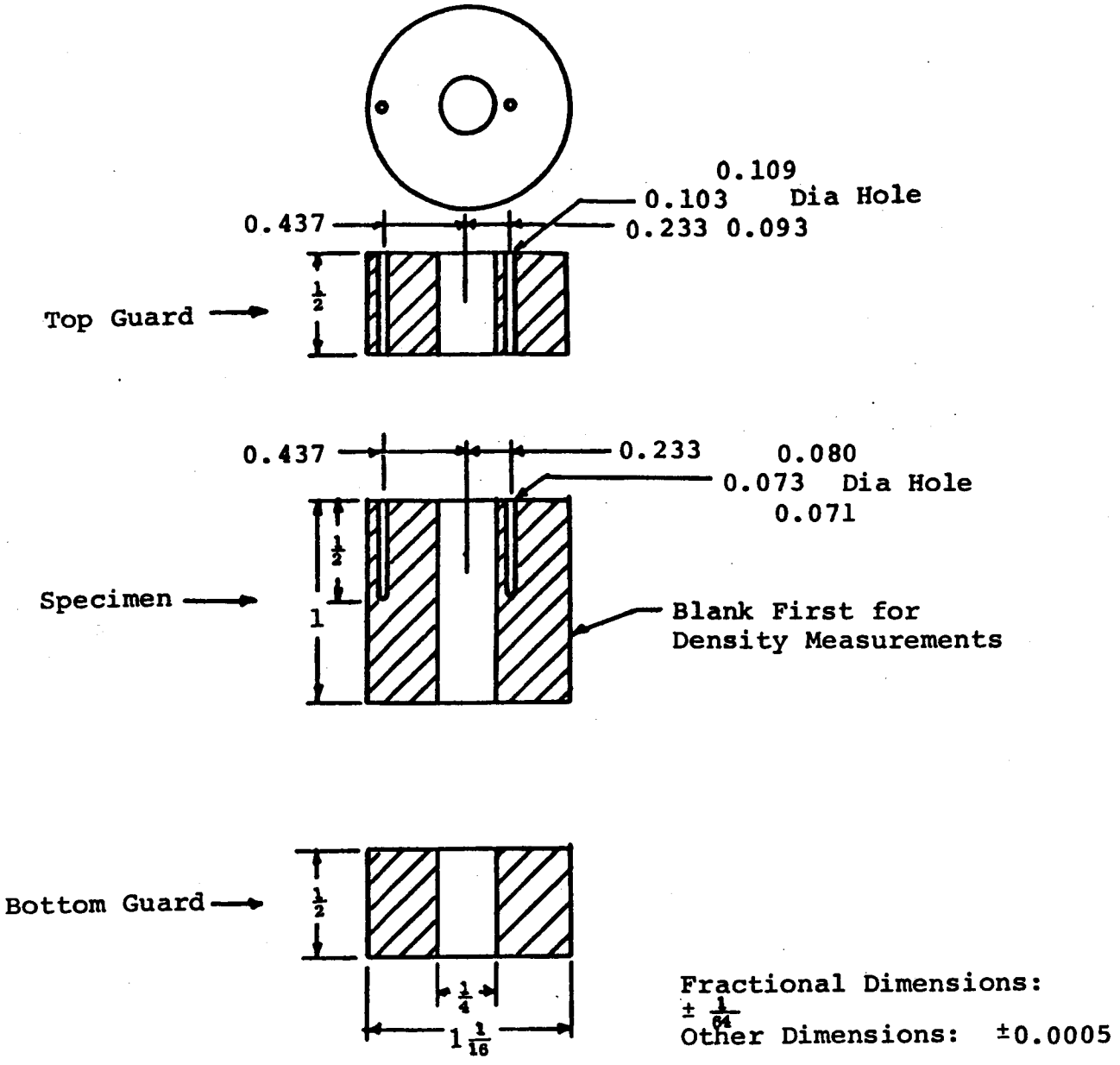

Figure 4. 1.06 Diameter Thermal Conductivity Specimen for Radial Inflow Apparatus

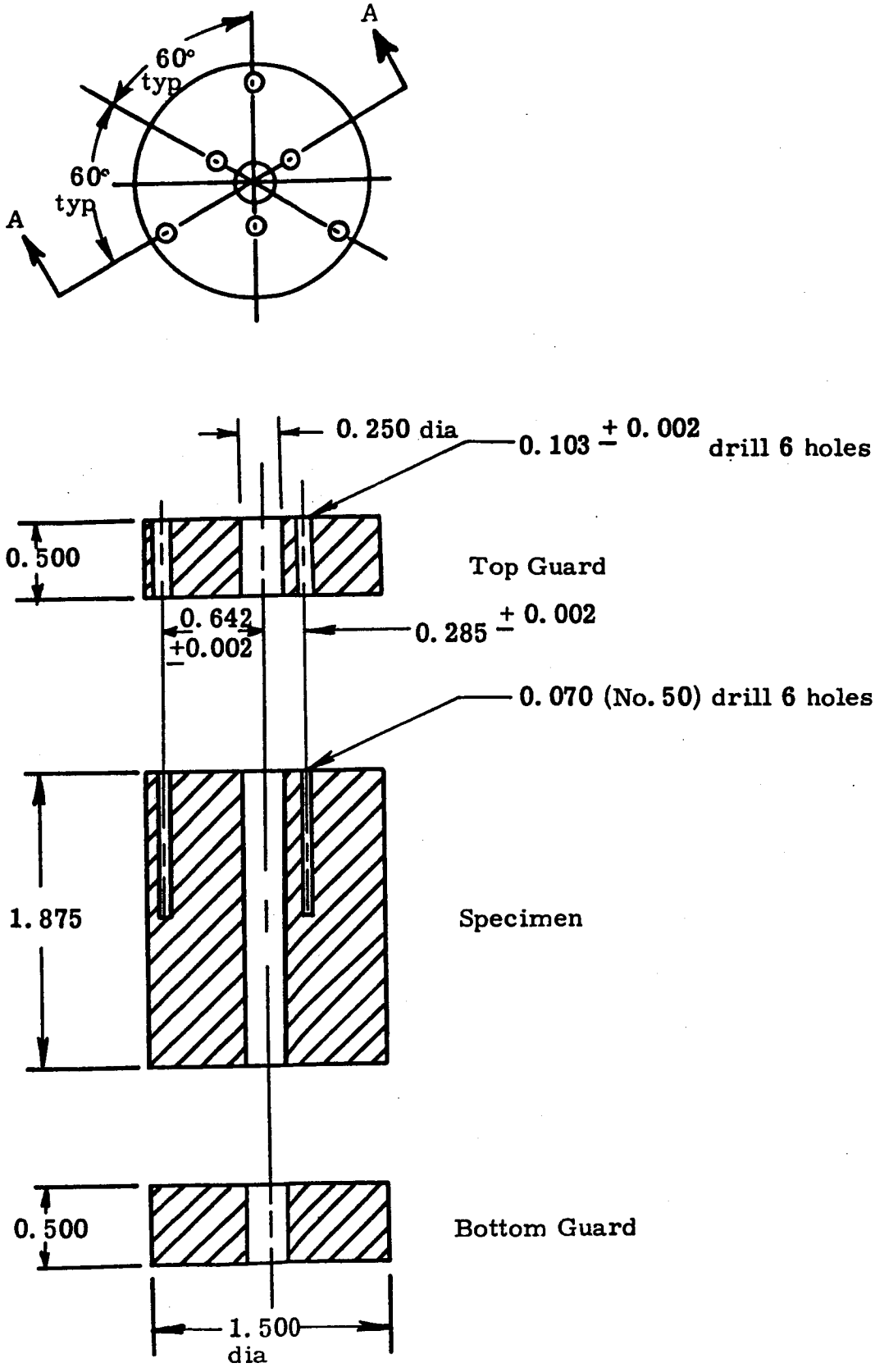

Figure 5. Dimensions of 1.50 Inch Diameter Specimen and Guards Used for Radial Inflow Thermal Conductivity Measurements

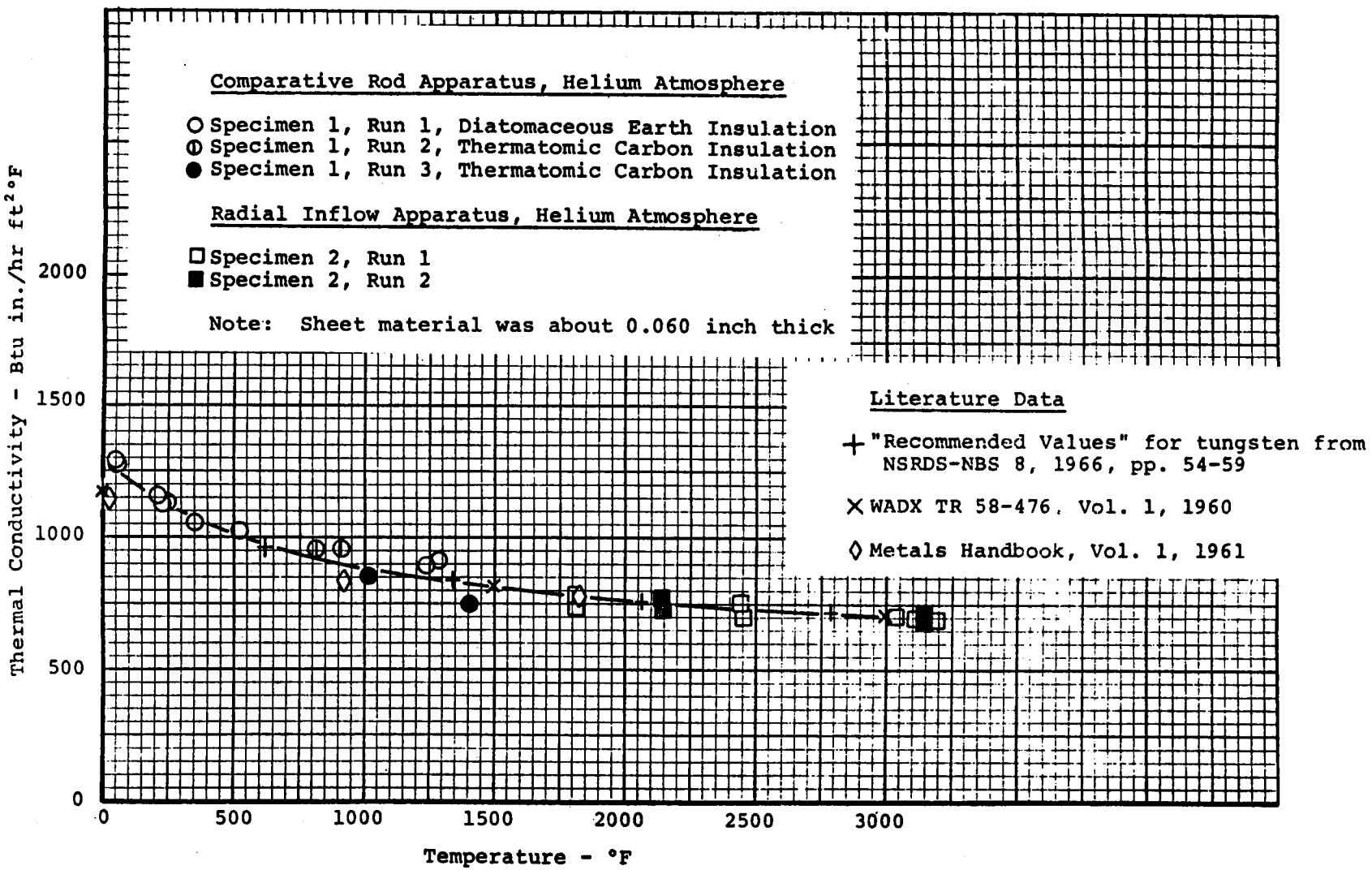

Figure 6. The Thermal Conductivity of Tungsten Sheet Parallel to the Plane of the Sheet

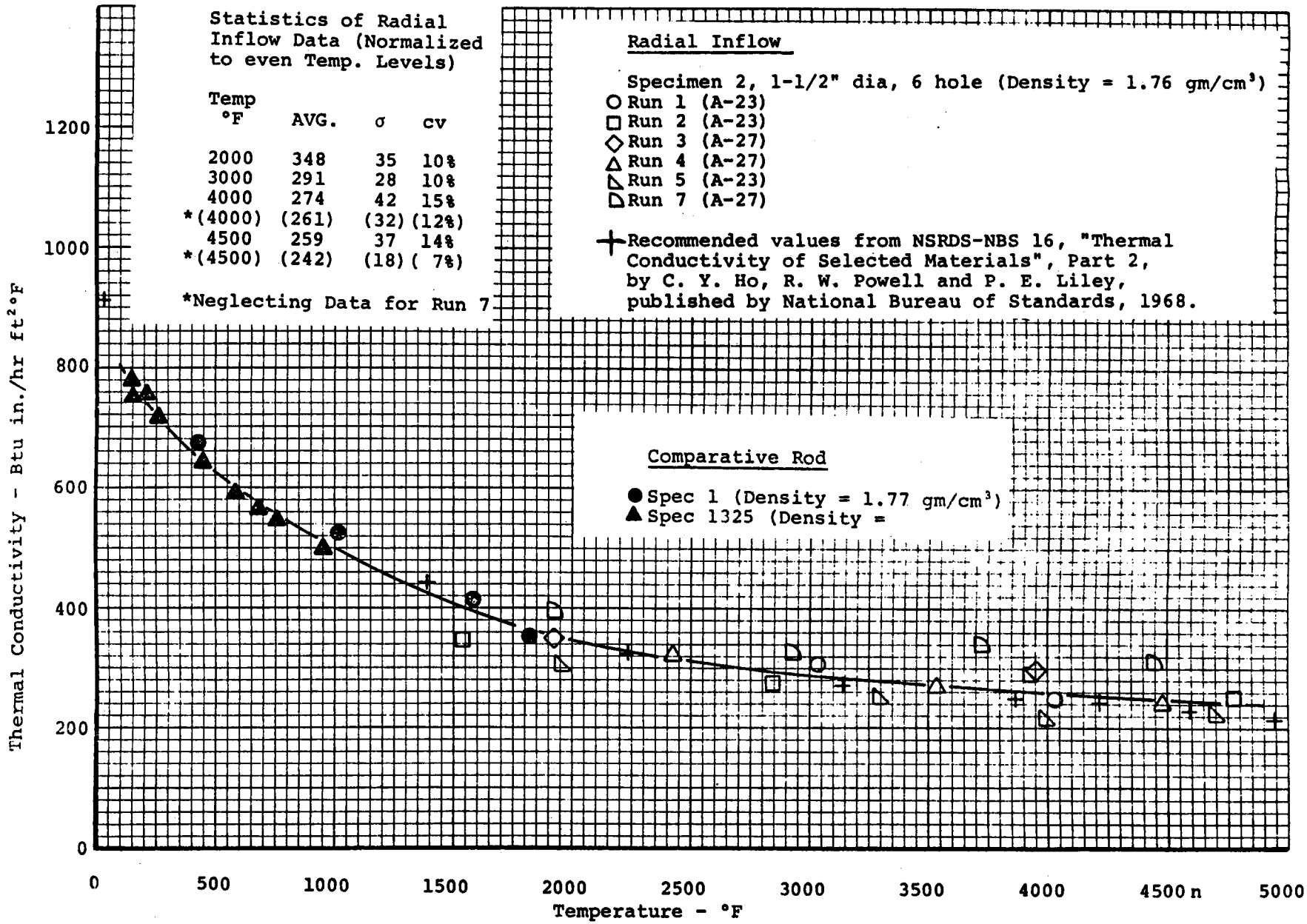

Figure 7. The Thermal Conductivity of ATJ Graphite, With Grain

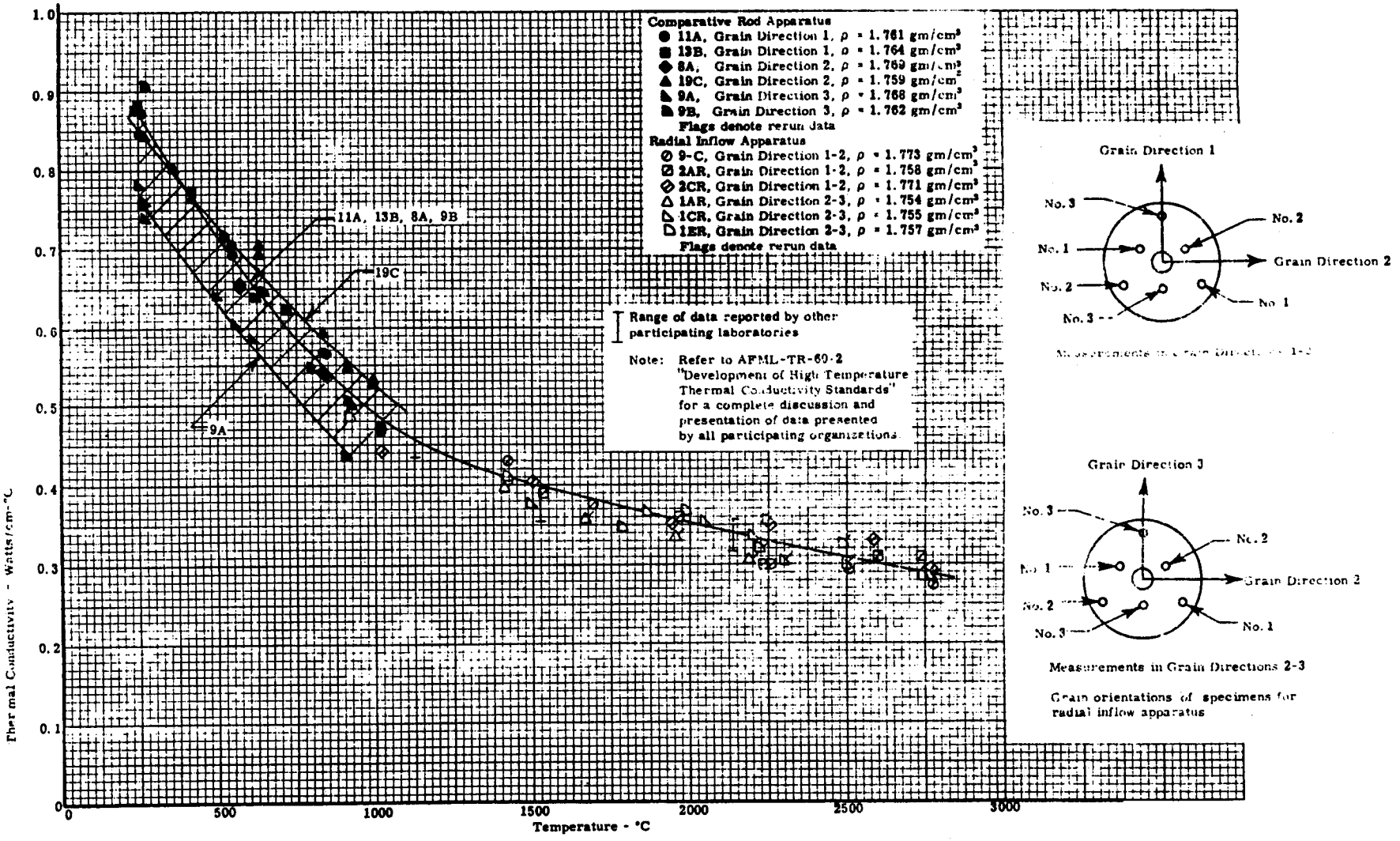

Figure 8. The Thermal Conductivity of AXM-5QI Graphite

APPENDIX E

HEAT CAPACITY TO 1000°F

HEAT CAPACITY TO 1000°F

The heat capacity to 1000°F is determined from data obtained in an adiabatic calorimeter. In this apparatus the heated specimen is dropped into a thermally guarded, calibrated cup, and the enthalpy is measured as a function of the increase in temperature of the cup. The heat capacity is the slope of the enthalpy versus temperature curve. A picture of the apparatus is shown in Figure 1.

A tubular furnace and a cold box are used to bring the specimens to temperature. By pivoting this equipment on a common post near the calorimeter, the samples are transferred to a position directly over the calorimeter cup. At this position the specimen is released from a suspension assembly that is triggered externally. Thermocouples located near the specimen are used to measure specimen temperature. The normal specimen size is about 1" x 1" x 1".

Elevated specimen temperatures are maintained by a manual setting of a variable voltage transformer, which controls the power input to the furnace. Cold sample temperatures are obtained by filling the cold box with dry ice and, when required, injecting liquid nitrogen vapors. The cold box consists of two concentric cylinders enclosed in a housing. The smaller cylinder (3" diameter by 16" high) is constructed of 1/4" mesh hardware cloth. The larger cylinder is made of galvanized sheet metal (15" diameter and 16" high). The annulus is partially filled with dry ice.

Specimens of the materials are heated or cooled to the desired temperature, and following a stabilization period, are dropped into the calorimeter cup. Adiabatic conditions are maintained during each run by manually adjusting cup guard bath temperature.

The covered cup of the drop-type adiabatic calorimeter is approximately 2-1/2" diameter by 2" deep. Three thermocouple wells are located in the bottom wall of the cup. The cup is mounted on cork supports, which rest in a silver-plated copper jacket. The jacket is immersed in a bath of ethylene glycol which is maintained at the temperature of the cup by means of a heater and copper cooling coils immersed in the liquid. Chilled trichloroethylene is circulated through the coils to cool the bath below ambient temperature when cold enthalpy measurements are made. A double-bladed stirrer maintains uniform bath temperature.

In the calorimeter six copper-constantan thermocouples, differentially connected between calorimeter cup and jacket, indicate temperature difference between cup and bath. The six thermocouples enable a difference of 0.03°F to be detected. This difference is maintained to within 0.15°F. During the runs, absolute temperature measurements of the cup are determined by means of the three thermocouple junctions, series connected, in the bottom of the calorimeter cup. All of the thermocouple readings are taken with instruments which permit readout to within 0.1°F; however, the system uncertainty is about 0.5°F.

The enthalpy of the specimen at any initial temperature is calculated from the following equation:

$$h = \frac{K}{W_S} (t_2 - t_1) \qquad (1)$$

where

h = enthalpy above t_2
K = calorimeter constant, 0.2654 Btu/°F
W_S = sample weight in lbs
t_1 = initial cup temperature in °F
t_2 = final cup temperature in °F

The calorimeter constant of 0.2654 Btu/°F was determined by measuring the enthalpy of an electrolytic copper specimen of known specific heat.

The enthalpy is referred to a common base temperature of 85°F using the following linear interpolation:

$$h_{85} = h \frac{(t_3 - 85)}{(t_3 - t_2)} \qquad (2)$$

where

h_{85} = enthalpy above the reference temperature of 85°F in Btu/lb
t_3 = initial sample temperature in °F

The base of 85°F is used because this is usually near the actual final cup temperature.

The enthalpy-temperature curve established is used to determine heat capacity (specific heat) by measuring its slope at different temperatures. This is done both graphically and by analytical methods which first fit the enthalpy data to an equation of the following type:

$$h_{85} = aT + bT^2 + cT^{-1} + d \qquad (3)$$

The temperature (T) employed usually is in degrees Rankine. While this equation may not provide the best definition of the enthalpy data over the entire temperature range, it does anticipate the theoretical behavior and is consistent with methods recommended in WADC TR 57-308 and by K. K. Kelley.[1] The derivative of this equation, the heat capacity, is used with the constant "c" adjusted so that the analytical solution agrees with the value determined graphically at 150°F. This technique is similar to that of Kelley in forcing the heat capacity equation through a known value. The equations are developed using a digital computer.

The accuracy of the apparatus has been confirmed by measuring the enthalpy of sapphire (SRM 734 from NBS) and other standard specimens. The results of the comparison on sapphire and other data indicate that the overall uncertainty of the apparatus is at ±3 percent.

---

1. Kelley, K. K., "Contributions to Data on Theoretical Metallurgy," Vol. XIII High Temperature Heat Content, Heat Capacity, and Enthalpy Data for Elements and Inorganic Compounds, Bulletin 584, U.S. Bureau of Mines, Nov. 1958.

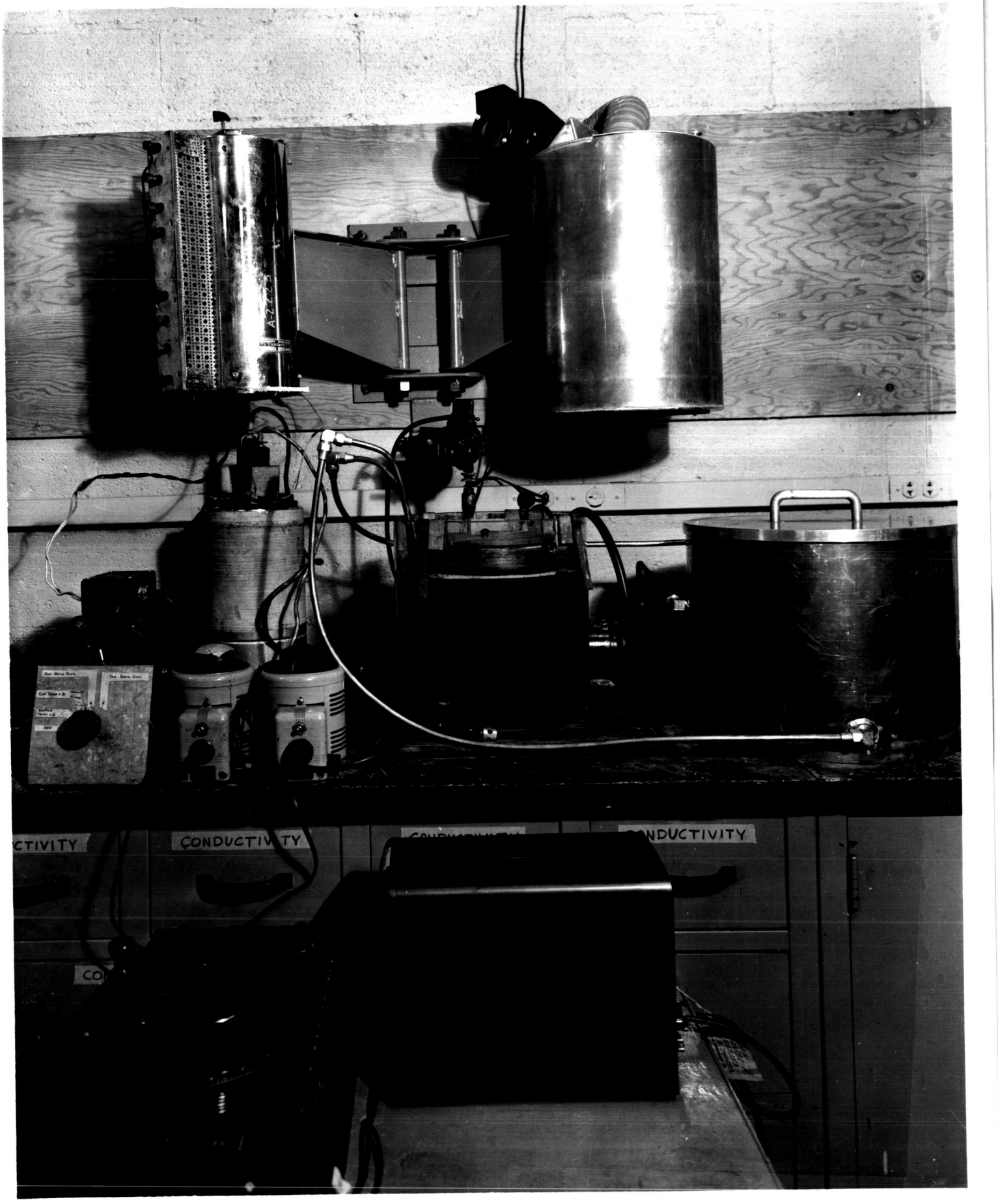

Figure 1. Heat Capacity Apparatus

APPENDIX F

HEAT CAPACITY TO 5500°F

HEAT CAPACITY TO 5500°F

The apparatus used for heat capacity employs the drop technique in which the specimen is heated in a furnace and then dropped into an ice calorimeter. The calorimeter contains a cup surrounded by a frozen ice mantle. Water at an inlet temperature of 32°F is circulated through an annulus surrounding the mantle in order to absorb heat leak from the surroundings. The entire system is insulated with glass wool. The enthalpy of the specimen is sensed as a change in volume of the water-ice system of the calorimeter as the ice melts. The annulus containing the flooded ice mantle communicates with the atmosphere through a mercury column in order that the change in volume can be read directly in a burette. An assembly drawing of the calorimeter is shown in Figure 1 and a picture of the calorimeter is shown in Figure 2. A picture of the ice mantle is shown in Figure 3. The specimen nominally is 3/4 inch diameter x 3/4 inch long.

The specimen is placed in either a graphite or stainless steel basket and heated in the furnace in a controlled atmosphere such as helium. The specimen and basket are dropped into the calorimeter and the volume change due to the resultant melting of ice is measured. The flutter valve immediately above the cup and the diaphragm valve immediately below the furnace are major features of the apparatus since the first blocks off radiation losses from the specimen up to the drop tube, and the second blocks radiation gains from the furnace down the drop tube just prior to dropping. The volume changes due to the baskets are measured and correction curves are established. Separate basket calibration minimizes the radiation error accompanying drop techniques. These errors are reported to be only about 0.5 percent[1]. Our theoretical calculations indicate even smaller errors from this source.

The heat necessary to melt enough ice to cause a volume change of 1 cc has been established by the U.S. National Bureau of Standards[2] at 3.487 Btu. This value is reported as the theoretical one for any ice calorimeter. Figure 4 shows a typical curve of mercury

---

[1] Furukawa, G.T., Douglas, McCoskey, and Ginnings, "Thermal Properties of Aluminum Oxide from 0° to 1200°K".

[2] Ginnings, D.C. and R. J. Corruccini, "An Improved Ice Calorimeter", NBS Research Journal, Volume 38, 1947, p583.

displacement versus time for one drop using a synthetic sapphire specimen. The correction for the stainless steel basket is subtracted from the measured mercury displacement and the result used to calculate specimen enthalpy above 32°F. The heat capacity, which is by definition the slope of the enthalpy versus temperature curve, is determined both graphically and analytically. The analytical approach is to fit the enthalpy data to an equation of the form

$$h_{32} = aT + bT^2 + cT^{-1} + d \qquad (1)$$

using a least squares technique. The derivative of this equation, the heat capacity, is computed with the constant "c" adjusted so that the analytical solution agrees with the graphical solution at 5000°F.[3] This technique is similar to that of Kelley in forcing the heat capacity equation through a known value[4]. The equations are developed using a digital computer.

A compilation of all errors has indicated that the apparatus is accurate to well within 5 percent uncertainty over the entire temperature range. Comparison of Southern Research Institute data on copper, Linde synthetic sapphire, and ATJ graphite all have confirmed this value.

---

[3] Pears, C.D., and J. G. Allen, "The Thermal Properties of Twenty-six Solid Materials to 5000°F or Their Destruction Temperatures", ASD-TDR-62-765.

[4] Kelley, K.K., "Contributions to Data on Theoretical Metallurgy", Volume XIII, High Temperature Heat Content, Heat Capacity and Enthalpy Data for the Elements and Inorganic Compounds, USBM 584, November, 1958.

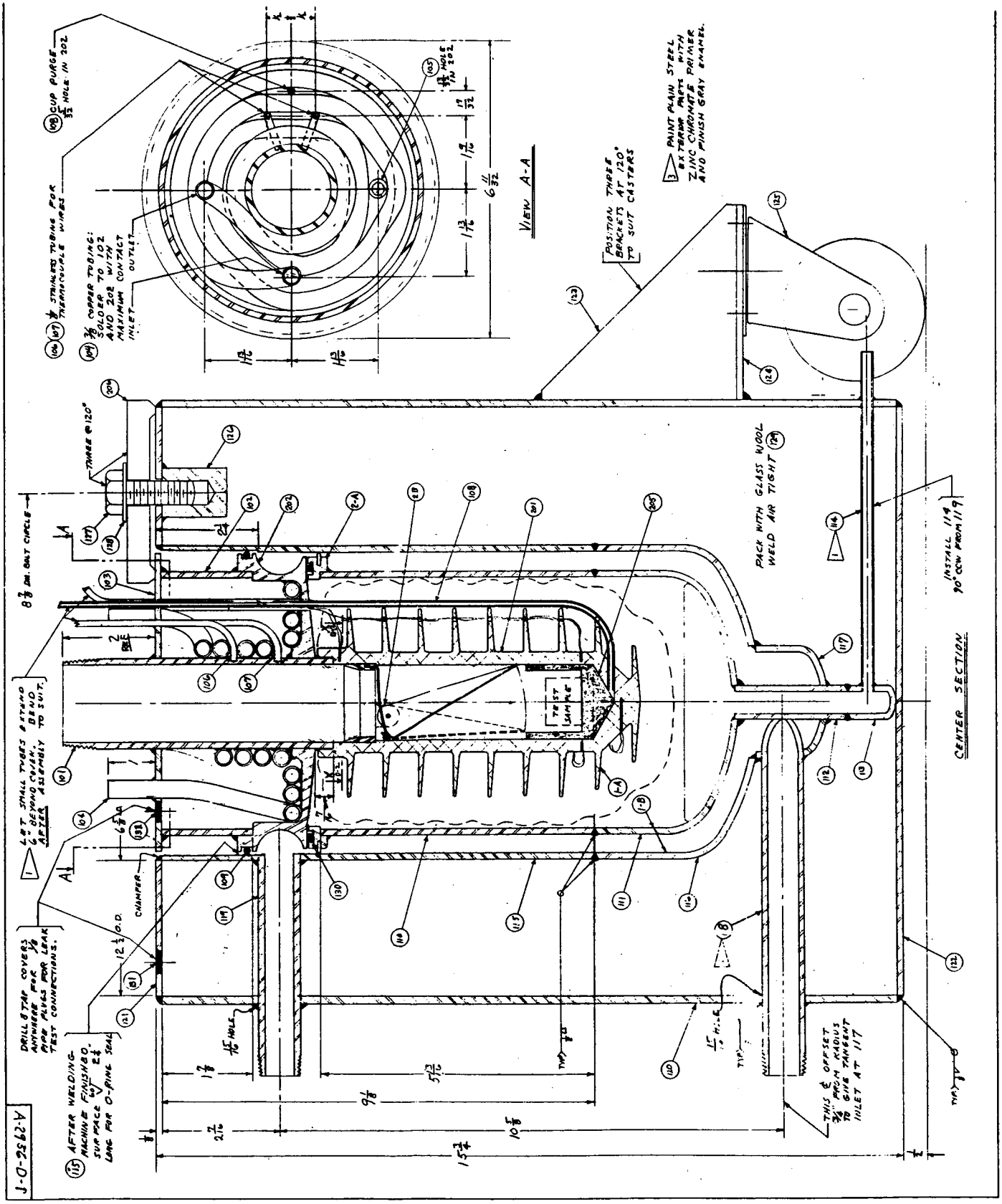

Figure 1. Ice Calorimeter, Drop Type - Specimens to 5500°F

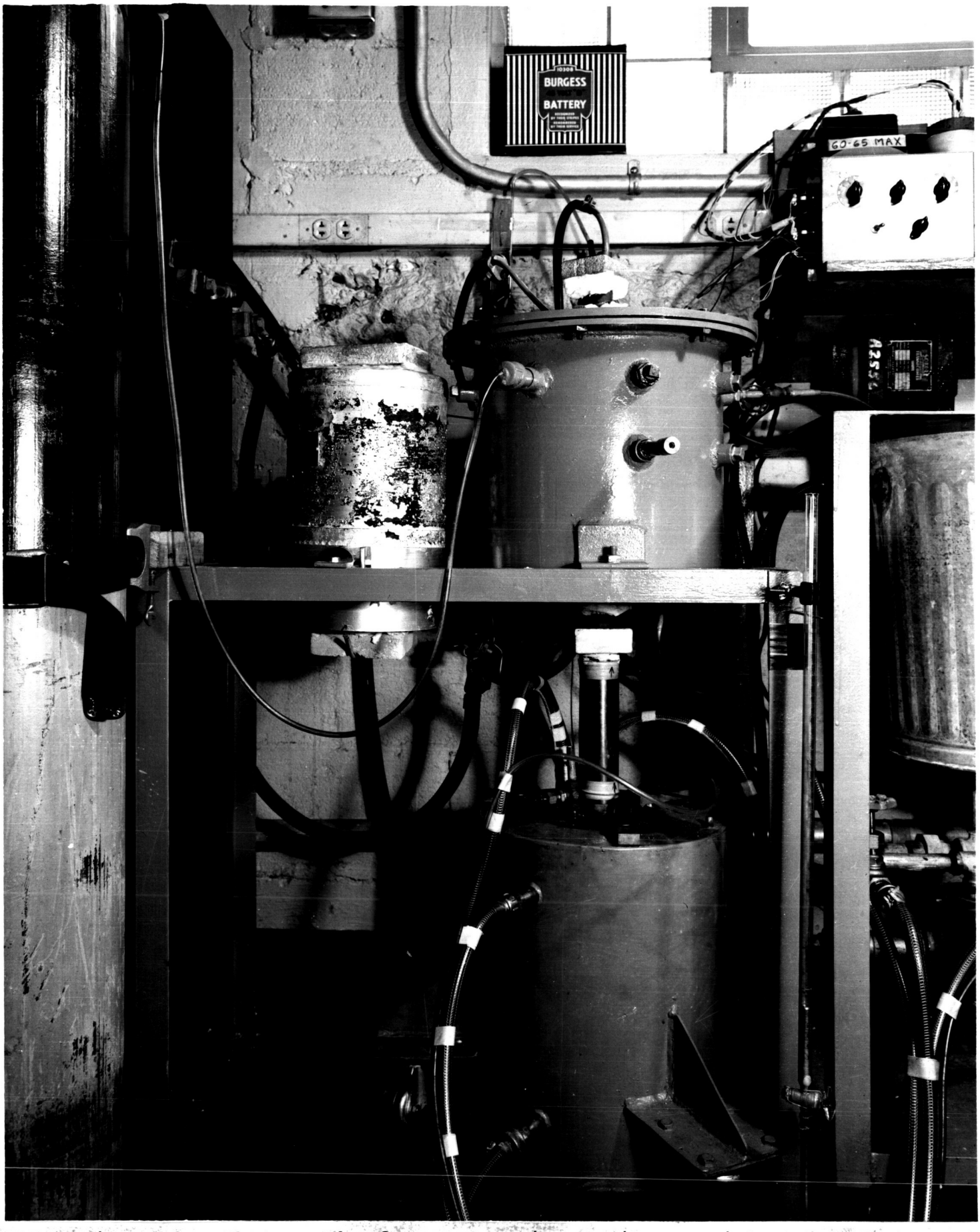

Figure 2. Photograph of Heat Capacity Equipment with Drop Shield Tube in Place

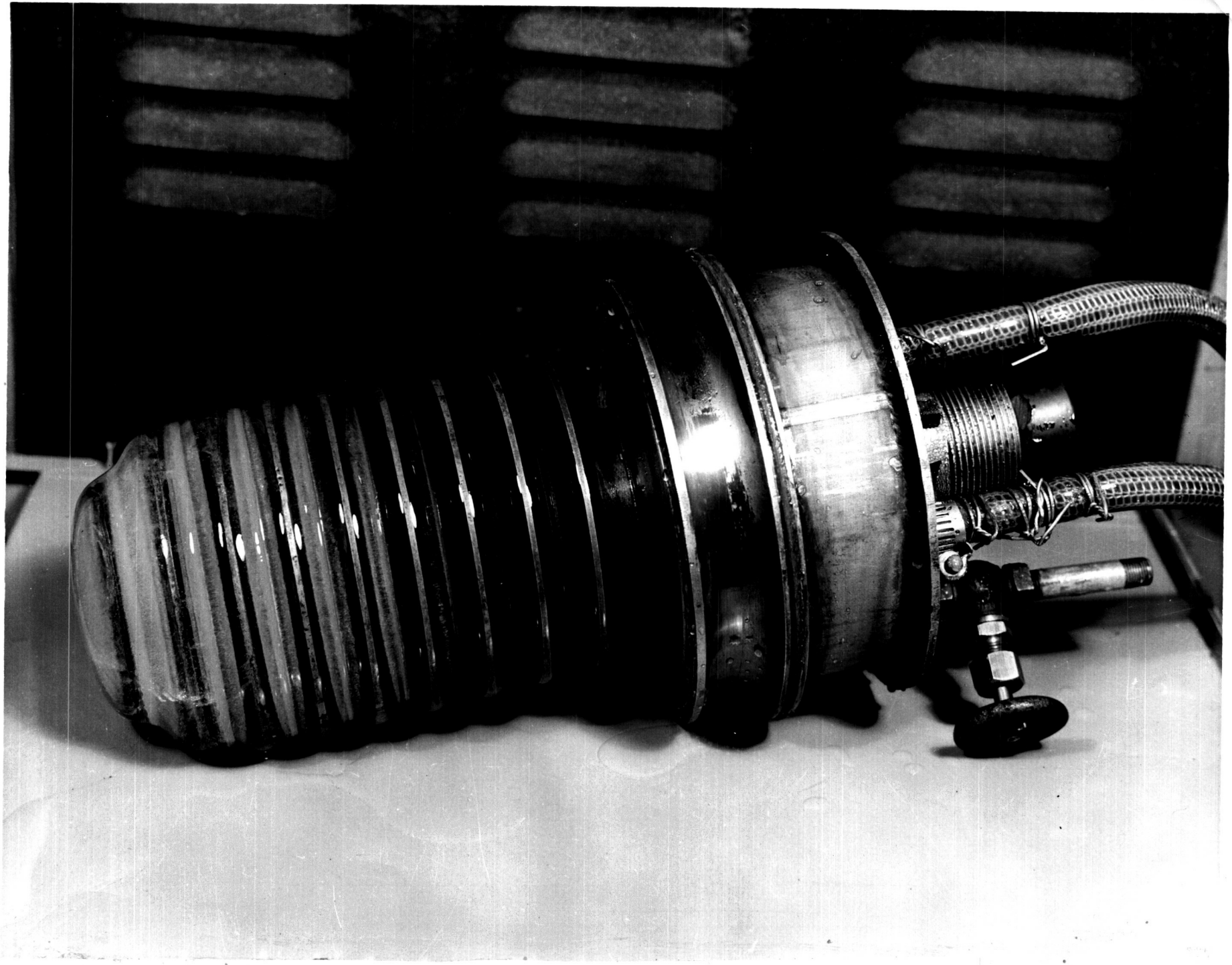

Figure 3. Photograph of Ice Mantle in Heat Capacity Ice Calorimeter

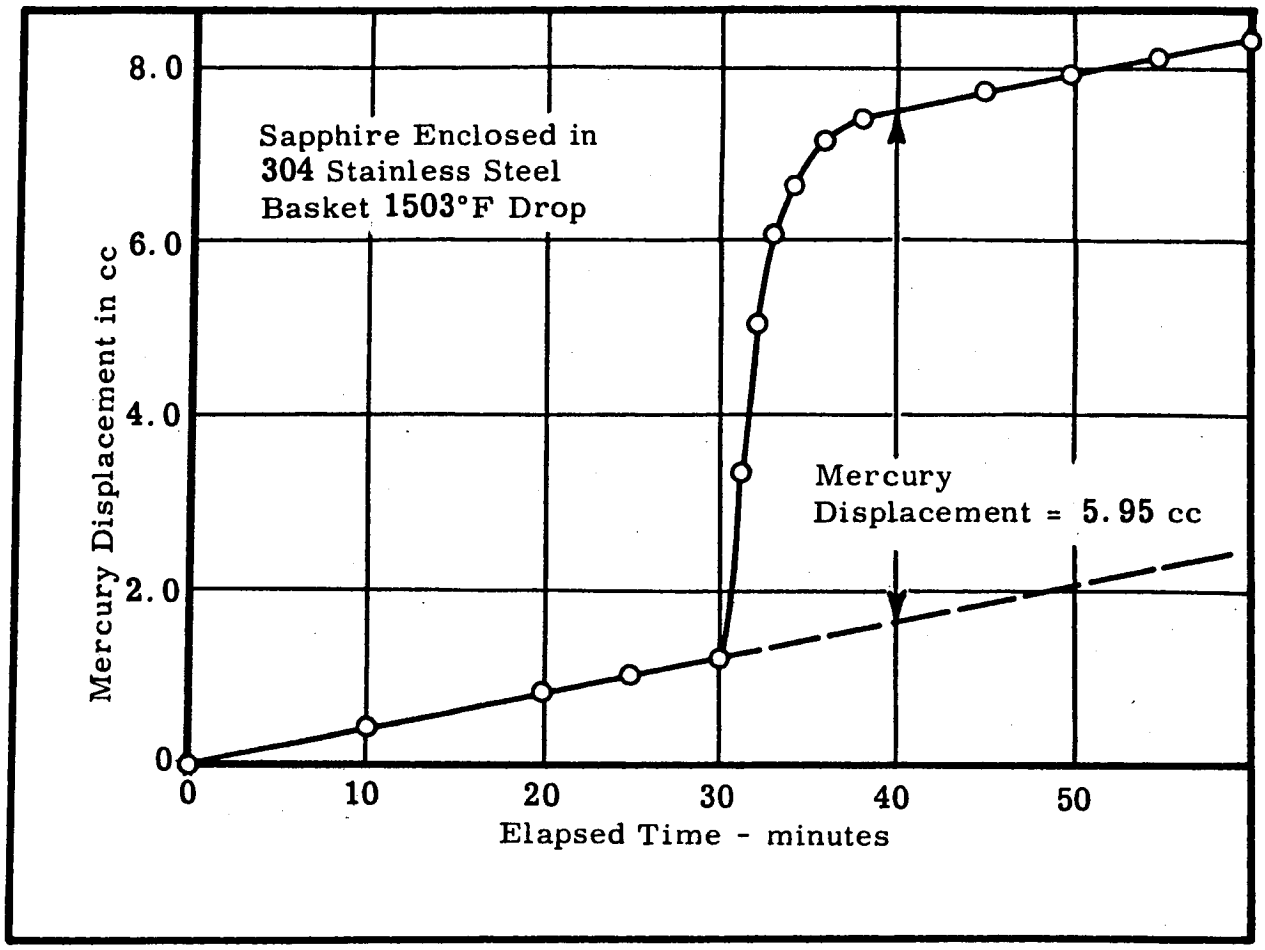

Figure 4. Mercury Displacement Due to Sapphire and 304 Stainless Steel Basket

APPENDIX G

PERMEABILITY TO 1000°F

PERMEABILITY TO 1000°F

We have two apparatus in which to make permeability measurements. One apparatus is designed for operation to 1000°F and the other is designed for room temperature measurements. These apparatus are basically the same in principle, except for the method in which pressure measurements are made. Static pressures across the specimen are measured with the room temperature apparatus, whereas the total pressure is measured in the 1000°F apparatus.

Room Temperature Apparatus

This apparatus is shown schematically in Figure 1. It consists of a copper housing and a copper specimen holder. An O-ring is used as a seal between the housing and the specimen holder. Gas is supplied to the specimen from a commercial gas cylinder. Static pressures are measured at the inlet and exit points to the housing. Flow rates are measured with either a bubble type flowmeter, a variable area flowmeter or a wet test meter; the type of instrument used to measure the flow rate depending upon the magnitude of the flow.

The specimen, which is 1 inch in diameter by 1/2 inch thick, is mounted in the housing as shown in Figure 2. The specimen is mounted on a shoulder approximately 1/64 inch wide and 1/64 inch deep. On the upstream side the specimen holder is bored out to a diameter of 1.5 inches and the annulus between the specimen and the holder is filled with silicone rubber (Dow Corning RTV-731 Silastic). This silicone rubber has been employed successfully as a sealant in prior permeability measurements.

High Temperature Apparatus

This apparatus is shown schematically in Figure 2. A detail cutaway view of the housing and specimen holder is shown in Figure 3. The apparatus as shown in these figures was designed for operation to 1000°F. Gas is supplied to the apparatus from a commercial gas cylinder. The volumetric flow rate is measured with a variable area flowmeter. The inlet pressure to the flowmeter is read with a mercury filled U-tube manometer. This pressure measurement is used to correct the indicated flowmeter reading to the volumetric flow rate at standard pressure. Between the flowmeter and the specimen housing, the gas passes through a preheater section. This consists of thin-walled stainless steel tubing which is resistively heated using low voltage and high current. Power is supplied

from a 25 KV step-down transformer, the input of which is regulated by a 220 V Powerstat. The gas then passes through the specimen and is exhausted to the atmosphere.

The pressures upstream and downstream of the specimen are measured with total pressure probes. These pressure monitors are connected to U-tube manometers such that the manometers read the pressure difference across the specimen and the gage pressure on the downstream side of the specimen.

Temperatures are measured with two chromel alumel thermocouples. One thermocouple is mounted in the stainless steel specimen holder. The other thermocouple is used to monitor the temperature of the gas leaving the downstream side of the specimen. The exposed junction of the gas thermocouple is placed so that the hot gas leaving the specimen impinges directly upon it.

Knife edges are machined on the faces of the housing and specimen holder. A copper gasket is used between these knife edges to provide a leak tight seal.

The specimen is mounted in a stainless steel housing as shown in Figure 4. The specimen rests in a recess approximately 1/64 inch wide by 1/32 inch deep. Above this recess the holder is bored out to a diameter of 1.5 inches. Normally, specimens used for the measurements are 1 inch in diameter by 1/2 inch thick. Smaller specimens may also be accommodated. The annulus between the specimen and the housing is filled with a sealing compound. A silicone rubber (Dow Corning RTV-731 Silastic) is used as the sealing compound for low temperature measurements. For high temperature runs, Sauereisen 31 cement is used as a sealant. Both of these sealing compounds have been used successfully in prior evaluations. A stainless steel washer is mounted on the exposed surface of the Sauereisen cement while it is still wet. This washer reduces the exposed area of the cement and serves as a secondary seal.

The procedure for setting up the specimen using the Sauereisen cement is as follows. The annulus is filled about 3/4 full with a fairly dry mix of the cement and then cured for about four hours at 250°F. Next, a wet wash is applied and the washer placed on top. The assembly is then cured for about four hours at 700°F.

Procedure

Ambient Temperature Runs - The procedure in making the runs at ambient temperature is as follows: when the wet test meter is used, the system is purged for about 30 minutes to remove residual gases from the meter. The pressure regulator is adjusted to give the desired pressure difference across the specimen. Several minutes are allowed for the system to stabilize. Then the measurements are made.

Elevated Temperature Runs - The procedure in making the runs at elevated temperatures is as follows: the housing is brought up to temperature with no gas flow through the apparatus. After the housing temperature stabilizes, the gas flow is turned on and the pressure regulator is set to give the desired pressure drop across the specimen. The gas preheater is then turned on and the input power is increased until the gas reaches the same temperature as the housing. At least two data points are taken at each pressure level to monitor that the two temperatures are in equilibrium and to reduce the risk of obtaining spurious readings.

General

During the runs the following data are recorded:

1. Atmospheric pressure.
2. Differential pressure across specimen.
3. Downstream gage pressure.
4. Pressure at flow instrument (at inlet to wet test meter or flowmeter; when flowmeter is used on the downstream side of housing no readings are taken because of the small pressure drop through the flowmeter venting to atmosphere).
5. Flowmeter readings.
6. Housing temperature.
7. Gas temperature.
8. Temperature at wet test meter (when used).

All flowmeter readings are converted to the volumetric flow rate at standard pressure.

DATA CORRELATION

Theory

Greenberg and Weger[1] concluded from a review of some of the literature on permeability that most of the data could be correlated with an equation of the type:

$$-\frac{dP}{dx} = \alpha \mu V + \beta \rho V^n \qquad (1)$$

where

$\frac{dP}{dx}$ = pressure gradient in the direction of flow

α = viscous flow coefficient (reciprocal of Darcy's constant, k)

V = instantaneous gas velocity

β = inertial flow coefficient

ρ = instantaneous gas density

μ = absolute viscosity

and where n is some number between 1 and 2.

Carman[2] selected the value of n as 2 to account for turbulent flow. Greenberg and Weger[1] also state that correlations of the data of Cornell and Katz indicate that the value of n should be 2 to account for inertial flow through consolidated media.

In equation (1), the first term on the right-hand side represents the resistance due to viscous flow. The second term on the right-hand side represents the resistance due to inertial flow. Inertial flow results from turbulence induced by the tortuous path the gas must follow through the porous material and also by high velocities. Both of these phenomena depend upon the kinetic energy of the fluid per unit volume, ρV^2. Thus, in developing equation (1) it was assumed that the expression for the inertial resistance could be superimposed upon the expression for the viscous resistance.

---

[1]See Refererences

Under steady-state conditions, the mass velocity of gas (for one-dimensional flow) through a porous media must be constant. By letting $\rho V = G$ and $n = 2$, equation (1) becomes

$$-\rho \frac{dP}{dx} = \alpha \mu G + \beta G^2 \tag{2}$$

where G = mass velocity.

Now, for an ideal gas

$$\rho = \frac{PM}{RT} \tag{3}$$

where

P = absolute pressure

M = molecular weight of gas

R = universal gas constant

T = absolute temperature

Substituting equation (3) into equation (2) and rearranging yields

$$-\frac{PM}{RT\mu G}\frac{dP}{dx} = \alpha + \frac{\beta G}{\mu} \tag{4}$$

or

$$-\frac{M}{RT\mu G}\int_{P_1}^{P_2} PdP = \left(\alpha + \frac{\beta G}{\mu}\right)\int_{0}^{L} dx$$

Integrating and rearranging equation (4) yields

$$\frac{MP_m\Delta P}{LRT\mu G} = \alpha + \beta\left(\frac{G}{\mu}\right) \tag{5}$$

where

$P_m = \frac{1}{2}(P_1 + P_2)$ = mean specimen pressure

$\Delta P = (P_1 - P_2)$ = differential pressure

L = thickness of specimen

Since G is a constant, one may write

$$G = \frac{Q_{STP}\,\rho_{STP}}{A} \tag{6}$$

where

Q_{STP} = volumetric flow rate at standard conditions

ρ_{STP} = gas density at standard conditions

A = total cross section of porous media normal to flow

Data Reduction

The dependent and independent variables in equation (5) are calculated for each data point. Then a plot of $MP_m\Delta P/LRT\mu G$ versus G/μ is made. Such a presentation is known as a Cornell and Katz plot. A straight line is drawn through the points thus plotted and the viscous and inertial coefficients obtained from the intercept and slope of the curve, respectively. Thus, for each specimen evaluated one viscous and one inertial coefficient are calculated at a given temperature level. Data are obtained over a sufficient range of the parameter (G/μ) to allow a good correlation and reduce the effects of spurious readings. The uncertainty in the reduced data is estimated to be ± 5 percent.

Some reduced data for a low-density phenolic-nylon char are presented in Figure 3. This figure shows typical data scatter about a straight line plotted through the data points. It has been our experience that the equation shown plotted in Figure 3, equation (5), correlates the data for porous materials which we have evaluated.

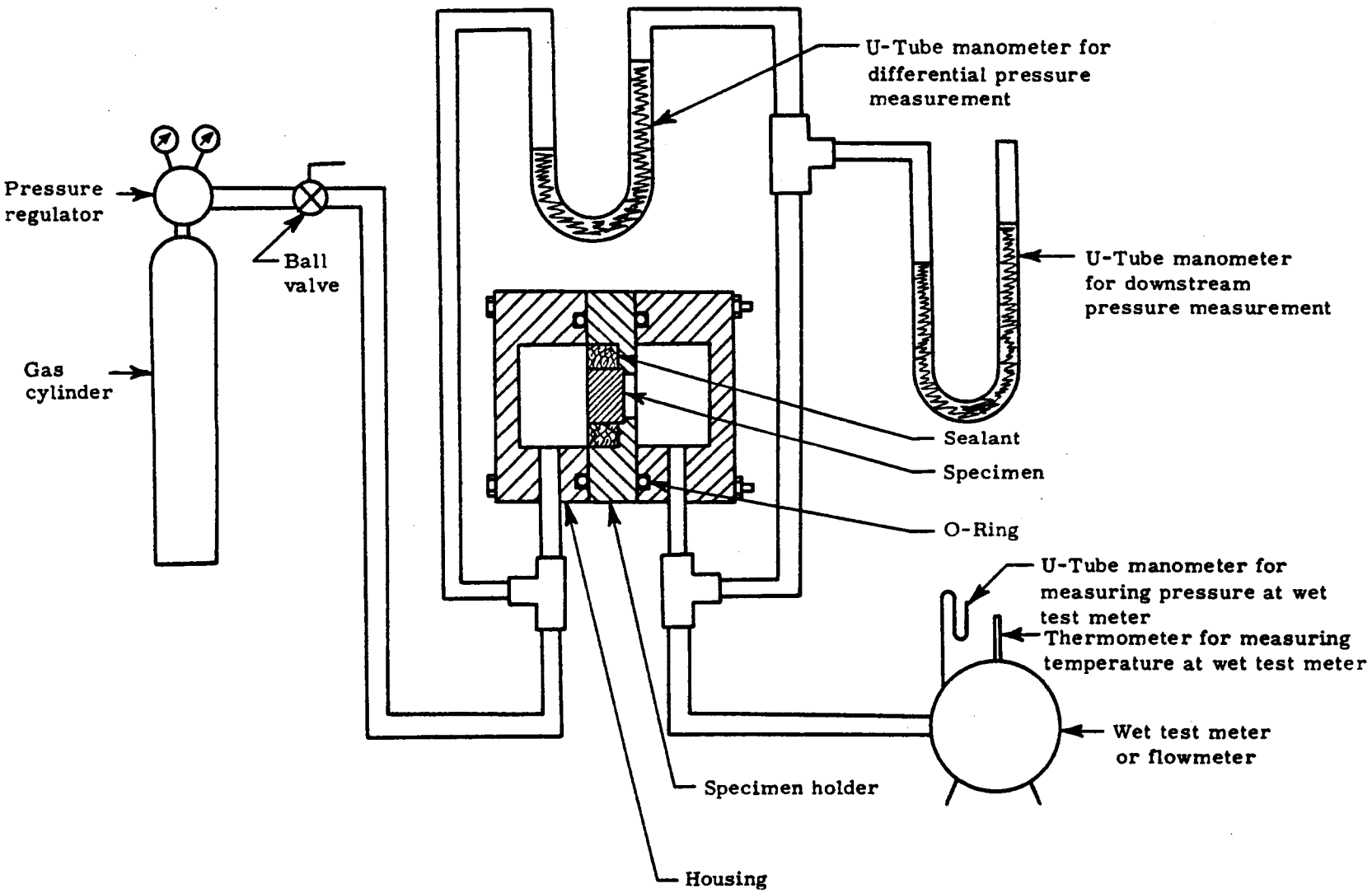

Figure 1. Permeability apparatus for room temperature permeability measurements

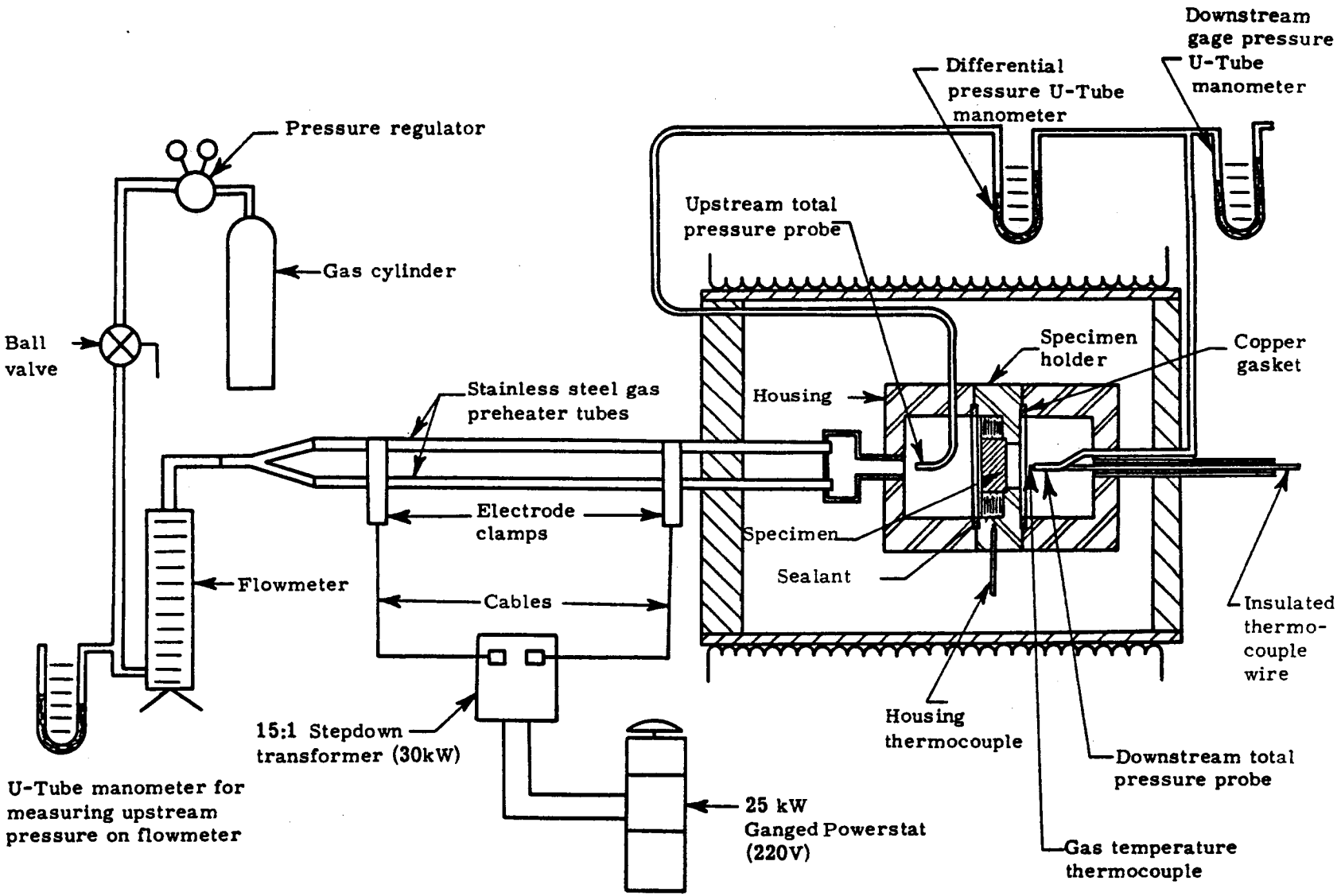

Figure 2. Permeability apparatus for measurements to 1000°F

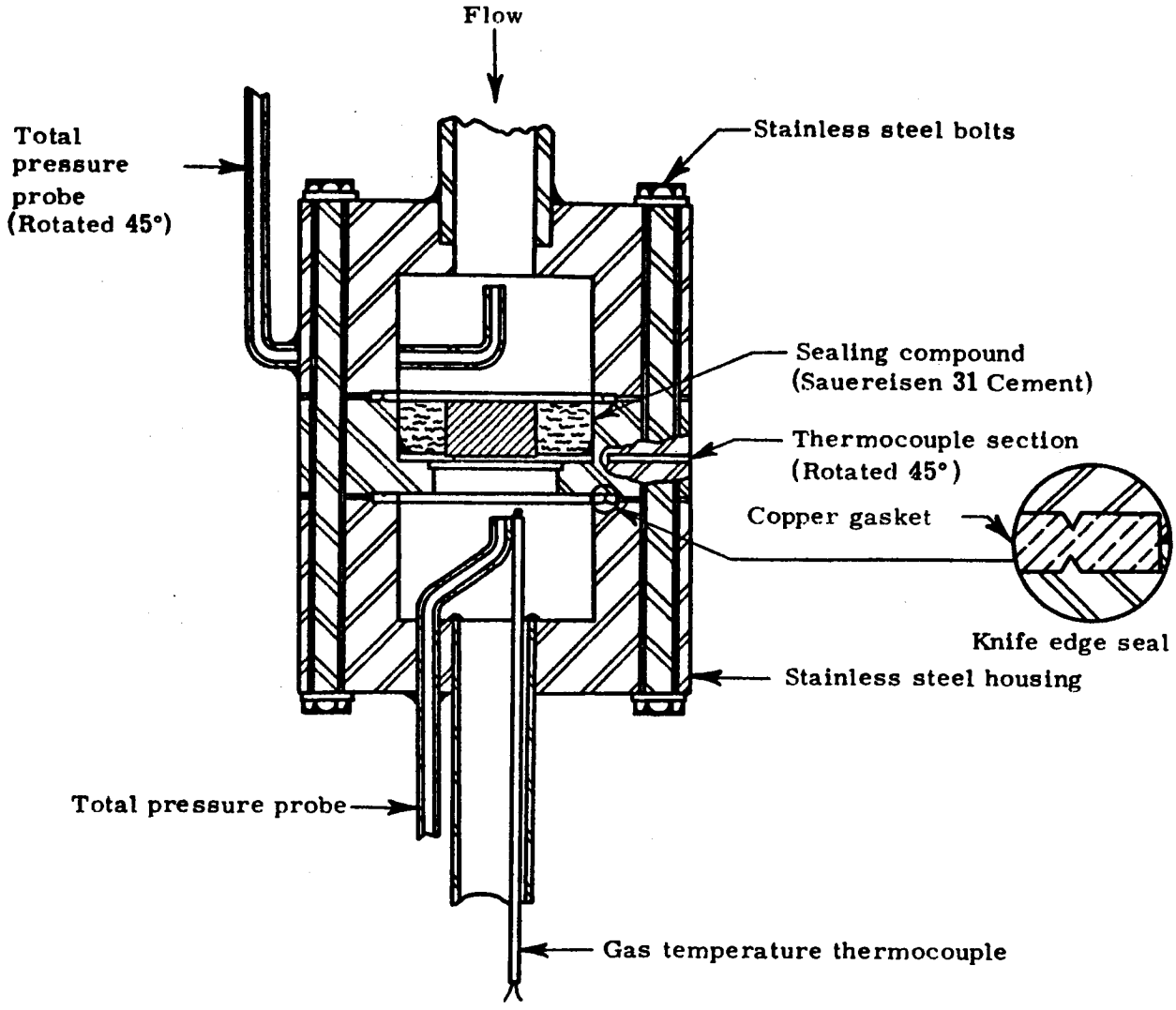

Figure 3. Details of specimen holder for high temperature permeability measurements

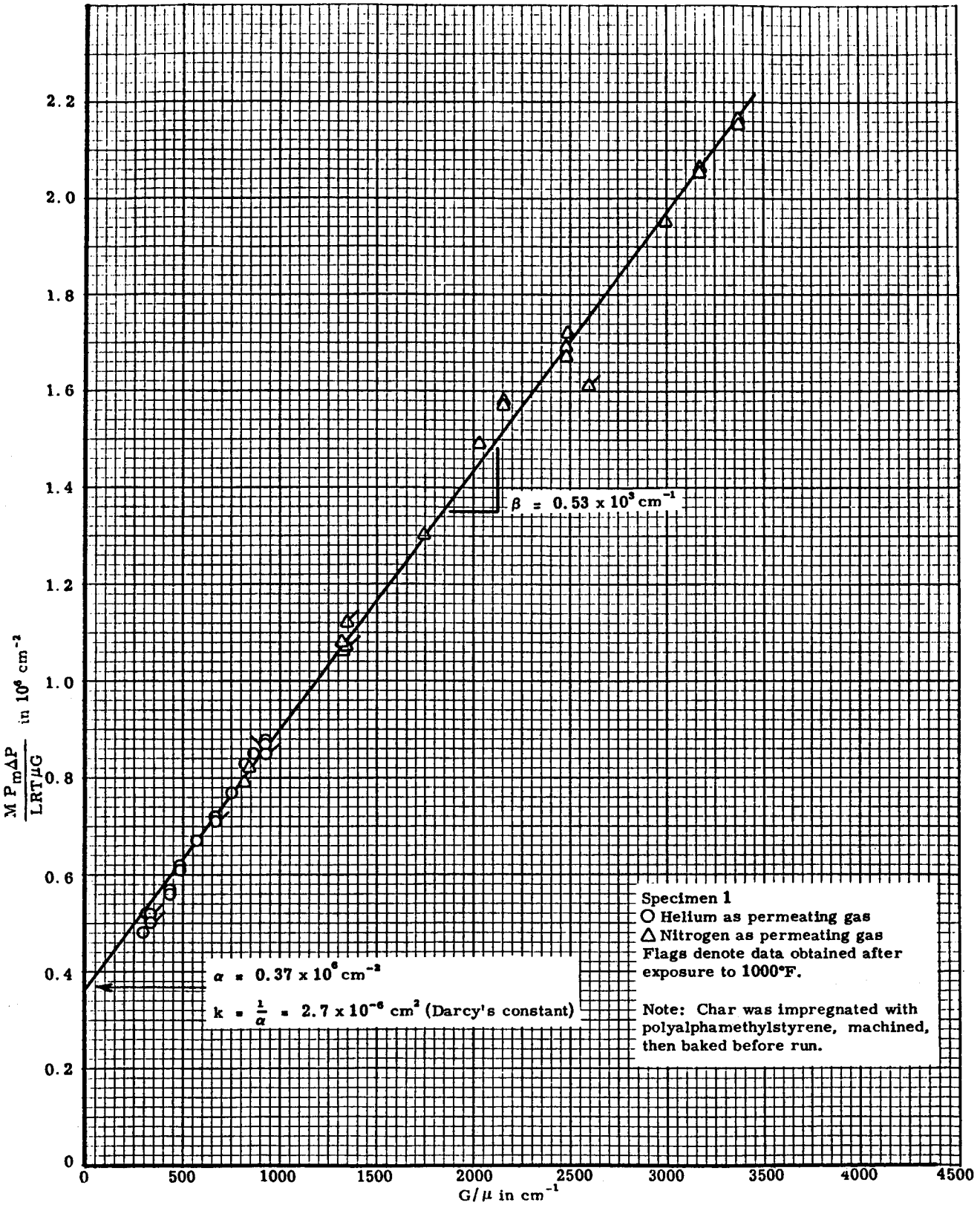

Figure 4. Cornell and Katz plot for low-density phenolic-nylon char perpendicular to the charring direction at room temperature

REFERENCES

1. Greenberg, D. B. and E. Weger, "An Investigation of the Viscous and Inertial Coefficients for the Flow of Gases through Porous Sintered Metals with High Pressure Gradients," Chemical Engineering Science 12, Pergamon Press Ltd., London, pp 8-19, 1960.

2. Carman, P. C., Flow of Gases through Porous Media, Academic Press, Inc., New York, 1956.